BMR JOURNAL
OF AUSTRALIAN GEOLOGY & GEOPHYSICS

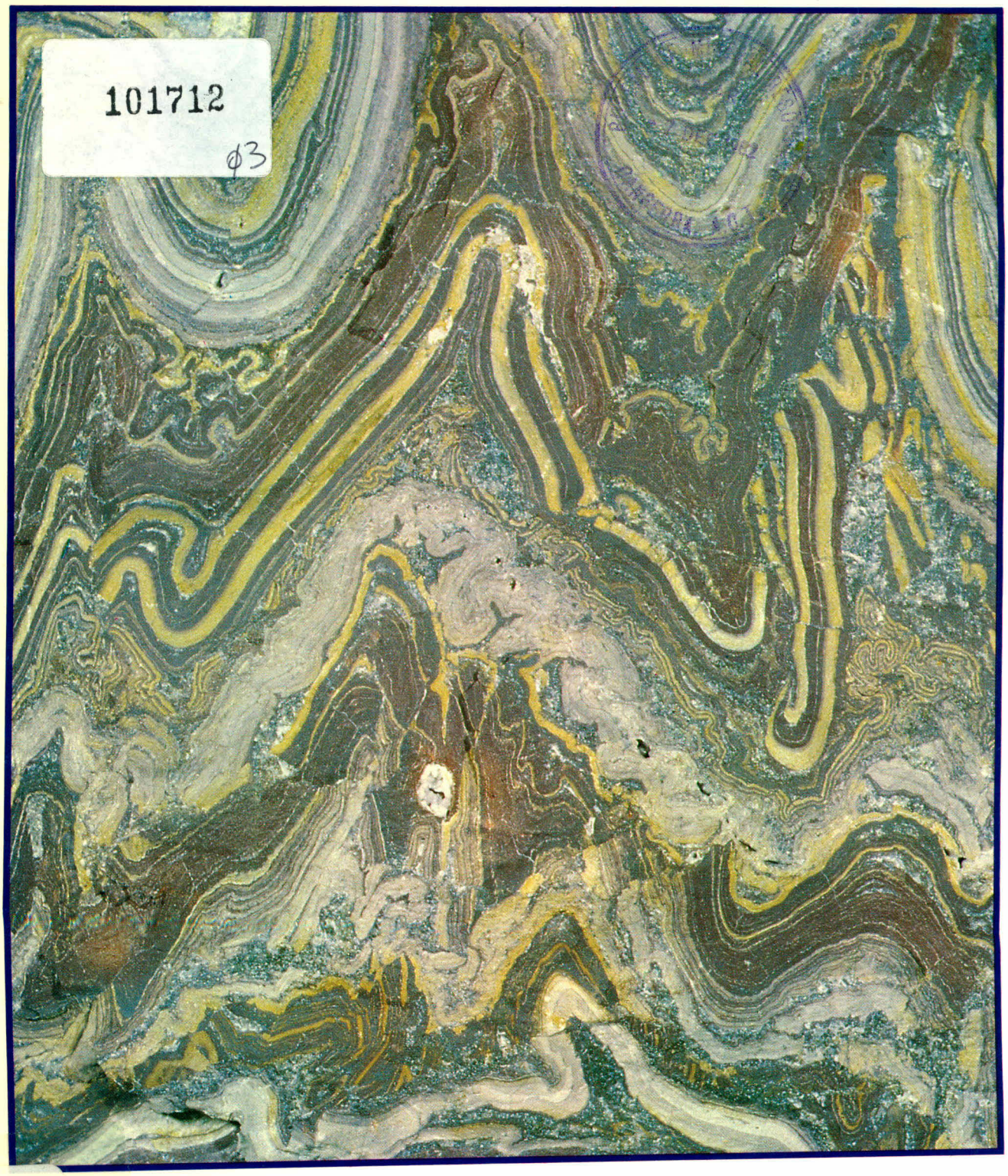

VOLUME 7 NUMBER 3 SEPTEMBER 1982

BMR JOURNAL
OF AUSTRALIAN GEOLOGY & GEOPHYSICS

VOLUME 7 NUMBER 3 SEPTEMBER 1982

CONTENTS

G. Playford
A latest Devonian palynoflora from the Buttons beds, Bonaparte Gulf Basin, Western Australia 149

G. F. Taylor & K. M. Scott
Evaluation of gossans in relation to lead-zinc mineralisation in the Mount Isa Inlier, Queensland 159

A. L. Jaques, D. H. Blake, & P. J. T. Donchak
Regional metamorphism in the Selwyn Range area, northwest Queensland 181

R. S. Nicoll
Multielement composition of the conodont *Icriodus expansus* Branson & Mehl from the Upper Devonian of the Canning Basin, Western Australia 197

P. Wellman & J. W. Williams
Extent of Archaean and Late Proterozoic rocks under the ice cap of Princess Elizabeth Land, Antarctica, inferred from geophysics 213

D. Denham, G. Bock, & R. S. Smith
The Appin (New South Wales) earthquake of 15 November 1981 219

NOTE

M. H. Tratt & R. V. Burne
Impregnation of unconsolidated sediment samples, using a large vacuum chamber 225

ABSTRACTS

New microform publications 227

Front cover: Gossan material of oxidised and partially leached lead-zinc-silver ore from Black Star open cut, Mount Isa. The mineralogy and geochemistry of gossans in the Mount Isa Inlier, northwest Queensland, are described in this issue in a paper by G. F. Taylor & K. M. Scott.

AUSTRALIAN GOVERNMENT PUBLISHING SERVICE CANBERRA 1982

Department of National Development and Energy, Australia

Minister: Senator the Hon. Sir John Carrick, K.C.M.G.

Secretary: A. J. Woods

Bureau of Mineral Resources, Geology and Geophysics

Director: R. W. R. Rutland

Editor, BMR Journal: I. M. Hodgson

The BMR Journal of Australian Geology & Geophysics is a quarterly journal of research and related activities. Contributions are from officers of the BMR, from BMR officers working in collaboration with others, or requested work sponsored by the BMR. In addition to articles the Journal may include shorter notes and discussion of papers published in it. Discussion of papers is invited from anyone.

Annual subscription to the Journal is $25 (Australian). Individual numbers, if available, cost $8.50. Subscriptions, etc., made payable to the Receiver of Public Moneys in Australian dollars should be sent to the Director, Bureau of Mineral Resources, Geology and Geophysics, P.O. Box 378, Canberra, A.C.T. 2601, Australia.

Other matters concerning the Journal should be sent to the Director, marked for the attention of the Editor, BMR Journal.

Cover design: Stuart Fereday.

The text figures in this issue were drafted by P. Jorritsma, P. Griffiths, & B. Pashley.

ISSN 0312-9608

Printed by Graphic Services Pty Ltd, 516-518 Grand Junction Road, Northfield, S.A. 5085

BMR Journal of Australian Geology & Geophysics, 7, 149-157

A LATEST DEVONIAN PALYNOFLORA FROM THE BUTTONS BEDS, BONAPARTE GULF BASIN, WESTERN AUSTRALIA

G. Playford[1]

A moderately well-preserved miospore flora has been obtained from the type section of the Late Devonian Buttons beds in the southwestern Bonaparte Gulf Basin, Western Australia. It is characterised by relatively abundant specimens of *Retispora lepidophyta* (Kedo) Playford, 1976 and by other trilete miospore species that collectively constitute the *R. lepidophyta* Assemblage as defined from the lower part of the Fairfield Group of the Canning Basin, Western Australia. On this basis, the Buttons beds are datable as latest Devonian, probably within the interval Fa2d to Tn1a or early Tn1b of Belgian terminology. This palynological age determination is somewhat younger than previous, faunally based age assessments of the Buttons beds, which have suggested, not altogether unequivocally, an earlier Famennian age (i.e., doIIβ–doIII, Fa1c–Fa2b). One new species of trilete cingulate miospores—*Lophozonotriletes varionodosus*—is instituted herein.

Introduction

In the Bonaparte Gulf Basin of northwestern Australia (Fig. 1), marine Devonian rocks are known from both outcrop and subsurface, and reach a thickness of at least 1800 m (Veevers & Roberts, 1968; Jones, 1968; Playford & others, 1975). Devonian sedimentation is believed to have begun in the early Frasnian (or perhaps late Givetian). Three depositional facies were recognised by Veevers & Roberts (1968): (a) the platform carbonate province, in the northwest of the basin; (b) the deeper-water, basinal shale province, known only from subsurface sections in the basin's north-central part; and (c) the platform conglomerate province to the southeast. The distribution of these provinces and correlation of their constituent rock units have been depicted by Veevers & Roberts (1968, figs. 4, 10) and Roberts & others (1972, correlation chart).

The present paper concerns the palynological characteristics of one of the basin's Late Devonian units, the Buttons beds; and is intended to supplement previously published biostratigraphic inferences based upon other palaeontological data from the unit.

Buttons beds

The Buttons beds are a marine unit that is developed in the southern and southeastern portion of the Bonaparte Gulf Basin (Jones, 1968, fig. 1), specifically in the transitional area between the two platform provinces and in the general vicinity of the Precambrian Pincombe Range inlier. As defined by Veevers & Roberts (1968, pp. 59–64), the Buttons beds incorporate over 300 m of sandy and silty limestone with subordinate dolostone and sandstone. The type section (no. 105 of Veevers & Roberts, p. 62; figs. 30, 35) is located in the bed of the Ord River, just north of Buttons Crossing (Fig. 2); it is 350 m thick, but neither the base nor top is exposed.

The Buttons beds are considered to represent shallow water, inshore and offshore lagoonal deposits on the landward side of the reef complex embodied by the partly equivalent Ningbing Limestone. Thus, they are regarded (Veevers & Roberts, 1968, p. 59) as being laterally contiguous with part, 'probably the lower part', of the Famennian to ?Tournaisian Ningbing Limestone, which constitutes an extensively outcropping reefal unit in the platform carbonate province (i.e. around the western margin of the Bonaparte Gulf Basin). Both the Ningbing Limestone and Buttons beds are believed to be conformable on the underlying uppermost member (Jeremiah Member) of the Frasnian to early Famennian Cockatoo Formation. At one locality, Sorby Hills (Veevers & Roberts, 1968, fig. 37), the Buttons beds are unconformable on Precambrian siltstone. The top of the unit, where exposed, is said to have a disconformable relationship with overlying Early Carboniferous limestone of the Burt Range Formation (Veevers & Roberts, 1968, pp. 67, 70).

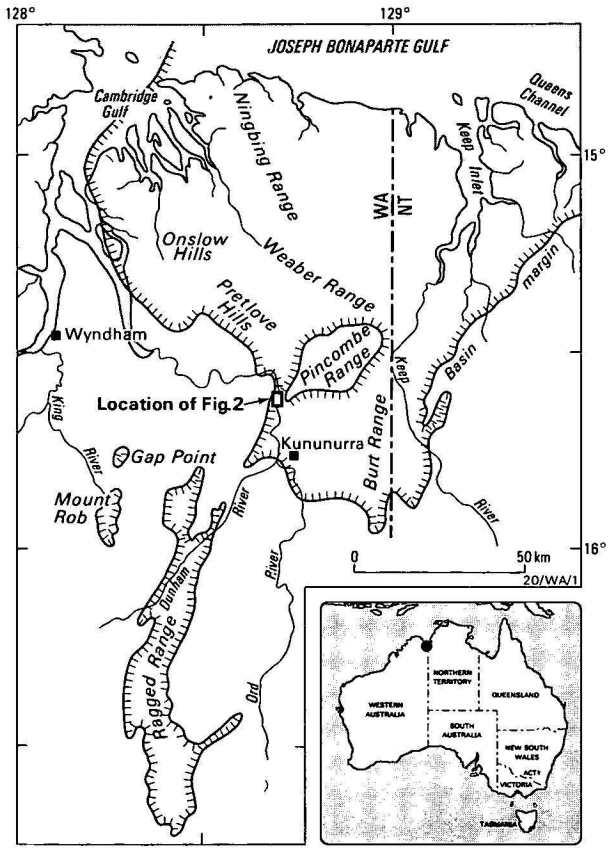

Figure 1. Locality map, Bonaparte Gulf Basin of Western Australia and Northern Territory.
After Veevers & Roberts (1968, fig. 5).

[1] Department of Geology and Mineralogy, University of Queensland, St Lucia, Queensland 4067.

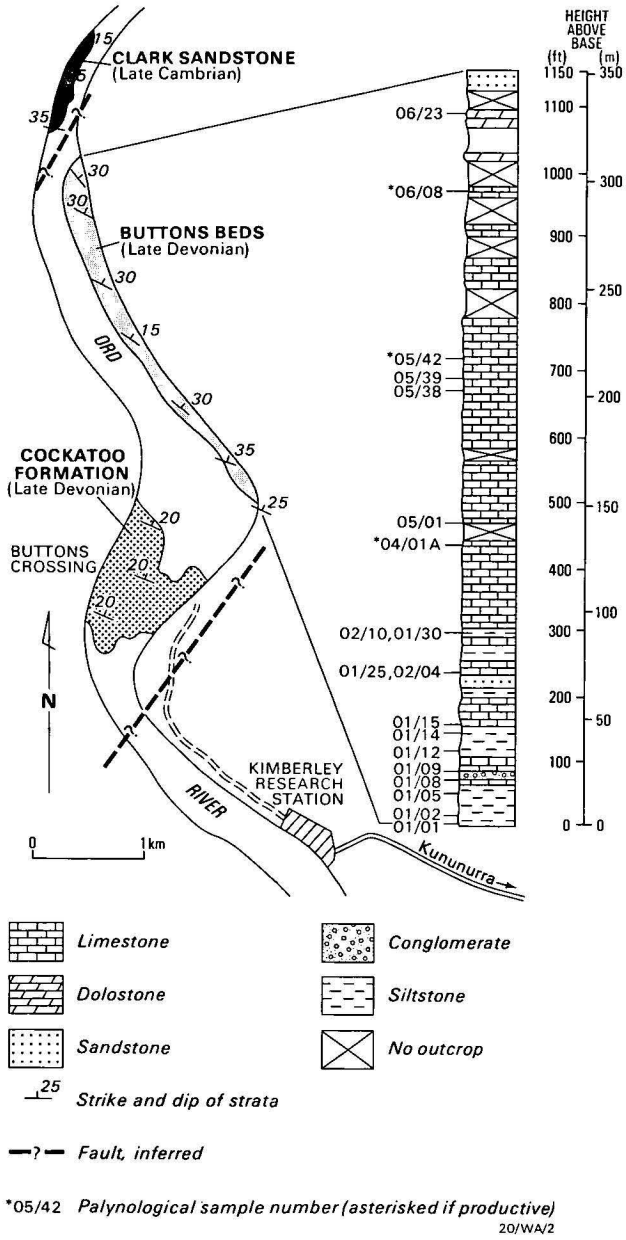

Figure 2. Map and stratigraphic column of the type section of the Buttons beds.
The column shows generalised lithologies and sampling levels. Adapted from Veevers & Roberts (1968, figs. 30, 35).

At the type section, the base of the Buttons beds was regarded by Veevers & Roberts (p. 62) as being 'probably conformable' on the Cockatoo Formation, although uncertainty exists (Veevers & Roberts, pp. 33–34) because of structural complexity and incomplete exposure. The top of the type Buttons beds was regarded by the same authors as being in faulted juxtaposition with the Cambrian Clark Sandstone.

Fauna and flora

Varied and often rich fossil assemblages have been reported from the Buttons beds, particularly at their type section (Veevers & Roberts, 1968, p. 62). Groups represented prominently include brachiopods (Roberts, 1971), ostracods (Jones, 1968), corals (Hill, 1954), calcareous algae (Veevers, 1970), bivalves, gastropods, stromatoporoids, crinoids, and lepidodendrid megaplants (viz. *Leptophloeum australe* (McCoy) Walton, 1926). Conodonts are infrequent (Druce, 1969). Plant microfossils have not previously been reported from the Buttons beds.

Previous age assessments

The age of the Buttons beds has been assessed hitherto e.g. Roberts & others, 1972, p. 470) from fossil evidence—afforded principally by ostracods, brachiopods, conodonts, and megaplants—and also from the unit's inferred lateral equivalence with part of the reefal Ningbing Limestone (dated as early Famennian to possibly early Tournaisian). The bulk of the palaeontological data hitherto available indicates a Late Devonian (Famennian) age.

Attempts to refine the dating and correlation of the Buttons beds have rested primarily on a conodont specimen, and also on ostracods and brachiopods. Chronological significance has been attached by Jones & Druce (1966), Roberts & others (1967), and Roberts & others (1972) to the occurrence of a conodont that Druce (1969, pp. 111, 156; pl. 34, figs. 4a,b) termed *Polylophodonta* sp. A. This form, represented by a single specimen from the Buttons beds type section (250 m above base), was said to indicate an early Famennian (doIIβ–doIII) age (Roberts & others, 1967, p. 573; 1972, p. 470). It should be noted, however, that two other species of the meagre conodont fauna recorded from the Buttons beds—namely *Hindeodella corpulenta* Branson & Mehl, 1934 and *Spathognathodus* aff. *S. robustus* (Branson & Mehl, 1934)—are suggestive of a younger (Tournaisian) age (see Druce, 1969, charts 2,5).

Jones (1968) proposed four, provisional, concurrent range zones based on ostracod faunas from the type section of the Button beds. The endemic complexion of these faunas inhibited their application in overseas correlation; but they were applied to correlation on a local scale, suggesting, inter alia, that the Buttons beds are equivalent to the lower part of the Ningbing Limestone (in turn dated by conodonts as early Famennian:

Figure 3. Miospores from the Buttons beds (type section).
Magnification X500 unless otherwise indicated.
a—*Granulatisporites frustulentus* Balme & Hassell emend. Playford, 1971; median focus (X750), sample 05/42, prep. D547/1, 106.1 6.3, CPC 22149. **b, c**—*Apiculatisporis morbosus* Balme & Hassell, 1962: **b**—proximal focus, sample 04/01A, prep. D526/7, 112.6 13.0, CPC 22150; **c**—median focus, sample 06/08, prep. D546/1, 107.0 20.2, CPC 22151. **d, e**—*Convolutispora fromensis* Balme & Hassell, 1962: **d**—median focus, sample 04/01A, prep. D526/1, 97.6 10.9, CPC 22152; **e**—proximal focus, sample 04/01A, prep. D526/1, 103.5 10.9, CPC 22153. **f**—*Camptotriletes balmei* Playford, 1976; median focus, sample 04/01A, prep. D526/1, 100.6 12.2, CPC 22154. **g**—*Reticulatisporites ancoralis* Balme & Hassell, 1962; proximal focus, sample 04/01A, prep. D526/1, 112.1 7.8, CPC 22155. **h, i**—*Brochotriletes textilis* (Balme & Hassell) Playford, 1976: **h**—proximal focus, sample 05/42, prep. D547/1, 107.8 21.6, CPC 22156; **i**—proximo-equatorial aspect, sample 04/01A, prep. D526/1, 111.1 6.6, CPC 22157. **j–n**—*Lophozonotriletes varionodosus* Playford sp. nov.: **j**—median focus, sample 04/01A, prep. D526/1, 112.3 10.5, CPC 22158; **k**—distal focus, sample 04/01A, prep. D526/8, 104.2 11.9, CPC 22159; **l**—distal focus, sample 06/08, prep. D546/1, 117.8 8.3, CPC 22160; **m**—distal focus, sample 04/01A, prep. D526/1, 102.4 6.9, CPC 22161; **n**—holotype, distal focus (X750), sample 04/01A, prep. D526/10, 109.1 12.7, CPC 22162. **o–p**—*Knoxisporites literatus* (Waltz) Playford, 1963: **o**—median focus, sample 04/01A, prep. D526/9, 103.5 13.8, CPC 22163; **p**—proximal focus, sample 04/01A, prep. D526/1, 112.4 22.5, CPC 22164.

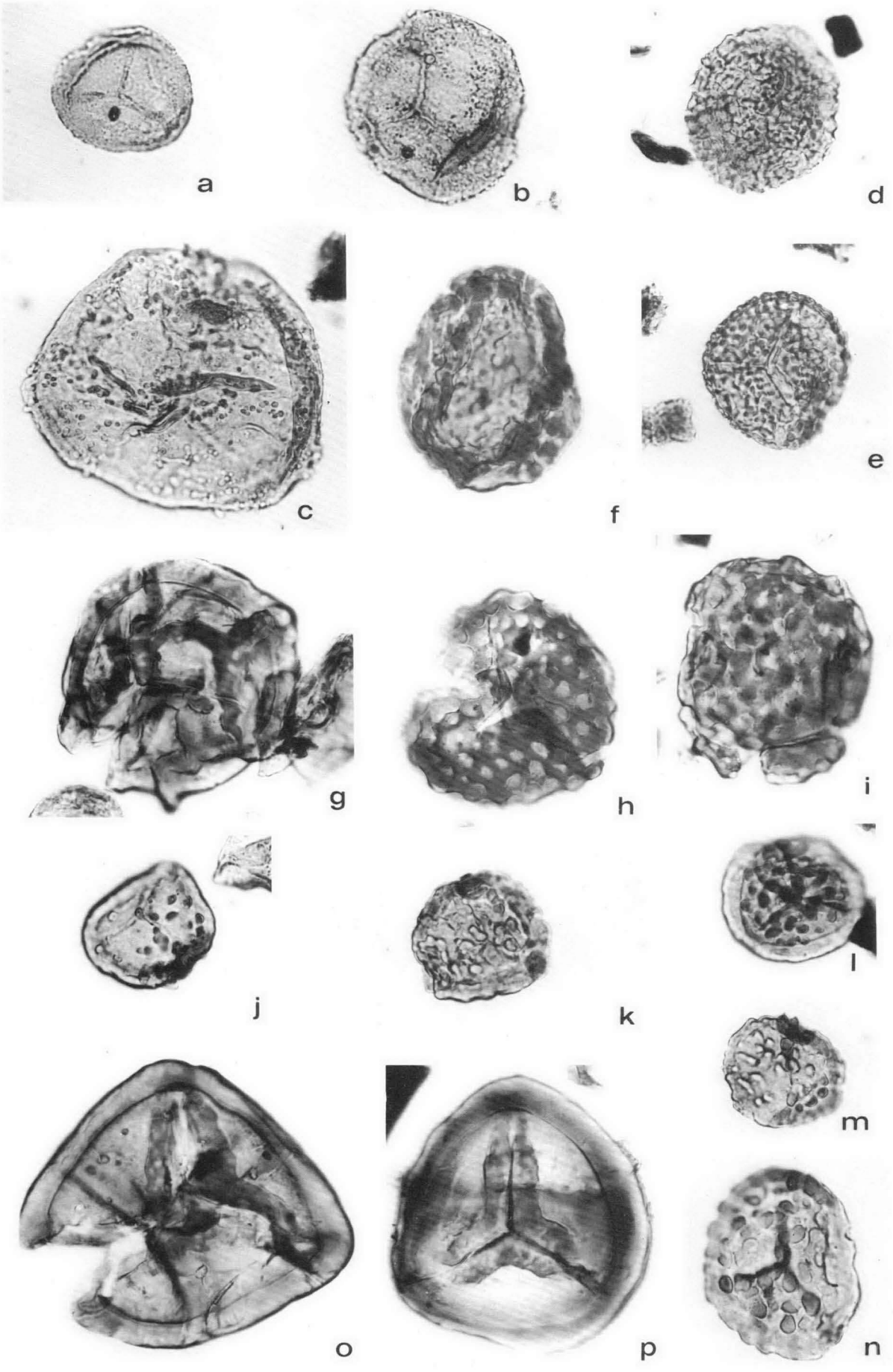
a
b
d
c
f
e
g
h
i
j
k
l
m
o
p
n

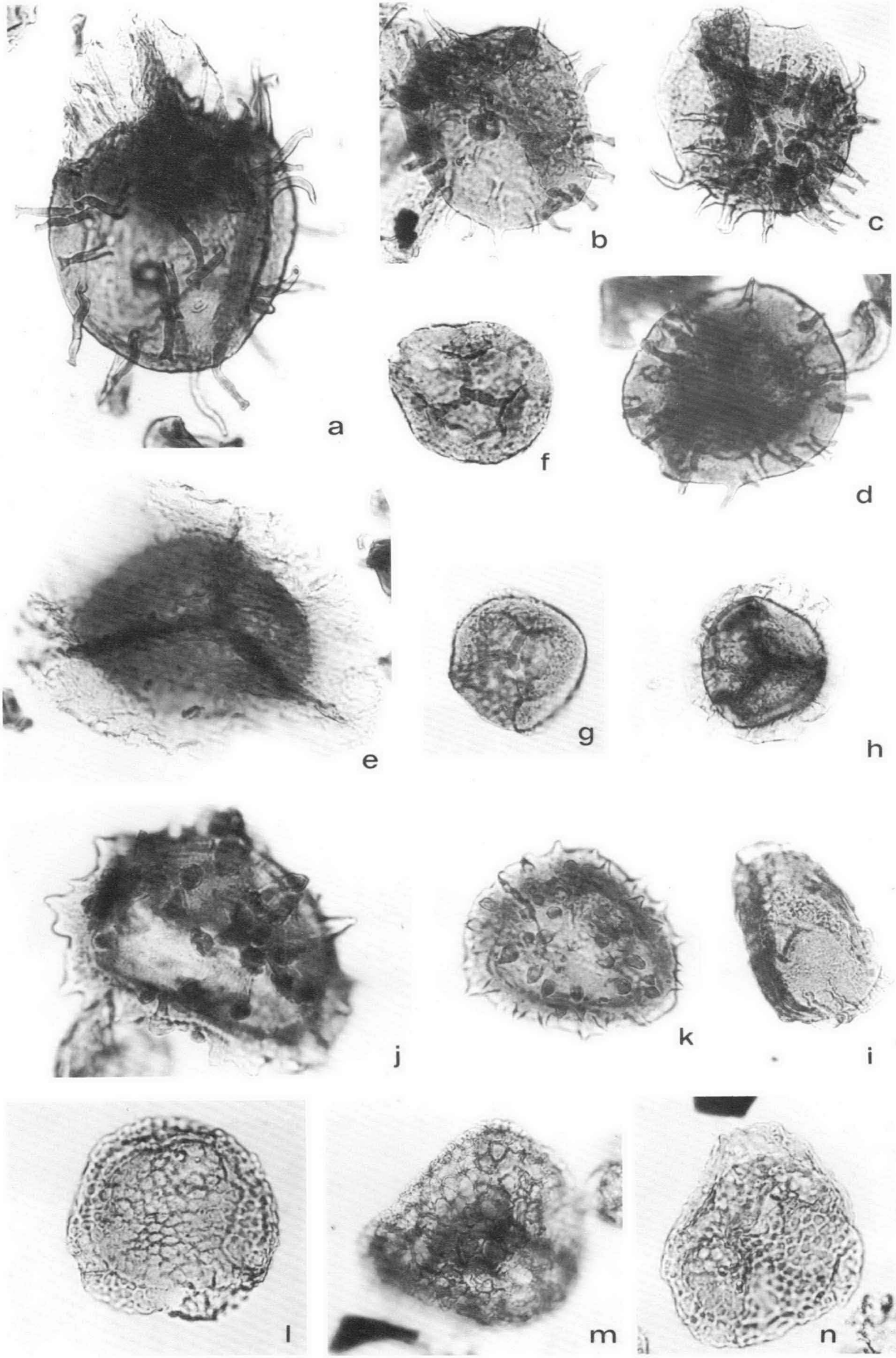
a
b
c
f
d
e
g
h
j
k
i
l
m
n

Druce, 1969, p. 19). Jones (1968) noted, however, that six species from his zonal sequence are also known to occur in the late Famennian of the northern Canning Basin.

From several horizons in the type section of the Buttons beds, Roberts (1971) recorded four species of articulate brachiopods, including *Cyrtospirifer ningbingensis* Roberts, 1971, the characteristic species of his *C. ningbingensis* Zone which he recognised throughout the major (Famennian) part of the Ningbing Limestone. Although he acceded to prior suggestions of an early Famennian dating for the Buttons beds, Roberts (1971, p. 14) pointed out that one of his new species, *Cyrtospirifer depressus* (from the Buttons beds in the Burt Range area), closely resembles two Russian species of probable latest Devonian age, and therefore implies 'a younger age than indicated by ostracods'.

In summary, therefore, the invertebrate and conodont evidence accrued thus far signifies a Late Devonian, and certainly post-Frasnian, age for the Buttons beds, but it cannot be taken as clearly indicative of either early Famennian or late Famennian-earliest Tournaisian.

Materials and methods

All samples examined in the present study were collected in 1978 by BMR officers (R. S. Nicoll, P. J. Jones) from the type section of the Buttons beds, in the vicinity of Buttons Crossing, about 3–6 km north of the Kimberley Research Station. As depicted in Figure 2, the type section extends along the east side of the Ord River, and the samples studied span virtually the full exposure, which accounts for some 350 m of strata, although, as mentioned earlier, the base of the unit is not exposed and its top is faulted. Nineteen samples from 17 horizons in the type section were processed for their palynomorph content. Of these, only three samples proved to contain plant microfossils, mainly spores, in moderate states of preservation. The remainder were barren in a palynological context, yielding only sparse, indeterminate organic matter.

Details of the palynologically productive samples are as follows: Sample 04/01A—medium grey, carbonaceous, calcareous siltstone; 131.1 m above exposed base; palynological preparation no. D526. Sample 05/42—light grey, silty limestone; 213.3–216.4 m above exposed base; palynological preparation no. D547. Sample 06/08—light grey, silty limestone; 289.6–292.6 m above exposed base; palynological preparation no. D546.

The nineteen samples were subjected to conventional laboratory procedures for the extraction and concentration of plant microfossils (e.g. Playford, 1971, pp. 9–10), although concentrated nitric acid (5–10 minutes treatment) was used as macerant rather than Schulze solution, and 0.5 per cent potassium hydroxide solution was the subsequent clearing agent. Heavy-liquid separation (zinc bromide solution, in carefully controlled steps, from S.G. 2.0 down to 1.5) was followed by fine screening (mesh size 170 μm) to achieve the optimum concentration of palynomorphs. Three strew slides and about 15 single-specimen slides were made from each productive residue, using glycerine jelly as mounting medium.

Slides were examined with a Zeiss Photomicroscope II (no. Mx3237 of the Department of Geology and Mineralogy, University of Queensland). Stage-coordinates for illustrated specimens (Figs. 3, 4) are from the mechanical stage of that instrument. The specimens are deposited permanently in the Commonwealth Palaeontological Collection maintained by the Bureau of Mineral Resources, Canberra. Registered specimen numbers (prefixed 'CPC') refer to the official catalogue of that collection.

Palynology

The three palyniferous samples contain assemblages that consist largely of trilete miospores with minor proportions (<2.5 per cent) of diminutive simple acritarchs, mainly of the *Micrhystridium* type, and in one case (sample 05/42) of scolecodont fragments. Quality of spore preservation was sufficient to permit confident identification to specific level; the most varied and abundant assemblage was obtained from sample 04/01A (20 species recognisable). The taxonomic composition of the spore floras is essentially similar in the three samples, 14 species being common to at least two samples (Table 1).

One of the commonly occurring forms, which has previously been recorded from the Canning Basin as '*Lophozonotriletes* sp. A' of Playford (1976), is formally instituted below as a new species. All other spore taxa could be identified as previously named species. *Retispora lepidophyta* (Kedo) Playford, 1976 is the most numerous (up to 10 per cent of miospore flora).

Systematic description

Genus *Lophozonotriletes* Naumova emend. R. Potonié 1958

Type species. *Lophozonotriletes lebedianensis* Naumova, 1953; by subsequent designation of Potonié (1958, p. 27).

Discussion. See Playford (1976, p. 28).

Figure 4. Miospores from the Buttons beds (type section), continued.
Magnification X500 unless otherwise indicated.
a–d—*Hystricosporites porrectus* (Balme & Hassell) Allen, 1965: **a**—equatorial aspect, sample 04/01A, prep. D526/3, 114.8 19.5, CPC 22165; **b**—distal focus, sample 04/01A, prep. D526/1, 100.0 22.9, CPC 22166; **c**—equatorial aspect (X250), sample 04/01A, prep. D526/4, 108.6 10.9, CPC 22167; **d**—median focus, sample 04/01A; prep. D526/2, 99.6 14.8, CPC 22168. **e**—*Cirratriradites impensus* Playford, 1976; median focus, sample 04/01A, prep. D526/1, 105.6 4.3, CPC 22169. **f, g**—*Diaphanospora depressa* (Balme & Hassell) Evans, 1970: **f**—proximal focus, sample 04/01A, prep. D526/2, 92.6 4.8, CPC 22170; **g**—proximal focus, sample 04/01A, prep. D526/12, 106.7 12.0, CPC 22171. **h**—*Diaphanospora riciniata* Balme & Hassell emend. Evans, 1970; median focus, sample 04/01A, prep. D526/2, 112.0 11.9, CPC 22172. **i**—*Diaphanospora perplexa* Balme & Hassell emend. Evans, 1970; median focus, sample 06/08, prep. D546/1, 94.6 5.5, CPC 22173. **j, k**—*Hymenozonotriletes scorpius* Balme & Hassell, 1962 emend. Playford, 1976: **j**—distal focus, sample 05/42, prep. D547/1, 105.2 3.6, CPC 22174; **k**—median focus, sample 04/01A, prep. D526/11, 105.5 14.2, CPC 22175. **l–n**—*Retispora lepidophyta* (Kedo) Playford, 1976: **l**—median focus (X750), sample 04/01A, prep. D526/2, 94.2 4.1, CPC 22176; **m**—distal focus, sample 05/42; prep. D547/1, 101.2 16.7, CPC 22177. **n**—distal focus (X750), sample 04/01A, prep. D526/1, 110.7 13.5, CPC 22178.

Table 1. Check list of palynological microfossils recorded from the three palynologically productive samples of the Buttons beds.

	Sample nos.			
	04/01A	*05/42*	*06/08*	*Illustrations*
Leiotriletes pulvereus Balme & Hassell, 1962	•			
Retusotriletes digressus Playford, 1976	•			
Granulatisporites frustulentus Balme & Hassell emend. Playford, 1971	•	•	•	Fig. 3a
Verrucosisporites nitidus (Naumova) Playford, 1964	•	•		
Apiculatisporis morbosus Balme & Hassell, 1962	•		•	Figs. 3b, c
Convolutispora fromensis Balme & Hassell, 1962	•			Figs. 3d, e
Camptotriletes balmei Playford, 1976	•			Fig. 3f
Reticulatisporites ancoralis Balme & Hassell, 1962	•	•		Fig. 3g
Brochotriletes textilis (Balme & Hassell) Playford, 1976	•	•		Figs. 3h, i
Knoxisporites literatus (Waltz) Playford, 1963	•		•	Figs. 3o, p
Lophozonotriletes varionodosus Playford sp. nov.	•	•	•	Figs. 3j–n
Hystricosporites porrectus (Balme & Hassell) Allen, 1965	•	•		Figs. 4a–d
Cirratriradites impensus Playford, 1976	•		•	Fig. 4e
Hymenozonotriletes scorpius Balme & Hassell emend. Playford, 1976	•	•	•	Figs. 4j, k
Auroraspora macra Sullivan, 1968	•			
Diaphanospora depressa (Balme & Hassell) Evans, 1970	•	•	•	Figs. 4f, g
Diaphanospora perplexa Balme & Hassell emend. Evans, 1970	•	•	•	Fig. 4i
Diaphanospora riciniata Balme & Hassell emend. Evans, 1970		•	•	Fig. 4h
Endosporites micromanifestus Hacquebard, 1957	•			
Grandispora clandestina Playford, 1976	•			
Retispora lepidophyta (Kedo) Playford, 1976	•	•	•	Figs. 4l–n
Acritarchs	•	•	•	
Scolecodonts		•		

Lophozonotriletes varionodosus sp. nov.
(Figs. 3j–n)

1976 *Lophozonotriletes* sp. A of Playford, pp. 30–31; pl. 5, fig. 9.

Diagnosis. Spores radial, trilete. Amb subcircular to roundly subtriangular; periphery gently, irregularly undulating. Laesurae distinct, more or less straight; simple or accompanied by very narrow lip development towards proximal pole; extending near or almost to cingulum's inner margin. Distal surface, including cingulum, conspicuously sculptured with verrucae that are somewhat variable in terms of shape, size, and spacing. Basal diameter of verrucae 2–11 μm (usually up to 6 μm), height 1.5–3.5 μm; basal outline varies from subcircular to irregularly rounded-elongate, tops from rounded to flattened. Verrucae mainly discrete (up to 10 μm apart), but sometimes coalescent basally in groups of 2, 3, or (rarely) 4. Proximal exine, and non-verrucate distal exine, laevigate to faintly scabrate.

Dimensions (15 specimens). Overall equatorial diameter 44 (56) 71 μm; diameter of spore cavity 33 (41) 60 μm.

Holotype. Preparation D526/10, 109.1 12.7, CPC 22162; Fig. 3n. Proximal aspect. Amb subcircular, equatorial diameter 45 μm overall, diameter of spore cavity 35 μm; narrowly lipped laesurae almost attain inner margin of cingulum; mainly discrete distal verrucae, 2–6 μm in basal diameter, 1.5–2 μm high, irregularly distributed (up to 6.5 μm apart); equatorial margin (of cingulum) irregularly undulant due to verrucate sculpture.

Type locality. Type section of Buttons beds, Ord River, Bonaparte Gulf Basin, Western Australia (see Fig. 2); sample 04/01A, 131.1 m above exposed base of section .

Name derivation. Lat., *vario*, to vary; *nodus*, swelling, knob.

Comparison. See Playford (1976, p. 31) for comparison with Russian Late Devonian/Tournaisian species described by Naumova (1953) and Kedo (1957, 1963).

Distribution. *Lophozonotriletes varionodosus* sp. nov. has been encountered in all three palyniferous samples of the Buttons beds examined herein (Table 1). It is known also from a latest Devonian sample of the Fairfield Group (i.e., Yellow Drum Sandstone), Canning Basin, Western Australia (Playford, 1976); and from the lower part of the Mount Eclipse Sandstone, Ngalia Basin, Northern Territory (Playford, unpubl. data).

Correlation and age of the palynoflora

All constituent miospore species of the Buttons beds palynoflora are known to occur in the lower part of the latest Devonian-Early Carboniferous Fairfield Group (i.e., Gumhole Formation and overlying Yellow Drum Sandstone: Druce & Radke, 1979) of the northern Canning Basin, Western Australia (see Balme & Hassell, 1962; Playford, 1976). Indeed, the majority of the species present have been reported as confined vertically to the lower Fairfield; while several (viz. *Granulatisporites frustulentus*, *Verrucosisporites nitidus*, *Convolutispora fromensis*, *Knoxisporites literatus*, *Diaphanospora* spp., and *Endosporites micromanifestus*) are known to extend into the younger part of the Fairfield Group (Laurel Formation). In terms of Playford's (1976) Fairfield assemblages, the Buttons beds palynoflora is unmistakably representative of the *Retispora lepidophyta* Assemblage. The latter occurs not only in the Gumhole Formation and Yellow Drum Sandstone, but has also been recovered from the lower part of the Mount Eclipse Sandstone of the Ngalia Basin, Northern Territory (Playford, unpubl. data), the lower part of the Gilberton Formation of the Georgetown Block, north Queensland (Foster & Playford, unpubl. data), and the Ravendale Formation of the Balcannia Trough, New South Wales (Evans, 1968; Roberts & others, 1972, p. 485).

Dating of the *Retispora lepidophyta* Assemblage has previously been discussed by Playford (1976, p. 55), who concluded that it is assignable to the latest Devonian, viz. latest Famennian, Fa2d, to Strunian (Etroeungt), Tnla, or early Tnlb, of Belgian terminology. This conclusion was based upon abundant published information that the widely reported, virtually ubiquitous, nominate taxon is confined vertically to the above-mentioned, immediately pre-Carboniferous interval (Fa2d–Tnla or early Tnlb); see, for instance, Streel (1974), McGregor (1979, p. 177, text-fig. 8). Moreover, the age assessment was consonant with microfaunal data from the Fairfield Group (see discussions by Playford, 1976, pp. 6–8, Druce & Radke, 1979, and references cited in both papers).

With respect to the distribution of *Retispora lepidophyta*, there have been some recent suggestions that its stratigraphic range might be somewhat less restricted than has hitherto been acknowledged. Firstly, it should be noted that several Russian palynologists (e.g. Raskatova, 1974; Kedo, 1974) have indicated intermittent and sparse representation of *R. lepidophyta* in older Famennian deposits, i.e. prior to the plenitude and consistency of occurrence of that species in latest Famennian-earliest Tournaisian strata.

Dr. P. J. Jones has courteously drawn the writer's attention to a paper by Chizhova & Bouckaert (1976), concerned primarily with a comparison of ostracod faunas in Devonian-Carboniferous boundary strata from Belgium and the Russian Platform. These authors (pp. 22–23) alluded to a publication by Nenastieva (1975), who had reported abundant representatives of *R. lepidophyta* (as '*Hymenozonotriletes lepidophytus*' and the varieties *minor* and *tener*) from the Zelenetsky 'Horizon' of the Timan-Pechora region in the north-eastern sector of European U.S.S.R. On palynological grounds, Sennova (1972) and Nenastieva (1975) correlated the Zelenetsky Horizon with the Kudeyarovsky and Ozersky Beds of the central Russian Platform, and with the Zavolzhsky Horizon of the Volga-Ural region, which are regarded as Fa2d–Tnla age equivalents (Reitlinger & others, 1979, fig. 1; McGregor, 1979, text-fig. 7). However, Chizhova & Bouckaert (1976) asserted that the ostracods and foraminiferids associated with Nenastieva's material favour an older age: specifically, early late Famennian (Fa2a$^{\beta}$–Fa2b), within the *Platyclymenia* (ammonoid) Zone. Reitlinger & others (1979, p. 33), following a detailed discussion of the lines of evidence available up to 1975, concluded that the question of the age of the Zelenetsky Horizon has yet to be resolved among Soviet palaeontologists, who date it variously 'as being equivalent to the *Platyclymenia*, *Gonioclymenia*, and/or basal *Wocklumeria* Zones, depending on the group of organisms on which the assessment is based'; i.e. within an age range of Fa2b–Fa2d (and possibly Tnla).

More recently, Dr. M. Streel (written communication, 18 January, 1982) has advised on his and Dr. T. V. Byvsheva's re-examination of Nenastieva's (1975) material. This confirmed Sennova's (1972) observations that 'true' *Retispora lepidophyta* makes its first appearance, not at the base of the Zelenetsky Horizon, but in the upper part of the lower ("*Entomozoe* beds") section of the Horizon. This assumes some importance in the light of the findings of Chizhova, Bouckaert, & others (1979) on conodont faunas from one of the boreholes (Vezhaiou 825) studied by Nenastieva (1975) and from another (Numylg 1) in the Timan-Pechora region. Bouckaert and his co-authors (p. 29) concluded that the lower portion of the Zelenetsky Horizon contains, successively, faunas of the *Palmatolepis marginifera* Zone, *Scaphignathus velifer* Zone, *Polygnathus styriacus* Zone, and of the lower and middle parts of the *Bispathodus costatus* Zone (see Fig. 5). Therefore, Chizhova, Bouckaert, & others (1979) considered that the *Entomozoe* beds correspond, in Belgian terminology, with the interval Fa2a–Fa2d (partly). Streel concluded his written communication by stating his belief that the introduction of *Retispora lepidophyta* postdates the middle *styriacus* Zone.

The upper stratigraphic limit of *R. lepidophyta* appears to be fully accepted as more or less coincident with the Devonian-Carboniferous boundary, notwithstanding current debate about the precise placement of that boundary and faunal criteria appropriate for its recognition (Paproth, 1980, p. 287; Van Veen, 1981, pp. 68–70). The latter author, however (p. 86), pointed to possible slight extension of the species into basal Carboniferous sediments in two sections of the Ardenno-Rhenish Basin.

From the above discussion, it seems clear that *R. lepidophyta* is abundantly characteristic of palynofloras of the latest Devonian (Fa2d to Tnla or early Tnlb), but that its introduction, in some regions at least, could well date from significantly earlier in the Famennian. There remains an obvious need for more adequate substantiation of these older occurrences (e.g. Raskatova, 1974) in terms of illustration/description of the spores and of associated, potentially age-definitive faunas (cf. Paproth & Streel, 1970; Sandberg & others, 1972; Becker & others, 1974).

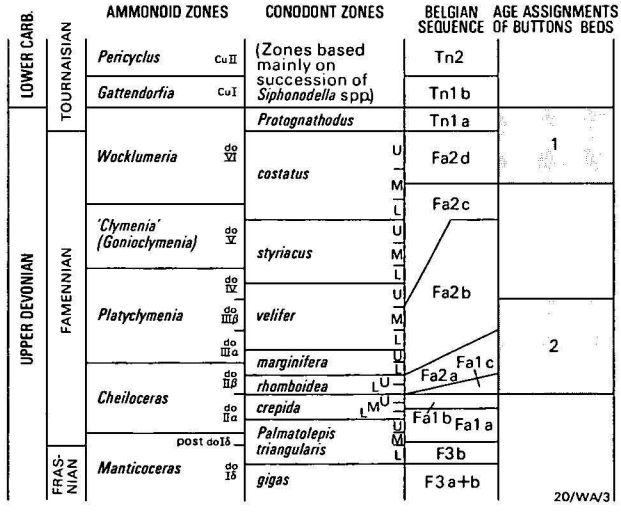

Figure 5. Chart showing disparate datings of the Buttons beds within the Late Devonian.

In extreme right-hand column, position 1 is based on palynological data presented herein; position 2 is based on palaeozoological data of previous authors as cited in text. Standard (European) subdivisions of the younger part of the Upper Devonian are adapted from Ziegler (1971, 1979) and House (1979); and of the initial part of the Lower Carboniferous from Ross (1979).

Taking into account the specific identity of the Buttons beds palynoflora with the faunally dated *Retispora lepidophyta* Assemblage of the lower Fairfield Group, as well as the above evaluation of the known distribution of *R. lepidophyta* itself, it seems reasonable to regard the subject palynoflora and its host sediments as latest Devonian in age. This is somewhat younger than the age proposed earlier on faunal grounds, although of course both assessments fall within the Famennian or at least the post-Frasnian Late Devonian interval (Fig. 5).

The stratigraphic implications of a latest Devonian dating are such as to:
(a) introduce a hiatus (disconformity), spanning much of the Famennian, between the Buttons beds and the underlying Jeremiah Member of the Famennian Cockatoo Formation;
(b) correlate the Buttons beds with the upper rather than the lower part of the Ningbing Limestone; and
(c) minimise or perhaps eliminate the supposed hiatus between the Buttons beds and the succeeding Early Carboniferous Burt Range Formation, as suggested, for instance, by Jones (1968, fig. 7) and Roberts & others (1972, correlation chart).

Acknowledgements

Drs. P. J. Jones and E. M. Truswell of the Bureau of Mineral Resources are thanked for the provision of samples and relevant stratigraphic data. Drs. Maurice Streel (Université de Liège, Belgium) and M. J. M. Bless (Naturhistorisch Museum, Maastricht, Netherlands) have been most helpful correspondents. Mrs. D. Phipps, of the Department of Geology and Mineralogy, University of Queensland, was responsible for palynological laboratory processing; and Misses P. Veness and R. Austin, of the same department, for typing of the manuscript. The research was undertaken with support from the Australian Research Grants Scheme.

References

BALME, B. E., & HASSELL, C. W., 1962—Upper Devonian spores from the Canning Basin, Western Australia. *Micropaleontology*, 8, 1-28.

BECKER, G., BLESS, M. J. M., STREEL, M., & THOREZ, J., 1974—Palynology and ostracode distribution in the Upper Devonian and basal Dinantian of Belgium and their dependence on sedimentary facies. *Mededelingen Rijks Geologische Dienst, Nieuwe Serie*, 25, 9-99.

CHIZHOVA, V., & BOUCKAERT, J., 1976—On correlation (Ostracoda) of Famennian and Tournaisian deposits of the French-Belgian Basin and the Russian Platform. *Service Géologique de Belgique, Preliminary Report*, 1-6-76, 18-32.

CHIZHOVA, V. A., BOUCKAERT, J., ALEKSEYEV, A. S., ARISTOV, V. A., BARSKOV, I. S., GAGIYEV, M. K., DREESEN, R., KONONOVA, L. I., LIPNYAGOV, O. M., OVNATANOVA, N. S., SIMAKOV, K. V., & KHALYMBADZHA, V. G., 1979—Correlation of Famennian and Tournaisian deposits of the U.S.S.R. and the French-Belgian Basin on conodonts. *Service Géologique de Belgique, Professional Paper* 5(161), 2-40.

DRUCE, E. C., 1969—Devonian and Carboniferous conodonts from the Bonaparte Gulf Basin, northwestern Australia, and their use in international correlation. *Bureau of Mineral Resources, Australia, Bulletin* 98.

DRUCE, E. C., & RADKE, B. M., 1979—The geology of the Fairfield Group, Canning Basin, Western Australia. *Bureau of Mineral Resources, Australia, Bulletin* 200.

EVANS, P. R., 1968—Upper Devonian and Lower Carboniferous miospores from the Mulga Downs Beds, N.S.W. *Australian Journal of Science*, 31, 45.

HILL, D., 1954—Coral faunas from the Silurian of New South Wales and the Devonian of Western Australia. *Bureau of Mineral Resources, Australia, Bulletin* 23.

HOUSE, M. R., 1979—Devonian in the eastern hemisphere. *In* ROBISON, R. A., & TEICHERT, C. (editors), Treatise on invertebrate paleontology, Part A. *Geological Society of America Incorporated & University of Kansas*, A183-A217.

JONES, P. J., 1968—Upper Devonian Ostracoda and Eridostraca from the Bonaparte Gulf Basin, northwestern Australia. *Bureau of Mineral Resources, Australia, Bulletin* 99.

JONES, P. J., & DRUCE, E. C., 1966—Intercontinental conodont correlation of the Palaeozoic sediments of the Bonaparte Gulf Basin, northwestern Australia. *Nature*, 211 (5047), 357-9.

KEDO, G. I., 1957—Spores from the Supra-salt Devonian deposits of the Pripyat Basin and their stratigraphic significance. *In* Palaeontology and biostratigraphy of BSSR, volume 2. *Akademiya Nauk Belorusskoy, Institut Geologicheskikh Nauk*, 3-43. (In Russian.)

KEDO, G. I., 1963—Spores of the Tournaisian stage of the Pripyat Basin and their stratigraphic significance. *In* Palaeontology and biostratigraphy of BSSR, volume 4. *Akademiya Nauk Belorusskoy, Institut Geologicheskikh Nauk*, 3-121. (In Russian.)

KEDO, G. I., 1974—The Devonian-Carboniferous boundary in the Pripyat Basin as revealed by palynological data. *In* Palynology of Proterophyte and Palaeophyte. *Nauka, Moscow*, 86-92. (In Russian.)

MCGREGOR, D. C., 1979—Spores in Devonian stratigraphical correlation. *Special Papers in Palaeontology*, 23, 163-84.

NAUMOVA, S. N., 1953—Spore-pollen assemblages of the Upper Devonian of the Russian Platform and their stratigraphic significance. *Akademiya Nauk SSSR, Trudy Instituta Geologicheskikh Nauk*, 143 (Geologicheskaya Seriya No. 60): 1-204. (In Russian.)

NENASTIEVA, V. E., 1975—Spore assemblages from the transitional Devonian-Carboniferous deposits of the Timan-Pechora province. *V kn: Geologia i poleznye iskopaemye Timano-Pechorii provintsii, Syktyvkar*, 61-7. (In Russian.)

PAPROTH, E., 1980—The Devonian-Carboniferous boundary. *Lethaia*, 13, 287.

PAPROTH, E., & STREEL, M., 1970—Corrélations biostratiraphiques près de la limite Dévonien/Carbonifère entre les faciès littoraux ardennais et les faciès bathyaux rhénans. *Les Congrès et Colloques de l'Université de Liège*, 55, 365-98.

PLAYFORD, G., 1971—Lower Carboniferous spores from the Bonaparte Gulf Basin, Western Australia and Northern Territory. *Bureau of Mineral Resources, Australia, Bulletin* 115.

PLAYFORD, G., 1976—Plant microfossils from the Upper Devonian and Lower Carboniferous of the Canning Basin, Western Australia. *Palaeontographica* (B), 158, 1-71.

PLAYFORD, P. E., COPE, R. N., COCKBAIN, A. E., LOW, G. H., & LOWRY, D. C., 1975—Phanerozoic. *In* The geology of Western Australia. *Geological Survey of Western Australia, Memoir* 2, 223-433.

POTONIÉ, R., 1958—Synopsis der Gattungen der Sporae dispersae. II. Teil: Sporites (Nachträge), Saccites, Aletes, Praecolpates, Polyplicates. Monocolpates. *Beihefte zum Geologischen Jahrbuch*, 31, 1-114.

RASKATOVA, L. G., 1974—A detailed stratigraphic subdivision of the Devonian of the Central Devonian Field in the light of palynological evidence. *In* Palynology of Proterophyte and Palaeophyte. *Nauka, Moscow*, 67-71. (In Russian.)

REITLINGER, E. A., SEMICHATOVA, S. V., BYVSHEVA, T. V., CHIZHOVA, V. A., KONONOVA, L. I., & LIPINA, O. A., 1979—The Devonian-Carboniferous boundary in the U.S.S.R. *In* WAGNER, R. H., HIGGINS, A. C., & MEYEN, S. V. (editors), The Carboniferous of the U.S.S.R. *Yorkshire Geological Society, Occasional Publication* 4, 23-42.

ROBERTS, J., 1971—Devonian and Carboniferous brachiopods from the Bonaparte Gulf Basin, northwestern Australia. *Bureau of Mineral Resources, Australia, Bulletin* 122.

ROBERTS, J., JONES, P. J., & DRUCE, E. C., 1967—Palaeontology and correlations of the Upper Devonian of the Bonaparte Gulf Basin, Western Australia and Northern Territory. *In* OSWALD, D. H. (editor), International symposium on the Devonian System. *Alberta Society of Petroleum Geologists, Calgary,* 2, 565-77.

ROBERTS, J., JONES, P. J., JELL, J. S., JENKINS, T. B. H., MARSDEN, M. A. H., MCKELLAR, R. G., MCKELVEY, B. C., & SEDDON, G., 1972—Correlation of the Upper Devonian rocks of Australia. *Journal of the Geological Society of Australia,* 18, 467-90.

ROSS, C. A., 1979—Carboniferous. *In* ROBISON, R. A., & TEICHERT, C. (editors), Treatise on invertebrate paleontology, Part A. *Geological Society of America Incorporated & University of Kansas,* A254-90.

SANDBERG, C. A., STREEL, M., & SCOTT, R. A., 1972—Comparison between conodont zonation and spore assemblages at the Devonian-Carboniferous boundary in the western and central United States and in Europe. *Septième Congrès International de Stratigraphie et de Géologie du Carbonifère, Krefeld 1971, Compte Rendu,* 1, 179-203.

SENNOVA, V. E., 1972—Upper Devonian spore-pollen assemblages of the Timan-Pechora province. *V kn: Geologia i neftegazonosnost Severovostoka Evropeiskoy chasti SSSR,* 11, 99-107.

STREEL, M., 1974—Similitudes des assemblages de spores d'Europe, d'Afrique du Nord et d'Amérique du Nord au Dévonien terminal. *Sciences Géologiques, Bulletin,* 27, 25-38.

VAN VEEN, P. M., 1981—Aspects of Late Devonian and Early Carboniferous palynology of southern Ireland. V. The change in composition of palynological assemblages at the Devonian-Carboniferous boundary. *Review of Palaeobotany and Palynology,* 34, 67-97.

VEEVERS, J. J., 1970—Upper Devonian and Lower Carboniferous calcareous algae and stromatolites from the Bonaparte Gulf Basin, northwestern Australia. *Bureau of Mineral Resources, Australia, Bulletin* 116, 173-88.

VEEVERS, J. J., & ROBERTS, J., 1968—Upper Palaeozoic rocks, Bonaparte Gulf Basin of northwestern Australia. *Bureau of Mineral Resources, Australia, Bulletin* 97.

ZIEGLER, W., 1971—Conodont stratigraphy of the European Devonian. *In* SWEET, W. C., & BERGSTRÖM, S. M. (editors), Symposium on conodont biostratigraphy. *Geological Society of America Memoir,* 127, 227-84.

ZIEGLER, W., 1979—Historical subdivisions of the Devonian. *Special Papers in Palaeontology,* 23, 23-47.

BMR Journal of Australian Geology & Geophysics, 7, 159–180

EVALUATION OF GOSSANS IN RELATION TO LEAD-ZINC MINERALISATION IN THE MOUNT ISA INLIER, QUEENSLAND

Graham F. Taylor[1] & Keith M. Scott[1]

Structural, textural, mineralogical, and geochemical properties of gossans associated with lead-zinc mineralisation in the Carpentarian Mount Isa Inlier of northwest Queensland have been studied. Mineralisation at Mount Isa, Hilton, and Lady Loretta is associated with abundant stratiform pyrite, which, upon oxidation, has formed prominent gossanous ridges at each deposit. The gossans, which have a laminated structure and occasional boxworks and casts after pyrite, generally carry only minor to trace levels of target and pathfinder elements. Where orebodies were close to the surface, cerussite and other secondary lead minerals are abundant, but Zn and Ag have been substantially leached from surface gossans. Immature gossans are found on the Dugald River and Pegmont deposits, both of which have low iron sulphide contents and a partially truncated profile. At Dugald River, the normally mobile elements (e.g. K, S, Zn, Cu, Cd, Tl) have been retained because of reaction between acid solutions and carbonate-rich wall rocks. The Pegmont mineralisation occurs in a quartz-magnetite-garnet-apatite banded iron formation, which, on oxidation, has given rise to a Mn-, Pb-, and Zn-rich gossan with abundant plumbogummite, pyromorphite, and coronadite. Gossans and ironstones from elsewhere within the Paradise Creek Formation, Soldiers Cap Group, Mount Isa Group, and Answer Slate often have similar laminated structures and mineralogy, but their variable geochemical signatures make direct comparison with other deposits difficult. Various statistical techniques have been used to evaluate these geochemical data in relation to gossans and ironstones of known association from throughout the Mount Isa Inlier. Although reflecting some known mineralogical and elemental associations, neither correlation coefficients nor R-mode factor analysis are of use in assigning group membership, because of the diverse geochemical characteristics of the ferruginous outcrops. Stepwise discriminant analysis using Pb, P, Ba, As, Zn, Mn, Co, S, and Sb was found to classify all gossans and ironstones into six geologically distinct groups.

Introduction

In the Mount Isa Inlier, as in other areas of Australia, the ability to distinguish gossans associated with economic base-metal mineralisation from those on 'barren' pyrite-pyrrhotite bodies and other numerous ironstone outcrops is important in mineral exploration. The pioneering work of R. Blanchard during 1930–1945 (Blanchard, 1968) relied heavily on textural observations, although he did attempt to rationalise the geochemistry of typical 'limonites' (Blanchard, 1944). A similar study of oxidised Mount Isa ore was made by Grondijs & Schouten (1937). A number of papers have addressed the characterisation of gossans and understanding of the weathered profile above base-metal mineralisation in the Mount Isa Inlier: Zimmerman (1964), Smith (1965), Derrick (1972), Green & others (1972), Glasson (1973), Taylor (1973), Bampton & others (1977), Scott & Taylor (1977), Taylor (1979), Hunter (1980), Orridge (1980), Nisbet & Joyce (1980), Rossiter (1980), Taylor & Appleyard (in press), Taylor & Scott (in press). In addition, many important contributions made by company geologists and consultants are contained in unpublished reports.

In 1973, the CSIRO Division of Mineralogy embarked on a program to determine mineralogical and geochemical features that could be used in the evaluation of gossans and ironstones in the Mount Isa Inlier. This paper reports the results of such studies of gossans associated with, and ironstones possibly related to, the various types of lead-zinc mineralisation. Initially, the data are considered in relation to the mineralogy and geochemistry of the fresh sulphides, the nature of gangue and wall rocks, and the weathering history. Statistical techiques are then evaluated to determine the possibility of characterising the gossans and ironstones from the geochemical data.

[1] CSIRO Division of Mineralogy, P.O. Box 136, North Ryde, NSW 2113

Geology and physical features of the Mount Isa Inlier

Significant lead-zinc(-silver) mineralisation occurs at three stratigraphic levels in the Mount Isa Inlier (Plumb & others, 1980, Fig. 1). The youngest deposits occur in the western succession within Upper Carpentarian carbonaceous and dolomitic shales of the Mount Isa Group (particularly the Urquhart Shale) and in the stratigraphically equivalent Paradise Creek Formation of the McNamara Group. In the eastern succession, Dugald River and prospects within the Answer Slate occur in similar slate-shales of the Mary Kathleen Group, but are stratigraphically lower. The oldest mineralisation also occurs in the eastern succession, within the Lower Carpentarian Soldiers Cap Group, and exhibits the highest grade regional metamorphism and greatest volcanic contribution in its host rocks. Carbonate-hosted galena mineralisation occurs in the Lawn Hill Formation, but is not considered here as it forms iron-poor outcrop.

The rocks of the Mount Isa Inlier occur as an immaturely dissected undulating plateau, 300–500 m above sea level. Twidale (1956) recognised three erosional surfaces, (a) pre-middle Mesozoic, (b) early to middle Tertiary, and (c) late Tertiary-Quaternary, all of which are believed to have been peneplains. The pre-middle Mesozoic surface is obvious in many parts of the region as iron-stained capping on plateau remnants and mesas, with large caves formed at the base. Lateritisation occurred during the early to middle Tertiary period, and lateritic rubble currently forms the surface in many low-lying areas.

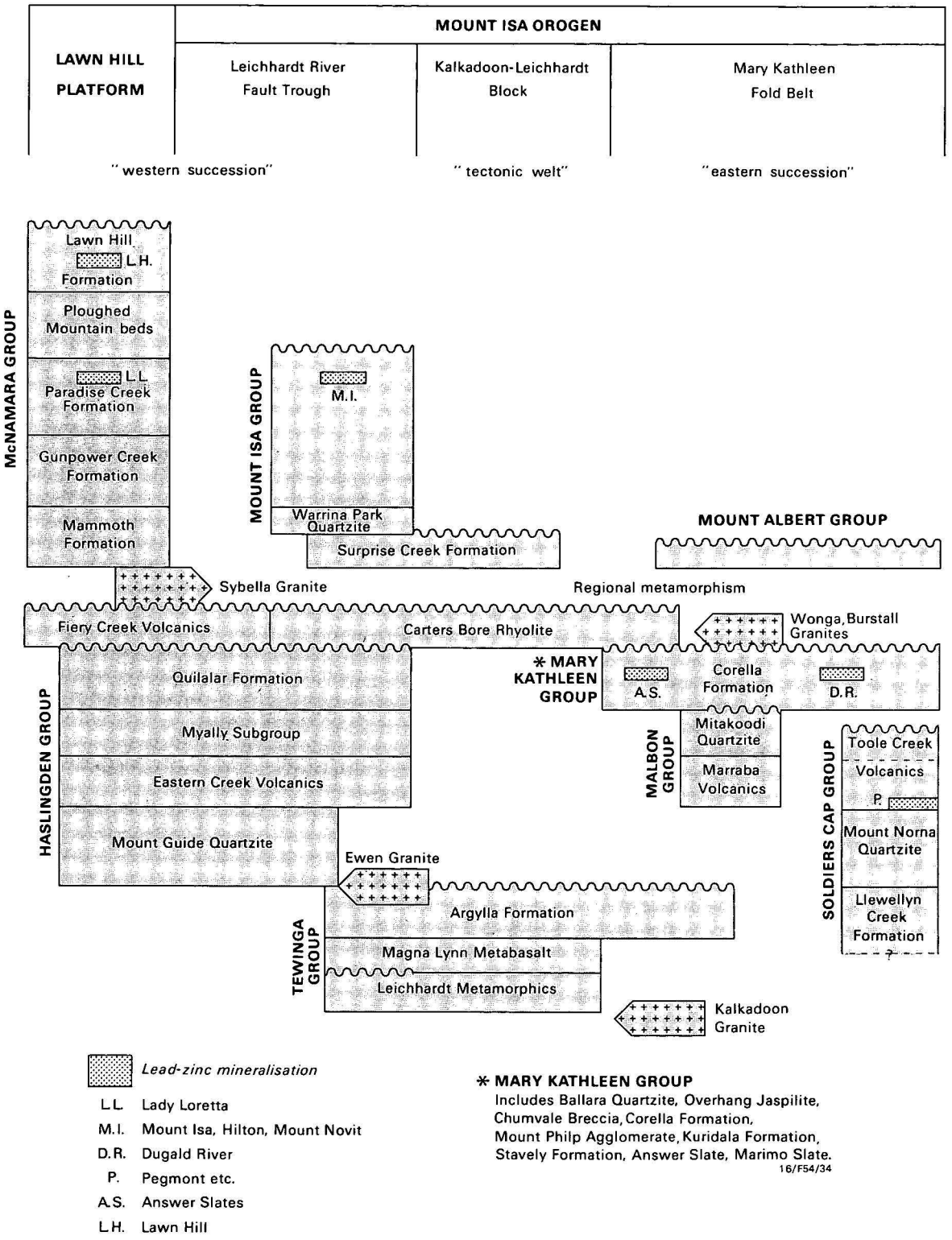

Figure 1. Stratigraphic correlation chart of the Mount Isa Inlier, showing approximate stratigraphic locations of lead-zinc(-silver) mineralisation.
After Plumb & others, 1980.

Detailed landforms can be attributed to the lithology and structure of the Proterozoic rocks. Thus, the central Kalkadoon-Leichhardt acid igneous complex ('tectonic welt' of Fig. 2) is represented by rough boulder-strewn surfaces; in the western succession dolomites and basaltic lavas generally produce low relief, and valleys with extensive alluvium form in shales and slates; and the calc-silicates of the highly folded, metamorphosed, and metasomatised eastern succession often form prominent outcrops, giving a very rough land surface. Quartzites form areas of greatest relief with deeply incised valleys.

Climate is tropical, with moderate rainfall (680 mm) to the north and low rainfall (300 mm) to the south, principally as summer storms. Average maximum daily

temperatures are high (> 30°C) with greatest diurnal and seasonal extremes in the south. Evaporation (~3700 mm) is much greater than precipitation, suggesting that there is an upward as well as downward movement of water in the weathered zone. Depth of complete weathering is highly variable: greater than 100 m in some areas of fracturing and faulting, to less than 20 m in areas of low relief. The base of complete oxidation closely corresponds to the standing water depth, except where mining activities have lowered the water table.

Samples and methods

Gossans associated with known lead-zinc mineralisation at Mount Isa, Hilton, Mount Novit, Lady Loretta, Dugald River, Pegmont, and Fairmile were sampled, as were weathered ironstone outcrops in the Lake Moondarra area and the Paradise Creek Formation at Goat Creek, six prospects within the Answer Slate, and eight prospects in the Squirrel Hills group (Fig. 2). Generally, sampling of the ferruginous outcrops and wall rocks was along traverses, but at some locations, representative grab samples were taken. In addition, sulphides from diamond-drill core or hand specimens from a majority of the deposits and prospects have been analysed.

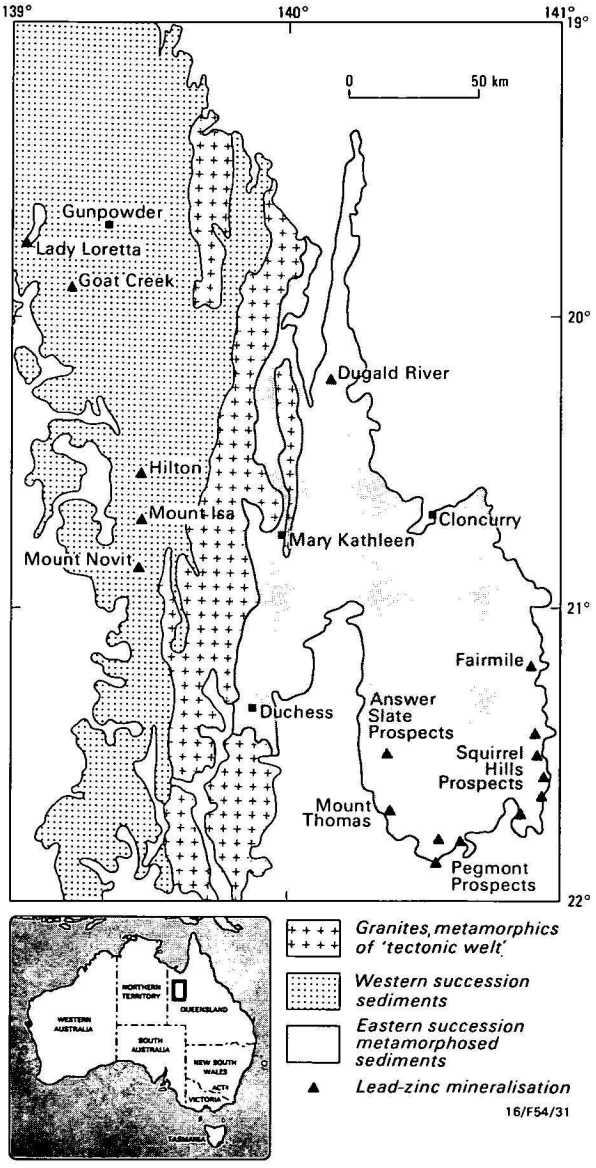

Figure 2. Proterozoic (Carpentarian) outcrop of the Mount Isa Inlier, showing lead-zinc deposits and prospects sampled in this study.

Samples were cut to give a slab for photography and optical microscopic examination, a polished petrographic mount for electron optical techniques, and a piece for curating. At least 200 g of each sample was crushed and ground to −75 μm for X-ray powder diffractometry and chemical analysis. Major elements, S, As, Ba, Bi, Co, Cr, Pb, Sb, Sn, Sr were determined by X-ray fluorescence spectrometry; Cu, Pb, Zn and Ag by atomic absorption spectrometry after total digestion; and Ag, Bi, Cd, Ga, Ge, In, Mo, Sb, Sn and Tl by semi-quantitative emission spectroscopy. Sulphides separated from diamond drill core and hand specimens by froth flotation or by use of a small dental drill were similarly analysed.

Gossan and ironstone descriptions

In this section, the geology, type of mineralisation, and weathering at each deposit and prospect are briefly described. These are summarised in Table 1, together with a landform classification based on the hierarchical system (Table 2) of Butt & Smith (1980). The texture, structure, mineralogy, and geochemistry of gossans, ironstones and any primary mineralisation are also described, with geochemical data presented as average values for the sake of simplicity. Mean values and ranges for each area are shown in Figure 3 and more detailed geochemical and mineralogical data are in reports and publications available at the CSIRO Division of Mineralogy, North Ryde, NSW.

Mount Isa

Stratiform lead-zinc-silver mineralisation occurs within the pyritic, tuffaceous middle part of the Urquhart Shale unit of the Mount Isa Group (Mathias & Clark, 1975). Gossanous outcrop, which occurs as a ridge up to 30 m above the surrounding plain, is generally related to the pyritic envelope about the orebodies, with the Nos. 1 and 2 orebodies having an extensive outcrop in the Black Star open pits at the northern end of the mine, and small outcrops of Nos. 6, 7, 11, 11/30, 11/60, and 12 orebodies occurring further to the south at Rio Grande (Smith, 1965). Complete oxidation extends to a depth of about 60 m and partial oxidation another 10–20 m. Mine drainage has caused the water table to fall from the original depth of 50 m, while surface outcrop has been altered by excavations for mine operations and buildings, with consequent contamination.

The distribution of Ag, Pb, and Zn through the weathered profile is described by Smith (1965). Whereas Ag is thoroughly leached to 30 m and Zn to 45 m, Pb is converted to secondary minerals and concentrated at the surface. Secondary Ag and Zn minerals occur in a transition zone lower in the profile. Samples from towards the base of complete oxidation in the Black Star open-cut, representing weathered, slightly cupriferous (~0.5% Cu) lead-zinc-silver mineralisation of Nos. 1 and 2 orebodies, are composed of quartz + goethite ± hematite +

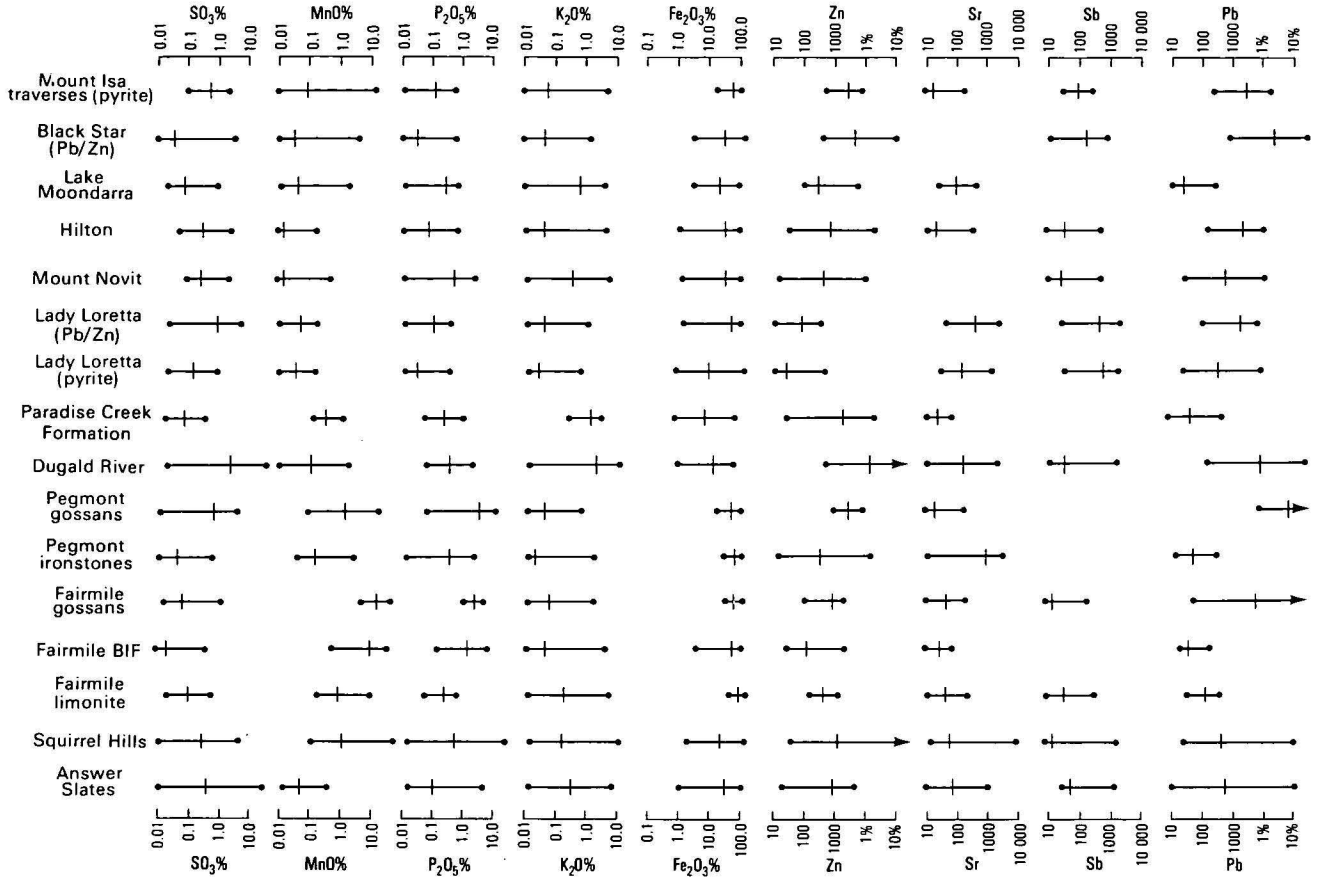

Figure 3. Ranges and geometric means for major and trace elements in gossans and ironstones from deposits and prospects in the Mount Isa Inlier.
Values in ppm unless indicated otherwise.

Table 1. Summary of location, type of mineralisation, nature of host rocks, depth of weathering, landform situation, type and number of samples of deposits and prospects used in this study.

Deposit/prospect	*Mineralisation*	*Host rock/gangue*	*Depth of weathering (m)*	*Landform situation (Butt & Smith, 1980)*	*Sampling technique*	*No. of samples* classified (Table 12)*
Black Star	gn-sph-(cpy)-py-po	qtz-dol-feld-ser(chl)	60	E1	Grab	19
Rio Grande BSD Bernborough	py-po-gn-sph-(cpy)	qtz-dol-feld-ser(chl)	60	E1	Traverses	37
Hilton	gn-sph-(cpy)-py-po	qtz-dol-feld-ser(chl)	?60	D1/E1	Traverses	38
Lady Loretta	sph-gn-py-bar	qtz-sid-dol-ser(chl)	100–150	E1	Grab	32
Dugald River	sph-gn-py-po	qtz-feld-cal-dol-ser-chl	20–35	E1	Traverses	27
Pegmont	gn-(sph)-py	qtz-mag-ap-gnt-ol-amp	50	D1/D2	Grab	52
Fairmile	gn-(sph)-py	qtz-mag-ap-gnt	<100	E1	Traverses	53
	py	qtz-ser-chl	<100	E2	Grab	5
Mount Novit	py-po-sph-gn	qtz-feld-dol-sid-mag-ser-chl	?60	E1	Traverses	44
Lake Moondarra	(?py)	qtz-feld-cal-sid-dol-ser-chl	?60–80	D2	Grab	16
Paradise Creek Fm	(py)	qtz-dol-cal-feld-ser-chl	50–60	D1/D2	Grab	13
Answer Slate	py-po-(gn)-sph-(cpy)	qtz-sid-cal-feld-dol-(fl)	?40	A1/A2	Traverses	58
Squirrel Hills	(gn)-(sph)-(cpy)-py-po	feld-qtz-amp-pyrox qtz-mag-ap-gnt-ol	30	D1/D2	Grab	52

Abbreviations: gn — galena; sph — sphalerite; cpy — chalcopyrite; py — pyrite; po — pyrrhotite; qtz — quartz; mag — magnetite; bar — barite; sid — siderite; dol — dolomite; ser — sericite; chl — chlorite; ap — apatite; gnt — garnet; cal — calcite; ol — olivine; feld — feldspar; amp — amphibole; pyrox — pyroxene; fl — fluorite

* This number of samples is generally greater than that shown in subsequent tables as some ferruginised wall rock samples are included.

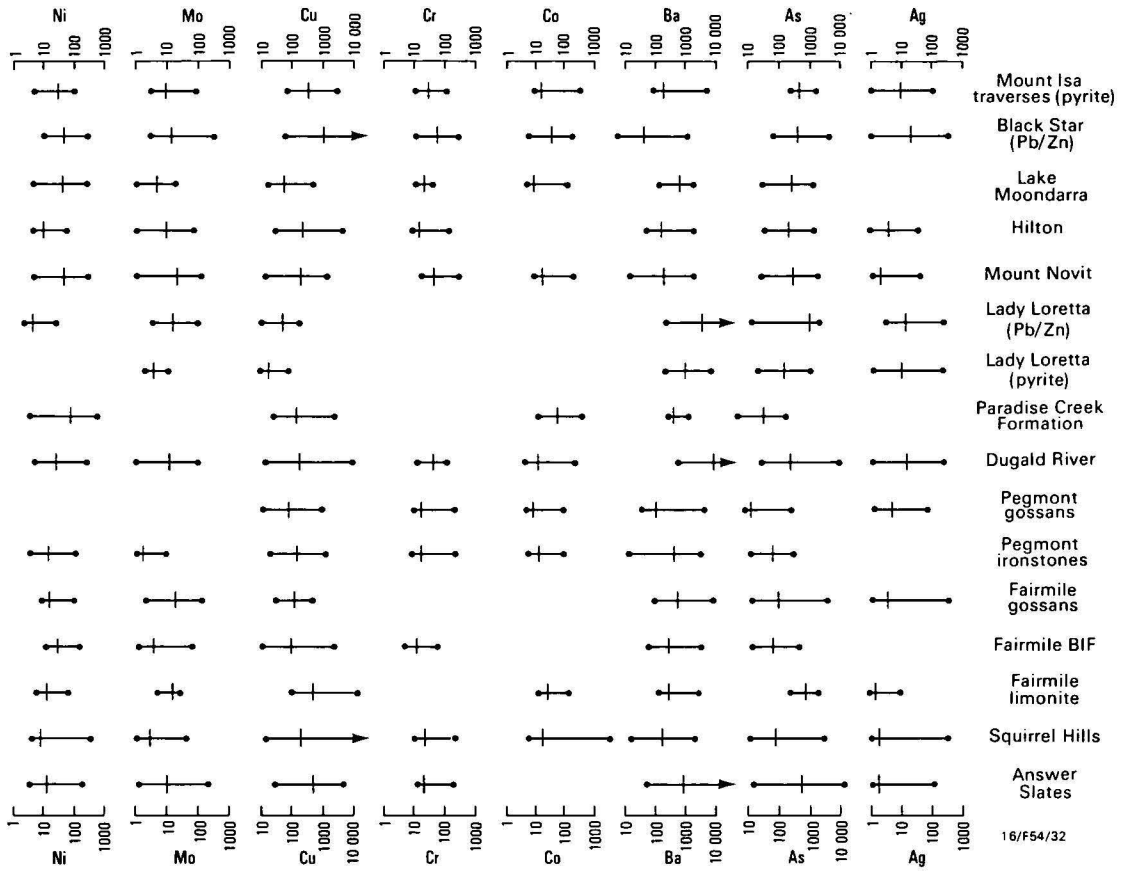

Table 2. Hierarchical classification of gossans and ironstones, based on landform situation and type of overburden (after Butt & Smith, 1980).

Weathering profile	*Landform situation*	*Type of overburden*	*Model*
Complete weathering profile	A, Low relief	None	A1
		In situ	A2
		Transported	A3
	B, Moderate relief	None	B1
		In situ	B2
		Transported	B3
	C, High relief	(May not exist)	
Partly stripped profile	D, Low relief	None	D1
		In situ	D2
		Transported	D3
	E, Moderate relief	None	E1
		In situ	E2
		Transported	E3
	F, High relief	None	F1
		In situ	F2
		Transported	F3
Bedrock fresh	G, Low relief	None	G1
		In situ	G2
		Transported	G3
	H, Moderate relief	None	H1
		In situ	H2
		Transported	G3
	I, High relief	None	I1
		In situ	I2
		Transported	I3

sericite + kaolinite ± cerussite ± secondary Pb minerals of the alunite-jarosite series*, and minor rosasite $(Cu,Zn)_2CO_3(OH)_2$, anglesite, coronadite and hemimorphite. In many of these samples the original finely bedded, often contorted and crenulated structure is retained (Fig. 4), with colloform iron oxides, sparry cerussite and euhedral quartz occurring in voids and partings. Other samples are sponge-like or cavernous masses of secondary limonite, cerussite, jarosite, and quartz, sometimes silicified or ferruginised, and represent solution deposition, possibly within solution cavities in the dolomitic shales. In both cases, boxworks or pseudomorphs after sulphides are extremely rare.

Trace elements associated with the most common sulphide minerals at Mount Isa are: Ag, Ba, Sb, Tl, and Zn with galena, Cd and In with sphalerite, As, Mo, and Tl with pyrite, and Mo with pyrrhotite (Scott & Taylor, 1979a). Except for Ba, In, and Tl, these elements also occur in the weathered subcrop at Black Star (Table 3). Concentrations of the trace elements in subcrop at Black Star are generally greater than in the surface gossans from Rio Grande, showing that highest concentrations of many trace elements occur lower in the gossan profile.

* These minerals have the general formula $AM_3(XO_4)_2(OH)_6$ where A = K, Na, Pb, Ba, Ca, Sr; M = Fe, Al; and XO_4 = SO_4, PO_4, AsO_4

Table 3. Average compositions of gossans from Mount Isa and Hilton: majors in wt%; traces in ppm.

	Mount Isa										
	Black Star			*BSD traverse*				*Bernborough traverse*			
	North	*South*	*Rio Grande*	*East slope*	*Crest*	*West slope*	*West flat*	*East flat*	*East slope*	*Crest*	*West slope*
No. of samples	6	11	5	6	3	5	4	2	5	3	4
	Subcrop		Outcrop	Outcrop				Outcrop			
Fe_2O_3	48.3	38.2	63.8	60.2	27.1	51.8	52.4	43.5	50.2	55.9	65.2
K_2O	0.05	0.21	0.01	0.40	0.06	0.02	0.40	2.85	1.22	0.01	0.26
P_2O_5	0.15	0.05	0.17	0.10	0.10	0.15	0.10	0.43	0.32	0.15	0.27
MnO	0.02	0.07	0.05	1.52	0.26	0.02	4.34	0.05	0.07	0.01	0.02
SO_3	0.25	0.19	0.42	0.41	0.36	0.47	0.37	0.65	0.34	0.26	1.03
Ag	14	41	5	17	8	4	43	4	15	28	23
As	1 190	410	1 010	390	230	440	340	910	560	590	500
Ba	56	48	35	1 750	330	220	1 250	490	150	20	96
Bi	1	1	<1	<1	<1	<1	<1	<1	<1	<1	<1
Cd	15	22	13	17	<3	4	18	<3	<3	<3	<3
Co	51	53	19	47	47	7	150	10	13	6	8
Cr	52	85	36	45	30	30	29	60	39	25	30
Cu	1 280	1 130	1 260	180	300	360	930	940	310	130	250
Ga	9	7	4	15	3	4	2	8	6	1	11
Ge	16	16	8	6	4	4	5	9	8	9	28
In	<1	<1	<1	<1	<1	<1	<1	<1	<1	<1	<1
Mo	8	77	33	9	10	19	8	11	10	10	8
Ni	62	100	30	24	57	34	48	80	36	37	20
Pb	22 200	94 300	5 200	1 180	1 950	1 440	10 900	480	4 590	5 780	12 600
Sb	140	340	140	85	70	88	93	40	69	130	170
Sn	1	1	<1	<1	<1	<1	<1	<1	1	<1	1
Sr	16	<5	5	43	52	56	8	210	29	<5	14
Tl	<1	<1	<1	<1	<1	<1	<1	<1	<1	<1	<1
Zn	4 400	8 100	2 890	2 200	1 800	2 300	3 900	2 650	4 980	4 600	4 140

Figure 4. Oxidised and partially leached lead-zinc-silver ore from Black Star open-cut, Mount Isa.
Composed essentially of iron oxides, cerussite and quartz, and retains original contorted and crenulated fine laminations of ore (13 cm across).

Surface ironstones from the southern end of the mine (BSD and Bernborough areas) are generally weathered pyritic shale that has been silicified or ferruginised with colloform limonite, manganese oxides, euhedral quartz, kaolinite, and alunite-jarosite forming in voids and partings. Some boxworks and pseudomorphs after pyrite are obvious, but derivation from massive sulphides is more commonly indicated by distinctive patches of hematite.

Each traverse across the main gossan ridge has been subdivided (Table 3) to show the effect of relief upon trace element distribution. The samples are gossans after the pyritic envelope that enclosed the lead-zinc mineralisation, and carry concentrations of both target and pathfinder elements (see Butt & Smith, 1980, for definitions). High concentrations of K_2O, Ba, and Sr reflect, in part, derivation from dolomitic shales. There is a strong tendency for the crests of the ridges to have lower target and pathfinder element contents, presumably as a result of hydromorphic dispersion. In the BSD traverse highest concentrations of target and pathfinder elements (except As) occur to the west, possibly reflecting higher trace element content of hangingwall pyrite. At Bernborough this is also true, except for Cu, Co, and Ni, which are higher in the footwall sequence, reflecting the leakage of Cu from the 1100 orebody (R. E. Russell & C. W. Robertson, personal communication, 1979).

The high target and pathfinder element contents of all gossans in the Mount Isa field reflect the lower mobility of these elements in an environment where acid solutions are buffered by carbonate in the wall rocks. However, because of the high iron sulphide content, these gossans do not exhibit the same immaturity as those at Dugald River (see below).

Hilton

The geology and mineralisation at Hilton are similar to that at Mount Isa (Mathias & Clark, 1975). Again, the gossans, occurring as seven isolated hills, represent

Hilton			Tombstone Hill		
13 Mile Hill	*Offset Hill*	*Handlebar Hill*	*East flat*	*East slope*	*West slope*
9	5	8	3	3	6
Outcrop					
25.7	51.6	24.9	64.1	48.8	45.5
0.05	0.48	0.22	0.01	0.02	0.02
<0.01	0.44	0.19	0.08	0.15	0.12
0.03	0.04	0.02	0.12	0.07	0.02
0.20	0.30	0.22	0.29	0.46	0.41
4	4	6	1	8	10
240	200	180	450	760	420
180	1 230	190	110	68	100
<1	<1	<1	1	1	<1
<3	<3	<3	<3	<3	<3
<10	<10	<10	10	50	10
29	15	20	10	15	15
120	320	800	800	900	360
6	6	5	<1	<1	<1
33	24	13	7	17	9
<1	<1	<1	<1	<1	<1
7	5	9	27	33	13
4	6	4	27	30	33
880	3 980	3 800	3 500	6 700	5 800
30	160	30	<30	<30	13
2	<1	<1	<1	<1	<1
35	90	40	6	16	8
4	<1	<1	<1	<1	<1
300	7 740	1 450	3 680	1 460	320

the pyritic envelope enclosing the lead-zinc mineralisation, the weathered portions of which are exposed only in costeans.

Of the two surface ironstone types recognised by Zimmerman (1964), the 'massive rounded, siliceous jaspers' represent variously silicified and ferruginised, often leached, contorted or disrupted Urquhart Shale, while the 'cavernous, earthy, iron-rich crust' is as a result of iron being deposited from solution. A third type, 'fine laminae and veins of limonitic material in silicified and leached shale' (Mathias & others, 1973) generally occurs in the wall rocks. These authors noted that the ironstones are strictly a surface feature, which suggests that the ferruginisation may be an accumulation of remnant Fe after leaching and erosion during lateritisation, which would make these outcrops unique in the Mount Isa Inlier.

Boxworks and pits are rare, although patches and veins of massive hematite are probably after pyrite. Other minerals present are quartz, goethite, and variable jarosite with minor kaolinite, feldspar, sericite, and chlorite. Those samples from costeans have abundant secondary lead minerals—cerussite, anglesite, and Pb-bearing alunite-jarosite minerals.

Geochemistry of samples from traverses across 13 Mile Hill, Tombstone Hill, Handlebar Hill, and Offset Hill (Table 3) is similar to that for traverses across the southern end of Mount Isa Mine, but with generally slightly lower average Ag, As, Cd, Co, Ni, Pb, Sb, and, possibly, Cu and Ga contents. Distribution of elements at Tombstone Hill (Table 3) is not as simple as at Mount Isa, the more mobile Cu and Zn being hydromorphically dispersed down the steeper eastern slope, while the less mobile Pb and As are more evenly distributed about the crest of the ridge.

Mount Novit

A prominent discontinuous gossanous ridge, with a strike length of about 8 km, occurs in the Breakaway Shale unit of the Mount Isa Group (Russell, 1978), 15 km south of Mount Isa. Diamond drilling has indicated that the southern and central sections of this ridge overlie a 20 m thick massive band of pyrite, pyrrhotite, and magnetite, with variable amounts of sphalerite, galena, marcasite, chalcopyrite, and arsenopyrite. An indistinct hangingwall ironstone ridge occurs at the extremities of the main ferruginous outcrop. Except that they occur in a stratigraphically lower unit of the Mount Isa Group, the ironstone ridges at Mount Novit are, at least superficially, similar to those at Mount Isa and Hilton.

Samples from eight traverses across strike and three from along strike have a characteristic mineralogy of quartz + goethite ± hematite ± Pb-bearing alunite-jarosite minerals ± sericite ± chlorite/kaolinite. Wall rocks become less ferruginous away from the lode, and are typically micaceous, but the hangingwall lode, where developed, has a similar mineralogy to that of the main lode horizon.

Outcrops range from structureless to delicately laminated after stratiform mineralisation, with contortion and brecciation of the laminae and infillings of 'buck' quartz being common. Silicification has tended to enhance the banding, whereas ferruginisation has, in many samples, obliterated it. Pits and voids, commonly with delicate boxworks, are either disseminated throughout the samples or densely packed along bedding planes. In some cases, large clasts of mineralisation have been replaced by goethitic boxworks.

Table 4. Average compositions of ironstone samples from various prospects at Mount Novit: majors in wt %; traces in ppm.

No. of samples	*Satellite* 3	*Window* 3	*Mt Novit* 1	*Gouger North* 4	*Gouger South* 2	*Smoko* 4	*Bradshaws* 4
Fe_2O_3	37.2	63.0	25.2	61.1	57.9	17.8	55.2
K_2O	1.79	0.85	0.06	0.02	0.26	0.04	0.62
P_2O_5	0.84	0.56	0.58	0.93	0.52	0.31	0.25
MnO	0.02	0.03	0.02	<0.01	0.03	<0.01	<0.01
SO_3	0.14	0.82	0.30	0.75	0.34	0.39	0.35
Ag	<1	3	2	6	6	14	3
As	120	730	310	750	570	260	450
Ba	200	200	610	90	270	140	75
Bi	1	<1	<1	1	<1	<1	<1
Cd	<1	<1	<1	<1	<1	<1	<1
Co	57	<10	<10	6	<10	11	29
Cr	<10	<10	<10	<10	<10	<10	<10
Cu	44	800	300	190	700	100	120
Ga	15	5	4	7	5	2	10
Ge	<3	<3	<3	14	<3	4	5
In	<1	<1	<1	<1	<1	<1	<1
Mo	3	9	10	190	23	73	58
Ni	170	6	6	73	<4	60	100
Pb	85	4 700	3 000	5 850	7 850	2 080	1 020
Sb	8	330	100	180	28	62	13
Sn	17	32	60	52	55	41	15
Sr	<10	<10	<10	<10	<10	<10	<10
Tl	2	<1	<1	<1	<1	<1	5
Zn	570	1 670	520	840	460	130	610

Table 5. Average compositions of ironstones from Lake Moondarra and the Goat Creek prospect within the Paradise Creek Formation: majors in wt %; traces in ppm.

	Lake Moondarra	*Goat Creek*
No. of samples	16	13
Fe_2O_3	27.4	30.2
K_2O	1.59	1.23
P_2O_5	0.29	0.25
MnO	0.19	0.35
SO_3	0.16	0.13
Ag	<1	<1
As	490	40
Ba	710	330
Bi	<1	<1
Cd	<1	<1
Co	<10	90
Cr	20	<10
Cu	90	370
Ga	7	10
Ge	<1	<1
In	<1	<1
Mo	5	1
Ni	28	120
Pb	50	75
Sb	<10	<10
Sn	<1	<1
Sr	120	22
Tl	<1	<1
Zn	270	3 300

Average compositions of samples from six of the ridges at Mount Novit (Table 4) are slightly more phosphatic than, but basically similar to, those from Mount Isa and Hilton. Trace element contents of wall rocks up to 20 m from the gossan are much lower, indicating general lack of hydromorphic dispersion.

Lake Moondarra area

Ironstones from the Moondarra Siltstone and Breakaway Shale units of the Mount Isa Group near Lake Moondarra, northeast of Mount Isa (Fig. 2), were assessed during this study. Samples from the Breakaway Shale are weathered and variously ferruginised, laminated shale with a mineralogy of quartz + hematite ± goethite ± trace microcline ± sericite ± chlorite ± talc ± kaolinite and occasional siderite or calcite, and may bear large casts after pyrite, now filled with specular hematite, 'pitch' limonite or kaolinite. The samples from the Moondarra Siltstone are of similar appearance, with brecciated shale fragments, large casts after pyrite, and dark manganese coatings, the mineralogy being dominated by the presence of calcite ± dolomite or siderite. Trace element levels in these ironstones are generally much lower than in gossan samples from Mount Isa and Hilton (Table 5).

Lady Loretta

The Lady Loretta lead-zinc-silver deposit occurs in dolomitic siltstones, pyritic carbonaceous shale, and sandstones of the Upper Paradise Creek Formation (Loudon & others, 1975), approximately 115 km north-northwest of Mount Isa (Fig. 2). The bulk of the mineralisation occurs in the northeast-trending Small Syncline; some minor intersections were encountered in drill core from the Big Syncline to the south. Prominent ironstone ridges of hematite, goethite, chert, and barite occur on the southeast and west sides of both synclines, immediately below a lateritised plateau surface, approximately 60 m above the surrounding plain. These outcrops represent the Ore Horizon, the underlying pyrite unit, and the enclosing siderite-rich units (G. R. Carr, personal communication, 1981) on the west side of the Small Syncline.

The Ore Horizon outcrop is a deep red hematitic gossan with some relict bedding, minor brecciation, and some small-scale faulting. Boxworks are rare, and often the gossans are completely featureless (Fig. 5). Some samples are completely silicified, with only remnant hematite as patches or along original bedding planes. Rare casts after pyrite occur in these siliceous samples. Other units form variously silicified and ferruginised shales and sandstones with large casts after siderite (Fig. 6) and often obvious bedding. Samples from the barite-rich zone are slightly ferruginised, massive, well-crystallised barite.

The composition of samples from five zones of outcrop is presented in Table 6, and shows that most elements are more abundant in outcrops of the Ore Horizon than in outcrops of the other units. Exceptions to this

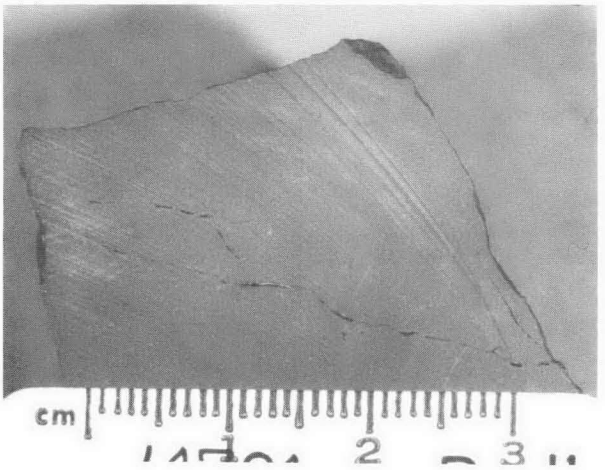

Figure 5. Massive hematite after lead-zinc mineralisation, Lady Loretta, with original structure completely obliterated.

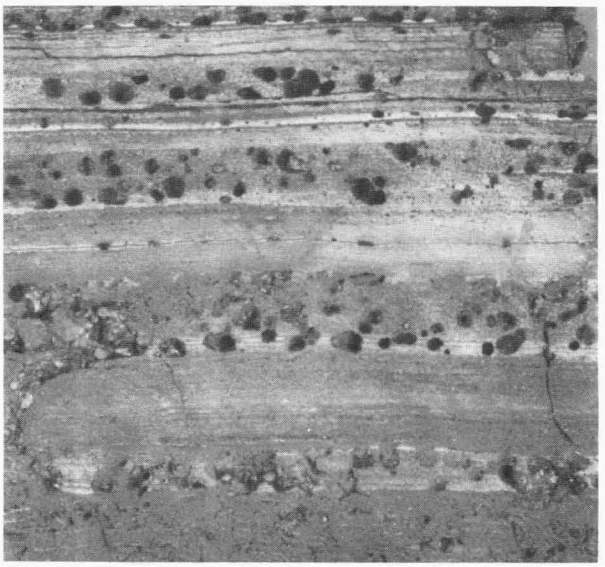

Figure 6. Ferruginised shale with large casts after siderite occurring in footwall of Lady Loretta mineralisation (10 cm across).

Table 6. Average compositions of samples from five zones of ferruginous outcrop at Lady Loretta: majors in wt %; traces in ppm.

	Small Syncline			*Big Syncline*	
	Ore	*Pyrite*	*Siderite*	*Pyrite*	*Barite*
No. of samples	11	4	5	6	2
Fe_2O_3	48.0	23.9	5.80	27.4	n.d.
K_2O	0.12	0.02	0.05	0.11	n.d.
P_2O_5	0.09	0.06	0.06	0.11	n.d.
MnO	0.05	0.04	0.03	0.06	n.d.
SO_3	1.12	0.15	0.17	0.42	n.d.
Ag	34	26	7	40	<1
As	1 080	280	76	470	55
Ba	22 700	850	510	2 470	33.4%
Bi	3	<1	<1	<1	<1
Cd	<1	<1	<1	<1	<1
Co	<10	<10	<10	<10	<10
Cr	<10	<10	<10	<10	<10
Cu	55	9	36	26	15
Ga	8	5	1	7	<1
Ge	19	30	6	44	8
In	<1	<1	<1	<1	<1
Mo	25	3	3	6	3
Ni	5	<5	5	<5	<5
Pb	1 630	890	212	2 140	90
Sb	610	530	60	95	<30
Sn	2	2	2	2	<1
Sr	750	370	55	290	1 020
Tl	<1	<1	<1	<1	<1
Zn	82	123	28	60	20

n.d. = not determined.

are Ba and Sr (in the barite-rich zone), Ge, which is greater in the pyritic horizons, Pb, which is higher in the pyritic horizon of the Big Syncline and may reflect a small pocket of rich mineralisation, and Zn, where it has been scavenged by iron oxides of the pyritic unit of the Small Syncline. Where high Pb levels occur, secondary lead minerals of the alunite-jarosite series have been detected, but usually the mineralogy is quartz, goethite, hematite, kaolinite, chlorite, and sericite.

Paradise Creek Formation

Ironstone outcrops are extremely abundant in the Paradise Creek Formation (and Gunpowder Creek Formation) immediately west of the Mount Gordon Fault Zone (Glasson, 1973; Bampton & others, 1977). Most are associated with copper mineralisation, and, of the ironstones described by Glasson, only those at Goat Creek can be considered as the possible product of weathering of stratiform lead-zinc mineralisation. These ironstones, which are variously ferruginised kaolinite, occur within gently dipping dolomitic shales, siltstones, and mudstones of the lower Paradise Creek Formation, which have been weathered to form rounded hills of low to moderate relief. Whereas the fresh rock consists of quartz, carbonates (often iron-rich), chlorite, sericite, feldspar, and organic carbon, the surface outcrop is quartz, goethite, kaolinite, sericite, and traces of hematite, suggesting that the iron oxides are derived from weathering of carbonates and, possibly, chlorite. Glasson (1973) noted that there is no relation between the high Zn content (1500–18000 ppm) of the ironstones and that of fresh rock (20–215 ppm). In addition to high Zn values, those of Ba, Co, Cu, Ni, and, to a lesser extent, Pb are also anomalous (Table 5), but again do not relate to their values in fresh core.

Dugald River

The Dugald River zinc-lead lode occurs in a clastic sedimentary basin of the Corella Formation 60 km northwest of Cloncurry (Fig. 2). It is a thin ($\leqslant$ 10 m) lenticular black carbonaceous shale-sulphide bed at the base of a slate-schist sequence that dips 70–75° to the west. A scapolitic calc-silicate rock occurs stratigraphically above the lode, with black argillaceous limestone and a black slate-hornfels in the footwall (Whitcher, 1975). Pyrrhotite, pyrite, and sphalerite occur in approximately equal proportions, together with subordinate galena, and traces of chalcopyrite, pyrargyrite, tetrahedrite, and arsenopyrite.

The lode crops out as a well-defined gossan, 2450 m long and up to 10 m wide, near the crest of a line of low ridges, 20 m above the surrounding alluvial-colluvial plain. Wall rocks of the gossan are often siliceous, and may be up to 2 m higher than the rest of the gossan. The Western Lode crops out over a strike length of 700 m to the west of the Dugald River Lode, but has no relief. Depth of oxidation is shallow (20–35 m), much of the gossan having been stripped by erosion (Taylor & Appleyard, in press) from an elevation similar to that of the top of the nearby Knapdale Quartzite.

Quartz, adularia, barite, goethite, hematite, Pb-bearing alunite-jarosite minerals, mica, kaolinite, carbonaceous matter ± montmorillonite occur in outcrop. Despite a high Zn content in the gossan (Table 7), there are only minute traces of smithsonite, goslarite, and hemimorphite; most of the Zn occurs in barite and manganese oxides, and absorbed onto phyllosilicates, iron oxides, and carbonaceous matter. Hemimorphite is more abundant in the immediate footwall, where it precipitated under more alkaline conditions, and also at the northern end of the lode, where mimetite, duftite, and native copper are significant constituents.

Because of the fine grain size of the ore, there are no boxworks, casts, or pseudomorphs after sulphide minerals. The stratiform nature of the mineralisation is often retained in the gossans (Fig. 7a), with folding, faulting, slumping, and other sturctures preserved. Gossans are commonly dark grey to black, with patches of light brown to yellow secondary lead minerals (Fig. 7b).

Analysis of fresh sulphides shows that Ag, As, Ba, Cd, Cu, Sb, and Tl (together with Hg and Se) contents are high in the ore, Ba occurring in the feldspar, hyalophane. Unlike mature gossans, the mobile elements are not completely leached, and significant anomalies of major and trace elements occur in both outcrop and subcrop of the Dugald River Lode (Table 7). Some trends are obvious: a decrease in Ag, As, Ba, Cd, Ge, Pb, and Sb north along strike; greater levels of Ag, Ba, Cd, Cu, Pb, and Tl, and lower As, Ga, and Ge in subcrop than in outcrop. Siliceous gossan from the Dugald River Lode and gossans from the Western Lode, and from a possible extension of it in the hangingwall, also contain significant anomalies of major and trace elements (Table 7).

Table 7. Average compositions of gossan outcrop and subcrop samples from the Dugald River prospect: majors in wt %; traces in ppm.

	DDH DR46	*13935N*		*14359N*				
No. of samples	*Fresh sulphide* 12	*Outcrop* 11	*Subcrop* 3	*Outcrop* 4	*Subcrop* 8	*Siliceous outcrop* 3	*Western Lode* 4	*'Hanging wall'* 4
Fe_2O_3	8.97*	35.3	16.4	16.4	17.7	1.81	6.38	50.6
K_2O	3.56	0.81	1.63	1.67	5.45	4.58	2.62	0.69
P_2O_5	0.24	0.65	0.15	0.29	0.62	0.14	0.67	0.47
MnO	2.01	0.60	0.63	1.13	0.20	0.03	0.07	0.05
SO_3	21.0†	6.32	10.1	1.00	12.3	0.85	1.30	n.d.
Ag	55	80	<100	1	40	14	4	80
As	540	1 340	350	320	140	180	230	1 950
Ba	2.55%	1.46%	4.00%	810	2.39%	2.49%	520	2.32%
Bi	<1	<1	<1	<1	<1	<1	<1	<1
Cd	380	10	80	<10	13	<3	<10	3
Co	9	19	30	40	35	10	10	13
Cu	310	415	740	45	215	450	400	540
Ga	10	20	7	12	6	11	21	10
Ge	12	10	5	4	2	5	16	10
In	<1	<1	<1	<1	<1	<1	<1	<1
Mo	15	33	19	5	42	14	5	20
Ni	30	16	15	50	105	35	15	40
Pb	1.75%	5.00%	11.6%	0.37%	1.79%	0.42%	1.48%	1.45%
Sb	23	110	50	<30	35	<30	32	160
Sn	6	<4	2	2	<4	3	2	20
Tl	60	2	15	2	30	10	10	13
Zn	13.5%	2.35%	12.4%	10.6%	5.16%	0.55%	1.80%	0.51%

* as Fe. † as S. n.d. = not determined.

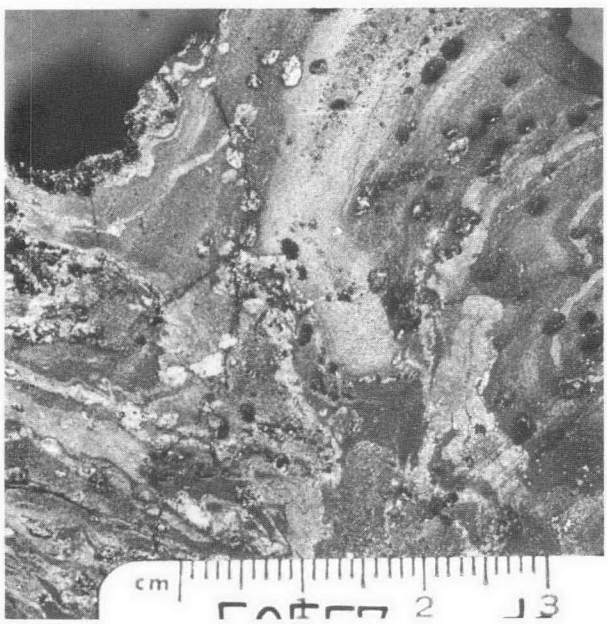

Figure 7. (a) Dugald River gossan sample, showing original structure of ore preserved in quartz, adularia, barite, iron oxides and carbonaceous matter.

(b) Dark massive gossan with lighter patches of secondary lead minerals of alunite-jarosite series (3 cm across).

Pegmont prospects

The Pegmont lead-zinc deposit, about 175 km southeast of Mount Isa (Fig. 2), is believed to occur in the Soldiers Cap Group (cf. Locsei, 1977; Stanton & Vaughan, 1979), which also hosts the Fairmile and Squirrel Hills prospects (see below). Galena, sphalerite, and magnetite, with lesser pyrrhotite, pyrite, and chalcopyrite, occur associated with a quartz-magnetite-garnet-apatite banded iron formation (BIF) (Stanton & Vaughan, 1979) in the Toole Creek Volcanics Member of the Soldiers Cap Group. The deposit consists of a single stratiform sheet up to 6 m thick, with an overall dip varying from horizontal to 20° southeast, and has been intensely folded (Orridge, 1980) and metamorphosed up to amphibolite grade.

The area is of low relief with occasional Cretaceous mesas rising to less than 30 m above alluvial plains, which are often covered with lateritic rubble. Oxidation extends to a depth of 50 m (Orridge, 1980). In the main area of mineralisation, soils are skeletal, with gossan outcrops rising up to 5 m through the soil (Fig. 8).

Outcrop occurs as ferruginous, jaspery, manganese-oxide stained masses, in which the original banded character of the mineralisation is well preserved. In addition, many samples have casts and delicate box-

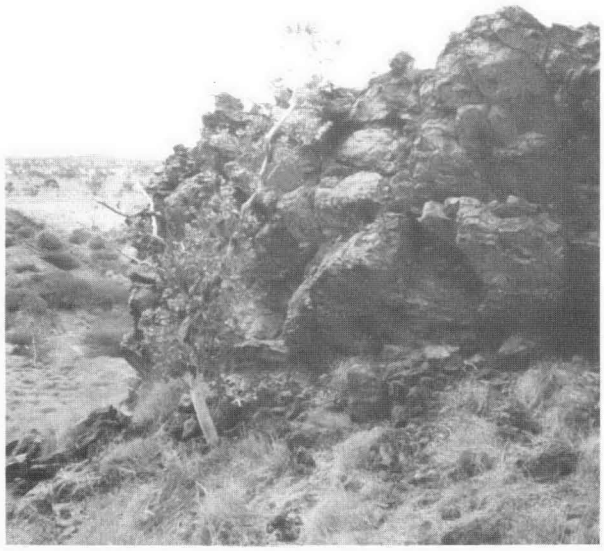

Figure 8. Gossan outcrop at Pegmont, showing manganese-coated jaspery BIF rising about 5 m above surrounding plain.

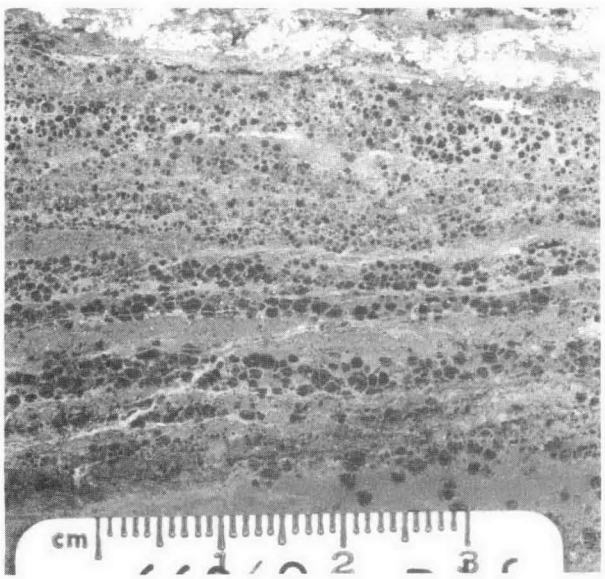

Figure 9. Pegmont gossan sample, showing original banding with casts and boxworks after fayalite.
Secondary lead minerals of alunite-jarosite series may constitute 25% of these gossans.

works after fayalite (Fig. 9), a characteristic not found elsewhere in the Soldiers Cap Group. The mineralogy is goethite ± plumbogummite ± graphite ± hematite ± corkite ± quartz ± coronadite ± pyromorphite ± spessartite and occasionally staurolite, talc, and kaolinite. In common with other deposits in north-west Queensland (Scott & Taylor, 1979b) and elsewhere (Baker, 1963), the secondary lead minerals of the alunite-jarosite series have formed from galena, with pyromorphite as the intermediate phase.

Apart from Ag and Cd, the trace element content of the ore is low (Table 8). It is, therefore, not surprising that outcrop samples have generally low (and variable) pathfinder element contents, except that there has been slight residual concentration of As, Ba, Cu, and Sr in the outcrop compared with fresh sulphide. The high levels of P_2O_5, MnO, and SO_3 reflect the original mineralogy and immaturity of the gossan.

Apart from the low iron sulphide content of the mineralisation, two other factors have contributed to the immaturity of the gossan profile: the high apatite content, which acts as a buffer to the formation of a highly acidic environment, and erosion of the upper part of the gossan, leaving only a shallow profile (as at Dugald River).

Other prospects near Pegmont (referred to as 'Pegmont ironstones') are also associated with the BIF and, except for the absence of casts and boxworks after fayalite, have a similar appearance to the Pegmont gossans. Those from Jolimont are characterised by high Ba and Sr, occurring as goyazite or gorceixite (hydrated Sr-Ba-Ca-Al phosphates), and Zn (Table 8), associated with abundant kaolinite. Banded outcrop from the Mount Thomas prospect, northwest of Pegmont (Fig. 2), has a very subdued geochemical signature (Table 8) similar to that of other prospects in the Soldiers Cap Group.

Fairmile

The Fairmile Prospect occurs in the Soldiers Cap Group approximately 65 km south-southeast of Cloncurry (Fig. 2). A prominent BIF folded into a tight syncline has a strike length of several kilometres. In both limbs of the most northerly section of outcrop, the quartz-magnetite-garnet-apatite BIF hosts pyrite-galena mineralisation.

Quartzite, garnet quartzite, and amphibolite form a prominent ridge up to 20 m above the surrounding plains, and remnants of Cretaceous peneplanation occur as mesas in the relatively heavily dissected region. The BIF occurs as a 2 m wide resistant unit up to 2 m above the general relief of the prominent ridge. Beneath a veneer of dark manganese oxides the outcrop retains its original banding, which is often highly folded and contorted (Fig. 10). There are no boxworks or casts after fayalite, although some bands are more porous than others, and may result from leaching of fine-grained fayalite. Depth of weathering and the nature of the weathered profile are not known, but it is assumed that the relatively low iron sulphide content and high apatite content have resulted in the formation of an immature profile. To the east of the most northerly outcrop of BIF, there is a restricted area of limonitic gossan, which contains boxworks and casts after pyrite.

The mineral assemblage of weathered BIF is hematite (martite) + goethite + magnetite + garnet (spessartite) + apatite ± cryptomelane, with accessory feldspar, chlorite, and mica. Secondary lead minerals, corkite, plumbogummite, and pyromorphite, distinguish gossan from other ironstone outcrops.

The geochemistry of the Fairmile gossans (Table 8) is similar to that of the Pegmont gossans, but with higher MnO, As, and Ba, and lower P_2O_5, Pb, and Zn content. Comparatively high levels of elements normally mobile in acid oxidising conditions confirm the immaturity of the profile. Outcrops of unmineralised BIF

Figure 10. Sample of Fairmile gossan showing intensely folded banding.
Mineral assemblage is hematite, magnetite, garnet, manganese oxides and secondary lead minerals.

have lower SO_3, Ag, As, Ba, Bi, Pb, Sb, Sr, and Zn values than the gossans, but higher Cu possibly reflects the existence of minor copper mineralisation associated with the BIF, an association known to occur elsewhere in the Soldiers Cap Group (e.g. Mount Norma approx. 40 km to the north).

The mineralogy (goethite, quartz ± hematite, ± feldspar) and geochemistry (Table 8) of the limonitic gossan are significantly different, with slightly anomalous Cu and Zn values.

Squirrel Hills prospects

Between Fairmile and Pegmont, the Squirrel Hills prospects occur in the Toole Creek Volcanics Member of the Soldiers Cap Group. The rocks of this unit consist of migmatites, quartzo-feldspathic gneisses, pelitic schists, quartzites, and amphibolites, which are commonly highly faulted and folded. Host rocks for the mineralisation are, typically, foliated quartz-garnet gneisses.

Much of the area comprises flat sandy plains with isolated hills and low ridges rising up to 20 m above the plains. The Corella Formation directly to the west has a greater relief and is the source of many streams that cut the Soldiers Cap Group and have deposited alluvium throughout the region. Mineralisation typically crops out as banded manganiferous gossan, and, although the gossan profile was not sampled, it is assumed to be immature over its average 30 m depth.

Sphalerite and pyrite are the most common sulphides, with minor galena and chalcopyrite. Galena appears

Table 8. Average compositions of samples from deposits

	Pegmont prospects			
No. of samples	*Pegmont Sulphide* 3	*Pegmont Outcrop* 32	*Jolimont* 6	*Mount Thomas* 9
Fe_2O_3	42.8	44.3	45.0	55.7
K_2O	0.13	0.08	0.37	<0.01
P_2O_5	2.73	3.57	0.61	0.55
MnO	3.50	2.41	0.20	0.39
SO_3	7.50	1.08	0.39	<0.01
Ag	11	11	<1	<1
As	<10	25	170	56
Ba	40	160	1 200	340
Bi	4	<1	7	<1
Cd	300	<10	<1	<1
Co	<10	<10	12	23
Cr	25	31	16	50
Cu	22	120	170	140
Ga	4	3	9	2
Ge	8	6	2	4
In	<1	<1	<1	<1
Mo	2	<3	3	<3
Ni	<4	4	11	55
Pb	7.54%	11.5%	40	<40
Sb	<30	<30	<30	<30
Sn	9	1	1	1
Sr	<10	38	1 300	280
Tl	<1	<1	<1	<1
Zn	2.97%	0.33%	1.03%	200

to have an affinity with magnetite, and chalcopyrite occurs with pyrrhotite in the footwall (Nisbet & Joyce, 1980). Marmatite replaces sphalerite, and pyrrhotite dominates over pyrite, where the host rocks are granuloblastic. Typical minerals in the quartzo-feldspathic gneiss are feldspar, quartz, amphibole, and pyroxene; where mineralisation is associated with BIF, they are olivine, quartz, garnet, apatite, magnetite, and mica.

Analyses of sulphide concentrates from various prospects show that Cd is the only element consistently associated with sphalerite; pyrite and pyrrhotite have variable As, Bi, Co, Cr, Cu, Ga, Ge, Mo, Ni, and Sn; Ag, Bi, Mo, Sb, and Sn are commonly associated with galena; and Co and Ni occur in chalcopyrite.

The mineralogy and geochemistry of gossans from Cowie, Marramungee, and Dingo are described by Nisbet & Joyce (1980), and the gross mineralogy of each of the studied prospects is detailed in Table 9. Quartz, hematite, goethite, magnetite, garnet, and carbonaceous matter are common to much of the outcrop; secondary lead minerals are of the alunite-jarosite series, and high Zn values are reflected in the occurrences of gahnite and hemimorphite. Zinc is also present in the secondary lead minerals, in manganese and iron oxides, and in pale apple-green nontronite. Lead may also occur as coronadite. None of these samples shows any characteristic boxworks or texture, although some of the original banded structure is retained.

Average composition of surface samples from each of the prospects (Table 8) shows extreme variation, which is possibly related to primary zonation (Taylor, 1979; Nisbet & Joyce, 1980). In many cases, the high levels of Pb, Zn, K_2O, P_2O_5, and SO_3 indicate the immaturity of the gossans, again reflecting the relatively low iron sulphide content of the mineralisation and stripping of the gossan profile.

and prospects associated with BIF in the Soldiers Cap Group: majors in wt %; traces in ppm.

Fairmile			*Squirrel Hills prospects*							
Gossan 30	*BIF* 23	*Limonitic gossan* 5	*Dingo* 7	*Zone A* 4	*Zone S* 4	*Camp Grid* 7	*Marramungee* 5	*Black Rock* 7	*Cowie North* 12	*Cowie South* 5
47.9	43.5	65.8	31.2	54.4	36.3	14.5	38.3	17.3	15.5	41.0
0.20	0.32	1.13	0.19	0.02	2.84	0.45	0.21	1.97	0.11	0.21
1.88	1.40	0.26	0.28	0.30	0.23	0.19	0.21	1.07	3.97	0.44
11.4	8.86	1.63	0.26	0.10	0.45	2.81	3.10	2.34	7.99	1.96
0.16	0.02	0.16	1.71	0.57	1.11	1.11	0.33	0.63	0.39	0.18
8	<0.3	1.3	32	<1	4	<1	2	40	2	1
240	85	780	130	60	1 000	98	24	190	400	120
710	340	370	150	210	530	430	45	170	150	110
5	<3	20	250	9	11	2	1	1	27	1
<1	<1	<1	<1	<1	<1	<1	<1	<1	<1	<1
10	13	26	53	100	42	10	18	58	10	90
11	15	<10	<10	<10	<10	<10	<10	<10	<10	<10
140	290	1 980	720	1 700	1 580	110	250	300	150	230
4	5	0.6	19	10	5	13	24	12	10	16
6	4	2	5	3	2	7	6	9	13	9
<1	<1	<1	<1	<1	<1	<1	<1	<1	<1	<1
25	16	16	5	6	9	5	1	11	3	4
20	38	20	4	200	38	4	4	32	4	15
1.26%	44	170	1.44%	2 000	2.35%	20	200	1.21%	7.58%	150
25	<10	70	<30	<30	500	<30	<30	<30	<30	<30
2	2	<1	9	2	19	1	1	2	4	8
60	30	60	33	130	230	81	26	50	1 060	58
<1	<1	<1	<1	<1	<1	<1	<1	<1	<1	<1
860	250	570	4 100	160	1 650	2 030	1 180	8.62%	6 000	1 530

Table 9. Gross mineralogy of gossans and ironstones from the Squirrel Hills prospects, as determined by X-ray diffraction.

Dingo
Quartz + hematite + goethite ± gahnite ± corkite ± garnet ± plumbogummite
Zone A
Quartz + goethite + hematite ± plumbogummite
Zone S
Quartz + goethite + hematite + carbonaceous matter ± corkite± plumbogummite ± feldspar
Camp Grid
Quartz + garnet + goethite + andalusite ± secondary Pb minerals ± gahnite ± hematite
Marramungee
Quartz + garnet ± goethite ± mica ± amphibole ± cryptomelane ± carbonaceous matter ± feldspar ± hematite
Black Rock
Quartz + goethite + hemimorphite ± garnet ± chlorite ± carbonaceous matter ± plumbogummite ± cryptomelane (coronadite) ± mica
Cowie North
Quartz + garnet + apatite + carbonaceous matter + plumbogummite ± goethite ± chlorite ± cryptomelane (coronadite)
Cowie South
Hematite + magnetite + quartz ± goethite ± garnet ± chlorite ± carbonaceous matter

If it is assumed that these outcrops in the Soldiers Cap Group have been leached to the same extent as the Pegmont gossan, it would appear that only Cowie North has sufficiently high Pb grades to warrant attention, whereas the Zn grades at Black Rock and possibly Cowie North are of interest (cf. Nisbet & Joyce, 1980). The extremely high Zn values at Black Rock are considered to represent concentration by reactive silica to form hemimorphite.

Answer Slate prospects

The Answer Slate is siliceous, sericitic, and carbonaceous, with some interbedded quartz siltstones and chert. It crops out about 50–100 km south of Cloncurry, and contains a number of prospects, comprising ferruginous outcrops associated with metadolerite sills.

Surface rocks are generally deeply leached and kaolinitic, a result of profound weathering (Twidale, 1956). A stable land surface is believed to have existed at about the same position as the present surface at least three times previously. Flat open country is most common, although the more siliceous or cherty lithology forms ridges of low relief. The gossans may occur on ridges, such as at Iris and Barite Ridge, or be barely visible above the plains, as at Venture (Fig. 11).

Mineralisation intersected by diamond-drill holes consists largely of pyrite and pyrrhotite with minor chalcopyrite, sphalerite, and galena in host rocks consisting of quartz, plagioclase, siderite (or calcite), sericite, and chlorite. At Barite Ridge, barite and fluorite are common and the feldspar is microcline. Analyses of pyrite concentrates from various prospects show that significant concentrations of Ag, As, Bi, Cd, Co, Cu, Ga, Mo, Ni, Pb, Sn, Tl, and Zn occur in the sulphide mineralisation (Scott & Taylor, 1980).

The mineralogy of surface gossans that contain rare boxworks and casts after pyrite is summarised in Table 10, and shows that they are essentially quartz, goethite, and hematite, with minor sericite, chlorite, and kaolinite derived from the shales and slates. Where there has been significant acid solution-wall rock interaction, jarosite has formed, and, as at Venture, where there is some Pb, secondary lead minerals of the alunite-jarosite series occur. An additional mineral found in some samples is cristobalite, which is believed to have formed by deposition of silica from weathered wall rocks (cf. Taylor & Sylvester, 1982).

Figure 11. Outcrop at Venture prospect partially obscured by alluvium and colluvium.
Such outcrops are only found by detailed ground surveys.

Table 10. Gross mineralogy of outcrop from prospects within the Answer Shale, as determined by X-ray powder diffraction.

Radke	Goethite + hematite + quartz + chlorite ± sericite ± talc ± rutile
Barite Ridge	Quartz + hematite + goethite ± barite ± kaolinite
Venture	Quartz + hematite + goethite ± sericite ± kaolinite ± jarosite ± secondary Pb minerals
Iris	Quartz + goethite + hematite ± sericite ± feldspar
New	Quartz + goethite ± hematite ± sericite ± jarosite ± cristobalite
Eastern	Quartz + hematite ± goethite ± kaolinite

The average composition of surface samples (Table 11) shows that Ag, As, Ba, Bi, Cu, Ga, Ge, Mo, Pb, Sb, Sn, and Zn are high, and Cd, Co, Ni, and Tl, which have generally been leached from the gossans, are low. Compositional variation along strike, particularly at Venture, is not shown by these average values. Lead contents up to 9 per cent, with associated high values of Ag, Cu, In, Mo, Sb, and Sn towards the southern end, may indicate the presence of localised galena mineralisation, as suggested by Gulson & Mizon (1979) on the basis of lead isotope studies.

Analysis of geochemical data

Despite the relatively wide use of graphical and statistical techniques to evaluate the geochemistry of gossans and ironstones in the Yilgarn Block of Western Australia (Clema & Stevens-Hoare, 1973; Joyce & Clema, 1974; Bull & Mazzucchelli, 1975; Travis & others, 1976; Moeskops, 1977; Smith, 1979; Smith & others, 1979), such techniques have not previously been applied to gossans and ironstones from the Mount Isa Inlier. Various univariate and multivariate statistical techniques, summarised by Andrew (1977a, 1979) and Ryall & Taylor (1981), have been used to ascertain those most relevant to gossan evaluation in the Mount Isa Inlier.

Table 11. Average compositions of ironstones from prospects in the Answer Slate: majors in wt %; traces in ppm.

No. of samples	*Radke* 7	*Barite Ridge* 4	*Venture* 26	*Iris* 12	*New* 7	*Eastern* 2
Fe_2O_3	50.3	38.4	25.8	30.9	45.6	48.6
K_2O	0.03	0.04	0.85	0.84	0.91	0.22
P_2O_5	0.07	0.08	0.36	0.18	0.01	0.02
MnO	<0.02	0.05	0.06	0.12	0.04	0.02
SO_3	0.39	28.2	1.09	0.40	7.56	0.55
Ag	3	<1	6	5	1	1
As	780	260	1 890	340	370	960
Ba	170	14.3%	1 330	360	430	470
Bi	4	30	6	16	13	30
Cd	<1	<1	<1	<1	<1	<1
Co	14	<10	<10	17	20	10
Cr	17	15	19	27	50	17
Cu	590	170	970	870	580	490
Ga	2	2	14	12	25	18
Ge	<1	3	12	5	4	11
In	<1	<1	3	<1	<1	5
Mo	38	4	22	7	5	11
Ni	60	<4	27	<11	40	6
Pb	1 240	170	9 000	130	770	1 920
Sb	130	<30	160	<30	50	35
Sn	8	2	130	15	11	8
Sr	25	250	220	85	160	30
Tl	<1	<1	<1	<1	<1	<1
Zn	750	45	840	130	500	390

Of the large number of major and trace element abundances determined during analysis of the gossans and ironstones, only five major and nineteen trace elements are reported. Silica, usually in the form of quartz (or cristobalite) derived from quartz gangue and the weathering of silicates, is not diagnostic, and its diluting effect on other elements can be gauged from the Fe_2O_3 content, with which it varies inversely. Similarly, Al derived from alumino-silicates is not diagnostic. The more readily leached Ca, Mg, and Na occur as carbonate or residual silicate gangue, and generally occur at or below the limit of detection. Titanium is essentially immobile and may possibly be used to determine the degree of dilution or concentration. None of the gossans studied is particularly enriched in Ti, with most values being less than 0.5 per cent. Thus, of the major constituents, only Fe, Mn, P, K, and S have been used in the statistical evaluation.

Range of values

To reduce the considerable geochemical variation at any one prospect, no data from ferruginised wall rocks have been considered. However, both residual* and deposited* ironstones and gossans have been analysed, which, because of dilution and the variable mobility of elements, gives rise to considerable variation in results.

* These terms are equivalent to 'indigenous' and 'exotic' of Blanchard (1968).

Concentration range and geometric mean for selected elements are depicted in Figure 3 for each gossan and ironstone suite. This grouping has been used to show the maximum ranges encountered in the gossans associated with the various styles of mineralisation in the Mount Isa Inlier. Other trace elements (Bi, Cd, Ga, Ge, In, Sn, Tl) have not been included, because they are generally at or below the limit of detection and have restricted concentration ranges.

Significant differences between the shale-hosted deposits and prospects and those associated with BIF south of Cloncurry are shown by the major elements in Figure 3, with the latter group having higher average Fe_2O_3, P_2O_5, and MnO, and lower K_2O and SO_3. Apart from the Soldiers Cap Formation, which includes ironstones from many diverse prospects, the range of values for P_2O_5, MnO, SO_3, and, in particular, Fe_2O_3 is more restricted than for the shale-hosted ironstones, while K_2O exhibits similar variations in both types. Range and mean value for gossans from the shale-hosted (Mount Isa, Dugald River and Lady Loretta) lead-zinc deposits show remarkable similarities, despite variations in the grade, nature of mineralisation, and host rocks.

The trace element contents of the Black Star, Dugald River, and Lady Loretta gossans again show some marked similarities (Fig. 3). The more acidic conditions at Lady Loretta are reflected in the lower Cu, Ni, Pb, and Zn contents, whereas the low Ba content in the Black Star gossans indicates its relatively low abundance in the Urquhart Shale.

Of the target elements, Pb is the most diagnostic for gossans directly associated with mineralisation, with large ranges and high means occurring in samples from Black Star, Dugald River, Pegmont, and Fairmile. At Lady Loretta the range is smaller and the mean, lower (Fig. 3), which, as previously indicated, reflects a greater degree of leaching, owing to high pyrite content. Large ranges but low means in the Squirrel Hills and Answer Slate prospects are related to the large number of ironstones sampled in each formation and the low grade mineralisation. Zinc is much less diagnostic, with both gossans (Black Star, Dugald River, Pegmont) and ironstones (Paradise Creek Formation, Soldiers Cap Formation) having large ranges and/or high means. Gossans associated with pyrite at Mount Isa, Hilton, and Mount Novit have higher means than gossans from Lady Loretta mineralisation (Fig. 3). These data emphasise the unreliability of using the Zn content of gossans and ironstones as an indicator of sphalerite mineralisation. The mean Ag values are significantly higher in gossans associated with shale-hosted mineralisation than in those associated with BIF, reflecting the original Ag content of the sulphides.

Ironstones and gossans in shales, except for those in the Paradise Creek Formation, have higher As contents than those associated with BIF, but there is no apparent correlation of As with Pb and Zn in the gossans. The distribution of Sb is even more erratic (Fig. 3), only the Black Star and Lady Loretta samples having mean values greater than 100 ppm. Similarly, Cu contents bear no relation to either the nature of host rocks or to underlying mineralisation, except that high means and large ranges occur in those samples from deposits and prospects with known copper mineralisation (in the hangingwall at Mount Isa, Hilton, and Dugald River, and in the footwall of a number of prospects in the Soldiers Cap Group). High values in the Fairmile limonitic gossan and Answer Slate are possibly related to minor copper mineralisation.

Cobalt and Ni ranges and means are generally restricted and non-diagnostic, even of gossans and ironstones associated with pyrite mineralisation. Both elements are commonly associated with iron sulphides, but upon oxidation are highly mobile in the acidic environment, only small amounts being adsorbed by goethite and phyllosilicates.

With only Black Star and Pegmont gossans having mean Ba values of less than 100 ppm, the Ba contents of gossans and ironstones from throughout the Mount Isa Inlier are high but, except for Lady Loretta and Dugald River, are not directly correlated with lead-zinc mineralisation.

Cumulative frequency plots—threshold

Histograms show that, in common with other gossans and ironstones (Andrew, 1979; Ryall & Taylor, 1981), the distribution of all elements other than Fe approximates lognormality. In using probability paper to determine threshold values from cumulative frequency plots (Sinclair, 1974, 1976), it is, therefore, necessary to make a log transformation. However, as only small numbers of samples, selected to represent an anomalous population, were taken at each deposit and prospect, threshold values have not been determined in this study.

Correlation matrices

Correlation matrices were initially determined using five major elements and nineteen trace elements, and then recalculated omitting those trace elements at or below the limit of detection (e.g. Bi, In, Sn, and Tl were not considered in the 'Mount Isa Traverse' group), to eliminate spurious correlations. From the sixteen matrices, those elements that correlate both positively and negatively, at the 99% confidence level, were examined for possible common trends.

The correlation coefficients do not contribute significantly to the evaluation of gossans and ironstones, although there are again differences between the shale-hosted and BIF-associated groups, reflecting essential differences in primary mineralogy and geochemistry. Thus, the strong positive correlations, Fe-As, K-Ga, As-Mo-Sb, Ba-Sr-S, and negative Fe-Ba occur essentially in the shale-hosted group. In the samples from the Paradise Creek Formation, there is a strong correlation between Fe-As-Co-Ni-Zn, and at Lake Moondarra, a possible correlation between Mn-Co-Ni-Zn, suggesting scavenging of trace elements by iron and manganese oxides, respectively. These do not, however, necessarily indicate non-gossanous ironstones, as the Dugald River gossans also have a strong Mn-Co-Ni-Zn correlation.

Primary and secondary mineralogy strongly influence the correlations: Ba commonly occurs with S as barite and alunite-jarosite minerals, but also correlates with K, presumably in sericite or residual feldspar as well as in K-Pb-Mn-oxides; Pb substitutes for K in secondary alunite-jarosite-type minerals, in which P, As, Sb, Mo, and Ge anions may substitute for SO_4^{2-}; trace elements are scavenged by iron and manganese oxides and alunite-jarosite-type minerals. Further discussion of the mineralogy in relation to the correlation matrices is included under 'Factor analysis' below.

Scattergrams

The use of scattergrams (Travis & others, 1976; Andrew, 1977b, 1979; Moeskops, 1977) to evaluate gossans and ironstones has met with some success, particularly if the group mean values are plotted instead of complete data sets, as the degree of overlap of each field is greatly reduced. Partitioning into three distinct groups, representing gossans on known lead-zinc mineralisation, ironstones (after BIF, ferruginous country rock, etc.), and gossans on pyrite mineralisation is best achieved by plotting Pb against major and trace elements. Some overlap of the fields is common, particularly between the two gossan populations, but plots of Pb vs Ba and Pb vs Cu separate each of the fields (Fig. 12), possibly because neither Ba, except at Lady Loretta and Dugald River, nor Cu contents are dependent on the lead-zinc mineralisation.

Factor analysis

In addition to computing the correlation matrices, R-mode factor analysis for each group of samples was determined using the Statistical Package for Social Sciences computer programs (Nie & others, 1975). The use of factor analysis in gossan evaluation is to explain the behaviour of groups of elements and to construct indices that permit scores to be calculated to ascertain group membership (factor score). Whereas Joyce & Clema (1974) were able to use principal component analysis to distinguish gossans derived from nickel-copper mineralisation in Western Australia because they have similar elemental signatures, the diverse geochemical characteristics of gossans associated with lead-zinc mineralisation in the Mount Isa Inlier preclude the use of either principal component analysis or factor analysis in determining group membership.

Many of the factors illustrate the behaviour of elements in the oxidised zone. Common associations that are readily explained are S-P-As-Pb-Sb-Ge (as secondary alunite-jarosite-type minerals), Ba-Sr-S-(Ag)-(Pb) (barite), Ba-Sr-K (alunite-jarosite minerals, sericite, and, possibly, feldspar), and adsorption of various elements by iron and manganese oxides. Other associations are unique to particular gossans or, in many cases, cannot be explained on known geological or mineralogical grounds. The use of factor or principal component analyses in the evaluation of gossans in the Mount Isa Inlier is, therefore, of doubtful value.

Discriminant analysis

Discriminant analysis has been shown by Bull & Mazzucchelli (1975), Andrew (1979), and Ryall & Taylor (1981) to be the most effective statistical technique in gossan evaluation, as it uses geochemical data to classify ironstones into known groups. Its effectiveness in classifying gossans and ironstones in the Mount

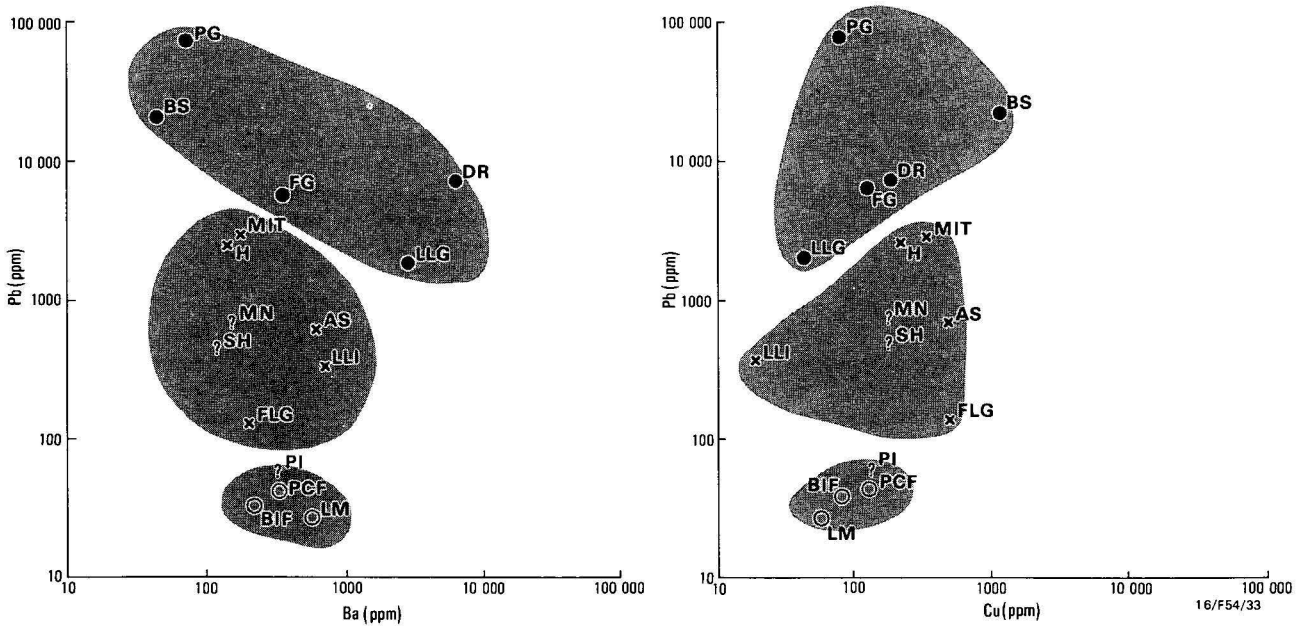

Figure 12. Scattergrams of geometric means of (a) Pb vs Ba and (b) Pb vs Cu for gossans and ironstones from deposits and prospects in the Mount Isa Inlier.
DR = Dugald River; BS = Black Star; PG = Pegmont gossan; FG = Fairmile gossan; LLG = Lady Loretta gossan; MIT = Mt Isa traverses; H = Hilton; MN = Mount Novit; AS = Answer Slate; SH = Squirrel Hills; LLI = Lady Loretta Ironstones; FLG = Fairmile limonitic gossan; PI = Pegmont ironstones; PCF = Paradise Ck Fm; BIF = barren BIF; LM = Lake Moondarra; • = gossan; X = pyritic gossan; O = ironstone; ? = unknown.

Table 12. Classification of gossan and ironstone samples by stepwise discriminant analysis, using (a) major and trace elements (bold type), and (b) trace elements only.

	Black Star		*Isa traverse*		*Ironstone*		*Dugald River*		*Pegmont gossan*		*BIF*	
* *Black Star*	**18**	17	**1**	2								
* *Isa Traverse*		5	**36**	32	**1**							
Lake Moondarra					**14**	5					**2**	11
Hilton		3	**36**	26	**1**		**1**	2		1		6
Mount Novit			**26**	21	**15**	10	**2**	2			**1**	11
Lady Loretta gossan			**11**	11								
Lady Loretta ironstone			**20**	9			**1**					12
* *Paradise Creek Fm.*					**13**	12						1
* *Dugald River*			**1**	2			**26**	25				
* *Pegmont gossan*							**1**	1	**31**	31		
Pegmont ironstone			**1**	1	**5**		**5**	5			**9**	14
Fairmile gossan				2				4	**13**	12	**17**	12
* *BIF*											**23**	23
Fairmile ironstone			**1**	2							**4**	3
Squirrel Hills		2	**8**	6	**15**	15	**10**	7	**10**	12	**9**	10
Answer Slate	**4**		**36**	29	**2**		**11**	5			**5**	24

* Type gossans and ironstones.

Isa Inlier has been tested using the computer program BMD 07M (Dixon, 1970) for stepwise analysis. The elements Fe, K, P, Mn, S, Ag, As, Ba, Co, Cu, Ga, Ge, Mo, Ni, Pb, Sb, Sr, and Zn were all used in the computation, using half the detection limit for values lower than the detection limit. All samples were classified into six groups, representing low Zn–high Pb gossans (Black Star, Mount Isa), gossans derived from pyritic envelopes enclosing lead-zinc mineralisation (pyritic gossans), ironstones on faults (from Paradise Creek Formation), high Pb-Zn gossans (Dugald River), gossans derived from mineralisation associated with BIF (Pegmont), and barren BIF. These six groups were selected as they are considered to best represent ironstones and gossans in the Mount Isa Inlier, and, as shown in Table 12(a), the classification proved satisfactory in correctly classifying the majority of samples in each group.

In decreasing order, the elements which best discriminate between the various gossans and ironstones are Pb, P, Ba, As, Zn, Mn, Co, S, and Sb. Both Pb and Zn are target elements; P and Mn occur commonly in the gossans and ironstones associated with BIF, the highest P levels occurring in the gossans; the gossans at Lady Loretta and Dugald River both have high Ba and S contents, and As and Sb are generally restricted to the shale-hosted deposits. However, there is no apparent unique association with Co, except that its values are highest in the Paradise Creek Formation ironstones.

Classification of samples from Lake Moondarra, Hilton, Mount Novit, Lady Loretta, and Fairmile gossan is also considered to be correct. Eleven gossan samples from Lady Loretta have been classified with samples from traverses at Mount Isa because both Pb, Zn, Ag, and some of the discriminant elements have been leached from the gossan by highly acidic solutions resulting from the oxidation of pyrite. Four samples of gossanous ironstone from Fairmile are incorrectly classified as BIF, with which they have no apparent mineralogical or geochemical affinity. Samples of ironstones from the Pegmont area, from prospects at Squirrel Hills, and from the Answer Slate prospects have been assigned to a number of groups (Table 12(a)), and reflect the large number of prospects sampled within each of the three areas (Tables 8 and 11). Inspection of the computer data indicates that the majority of both groups and individual samples have been correctly assigned and accurately reflect the nature of underlying mineralisation and physico-chemical conditions in the oxidised environment.

Separation of the 16 groups of gossans and ironstones is best illustrated by a plot of group means for the first two canonical variates (Fig. 13). Greatest separation (canonical variate I) is due to high levels of P_2O_5 and MnO in BIF-associated ironstones and gossans and the chalcophile elements Zn, As, and Sb in shale-hosted outcrop. Canonical variate II is dominated by Pb, giving good separation of the Pegmont gossans (geometric mean = 11.5 per cent), but lesser separation of other groups, which have mean Pb values ranging from 50 ppm (Lake Moondarra ironstones) to approx. 5 per cent (Dugald River, Fairmile, Black Star gossans). Of the remaining discriminant elements, Ba contributes significantly to canonical variate III, Co to IV, and SO_3 to V.

Four distinct groupings representing immature Pb/Zn-rich gossans, gossans on pyrite-rich mineralisation, ironstones, and BIF-associated outcrop are shown in Fig. 13. Whereas the first three groupings are relatively compact, the great diversity of mineralisation and geochemistry of the BIF-associated outcrop has resulted in a significant spread of means. Further subdivision into gossans on known mineralisation (e.g. Pegmont, Fairmile) and barren BIF is possible, with the mean for the Squirrel Hills prospects lying between both subgroups and those of shale-hosted affinity. Canonical plots for individual samples produce overlapping fields, which may be ascribed to real significant differences in properties of the outcrop, which are reflected in Table 12(a).

An additional classification was attempted using the 13 trace elements only. The results (Table 12(b)) are, with a few exceptions, less accurate than when some major elements are used in the analysis, e.g. 11 of the Lake Moondarra samples have been classified as BIF, whereas the majority are obviously ironstones similar to those occurring in the Paradise Creek Formation. To further test the validity of the technique, the program was re-run using only the nine elements

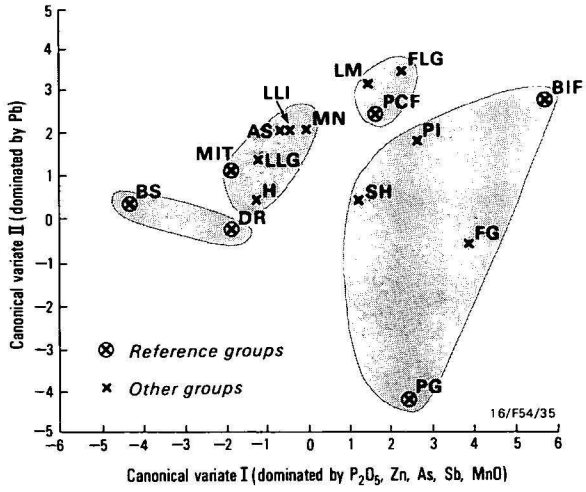

Figure 13. Plot of canonical variate means for each group of gossans and ironstone.
Abbreviations as for Fig. 12.

previously selected. This classification is similar to that in Table 12(a), with minor differences being due to elimination of less significant discriminant variables (e.g. Ni, which has a significant contribution to canonical variate II).

Discussion and conclusions

Texture

Evaluation of gossans from the Mount Isa Inlier by macro-textural features is of limited value, particularly in relation to fine-grained stratiform lead-zinc mineralisation. In general, only the coarser-grained disseminated mineralisation gives rise to recognisable casts and boxworks and, even then, pyrite is the main progenitor. Oxidation of fine-grained massive pyrite (pyrrhotite)-galena-sphalerite mineralisation results in the in-situ formation of the fine-grained massive goethite and hematite, and with possible subsequent flooding by solution-deposited iron oxides and silica, the textures are usually difficult to quantify; furthermore, as noted by Zimmerman (1964), prior experience is needed.

Some of the most distinctive textures are often gangue and wall-rock minerals, e.g. casts and boxworks after fayalite. If these minerals are known to be associated with the mineralisation, the textures and casts may be diagnostic. Generally, however, shales, carbonaceous shales, dolomitic shales, BIF, and gneisses seldom form diagnostic textures upon oxidation or reaction with the oxidising mineralisation.

Structure

Of greater significance is the remnant structure of the fine-grained laminated mineralisation, occurring as iron oxides with the laminations enhanced by partings or voids where sulphides have been leached from the host rocks (e.g. Fig. 8). Folding, slumping, brecciation, and other sedimentary and tectonic features are often preserved in the gossans, and may be recognised as representing economic mineralisation. However, all these features are obliterated on the surface of outcrops, where subsequent weathering, lateritisation, and solution-deposition of iron and manganese oxides and silica often form thick structureless coatings. It is only upon breaking the ferruginous rocks that diagnostic structures can be recognised. There is, of course, the problem of distinguishing between fine-grained pyrite (± pyrrhotite) with minor base metal sulphides and economic galena-sphalerite mineralisation.

Mineralogy

Optical microscopy, X-ray powder diffractometry, scanning electron microscopy, and the electron microprobe have been used to determine the mineralogy of ironstones, gossans, and the products of reactions between oxidising sulphides and wall rocks. This and other studies (Taylor & Sylvester, 1982; Taylor & Appleyard, in press; Taylor & Scott, in press) have shown that both qualitative and semi-quantitative mineralogical determinations, particularly of the commonly occurring minerals, quartz, hematite, goethite, sericite, chlorite, and kaolinite, are most effectively achieved by X-ray powder diffractometry. Specific identification of secondary minerals of lead, zinc (silver), and associated elements is more difficult, particularly if the minerals represent less than 0.5 per cent of the total volume. Distribution of elements between mineral phases and identification of rare minerals can only be determined by X-ray powder diffractometry under the most exceptional circumstances, and an electron microprobe or scanning electron microscope fitted with energy dispersive X-ray and Robinson back-scattered electron detectors (Robinson & Nickel, 1979; Nickel, 1981) was used.

X-ray powder diffractometry is of most use in the mineralogical mapping of ferruginous outcrops to delineate the extent of the gossan, to distinguish ferruginised wall rock or gangue from the gossan, and to outline the most prospective portion of the gossan. At the Venture prospect within the Answer Slate, the most prospective zone in the roughly 2 km long outcrop was outlined by the presence of Pb-bearing alunite-jarosite minerals. Similarly, the mineralisation at the northern end of the Fairmile prospect is indicated by secondary Pb-rich alunite-jarosite minerals, which, in this case, are readily recognisable in hand specimens. Of particular use to the exploration geologist is the facility with which outcrops can be compared, e.g. ironstones at Lake Moondarra differ from those at the southern end of the Mount Isa lode by having abundant carbonate and less alunite-jarosite, suggesting that they are ferruginised country rock that may have contained disseminated pyrite.

The mineralogy may also give valuable information concerning which part of the gossan profile is exposed at the surface. In a fully developed mature gossan profile, distinctive zones are recognisable (Taylor & others, 1980), the lower of which may be exposed at the surface by rapid erosion (e.g. the truncated profile at Dugald River). In these and immature gossans (e.g. Pegmont), the mineralogy (and geochemistry) may more nearly reflect the nature of the underlying mineralisation than the highly leached oxide zone.

Although not attempted in this study, semi-quantitative mineralogical data can be incorporated with geochemical data in the statistical analyses to evaluate the gossans and ironstones.

Geochemistry

In the Mount Isa Inlier, multi-element geochemistry has been shown to be an effective method of evaluating gossans associated with stratiform lead-zinc mineralisation. The assessment of a single ironstone outcrop or prospect from its Pb and/or Zn content alone may be misleading, as Zn is generally highly mobile in the oxidising environment and may move long distances from its source, while Pb is less mobile but readily scavenged by alunite and jarosite, which commonly form upon the oxidation of pyritic shales. The presence of pathfinder elements such as As, Sb, Ba, which are often less mobile than the target elements, gives added significance to anomalous values of Pb and Zn.

By far the most successful method of gossan evaluation is to compare multi-element geochemical data with that from known gossans and ironstones. This study has shown that stepwise discriminant analysis is the most effective method of evaluating the geochemical data provided that:

1. sufficient samples from known gossans and ironstones are analysed for use as test cases. In this respect, recognition of the various types of ferruginous outcrop within the Mount Isa Inlier was critical to the correct classification of unknown samples;

2. the distribution of the geochemical data must be determined, as the statistical theory of discriminant analysis assumes a multivariate normal distribution of the variables. As in other areas, the major elements tend to be normally distributed, while trace elements tend to lognormality. From the resulting histograms, cumulative frequency plots can also be constructed for the determination of threshold values (Sinclair, 1974; 1976); and

3. a range of major and trace elements must be determined for an accurate classification.

As only a few samples from shale-hosted deposits or prospects meet the high Pb and/or Zn requirements for classification as Black Star type or Dugald River type, the greatest value of the statistical classification is in distinguishing between gossans derived from pyritic-Pb-Zn horizons of the Mount Isa type and essentially barren pyrite, as at Lake Moondarra and within the Paradise Creek Formation. Similarly, within the Soldiers Cap Group, classification into Pegmont type and barren BIF type is accomplished, and in some instances shale-hosted groups identified, despite the greater degree of metamorphism (Table 12).

Stepwise discriminant analysis has correctly categorised an estimated 90 per cent of the samples collected during this study. If data on a range of gossans and ironstones are unavailable, discriminant analysis can be used to distinguish between two groups.

Other statistical techniques, such as linear correlation and factor analysis, are of little use in categorising ironstones and gossans, but do help in understanding the mechanisms of gossan formation (Taylor & Appleyard, in press). This is particularly true if semi-quantitative mineralogical data are included.

Gossan types

The physical and chemical characteristics of gossans depend on the original nature of the mineralisation, the composition of host rocks, geology, climate, and geomorphology. Of these, only the climate (both past and present) is common throughout the Mount Isa Inlier, so that there is a great diversity between all gossans and ironstones.

Because of the relatively low iron sulphide content in some of the lead-zinc mineralisation and the buffering effect of carbonate and other minerals in the wall rocks, many of the gossans are immature, in that they exhibit high levels of target and pathfinder elements and indistinct zoning within the profile. This is not true at Lady Loretta, where highly acidic conditions have caused most of the trace elements from the surface gossans to be leached out. Recent leaching has further reduced the trace element contents of outcrops, and, in most gossans, trace element levels in subcrop are significantly higher.

All gossans have been at least partially stripped, but at Dugald River rapid erosion has exposed the lowermost sulphate zone of the profile. In other areas, oxidation is to a much greater depth, owing to minimal stripping of more resistant rock types. Where the relief is greater, hydromorphic dispersion of trace elements into ferruginised wall rocks is greater, thus giving a larger target.

Minerals of the alunite-jarosite series are common, owing to the reaction between oxidising pyrite and shales. Where galena is present, secondary Pb-bearing alunite-jarosite minerals form, often with pyromorphite as the intermediate phase. In those deposits where apatite is a major constituent, phosphate may totally replace sulphate, while arsenate and other anions are minor substitutes. Other secondary lead minerals found in the gossans are coronadite and cerussite, where Mn and CO_2 levels, respectively, are high in the wall rocks. Specific zinc minerals are rare, even in those gossans with a high Zn content, most of the Zn being incorporated in the structure of, or adsorbed by, other secondary minerals.

Quartz, goethite, and hematite are the most common minerals in all gossans, the relative proportions depending on the original mineralogy, oxidising sulphide-wall rock reactions, and subsequent introduction by solution deposition, e.g. goethite formation is favoured by more acidic conditions than hematite (Wilhelm & Kosakevitch, 1978). Other minerals that are less common are kaolinite, sericite, remnant feldspar, remnant chlorite, and, in the BIF-associated gossans, magnetite and garnet. Various manganese oxides form crusts on the surface of gossans, particularly those associated with BIF, and may effectively scavenge a variety of trace elements.

This study has shown that the gossans of the Mount Isa Inlier differ from each other and that no single

technique can categorise the gossans and ironstones. Stepwise discriminant analysis of multi-element geochemical data has been shown to be the most effective technique, particularly if combined with mineralogical observations.

Acknowledgements

This study was made possible by the interest and co-operation of the management of Amoco Minerals Australia Co., Anaconda Australia Inc., Carpentaria Exploration Company Pty Ltd., CRA Exploration Pty Limited, Eastern Copper Mines N.L., Falconbridge (Australia) Pty Ltd., ICI Australia Ltd., Mines Exploration Pty Ltd., Mount Isa Mines Ltd., Newmont Proprietary Limited, Placer Exploration Ltd., Triako Mines N.L., and Union Miniere Development and Mining Corp. Ltd. who provided access to the deposits and prospects and to unpublished company data. The many geologists from each of these companies and from the Bureau of Mineral Resources were always willing to discuss the many aspects of this study and their local knowledge was of great help to us.

Our many colleagues at the North Ryde Laboratories of the Institute of Energy and Earth Resources who have prepared and analysed the samples have made an enormous contribution to this study. We thank them all most sincerely for their cheerfulness and expertise in providing the necessary data.

Discussions with John Wilmshurst, Nick Fisher, and Bill Ryall have greatly increased our understanding of gossan formation and data handling, while the manuscript has been improved as the result of suggestions by Ernie Nickel and Dave Whitford. Each of these colleagues is thanked for his help.

References

ANDREW, R. L., 1977a—Sulphide weathering and the evaluation of gossans in mineral exploration. *Minerals Science and Engineering*, 9, 119-50.

ANDREW, R. L., 1977b—Evaluation of copper-zinc gossans in southern Africa (abstract). *Transactions of the Institute of Mining and Metallurgy* (Section B), 86, 165-7.

ANDREW, R. L., 1979—The geology, mineralogy and geochemistry of selected base metal gossans in Southern Africa. *Ph.D. Thesis, Imperial College of Science and Technology, London* (unpublished).

BAKER, W. E., 1963—Hinsdalite pseudomorphous after pyromorphite, from Dundas, Tasmania. *Proceedings of the Royal Society of Tasmania*, 97, 129-32.

BAMPTON, K. F., COLLINS, A. R., GLASSON, K. R., & GUY, B. B., 1977—Geochemical indications of concealed copper mineralisation in an area northwest of Mount Isa, Queensland, Australia. *Journal of Geochemical Exploration*, 8, 169-88.

BLANCHARD, R., 1944—Chemical and mineralogical composition of twenty typical 'limonites'. *American Mineralogist*, 29, 111-4.

BLANCHARD, R., 1968—Interpretation of leached outcrops. *Nevada Bureau of Mines, Bulletin* 66.

BULL, A. J., & MAZZUCCHELLI, R. H., 1975—Application of discriminant analysis to the geochemical evaluation of gossans. *In* ELLIOT, I. L., & FLETCHER, W. L. (editors), Geochemical exploration 1974. *Elsevier, Amsterdam*, 219-26.

BUTT, C. R. M., & SMITH, R. E., 1980—Conceptual models in exploration geochemistry, 4—Australia. *Elsevier, Amsterdam.*

CLEMA, J. M., & STEVENS-HOARE, N. P., 1973—A method of distinguishing nickel gossans from other ironstones on the Yilgarn Shield, Western Australia. *Journal of Geochemical Exploration*, 2, 393-402.

DERRICK, G. M., 1972—Geochemistry of gossans from the Mount Isa-Cloncurry region, northwest Queensland (abstract). *Geological Society of Australia, Joint Specialist Groups Meeting, Canberra*, B7-8.

DIXON, W. J. (editor), 1970—BMD Biomedical computer programs. (2nd edition). *University of California Press.*

GLASSON, K. R., 1973—A study of anomalous copper-lead-zinc values in relation to rock types and weathering profiles in an area north of Mount Isa. *Proceedings of the Australasian Institute of Mining and Metallurgy Western Australian Conference*, 27-40.

GREEN, D. C., GREGORY, P., & COOPER, W., 1972—Red rock and gossan geochemistry, Duchess-Malbon River area, N.W. Queensland (abstract). *Geological Society of Australia, Joint Specialist Groups Meeting, Canberra*, B5-7.

GRONDIJS, H. F., & SCHOUTEN, C., 1937—A study of the Mount Isa ores. *Economic Geology*, 32, 407-50.

GULSON, B. L., & MIZON, K. J., 1979—Lead isotopes as a tool for gossan assessment in base metal exploration. *Journal of Geochemical Exploration*, 11, 299-320.

HUNTER, M. J., 1980—Esperanza Z2 Cu deposit, Mt Isa Belt, Qld. *In* BUTT, C. R. M., & SMITH, R. E. (editors). Conceptual models in exploration geochemistry, 4—Australia. *Elsevier, Amsterdam*, 163-6.

JOYCE, A. S., & CLEMA, J. M., 1974—An application of statistics to the chemical recognition of nickel gossans in the Yilgarn Block, Western Australia. *Proceedings of the Australasian Institute of Mining and Metallurgy*, 252, 21-4.

LOCSEI, J., 1977—Pegmont: a stratiform lead-zinc deposit in the Precambrian of northwest Queensland. *Proceedings of the Australasian Institute of Mining and Metallurgy*, 262, 25-7.

LOUDON, A. G., LEE, M. K., DOWLING, J. F., & BOURN, R., 1975—Lady Loretta silver-lead-zinc deposit. *In* KNIGHT, C. L. (editor), Economic geology of Australia and Papua New Guinea. Volume 1—Metals. *Australasian Institute of Mining and Metallurgy, Monograph* 5, 377-82.

MATHIAS, B. V., & CLARK, G. J., 1975—Mount Isa copper and silver-lead-zinc orebodies—Isa and Hilton Mines. *In* KNIGHT, C. L. (editor), Economic geology of Australia and Papua New Guinea. Volume 1—Metals. *Australasian Institute of Mining and Metallurgy, Monograph* 5, 351-72.

MATHIAS, B. V., CLARK, G. J., MORRIS, D., & RUSSELL, R. E., 1973—The Hilton deposit—stratiform silver-lead-zinc mineralisation. *In* FISHER, N. H. (editor), Metallogenic provinces and mineral deposits in the southwestern Pacific. *Bureau of Mineral Resources, Australia, Bulletin* 141, 33-58.

MOESKOPS, P .G., 1977—Yilgarn nickel gossan geochemistry —a review with new data. *Journal of Geochemical Exploration*, 8, 247-58.

NICKEL, E. H., 1981—The application of the scanning electron microscope in gossan research. *Bulletin Mineralogie*, 104, 292-7.

NIE, N. H., HULL, C. H., JENKINS, J. G., STEINBRENNER, K., & BENT, D. H., 1975—Statistical package for the social sciences. (2nd edition). *McGraw-Hill, New York.*

NISBET, B., & JOYCE, P., 1980—Squirrel Hills Zn-mineralisation, Mt Isa Belt, Qld. *In* BUTT, C. R. M., & SMITH, R. E. (editors), Conceptual models in exploration geochemistry, 4—Australia. *Elsevier, Amsterdam*, 169-74.

ORRIDGE, G. R., 1980—The Pegmont Pb-Zn deposit, Mt Isa Belt, Qld. *In* BUTT, C. R. M., & SMITH, R. E. (editors), Conceptual models in exploration geochemistry, 4—Australia. *Elsevier, Amsterdam*, 166-9.

PLUMB, K. A., DERRICK, G. M., & WILSON, J. H., 1980—Precambrian geology of the McArthur River-Mount Isa region, Northern Australia. *In* HENDERSON, R. A., & STEPHENSON, P. J. (editors), The geology and geophysics of northeastern Australia. *Geological Society of Australia, Queensland Division,* 71-88.

ROBINSON, B. W., & NICKEL, E. H., 1979—A useful new technique for mineralogy: the backscattered electron/low-vacuum mode of SEM operation. *American Mineralogist,* 64, 1322-8.

ROSSITER, A. G., 1980—The Cloncurry 8 Cu anomaly, Mt Isa Belt, Qld. *In* BUTT, C. R. M., & SMITH, R. E. (editors), Conceptual models in exploration geochemistry, 4—Australia. *Elsevier, Amsterdam,* 249-52.

RUSSELL, R. E., 1978—The Mount Novit Pb-Zn-Ag deposit —variations on a Mount Isa theme (abstract). *Third Australian Geological Convention, Townsville.*

RYALL, W. R., & TAYLOR, G. F., 1981—Gossan evaluation manual for use in the Kingdom of Saudi Arabia. *Ministry of Petroleum and Mineral Resources, Jiddah, Technical Record* RF-TR-01-3 (copies available from G. F. Taylor).

SCOTT, K. M., & TAYLOR, G. F., 1977—Geochemistry of the Mammoth copper deposit, northwest Queensland, Australia. *Journal of Geochemical Exploration,* 8, 153-68.

SCOTT, K. M., & TAYLOR, G. F., 1979a—Analyses of samples from DDHs P70E, V69E and M14E, Mount Isa Mines. *CSIRO Minerals Research Laboratories* (unpublished report).*

SCOTT, K. M., & TAYLOR, G. F., 1979b—Exploration geochemistry research, Soldiers Cap Group, Queensland, V —Composition of garnets and secondary minerals. *CSIRO Institute of Earth Resources* (unpublished report).*

SCOTT, K. M., & TAYLOR, G. F., 1980—Implications of sulfide geochemistry for exploration in the Agate Downs area, N.W. Queensland. *CSIRO Institute of Earth Resources* (unpublished report).*

SINCLAIR, A. J., 1974—Selection of threshold values in geochemical data using probability graphs. *Journal of Geochemical Exploration* 3, 129-49.

SINCLAIR, A. J., 1976—Applications of probability graphs in mineral exploration. *The Association of Exploration Geochemists Special Volume* No. 4.

SMITH, R. E., 1979—Exploration geochemical methods for the Bangemall Basin, Western Australia. *In* GLOVER, J. E., GROVES, D. I., & SMITH, R. E. (editors), Pathfinder and multi-element geochemistry in mineral exploration. *University of Western Australia, Extension Service Publication* 4, 83-98.

SMITH, R. E., MOESKOPS, P. G., & NICKEL, E. H., 1979—Multi-element geochemistry at the Golden Grove Cu-Zn-Pb-Ag deposit. *In* GLOVER, J. E., GROVES, D. I., & SMITH, R. E. (editors), Pathfinder and multi-element geochemistry in mineral exploration. *University of Western Australia, Extension Service Publication* 4, 30-41.

SMITH, W. D., 1965—The broader aspects of secondary mineralisation at Mount Isa, Queensland. *Proceedings of the Australasian Institute of Mining and Metallurgy,* 217, 33-8.

STANTON, R. L., & VAUGHAN, J. P., 1979—Facies of ore formation: a preliminary account of the Pegmont deposit as an example of potential relations between small 'iron formations' and stratiform sulphide ores. *Proceedings of the Australasian Institute of Mining and Metallurgy,* 270, 25-38.

TAYLOR, G. F., 1973—The geochemistry of siderite in relation to ironstone in the Paradise Creek Formation, northwest Queensland. *Journal of Geochemical Exploration,* 2, 367-82.

TAYLOR, G. F., 1979—Pathfinder-element geochemistry in base-metal exploration, northwest Queensland. *In* GLOVER, J. E., GROVES, D. I., & SMITH, R. E. (editors), Pathfinder and multi-element geochemistry in mineral exploration. *University of Western Australia, Extension Service Publication* 4, 60-82.

TAYLOR, G. F., WILMSHURST, J. R., BUTT, C. R. M., & SMITH, R. E., 1980—Gossans and ironstones. *In* BUTT, C. R. M., & SMITH, R. E. (editors), Conceptual models in geochemical exploration, 4—Australia. *Elsevier, Amsterdam,* 118-22.

TAYLOR, G. F., & SYLVESTER, G. C., 1982—Analysis of a weathered profile on sulphide mineralisation at Mugga Mugga, Western Australia. *Journal of Geochemical Exploration,* 16, 105-34.

TAYLOR, G. F., & APPLEYARD, E. C. (in press)—Weathering of the zinc-lead lode, Dugald River, northwest Queensland. I. The gossan profile. *Journal of Geochemical Exploration.*

TAYLOR, G. F., & SCOTT, K. M. (in press)—Weathering of the zinc-lead lode, Dugald River, northwest Queensland. II. Surface mineralogy and geochemistry. *Journal of Geochemical Exploration.*

TRAVIS, G. A., KEAYS, R. R., & DAVISON, R. M., 1976—Palladium and iridium in the evaluation of nickel gossans in Western Australia. *Economic Geology,* 71, 1229-43.

TWIDALE, C. R., 1956—Chronology of denudation in northwest Queensland. *Bulletin of the Geological Society of America,* 67, 867-82.

WHITCHER, I. G., 1975—Dugald River zinc-lead lode. *In* KNIGHT, C. L. (editor), Economic geology of Australia and Papua New Guinea. Volume 1—Metals. *Australasian Institute of Mining and Metallurgy, Monograph* 5, 372-6.

WILHELM, E., & KOSAKEVITCH, A., 1978—Chapeaux de fer rapport de synthese. *Bureau de Recherches Geologiques et Minieres, Orleans.*

ZIMMERMAN, D. O., 1964—Gossans at Northern Leases, Mount Isa, as visible geochemical anomalies. *In* WOODCOCK, J. T., MADIGAN, R. T., & THOMAS, R. C. (editors), *8th Commonwealth Mining and Metallurgical Congress, Publications,* 6, 359-67.

* CSIRO unpublished reports are available at the Division of Mineralogy, North Ryde.

BMR Journal of Australian Geology & Geophysics, 7, 181–196

REGIONAL METAMORPHISM IN THE SELWYN RANGE AREA, NORTHWEST QUEENSLAND

A. L. Jaques[1], D. H. Blake[1], & P. J. T. Donchak[2]

The Selwyn Range, which lies at the eastern margin of the Mount Isa Inlier, consists of pelitic, psammitic, and calcareous sedimentary and basic igneous rocks, which have been intruded by granite plutons and regionally metamorphosed to amphibolite grade. Three metamorphic zones, based mainly on pelitic assemblages, have been recognised in the main prograde sequence: a lower grade (biotite) zone equivalent to uppermost greenschist/lower amphibolite facies, an andalusite-almandine-staurolite zone of amphibolite grade, and an eastern upper amphibolite grade zone (sillimanite and sillimanite-K-feldspar). Superimposed on the prograde sequence is a variable retrograde assemblage related to later folding. Regional metamorphic isograds are unrelated to the granitoids, which include both pre-tectonic or syn-tectonic and post-tectonic types. Comparisons with experimentally determined reactions and calculations from various geobarometers for higher grade rocks indicate metamorphic pressures of 3–4 kb (300–400 MPa). Cation exchange equilibria (mainly garnet-biotite) and experimentally determined dehydration reactions indicate equilibration temperatures of ~450–680°C for the prograde sequence; the staurolite and almandine isograds are estimated to be at ~550°C, the sillimanite isograd ~600°C, and the K-feldspar isograd ~660°C.

Introduction

The Mount Isa Inlier consists of Proterozoic igneous and sedimentary rocks which have been subjected to several periods of deformation and metamorphism. The grade of the metamorphism is generally stated to be of greenschist to amphibolite facies (e.g. Carter & others, 1961), but few detailed studies of the metamorphic rocks have been made. In this paper we present a petrologic study of regionally metamorphosed sedimentary and basic igneous rocks in the Selwyn Range area in the southeastern part of the Mount Isa Inlier, with the aim of defining more closely the grade of metamorphism. The observed mineral assemblages indicate prograde metamorphism ranging from upper greenschist/lower amphibolite to uppermost amphibolite facies. Various geothermometers and geobarometers have been used to estimate the P-T conditions during this metamorphism and during subsequent retrograde events.

The study is based on samples collected during regional mapping of the Selwyn Range area in 1978–79, undertaken as part of BMR's program to provide geological maps at 1:100 000 scale of the Mount Isa Inlier. Petrographic summaries are given in the data records accompanying the preliminary maps by Blake & others (1979) and Donchak & others (1979). About forty rocks were examined by electron microprobe following the energy-dispersive method of Reed & Ware (1975) and Ware (1981). Chemical analyses of selected samples of the various rock types will be presented in a report on the geochemistry of rocks from the Mount Isa region (Wyborn, in preparation). Additional analyses are given in Walker & others (1960), Glikson & others (1976), Glikson & Derrick (1978), and Rossiter & Ferguson (1980). Notations used in this paper are given in an appendix. All samples have BMR numbers and the prefix 7853.

Regional geology

The Selwyn Range lies to the south of Cloncurry and forms part of the eastern sedimentary-volcanic succession of Plumb & others (1980), comprising an easternmost sequence of dominantly pelitic and psammitic sediments with minor basic volcanics (Soldiers Cap Group), a central belt of dominantly calcareous and calc-magnesian silicate (calc-silicate) rocks (Doherty Formation), and a western belt of psammitic sediments and volcanics (acid and basic) with subordinate pelitic and calcareous rocks (Tewinga, Malbon, and Mary Kathleen Groups). All formations have been extensively intruded by granitoids (Fig. 1). Recent U-Pb zircon and Rb-Sr dating indicates that the rocks probably range in age from about 1770–1720 m.y. or younger, and were regionally metamorphosed between 1670 and 1490 m.y. ago (Page, 1978, in preparation). Details of the regional geology have been given by Blake & others (1979) and Donchak & others (1979). Blake (1980) re-examined the stratigraphy of the Mount Isa region, proposing alternative correlations to those of Carter & others (1961) and Plumb & others (1980).

The Proterozoic formations are regionally metamorphosed, and are tightly to isoclinally folded about northerly trending fold axes. Two main, and one minor, phases of folding have been recognised. The first recognised folds (F_1) are isoclinal with mainly subvertical axial planes, and represent the most intense deformation in the area. S surfaces associated with this deformation event (D_1) range from fracture cleavages to well-developed axial-plane foliations defined by alignment of mica, amphibole, or sillimanite. Second generation (F_2) folds related to a later deformation (D_2) are generally tight to open, north to northeasterly plunging structures, and in pelitic rocks are represented by small crenulations of the S_1 foliations and the development of lineations (mainly mica and chlorite). Folds associated with a third deformation event (D_3) are open, southeasterly trending structures, and are only evident in the outcrops of Soldiers Cap Group pelites in the far northeast. The similarity of the F_1 and F_2 folds in all units suggests that all the Precambrian formations have undergone the same two deformations, D_1 and D_2 (Donchak & others, 1979). The prograde metamorphic assemblages relate to the dominant metamorphic episode M_1 and are associated with the main (D_1) deformation event .

Recent geological mapping (Blake & others, 1979; Donchak & others, 1979) and geochemical studies (L. A. Wyborn, 1981; personal communication, 1982) have shown that the granites of the Selwyn Range

[1] Bureau of Mineral Resources, P.O. Box 378, Canberra City, ACT 2601.
[2] Geological Survey of Queensland, G.P.O. Box 194, Brisbane, Qld 4001.

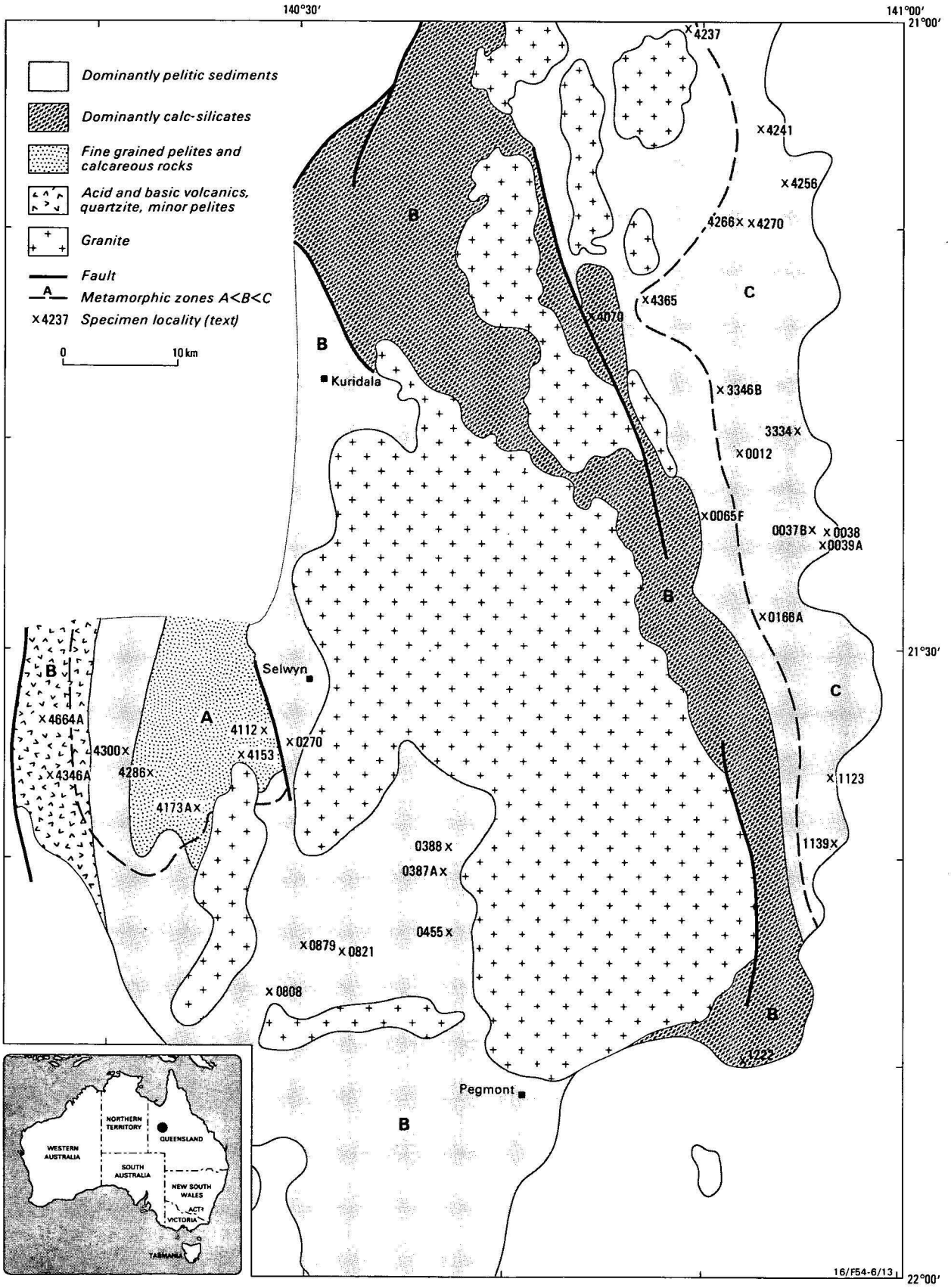

Figure 1. Simplified geological map of Selwyn Range area showing distribution of metamorphic zones.

area (the Williams Granite of Carter & others, 1961; Joplin & Walker, 1961) include at least two types. Some granitoids are post-metamorphic or, possibly, late syn-metamorphic, since they cut F_1 and F_2 structures and contain xenoliths of country rock amphibolite, gneiss, calc-silicate rocks, and schist. Others are syn-tectonic or pre-tectonic; they are foliated parallel to S_1, have irregular contacts with the country rocks (commonly 'lit-par-lit' type), and associated pegmatitic and aplitic veins are tightly folded. Most granites, however, show some petrographic evidence of metamorphic recrystallisation; the relationship of the granites to D_2 and D_3 is not known. Some of the late syn-metamorphic or post-metamorphic granites have narrow contact aureoles of hornfels, in which cordierite, andalusite, or sillimanite are locally developed.

Metamorphic zoning

Three prograde regional metamorphic zones, designated A, B, and C (Fig. 1), and defined mainly on the basis of mineral assemblages in pelitic rocks, roughly parallel the regional foliation and dominant fold trends. Metamorphic grade increases both to the west and east from a lower grade zone in the southwest of the area, with the highest grade rocks being in the east (zone C, Fig. 1). Typical mineral assemblages in each of the three zones are summarised in Table 1.

Zone A rocks—mainly weakly metamorphosed slate, siltstone, and limestone with some marble, phyllite, and fine mica schist—are equivalent to the biotite grade of the upper greenschist facies. Primary sedimentary and igneous structures and textures, including cross-bedding, convolute bedding, ripple marks, and slump structures in clastic sediments and subophitic textures in metadolerites, are well preserved.

Zone B rocks are more recrystallised than those of zone A, typically have a pronounced schistose fabric, and include porphyroblastic mica schist, granular-textured calc-silicate rocks and amphibolite. The boundary between zones A and B is taken to be the first appearance of staurolite, andalusite, or almandine in pelitic rocks, the first appearance of diopside in calcareous rocks, and the coexistence of the assemblage green hornblende ± oligoclase (An_{17} or higher) in basic rocks (Table 2). While these isograds do not coincide exactly, they are sufficiently close to enable division into the three zones at this scale. The staurolite-grade and almandine-grade rocks of zone B are equivalent to the lower middle amphibolite facies.

Zone C, defined by the presence of sillimanite in pelitic rocks, is restricted to the easternmost part of the area, where it forms a belt up to 12 km wide. Metabasites in this zone contain green-brown amphibole and some contain clinopyroxene or garnet. All rocks in the zone are strongly recrystallised, mostly to coarse porphyroblastic mica schist and granoblastic gneiss. Primary structures and textures are generally only poorly preserved. Veins (commonly pegmatitic) of qz+kfs+ab (± tour, mu) are common in pelitic and psammitic sequences, and are thought to represent anatectic melts.

Pelitic and psammitic rocks

Protolith compositions

The pelites and psammites consist of metamorphosed shale, siltstone, greywacke, quartz sandstone, and arkose. Many of the pelites in zones B and C (Soldiers Cap Group and Kuridala Formation) are richer in Al_2O_3 and poorer in MgO (<2 wt%) than typical pelites, whereas most of those in zone A are relatively poor in Al_2O_3 and many are calcareous. Staurolite-bearing metapelites typically have Mg/(Mg+Fe) ratios of 0.2–0.35. Strata richer in Fe, including banded iron formations, are common in the east and south. At one such locality in the south, Pegmont prospect, banded iron formation with associated Pb-Zn mineralisation contains fayalite, garnet, hornblende, grunerite, clinopyroxene, and greenalite (Stanton & Vaughan, 1979).

Mineralogy

Muscovite. Muscovite and biotite occur in rocks of appropriate composition in all three zones, typically defining S_1. In low-grade rocks muscovite forms porphyroblasts and fine aggregates interstitial to quartz and feldspar. It shows a range in composition (27–35% Al_2O_3, 0.3–1% Na_2O, 1–4.5% total Fe as FeO) and exhibits limited solid-solution towards phengite. In higher grade rocks it has low Fe and high Al_2O_3 contents, and approximates the ideal muscovite composition with two octahedral cations. The distribution coefficient for Fe-Mg exchange between muscovite and biotite, $K_{D\ mu\text{-}bi}^{Fe\text{-}Mg}$, lies in the range 0.7–1 and does not appear to change with metamorphic grade. Retrograde sericitic muscovite commonly replaces aluminosilicate minerals, especially sillimanite; the sericite is discordant to S_1 and commonly forms a crenulation foliation, S_2. The retrograde muscovite is generally more Mg-rich, and has a higher Na/(Na+K) ratio and X_{A1} than prograde muscovite (Table 2).

Biotite. In zone A biotite forms green-brown lepidoblastic flakes elongated parallel to cleavage-bedding traces, whereas in higher-grade gneissic rocks it is red-brown and more equidimensional. Retrograde biotite defines an S_2 foliation oblique to S_1 along the limbs of small scale F_2 crenulations. Biotite compositions change from Mg-rich varieties with low Al_2O_3 content (Mg_{80}, 14–15% Al_2O_3) at low grade to more Fe and Al-rich compositions ($M_{30\text{-}40}$, 18–20% Al_2O_3) at higher grade. The Mg/(Mg+Fe) ratio of biotite is greater than that of coexisting staurolite and almandine, as is typical of equilibrated assemblages. $K_{D\ st\text{-}bi}^{Fe\text{-}Mg}$ decreases with increasing grade from ~4 near the staurolite isograd to ~3 near the staurolite-out reaction boundary. Similarly, $K_{D\ ga\text{-}bi}^{Fe\text{-}Mg}$ also decreases with increasing metamorphic grade. Retrograde biotite typically has higher Mg and lower Ti and Al contents than prograde biotite (Table 2).

Staurolite. Staurolite occurs as porphyroblasts, commonly containing numerous inclusions of quartz, in Fe-rich metapelites and metagreywackes in zone B. Analyses show a slight deficiency in Si compared with the ideal unit cell formula of $H_2Fe_4^{2+}Al_{18}Si_8O_{48}$, and significant amounts of Zn and TiO_2 (up to 0.5 wt%).

Chlorite. Prograde chlorite is present in zone A rocks and is also sporadically developed in the lower part of zone B. At one locality in zone B, qz+bi+mu+ga+ab

Table 1. Summary of petrography: dominant mineral assemblages in zones according to rock type.

Pelitic	*Psammitic*	*Calcareous**	*Basic*
Zone A			
qz + mu ± chl qz + mu + bi ± fs (+ tour, Fe-oxide, pyrite, graphite)	qz + fs + mu ± bi (± tour, Fe-oxide)	qz + cc + hm qz + mu + bi + cc ± epi qz + ab + cc + chl ± epi qz + dol ± mu qz + fs + tr + cc ± chl ± mu	qz + ab + epi + chl + act ± blue/green hbl + sph ± bi ± cc ab + epi + gr + cc
Zone B			
qz + mu + bi ± fs qz + mu + bi + and ± fs ± chl qz + mu + bi + ga ± and qz + mu + bi + st ± and qz + mu + bi + st + ga (± mag, ilm)	qz + fs ± mu ± bi qz + bi + mu + ga ± fs (± ap, Fe-Ti oxide, zircon, tour)	pl — hbl ± scap ± qz ± sph ab + hbl + cpx ± scap ± qz ± kfs (± epi, ap, ilm, mag)	pl (oligoclase) + green hbl + epi + ilm ± qz ± act pl + green hbl + cpx + ilm ± qz (± epi, cc, ap, kfs, bi)
Zone C			
qz + bi + mu ± fs qz + bi + mu + ga ± fs qz + bi + mu + si ± ga ± fs qz + bi + kfs + si ± ga (± mag, ilm)	qz + fs ± mu ± bi qz + fs + ga ± mu qz + pl + kfs + bi + si	qz + pl + green hbl + cpx + sph qz + pl + green hbl + cpx + gr (± ap, epi, mag)	pl (An_{20-35}) + green/brown hbl + sph ± ilm ± qz pl (An_{35-68}) + green/brown hbl ± cpx ± ilm ± mag pl (An_{40-95}) + green/brown hbl ± cpx ± ga + ilm ± mag

* This group includes calcareous pelites, calc-magnesian silicates etc. (see text).

Table 2. Compositions of coexisting phases in pelitic and psammitic rocks.

	Ga				*Bi*			*Pl*		*Kfs*		*Mu*			*St*	
Sample	*Mg*	X_{Ca}	X_{Mn}	X_{Fe}	*Mg*	X_{Ti}	X_{Al}	X_{Ca}	X_{Na}	X_K	X_{Na}	*Mg*	*Na/(Na+K)*	X_{Al}	*Mg*	Al_2SiO_5
Zone B																
0879	9.8	0.038	0.026	0.884	39.3	0.029	0.173	—		—		43.8	0.139	0.947	14.8	—
	(8.7	0.035	0.026	0.857)	(39.9	0.032	0.167)					(41.8	0.151	0.952)		
0387A	8.4	0.013	0.088	0.823	34.0	0.035	0.137	0.019	0.977	—		42.7	0.161	0.948	—	—
	(7.2	0.017	0.092	0.827)	(35.3	0.036	0.143)									
0388	8.1	0.017	0.054	0.853	32.6	0.040	0.148	—		—		36.2	0.114	0.942	—	A
	(7.8	0.015	0.089	0.826)	(38.1	0.037	0.159)					(44.2	0.176	0.956)		
4237	8.7	0.010	0.016	0.889	32.7	0.029	0.150	—		—		38.6	0.189	0.945	13.9	A
Zone C																
4241	11.8	0.087	0.049	0.762	40.6	0.039	0.123	0.654	0.340	—			—		—	A
	(7.8	0.106	0.055	0.773)	(41.2	0.041	0.118)									
3346B	11.8	0.063	0.111	0.728	40.0	0.048	0.186	—		—		50.1	0.078	0.915	—	S(A)
	(9.8	0.070	0.167	0.689)	(40.9	0.045	0.224)									
0039A	10.8	0.007	0.049	0.841	35.8	0.085	0.146	0.057	0.931	0.926	0.065	36.3	0.053	0.905	—	S
	(10.7	0.006	0.049	0.843)	(43.0	0.044	0.184)									
4256	12.0	0.033	0.072	0.787	36.9	0.035	0.200	—		—		40.6	0.149	0.921	—	S
	(10.4	0.024	0.070	0.811)	(39.3	0.035	0.249)									
3334	11.9	0.153	0.142	0.621	36.3	0.059	0.076	0.358	0.633	—			—		—	—
	(11.5	0.154	0.140	0.625)	(37.3	0.059	0.094)									

Compositions given in parenthesis refer to retrograde assemblages (S_2, S_3). For garnet: X_i = i/(Fe+Mn+Mg+Ca); for biotite and muscovite: X_i = i/(Ti+Al^{VI}+Fe+Mn+Mg). A = Andalusite, S = sillimanite.

schist associated with andalusite-bearing metapelites contains Fe-rich, strongly zoned (Mg_{27-37}) chlorite: the most Mg-rich chlorite has a higher Mg/Fe ratio than coexisting almandine and biotite, suggesting equilibration at almandine grade. Retrograde chlorite, most commonly replacing almandine, is generally discordant to S_1, and probably related to D_2 or D_3.

Garnet. Almandine, generally as porphyroblasts, occurs in metapelites and some psammitic rocks (e.g. garnetiferous quartzite etc.) of zones B and C. Apart from the more Ca-Mn-rich garnets in a calcareous metarenite, the garnets have very low CaO and MgO contents ($X^{ga}_{Alm} \geqslant 0.8$, Table 2) and are commonly zoned with respect to Fe and Mg, rims being up to 4 mol % more almandine-rich than the cores in some higher grade rocks. $K^{Fe\text{-}Mg}_{D\ ga\text{-}bi}$ decreases with increasing metamorphic grade, from ~6 in zone B to ~3 in zone C. Relict garnet and garnet rims that equilibrated with S_2 (or S_3) biotite have higher K_D (~6–7), consistent with re-equilibration at lower temperature.

Andalusite. Andalusite porphyroblasts, commonly poikilitic, are widespread in zone B pelites. Microprobe analyses show little deviation from the ideal Al_2SiO_5 formula, apart from minor amounts of Fe and Mg (<0.25% Fe as FeO, MgO).

Sillimanite. Sillimanite forms prismatic aggregates (clusters of which resemble nodular porphyroblasts after former andalusite) and felted fibrolitic aggregates in zone C pelites. Sillimanite is the stable aluminosilicate phase in zone C, but andalusite occurs with sillimanite (commonly in aggregates) over a narrow interval near the boundary with zone B. Fibrolitic sillimanite also occurs in contact aureoles of some granite plutons. Sillimanite is commonly replaced by retrograde sericite.

Cordierite. Regional metamorphic cordierite is found only in K-poor, highly magnesian rocks (dolomitic marls?), commonly with anthophyllite and, in places, garnet (Carter & others, 1961). Cordierite in pelitic rocks is confined to the contact aureoles of granitoids; typical assemblages are cd+bi+and+kfs and cd+bi+si+kfs.

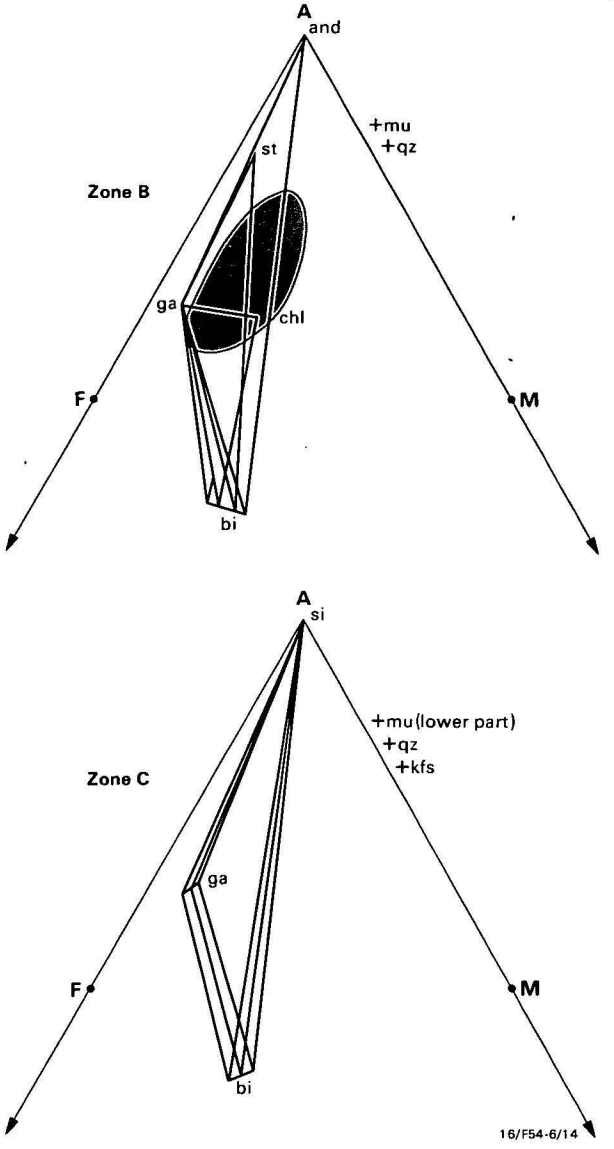

Figure 2. AFM diagrams (Thompson, 1957) for pelitic assemblages in zones B and C.
Stippled field represents approximate compositional range of Selwyn pelites.

Mineral parageneses

The prograde mineral assemblages of the pelitic rocks are shown on the AFM diagrams (Fig. 2) in the KFMASH system (J. B. Thompson, 1957; A. B. Thompson, 1976). The dominant assemblage in zone A is qz+mu+bi (± minor phengite, chl).

In zone B formation of almandine may have taken place by reactions involving chlorite and quartz, such as the discontinuous reaction (1) chl+ qz → ga + H_2O (e.g. Hsu, 1968) or, more likely, by continuous reactions, such as (2) chl + $bi_{(1)}$ + qz → ga + $bi_{(2)}$ + H_2O. Andalusite may have formed by analogous reactions involving chlorite and muscovite, such as (3) chl + mu + qz → and + bi + H_2O. On the other hand, the close spatial association of the andalusite and almandine isograds, together with the Fe-rich nature of chlorite coexisting with almandine, suggests the reaction (4) Fe-rich chl + mu + qz → ga + bi + and + H_2O. Formation of staurolite with the typical parageneses st+ga+bi and st+and+bi probably proceeded by the continuous reaction (5) chl + mu → st + bi + qz + H_2O rather than reactions involving garnet, such as (6) chl + mu + ga → st + bi + qz + H_2O, since petrographic evidence of significant breakdown of garnet at or near the staurolite isograd is lacking. Chlorite appears to have been consumed in most pelites in the lower part of zone B, and, over most of the zone, reaction of staurolite-bearing assemblages may have been continuous, e.g. (7) st + mu + qz → bi + Al_2SiO_5 + H_2O, as suggested by the trend towards Fe-end members (Fig. 3). This trend is consistent with the T-X_{Mg} variation described by Thompson (1976). The upper stability of staurolite is limited by the reactions (8) st + mu + qz → Al_2SiO_5 + ga + bi + H_2O, and (9) st + qz → Al_2SiO_5 + ga + H_2O. Staurolite appears to have broken down in the andalusite rather than the sillimanite field, since staurolite and sillimanite do not coexist and the four phase assemblage st+and+ga+bi

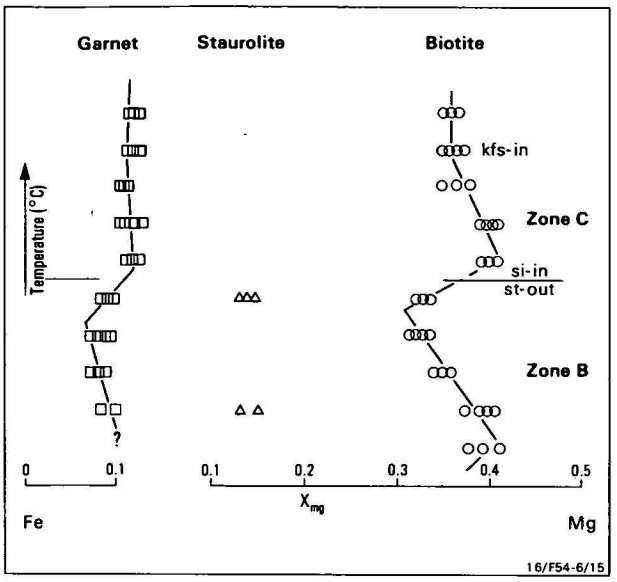

Figure 3. Variation in prograde mineral X_{Mg} with increasing metamorphic grade for Selwyn pelites.
Compare with schematic isobaric T-X_{Mg} loops for discontinuous reactions (e.g. Thompson, 1976; Yardley & others, 1980).

(+mu,qz) occurs near but below the sillimanite isograd. Reaction (8) is discontinuous, but reaction (9) causes staurolite to become increasingly magnesian as it breaks down (Yardley & others, 1980). Although the four phase assemblage shows petrographic evidence of almandine growth (with staurolite decomposition), the reversal of the Fe-Mg trend at the staurolite-out boundary (Fig. 3) suggests that reaction (9) may have been significant.

In zone C, andalusite persists into the sillimanite zone over a short interval before being replaced by sillimanite. Typical parageneses in zone C are qz+mu+bi +ga+si and qz+kfs+si+bi±ga. Above the staurolite zone, reaction may have been largely by (10) ga + mu → bi + si + qz. Muscovite coexists with quartz in the lower part of the sillimanite zone, but not at higher grade in the easternmost gneisses, where the sillimanite-K-feldspar (or 'second sillimanite') isograd is reached. The muscovite breakdown reaction, (11) mu + qz → kfs + si + H_2O, is commonly regarded as defining the boundary between medium and high grade metamorphism (e.g. Winkler, 1979). Mineral pairs in the upper part of zone C show little Fe-Mg variation (Fig. 3), suggesting cation exchange reactions were dominant.

Calcareous rocks

Protolith compositions

The calcareous rocks range from impure limestone to calcareous pelite to calc-silicate rocks, which make up the bulk of the extensive Doherty Formation. The calc-silicate rocks include both finely laminated and brecciated types, and consist predominantly of calcic-amphibole and diopsidic-pyroxene-bearing assemblages. Chemical analyses typically show up to 20% CaO + MgO, moderate SiO_2 and Al_2O_3 contents (50–60% SiO_2, 8–13% Al_2O_3), and comparatively high alkali contents (up to 5% Na_2O, 4% K_2O); those with moderate or high TiO_2 (and Zr, Y etc) contents may be carbonated basic rocks. Those with very high MgO contents (up to 12%), and correspondingly high MgO/FeO ratios are probably metamorphosed dolomitic marls or silts, whereas those richer in SiO_2 (up to 72%), poorer in MgO (<7%, commonly <2%), and poor in TiO_2, and occurring within dominantly

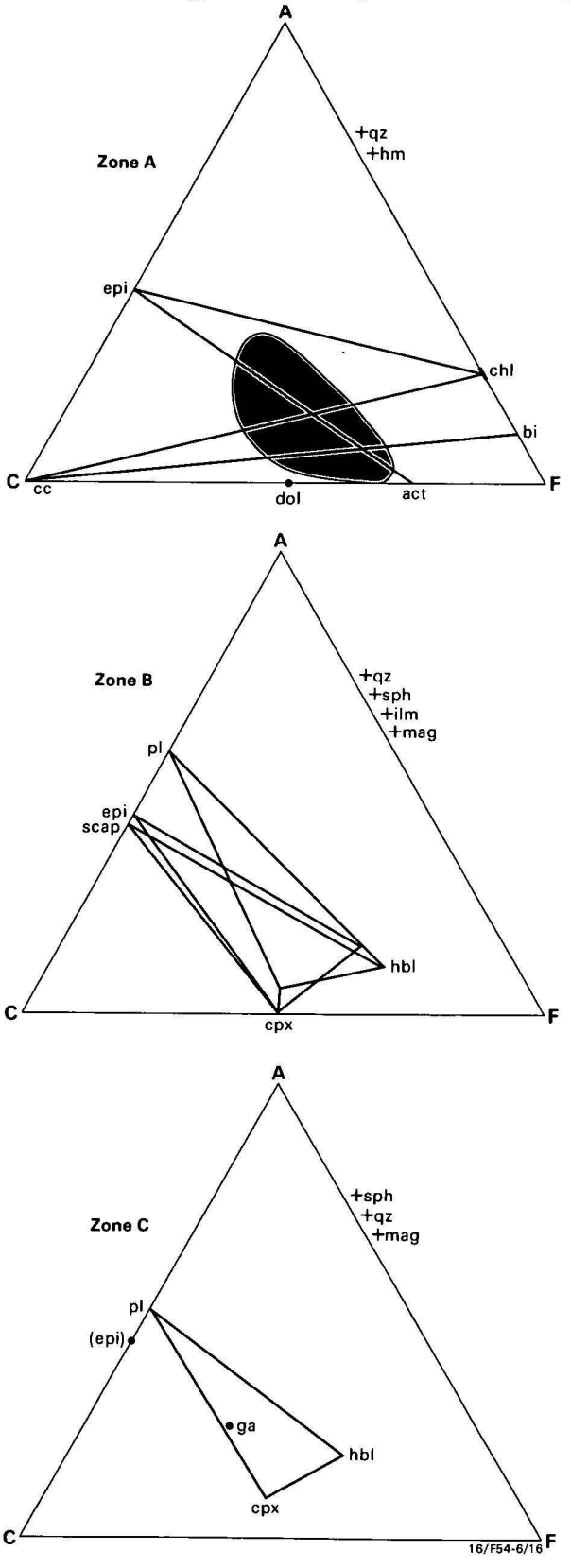

Figure 4. ACF diagrams for Selwyn calc-silicate assemblages.
Stippled area represents the field of Selwyn calc-silicates (note: field does not include limestones and marbles etc.).

pelitic sequences, represent metamorphosed calcareous shale and siltstone. Walker & others (1960) discussed the effects of metasomatism and the chemical convergence of metabasites and calc-magnesian silicates in the Mount Isa region. This convergence is shown by the overlap of some of the calc-silicate rocks with the metabasite field on the ACF diagram in Figure 4.

Mineralogy

Feldspar. Albite (An_{9-1} $Or_{2-0.5}$), but in some cases K-feldspar (microcline), occurs in most calc-silicate rocks. Highly calcic plagioclase (An_{86-90}) coexists with ga+cpx+epi+hbl in some high-grade calc-silicate gneisses with high CaO/Na_2O ratios (up to 25).

Amphibole. Amphibole is present in most of the calcareous rocks. In zone A, it is typically pale-coloured tremolite containing little Na. In zone B, the amphibole ranges from weakly pleochroic blue-green magnesiohornblende to strongly pleochroic (straw yellow to olive or turquoise green) edenitic hornblende, or Cl and K-rich ferropargasite (Table 3). Variation in composition with metamorphic grade is shown by the decrease

Table 3. Representative microprobe analyses of amphiboles in calc-silicates.

Zone	*A*	*B*	*B*	*B*	*C*
sample	*4173*	*0270*	*0455*	*1222*	*0037B*
SiO_2	54.31	49.28	36.88	44.72	36.95
TiO_2	nd	0.13	10.11	0.96	0.74
Al_2O_3	3.14	4.37	13.40	8.13	13.30
FeO	6.91	15.71	29.26	16.98	30.42
MnO	0.15	nd	1.11	nd	0.12
MgO	19.76	13.90	0.92	12.22	1.99
CaO	12.57	12.05	11.40	11.52	11.76
Na_2O	0.66	1.21	0.89	1.85	0.91
K_2O	nd	0.78	2.87	0.95	1.88
Cl	0.05	nd	2.03	0.11	0.81
Total	97.55	97.44	98.87	97.44	98.88
			Cations per 23 O		
Si	7.634	7.316	6.089	6.748	5.996
AlIV	0.366	0.684	1.911	1.252	2.004
AlVI	0.155	0.080	0.697	0.195	0.541
Ti	—	0.015	0.014	0.109	0.090
Fe	0.812	0.764	4.040	2.143	4.129
Mn	0.018	—	0.115	—	0.016
Mg	4.139	3.077	0.225	2.749	0.481
Ca	1.882	1.917	2.017	1.862	2.045
Na	0.179	0.348	0.286	0.542	0.287
K	—	0.148	0.605	0.183	0.389
Total	15.195	15.535	15.999	15.783	15.978
$\frac{100\,Mg}{(Mg+Fe)}$	83.6	80.1	5.3	56.2	10.4

nd = not detected.

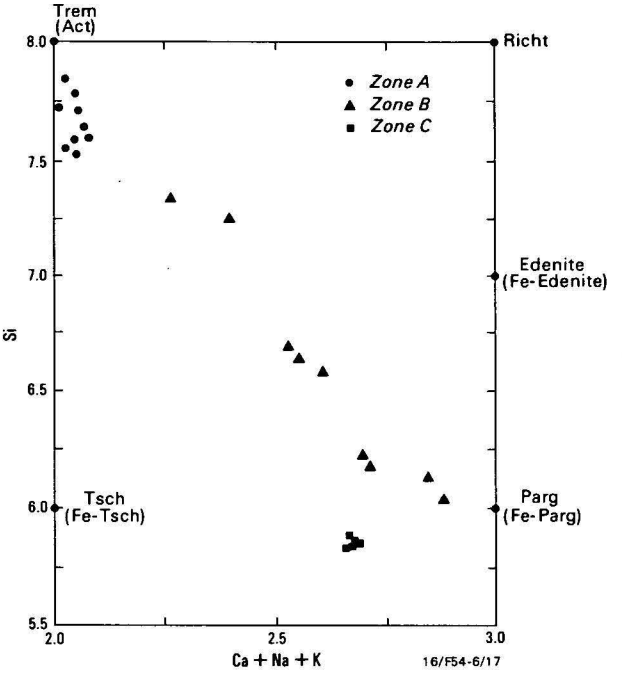

Figure 5. Variation of Ca + Na + K with Si (per 23 O) in amphiboles from calc-silicates.
Trem = tremolite, Act = actinolite, Richt = richterite, Tsch = tschermakite, Parg = pargasite.

Table 4. Representative microprobe analyses of clinopyroxenes in calc-silicates and metabasites.

	Calc-silicates				*Metabasites*				
Zone	*B*	*B*	*B*	*C*	*B*	*B*	*C*	*C*	*C*
Sample	*0270*	*0455*	*1222*	*0037B*	*4070*	*0065F*	*0012*	*4270*	*1139*
SiO_2	52.59	48.15	52.52	48.78	51.10	52.40	52.94	49.96	49.48
TiO_2	nd	nd	nd	0.11	nd	nd	nd	nd	0.18
Al_2O_3	0.48	0.56	0.95	1.38	0.18	0.31	0.66	0.71	1.56
FeO	11.10	26.71	10.52	22.45	15.77	11.33	8.95	18.19	19.14
MnO	0.15	1.71	nd	nd	0.62	nd	0.26	0.31	0.28
MgO	11.94	0.51	12.17	3.96	8.89	12.05	12.85	6.72	6.31
CaO	23.06	22.65	22.55	22.90	23.57	23.52	24.25	23.16	23.05
Na_2O	0.75	nd	1.18	0.26	0.18	0.12	nd	0.22	0.18
Total	100.06	100.29	99.89	99.84	100.31	99.73	99.90	99.28	100.18
				Cations per 6 O					
Si	1.989	1.977	1.982	1.956	1.979	1.989	1.987	1.976	1.947
AlIV	0.011	0.023	0.018	0.044	0.008	0.011	0.013	0.024	0.053
AlVI	0.010	0.004	0.024	0.021	—	0.003	0.016	0.009	0.019
Ti	—	—	—	0.003	—	—	—	—	0.005
Fe	0.351	0.917	0.332	0.753	0.511	0.360	0.281	0.602	0.630
Mn	0.005	0.060	—	—	0.020	—	0.008	0.010	0.009
Mg	0.673	0.031	0.685	0.237	0.513	0.682	0.719	0.396	0.370
Ca	0.934	0.997	0.912	0.984	0.978	0.956	0.975	0.981	0.972
Na	0.055	—	0.086	0.020	0.014	0.009	—	0.017	0.014
Total	4.028	4.009	4.039	4.018	4.023	4.009	3.999	4.016	4.019
X_{Ca}	47.7	51.2	47.3	49.9	48.9	47.9	49.4	49.6	49.3
X_{Mg}	34.4	1.6	35.5	12.0	25.6	34.1	36.4	20.0	18.8
X_{Fe}	17.9	47.2	17.2	38.1	25.5	18.0	14.2	30.4	31.9

nd = not detected.

in Si and increase in tetrahedral Al with increasing alkali content in the structural formulae (Fig. 5). Ti content in amphibole also correlates broadly with increasing metamorphic grade, but is also determined by the activities of various components in such equilibria as (12) $Ca_2Fe_4TiAl_2Si_6O_{22}(OH)_2 + O_2 \rightarrow$ an + ilm + mag + H_2O and (13) Sph + $Ca_2Fe_4TiAl_2Si_6O_{22}(OH)_2 \rightarrow$ an + Fe-act + ilm + H_2O (England, 1971; personal communication 1981).

Clinopyroxene. Clinopyroxene is common in calc-silicate rocks in zones B and C, where it ranges in composition from relatively magnesian salite to hedenbergite ($Ca_{49-51}Mg_{41-2}Fe_{10-47}$) in more iron-rich rocks. Alumina contents (Table 4) are low (generally <1 wt%), as is typical of amphibolite facies clinopyroxene, and calculated Fe^{3+} contents are comparatively high (~0.1–0.3). Some contain an appreciable amount of Na, indicating significant contents of acmite molecule.

Garnet. Pink garnet, rich in grossular and andradite, and commonly containing inclusions of quartz and ilmenite, occurs in a number of zone C calc-silicates. A representative garnet composition is given in Table 5.

Scapolite. Scapolite is widespread in calc-silicate rocks of the Duchess area to the immediate west (Edwards & Baker, 1954; Carter & others, 1961), but in the Selwyn Range it occurs only sporadically in the calc-silicate rocks of zone B, mainly as poikiloblastic anhedra. Microprobe analyses show that the scapolite is commonly meionitic (Me_{60-70}, ~1% Cl), in keeping with the high CaO/Na_2O of the host rock. Ramsay & Davidson (1970), however, found no correlation in the Mary Kathleen area between host rock and scapolite Ca/Na ratios, and proposed that the availability of chlorine was the main factor in controlling scapolite composition. Totals obtained in the microprobe analyses lie in the range 95–96%, suggesting 4–5% $CO_2 + H_2O$.

Table 5. Representative microprobe analyses of garnets in calc-silicates and metabasites.

	Calc-silicate	*Metabasites*		
Zone	*C*	*C*	*C*	*C*
Sample	*0037B*	*0166A*	*4270*	*1139*
SiO_2	37.72	37.48	37.52	37.34
Al_2O_3	17.23	21.24	19.84	20.29
FeO	21.97	28.28	20.34	26.12
MnO	0.24	3.18	1.24	2.21
MgO	0.31	2.43	0.44	1.08
CaO	22.25	8.10	20.09	12.72
Total	99.72	100.71	99.46	99.75
	Cations per 12 O			
Si	2.990	2.964	2.968	2.981
AlIV	—	0.036	0.032	0.019
AlVI	1.610	1.943	1.817	1.891
Fe3+	0.412	0.096	0.212	0.128
Fe2+	1.045	1.774	1.134	1.615
Mn	0.016	0.214	0.083	0.150
Mg	0.037	0.287	0.052	0.128
Ca	1.890	0.686	1.703	1.088
X_{Ca}	55.8	24.1	54.9	36.8
X_{Mg}	1.1	10.1	1.7	4.3
X_{Fe}	43.1	65.8	43.4	58.9

Fe^{3+} calculated on basis of stoichiometry.

Epidote, apatite, sphene. These minerals are ubiquitous in zones B and C calc-silicate rocks, and are locally abundant. Microprobe analyses of epidote closely approximate the $Ca_2FeAl_2Si_3O_{12}(OH)$ formula, whereas apatites generally have low Cl contents, consistent with hydroxyapatite. Sphene is pale coloured and typically occurs in granular aggregates. Microprobe analyses indicate some substitution of Al, Fe^{3+}, and V for Ti, and Al for Si; a typical sphene analysis is $(Al_{0.67}V_{0.01}Ti_{3.23}Fe_{0.06})\ Ca_{4.14}Si_{4.16}O_{20}$.

Carbonate. Calcite is the most common carbonate; dolomite occurs sporadically in zone A rocks. Microprobe analyses of calcite show little substitution of Mg, Mn or Fe for Ca (X_{Ca} ~0.99).

Mineral parageneses

Low-grade calcareous rocks are dominated by the assemblage qz+cc+ab+epi+tr; at higher grade this assemblage is replaced by hbl+di+ab±epi±qz±ap±gr (Fig. 4). Diopside formation is likely to have occurred mainly by the continuous reaction (14) tr + cc + qz $\rightarrow$ di + CO_2 + H_2O, rather than the reaction (15) dol + qz $\rightarrow$ di + CO_2, which takes place only within a restricted range of X_{CO_2} and over a small temperature range (e.g. Slaughter & others, 1975), since dolomite does not appear to be widespread at low grade. The isobaric equilibrium curves for reaction (14) lie within a comparatively narrow temperature range for large variations in X_{CO_2}, where $X_{CO_2} \geqslant 0.4$, but is strongly dependent on P_{fluid} (Slaughter & others, 1975). The absence of calcite and the very low a_{Tr}^{hbl} in amphiboles from most zone B (and all zone C) calc-silicate rocks indicate that reaction (14) took place in the lowermost part of zone B.

Grossular-rich garnet, co-existing with qz+epi+pl+hbl+sph+ap+cpx+mag (Fig. 4) occurs in a calc-silicate band in zone C. This assemblage is stable only under relatively high f_{O_2}. Formation of grossular garnet may have proceeded by reactions such as (16) zo + qz $\rightarrow$ gr + an + H_2O, (17) an + di $\rightarrow$ gr + pyrope + qz, and (18) an + hd = 1/3 alm + 2/3 gr + qz. The andradite component of garnet may be related to such equilibria as (19) hd + cc + $O_2 \rightarrow$ ad + qz + CO_2, and (20) hd + $O_2 \rightarrow$ ad + qz + mag (e.g. Taylor & Liou, 1978).

Metabasic rocks

Protolith compositions

Metabasites are widespread and range from slightly recrystallised metadolerite with well preserved ophitic and subophitic textures through to completely recrystallised granoblastic amphibolite with no relict igneous textures or structures. The average grainsize in the recrystallised rocks increases with metamorphic grade, from 0.2–0.4 mm in zone B to 0.4–0.6 mm in zone C. Garnet porphyroblasts in zone C amphibolites are up to 5 mm across and commonly contain inclusions of quartz and magnetite or ilmenite. The metabasites exhibit large variations in Ca-Mg-Fe (8–17% CaO, 8–14% FeO; Mg_{24-53}), as shown on the ACF diagram (Fig. 6). Samples with either high Na_2O (up to 4%) and low CaO contents, or with excessively high CO_2 and CaO contents (up to 17%) are thought to have been

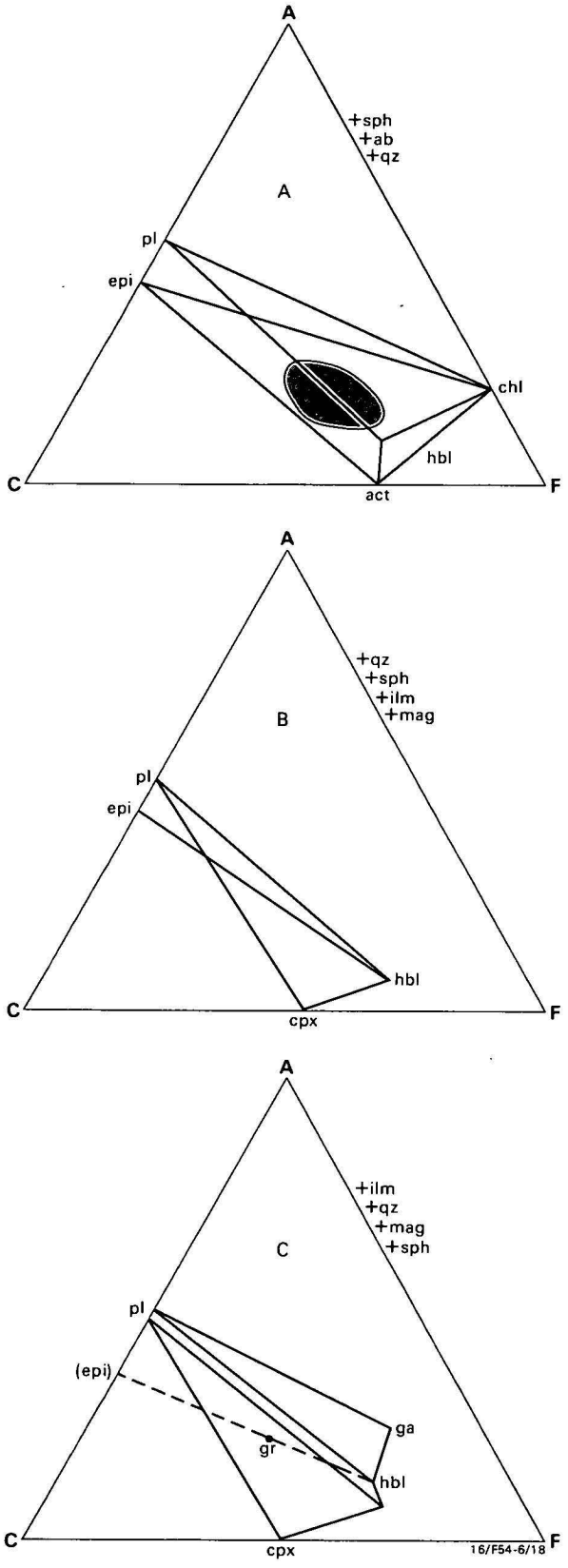

Figure 6. ACF diagrams for Selwyn metabasites.
Stippled area represents field of Selwyn metabasites.

chemically modified during (or before) regional metamorphism. All the samples are of tholeiitic affinity and similar to continental tholeiites (Glikson & others, 1976; Glikson & Derrick, 1978). Some of the metadolerites have low TiO_2 and Zr contents (e.g. 0.55% TiO_2, 22 ppm Zr; see also Rossiter & Ferguson, 1980), lower than the most Ti-poor Karroo dolerites (e.g. Le Roex & Reid, 1978).

Mineralogy

Plagioclase. Metadolerites in zone A are characterised by the retention of primary igneous plagioclase (An_{71-35}), which is commonly zoned by 20 mol. % or more. Plagioclase in recrystallised zone B amphibolites is of oligoclase composition, An_{17-22}, whereas more calcic plagioclase (typically An_{40}) occurs in higher grade metabasites (Table 6). The most calcic plagioclases (An_{82-94}) occur in garnet amphibolites with high CaO/Na_2O ratios.

Amphibole. Actinolite is the most common amphibole in zone A metadolerites but in some rocks it coexists with blue-green amphibole of magnesiohornblende to tschermakitic hornblende composition. Straw-yellow to khaki or olive-green hornblende (magnesiohornblende to hastingsite) predominates in zone B metabasites, but actinolite is present in some rocks near the lower boundary of the zone. Zone C metabasites contain yellow-brown to khaki or olive-green pargasitic hornblende. Representative analyses are given in Table 7.

Table 6. Compositional data for hbl-pl pairs.

Sample	*An (range)*	*Na(M4)*	*Ca(M4)*	*ln K*
		Zone A		
4173A	2.2 (2–4)	0.13	1.87	—6.495
4300	~10* (37–71)	0.03	1.97	—6.382
4153	~10* (35–61)	0.06	1.94	—5.673
4286	16 (16–54)	0.06	1.94	—5.134
		Zone B		
0270	4 (3–5)	0.10	1.90	—6.122
1222	10 (9–10)	0.12	1.88	—4.949
4664	19 (17–20)	0.07	1.93	—4.767
0065F	19 (17–21)	0.08	1.92	—4.628
0821	20 (19–21)	0.10	1.90	—4.331
4346	26 (21–29)	0.15	1.85	—3.558
		Zone C		
0037B	88 (86–90)	0.002	1.998	—4.914
0038	11 (9–12)	0.25	1.75	—4.037
1139	82 (82–83)	0.009	1.991	—3.925
4270	40 (36–45)	0.07	1.93	—3.722
1123	33 (28–33)	0.13	1.87	—3.374
4266	20 (20–21)	0.25	1.75	—3.332
4365	43 (41–43)	0.11	1.89	—3.126
3334	36 (33–37)	0.18	1.82	—2.935
0012	67 (65–67)	0.07	1.93	—2.609

* Assumed 'ideal' compositions.

Table 7. Representative microprobe analyses of amphiboles in metabasites.

Zone	*A*		*A*		*B*	*B*	*B*	*C*	*C*	*C*
Sample	*4153*		*4300*		*4346*	*4664*	*0065F*	*0012*	*0166A*	*4270*
SiO_2	53.41	39.93	52.70	44.03	41.19	44.86	40.74	47.08	43.91	38.27
TiO_2	nd	0.43	nd	0.41	0.53	0.40	1.09	0.67	0.93	0.86
Al_2O_3	2.82	13.13	3.30	12.88	13.44	8.25	9.96	8.44	10.63	14.00
V_2O_3	nd	0.15	nd	nd	0.13	nd	0.13	nd	0.15	nd
FeO	13.16	20.43	11.68	14.36	21.31	18.65	23.06	14.25	20.52	26.74
MnO	0.13	0.20	0.14	nd	0.24	0.19	nd	0.26	0.18	nd
MgO	15.62	7.84	16.03	11.31	7.50	10.93	8.04	12.96	8.38	3.36
CaO	12.78	11.81	12.76	12.44	11.50	12.06	11.67	12.31	11.36	11.48
Na_2O	0.19	1.43	0.27	1.58	1.48	1.02	1.99	1.14	1.05	1.61
K_2O	nd	0.76	0.07	0.19	0.52	0.81	0.83	0.21	0.49	1.54
Cl	nd	0.46	0.10	0.13	0.25	0.15	1.44	0.08	0.07	0.14
Total	98.12	96.57	97.05	97.33	98.09	97.32	98.95	97.39	97.68	98.00
					Cations per 23 O					
Si	7.675	6.232	7.624	6.521	6.299	6.816	6.369	6.943	6.666	6.078
AlIV	0.325	1.768	0.376	1.479	1.701	1.184	1.631	1.057	1.334	1.922
AlVI	0.153	0.646	0.186	0.770	0.722	0.293	0.205	0.410	0.568	0.700
Ti	—	0.050	—	0.045	0.061	0.045	0.128	0.075	0.107	0.103
V	—	0.018	—	—	0.016	—	0.016	—	0.019	—
Fe	1.582	2.667	1.413	1.779	2.726	2.370	3.015	1.757	2.605	3.552
Mn	0.016	0.027	0.018	—	0.031	0.024	—	0.032	0.023	—
Mg	3.345	1.825	3.457	2.497	1.709	2.475	1.873	2.849	1.895	0.795
Ca	1.968	1.975	1.977	1.974	1.884	1.964	1.955	1.944	1.848	1.954
Na	0.045	0.433	0.077	0.453	0.439	0.302	0.604	0.325	0.308	0.496
K	—	0.152	0.012	0.036	0.101	0.158	0.166	0.040	0.096	0.312
Total	15.109	15.793	15.139	15.554	15.689	15.669	15.921	15.431	15.468	15.912
$\frac{100\,Mg}{(Mg+Fe)}$	67.9	40.6	71.0	58.4	38.5	57.1	38.3	61.9	42.1	18.3

nd = not detected.

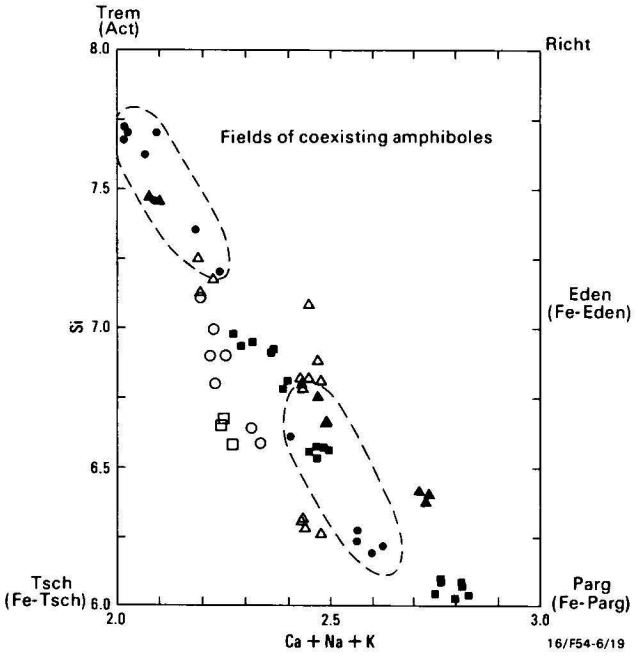

Figure 7. Variation of Ca + Na + K with Si (per 23 O) in amphiboles from Selwyn metabasites.
Open symbols = quartz-bearing, filled symbols = quartz-free. Dots = zone A, triangles = zone B, squares = zone C. Abbreviations as in Figure 5.

Two substitutions are evident with increasing grade of metamorphism (Fig. 7), the most common being a transition from actinolite to pargasitic hornblende in metabasites poor in quartz and chlorite. Metabasites of this group in zone A show a compositional gap between actinolite and hornblende (Fig. 7). The other substitution occurs in metabasites with modal quartz and chlorite (low grade), and involves formation of tschermakite and a trend toward edenite with increasing metamorphic grade. In these metabasites there is no indication of a miscibility gap between actinolite and hornblende. The transition from actinolite to tschermakitic hornblende involves the substitution (Al, Fe)$^{M(1)\text{-}M(3)}Al^{iv}$=(Mg, Fe)$^{M(1)\text{-}M(3)}Si^{iv}$ and, since epidote and Al-rich chlorite as well as calcic plagioclase occur in the zone A metadolerites, probably involved the reactions (21) act + Al-chl + epi + qz → Tschermakite + H_2O, and (22) act + Al-chl + an → Tschermakite + H_2O. The other trend, toward edenite, involves the substitution (Na,K)$^{A}Al^{iv}$=A site.□Si^{iv}, and probably involves the reaction (23) ab + epi → edenite + qz. Combination of these substitutions produces pargasitic hornblende (Figs. 7, 8). On the other hand, from his study of the Soldiers Cap amphibolites in the Cloncurry area, England (1971) concluded that, because of the rarity of chlorite, Fe-oxide minerals were important in introducing Al and Fe^{3+} into calciferous amphibole. In low pressure terrains edenite substitution becomes important at higher grade, whereas amphiboles in high P/T regimes characteristically show tschermakite enrichment with increasing metamorphic grade, consistent with the small dP/dT of the edenite-forming reaction (Grapes & Graham, 1978). Over all, the amphiboles of the Selwyn metabasite trend toward pargasite with increasing grade; this implies moderate pressures, and is consistent with the absence of kyanite and regional cordierite and the presence of almandine in pelitic rocks.

Ilmenite, magnetite, sphene. Ilmenite, formed by oxidative exsolution from primary, igneous titaniferous magnetite occurs as (III) lamellae in magnetite in zone A metadolerites. In zones B and C ilmenite occurs as a discrete recrystallised phase. Magnetite is an accessory in most metabasites. Sphene is common in all three zones, but is most common in zones B and C,

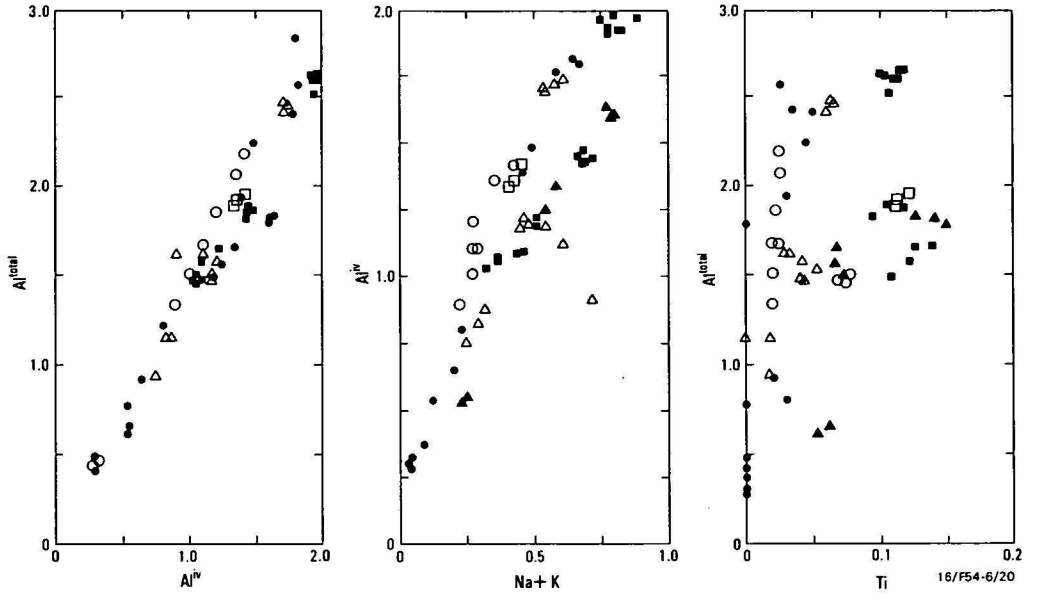

Figure 8. Variation of Al^{total} versus Al^{iv}, Al^{iv} versus Na+K and Al^{total} versus Ti content for Selwyn metabasites. Symbols as in Figure 7.

where it occurs as granoblastic grains and, in oxidised assemblages, is associated with hematite. Sphene is absent in almandine-garnet amphibolites where ilmenite is the stable phase.

Clinopyroxene. Granular, pale green to neutral-coloured clinopyroxene of diopside-salite composition (Table 4) occurs in calcic metabasites in the higher grade parts of zone B and in zone C. The high Ca contents of the pyroxenes are typical of metamorphic clinopyroxene in amphibolite facies terrains; no correlation of Ca content and metamorphic grade was observed. Al and Na contents are low ($\leqslant$1.3, 0.3 wt% respectively, Table 4), consistent with a low pressure origin.

Garnet. Grossular-rich garnet ($Ca_{56-37}Mg_{2-5}Fe_{42-58}$) is developed in the more Ca-rich metabasites and para-amphibolites ($CaO/Al_2O_3 \geqslant 1$). Almandine-garnet (~8% CaO), typically without clinopyroxene, occurs sporadically in Fe-rich (14–15% Fe as FeO) ortho-amphibolites (Table 5). $K_{D_{ga-cpx}}^{Fe\text{-}Mg}$ for grossular-rich garnet amphibolites is between 8 and 17.

Epidote. Epidote exists with comparatively sodic plagioclase ($<An_{30}$) in metabasites of zones A and B, a characteristic of the epidote-amphibolite facies, but it disappears with increasing metamorphic grade. Microprobe analyses indicate negligible Mn contents and moderately high Fe/(Fe+Al) ratios ~0.3; a typical analysis is $Ca_{2.01}Fe_{0.83}Al_{2.16}Si_{2.56}O_{12}$.

Mineral paragenesis

Prograde mineral parageneses are shown on the ACF diagrams (Fig. 6). The low grade metabasites are characterised by the assemblage chl+epi+act+blue/green hbl (tschermakite-rich)+pl. Sodic plagioclase ($<An_{16}$) is the stable composition, but relict igneous compositions are common. At higher grade, actinolite disappears and hornblende changes in composition by reactions (21), (22), and (23) to green magnesio-hornblende-hastingsite and coexists with more calcic plagioclase and, in calcic bulk compositions ($CaO \geqslant Al_2O_3$), commonly with calcic clinopyroxene formed by reaction (14). At higher grade, rocks of appropriate composition contain the parageneses pl(andesine) + green/brown hbl + ga. Garnet in quartz-free assemblages in rocks with excess CaO is grossular-rich ($X_{Ca} \geqslant 0.5$) and may have formed by quartz-consuming reactions, such as (16) or the reaction (24) an + qz + cc $\rightarrow$ gr + CO_2. The garnet in quartz-bearing assemblages without excess CaO is more almandine-rich ($X_{Fe} \geqslant 0.5$) and may have formed by reactions such as (18).

Conditions of metamorphism

P-T conditions of metamorphism have been estimated by comparison with petrogenetic grids of experimentally determined univariant curves and invariant points, and have been calculated from experimentally calibrated cation-exchange equilibria and thermodynamic relations. Although reactions may have been divariant, with reactants consumed by continuous reactions before the temperatures for limiting discontinuous reactions were reached, such univariant reactions do provide limits to assemblage stability (cf. Yardley & others, 1980).

Pressure

Pressures attained during metamorphism may be inferred from the absence of cordierite in favour of the assemblages ga+and+st and ga+bi+si in pelites. Comparison with Thompson's (1976) petrogenetic grid for discontinuous reactions in the system KFMASH indicates an upper limit to the cordierite stability field of 3.8–4.8 kb (max), above which the assemblage bi+si±chl is stable. Newton & Wood (1979) showed that the stability field of cordierite is promoted to higher pressures in H_2O-bearing systems, and presented (Mg, Fe) isopleths of coexisting garnet and cordierite. Examination of these isopleths leads to the suggestion that the Selwyn pelites with $X_{Mg}^{ga} \leqslant 0.1$ formed at pressures above 2.5 kb (anhydrous) and possibly higher than 4 kb (hydrous). Pressures in the higher grade part of zone B and in zone C must have

exceeded the invariant point for the assemblage cd+and+bi+st+ga, hence were greater than 3kb at 600°C (cf. Newton & Wood, 1979), but were lower than the Al_2SiO_5 triple-point pressure for andalusite-bearing pelites. The position of the triple point is uncertain. Wall & Essene (1972) noted that the triple-point pressure is closely defined by the andalusite-kyanite, kyanite-sillimanite intersection, but temperature was less well constrained. Greenwood (1976) suggested from petrographic observations that the andalusite-sillimanite boundary of Holdaway (1971) was at too low a temperature and proposed that the curve be placed 50°C higher. Thermodynamic data, however, favour the Holdaway data (e.g. Anderson & others, 1977; Day & Kumin, 1980). If the Holdaway data, drawn to give the highest triple-point temperature consistent with Holdaway's brackets, and the constraints of Weill (1966) and Anderson & others (1977) are accepted (Yardley & others, 1980), total pressures of 3–4 kb are implied for zone B assemblages.

Pressures have been calculated for the assemblage qz+bi+mu+ga+pl, using the empirical geobarometer proposed by Ghent & Stout (1981) and the compositional data in Table 2. The pressure calculated for a sillimanite-bearing pelite (Table 8) is in good agreement with that calculated from the reaction (25) ga + si + qz = 3 an (Ghent, 1976) and from the Fe-Mg garnet-biotite exchange reaction (Ferry & Spear, 1978), using the data in Table 2. Pressures calculated for a zone B pelite (qz+bi+mu+pl+ga+and) by analogous reactions involving andalusite (Ghent, 1976; Ghent & Stout, 1981) lie well within the kyanite stability field, implying either lack of equilibration or large deviations from the ideal (as also found by Yardley & others, 1980).

The pressures calculated for the pelites are supported by those calculated using the cpx-qz-pl geobarometer as calibrated by Ellis (1980). A para-amphibolite and a calc-silicate rock from zone C near the si-kfs isograd both gave nominal pressures of ~4 kb (Table 8), assuming temperatures interpolated from adjacent pelitic horizons using garnet-biotite geothermometry.

Perkins & Newton (1981) presented a calibration of reaction (17) for use as a geobarometer for the assemblage ga+cpx+pl+qz. However, the high Mn content of the garnets in the Selwyn rocks (Mn≥Mg) renders this barometer inapplicable. An attempt was made to use the analogous reaction in the Fe-system (reaction 18) to estimate pressures, since ΔV_r is comparatively large (2.461 kJ bar^{-1}). Available thermochemical data (Helgeson & others, 1978) indicate that ΔS_r is also large (−0.059 kJ $deg^{-1}mol^{-1}$). Since $\Delta H_{f,Alm}$ is poorly known, ΔH_r was derived empirically by calibration of the reaction against the P-T conditions derived for sample 78530037B (using the compositional data in Tables 4–6) from other geobarometers (Table 8) and a temperature of 650°C derived from garnet-biotite geothermometry (Table 9). This gives the expression (26) $-RT \ln K = -53.22 + 0.059T + 2.461P$, where $K = \frac{(a^{ga}_{Gr})^{2/3} \cdot (a^{ga}_{Alm})^{1/3} \cdot a^{qz}_{SiO_2}}{(a^{pl}_{An}) \cdot (a^{cpx}_{Hd})}$ and

T is in degrees Kelvin and P is in kilobars. The following activity in composition relationships have been adopted: $a^{ga}_{Gr} = (X^{ga}_{Ca})^3$, $a^{ga}_{Alm} = (X^{ga}_{Fe})^3$, $a^{qz}_{SiO_2} = 1$, $a^{pl}_{An} = X^{pl}_{Ca}$, and $a^{cpx}_{Hd} = (X_{Ca,M1} \cdot X_{Fe,M2})$. Insertion of ΔH_f data (Helgeson & others, 1978) for the other phases in the reaction, and assuming the empirically derived ΔH_r, gives a calculated value for $H_{f,Alm}$ of 5343.9 kJ, which compares with the 5328.6 kJ value cited by Ghent & Stout (1981).

A similar pressure, ~4 kb (Table 8), was obtained for the ga+cpx+pl+qz assemblage in para-amphibolite 78531139, using the above equation (26) together with the compositional data in Tables 4–6, and assuming an equilibration temperature of 650°C (as estimated for pelitic assemblages near the si-kfs isograd).

Table 8. Estimated pressures (bars).

Sample	P_1	P_2	P_3	P_4	P_5
0039A	—	4392	3916	3951	—
1139	3988				3991
0037B	4129				

P_1 = cpx-qz-pl (Ellis, 1980); P_2 = ga-si-qz-pl (Ghent 1976); $P_{3,4}$ = ga-mu-bi-pl (Ghent & Stout, 1981); P_5 = cpx-ga-qz (see text).

Table 9. Temperatures (°C) calculated from ga-bi and hbl-pl pairs.

Sample	*ga-bi*	*pl-hbl*[1]	*pl-hbl*[2]	*Retrograde* (ga-bi)
		Zone A		
4173A		379	428	
4300		383	434	
4153		411	473	
4286		434	505	
mean		402 ± 26	460 ± 36	
		Zone B		
0879	554			506
0387A	573			504
0388	581			494
4237	607			
0270		393	448	
1222		442	516	
4664		450	528	
0065F		456	537	
0821		470	558	
4346		509	616	
	578 ± 22	452 ± 38	534 ± 55	501 ± 6
		Zone C		
4241	609			462
3346B	618			535
0039A	648			538
4256	678			578
3334	685	544	670	651
0037B		443	518	
0038		485	579	
1139		490	588	
4270		501	603	
1123		519	632	
4266		522	635	
4365		533	653	
0012		563	701	
	648 ± 34	511 ± 36	620 ± 55	553 ± 69

[1] Calibration of Spear (1980).
[2] Calibration given in text.

Temperatures

Equilibration temperatures may be estimated by comparison with the experimentally determined univariant dehydration reactions in pelites shown in Figure 9. The lower stability limit of staurolite, commonly taken

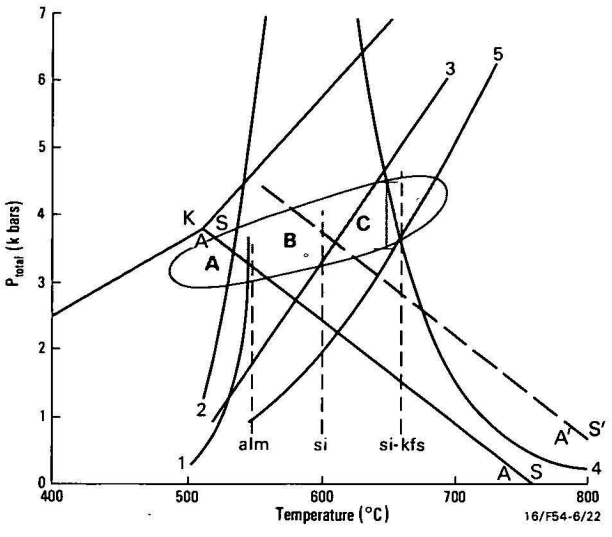

Figure 9. P-T diagram indicating estimated equilibration conditions for Selwyn metamorphics (stippled) zones A, B and C.

Dashed lines, alm, si, and si-kfs, indicate temperatures for these isograds based on ga-bi geothermometry. Aluminosilicate phase boundary (K-A-S) based on Holdaway (1971), after Yardley & others (1980); A′-S′ = suggested position of and-si phase boundary (see text). Reaction (1) chl+qz → alm + H_2O (Hsu, 1968), (2) lower limit of staurolite (Richardson, 1968; Hoschek, 1969), (3) st+mu+qz → Al_2SiO_5 + bi + H_2O (Hoschek, 1969), (4) water-saturated granite melting curve (Tuttle & Bowen, 1958; Merrill & others, 1970), (5) mu+qz → kfs + Al_2SiO_5 + H_2O (Chatterjee & Johannes, 1974; Helgeson & others, 1978).

as the boundary between the greenschist and amphibolite facies (e.g. Winkler, 1979), lies close to the curve for the formation of almandine by reaction (1) (Hsu, 1968), and has been determined by Richardson (1968) and Hoschek (1969) as 530–550°C at 3–4 kb. The upper stability limit of staurolite is not well constrained below 10 kb. The data of Slaughter & others (1975) suggest that reaction (14) takes place at ~550–600°C for P_{fluid} ~3–4 kb and $X_{CO_2} \geqslant 0.5$. The absence of the assemblage tr+cc+qz+di in all except the lower part of zone B and the very low a_{Tr} in amphibole at higher grade are consistent with the location of reaction (14) close to the staurolite and garnet isograds. The dehydration reaction involving the breakdown of muscovite and quartz (reaction 11) is well established (Chatterjee & Johannes, 1974; Helgeson & others, 1978) and, at $P_{H_2O} = P_{Total}$, intersects the water-saturated granite solidus at ~660°C and 3.8 kb. The presence of abundant quartzo-feldspathic (qz+ab±mu±kfs) veins and segregations in pelitic gneisses and schists at and above the si-kfs isograd suggests an origin by anatexis, i.e. synmetamorphic melts, as a direct consequence of the muscovite breakdown reaction. This implies minimum equilibration temperatures of ~660°C for the highest grade rocks.

Temperatures have also been estimated by several exchange equilibria. In these calculations, a pressure of 4000 bars has been assumed for zone C and a slightly lower pressure, 3500 bars, assumed for zones A and B.

Garnet-biotite. The strongly temperature-dependent Fe-Mg exchange reaction between garnet and biotite has been calibrated experimentally by Ferry & Spear (1978). Temperatures calculated from the compositional data in Table 3 range from ~550°C at a point slightly above the staurolite-isograd to ~600°C at the sillimanite isograd and to ~650–670°C at the si-kfs isograd (Table 9). Higher temperatures, ~700–720°C, are indicated by ga-bi pairs in calcareous psammitic gneisses in the easternmost outcrops of zone C, but, since the garnet here is rich in Ca and Mn and the Al^{vi} content in the biotite is low, these estimates are probably too high. The likely ranges in temperature are therefore of ~60°C for zone B and ~70°C for zone C.

The calculated temperatures agree well with those predicted from univariant dehydration reactions involving staurolite and garnet formation and the breakdown of muscovite + quartz. The maximum temperatures for the stability of staurolite, based on coexisting garnet-biotite pairs, are consistent with the upper stability field of staurolite shown in Figure 9. However, the P-T conditions defined for the Selwyn sillimanite isograd do not agree with Holdaway's (1971) aluminosilicate phase diagram, and imply stability (or meta-stability) of andalusite to higher grade. The P-T field defined for the Selwyn pelites is more consistent with the andalusite-sillimanite curve proposed by Greenwood (1976) (Fig. 9).

Plag–Hbl. Spear (1980) presented an empirical calibration of the NaSi-CaAl exchange between plagioclase and amphibole, and suggested its use as a geothermometer. However, calculation of K_D for the reaction, where $K_D = \frac{X_{Ca}}{X_{Na,pl}} \cdot \frac{X_{Na}}{X_{Ca\ M4,amph}}$, involves assignment of Na in the amphibole M4 site, which is critically dependent on the ferric iron content of the amphibole. We have followed the method favoured by Leake (1978) to estimate Fe^{3+} in amphibole, i.e. (Si+Ti+Al+Cr(V)+Fe^{3+}+Mn+Fe^{2+}+Mg) = 13. This method results in maximum ferric iron content (Fe^{3+}/(Fe^{3+}+Fe^{2+}) ~0.1–0.3) and Na,M4 values and the lowest K_D values (highest temperatures). The variation of plagioclase composition (av. mol. %An) with coexisting amphibole composition (Na,M4) for amphibolites and calc-silicate rocks is shown in Figure 10. The mineral pairs show a systematic orientation of tie lines, indicating attainment of equilibrium at lower, medium and higher metamorphic grades (cf. Spear, 1980, figs. 2, 7). Nominal temperatures calculated from Spear's (1980) empirical calibration (Table 9) show an over-all increase in temperature from zone A to zone C of about 150°C, consistent with the range recorded by the garnet-biotite geothermometer. However, the temperatures calculated by the plag-hbl geothermometer are significantly lower, and the difference is much greater than the ± 50°C uncertainty suggested by Spear (1980). This may be due to the solid solutions being strongly non-ideal, as indicated by the large variation of ln K_D with X_{An} for rocks within the same zone (Table 6); there are also uncertainties in the pressure dependence of the reaction. An alternative empirical calibration of the partitioning of NaSi-CaAl between plagioclase and hornblende has been made using the compositional data (Table 7) for 5 Selwyn amphibolites (X_{An} = 20–40) and assuming equilibration temperatures estimated from garnet-biotite equilibria in adjacent pelite horizons. Regression of the data points gave the expression (27) $\ln K_D = -\frac{9752}{T°K} + 7.407$ (r=0.925). Temperatures calculated by this

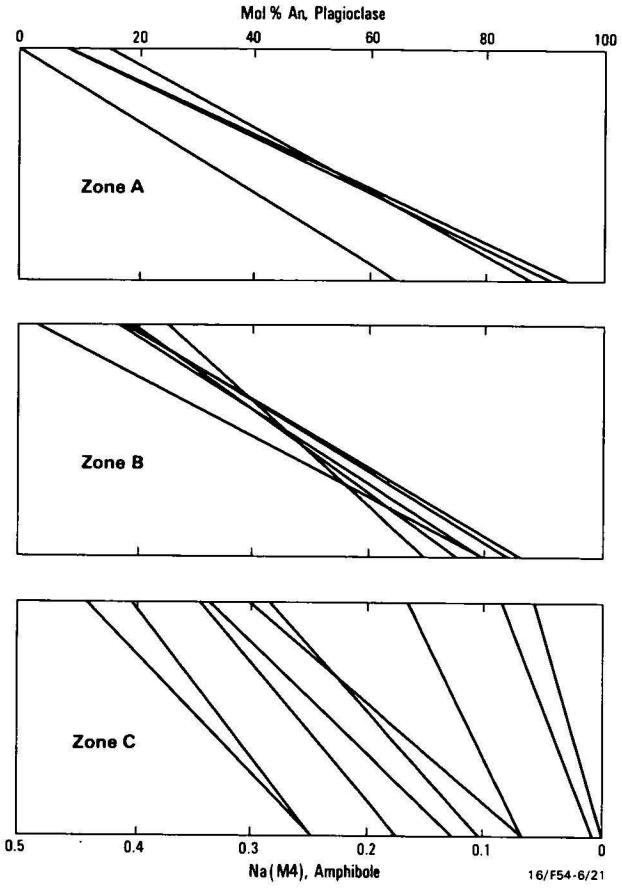

Figure 10. Variation of Na(M4) in amphibole with An content in co-existing plagioclase for Selwyn calc-silicates and amphibolites.
Note rotation of tie lines at higher metamorphic grade.

equation range from ~450°C for the lowest grade (zone A) metabasites to ~700°C for the highest grade amphibolites (Table 9), and are more consistent with those estimated by other means.

Other geothermometers. Temperatures for ga+cpx-bearing assemblages have been estimated using the Fe-Mg exchange between garnet and clinopyroxene (Ellis & Green, 1979). Nominal temperatures of ~770°C were obtained for two zone C ga-cpx amphibolites, and an even higher temperature, ~900°C, for a ga-cpx calc-silicate rock. These anomalously high temperatures probably arise because the Selwyn garnets are richer in Fe, Ca, and Mn than those used in the experimental calibration, and at these comparatively low-grade conditions departures from the ideal are greater. Meaningful temperature estimates could not be obtained using the two feldspar geothermometer (Powell & Powell, 1977; Stormer & Whitney, 1977), because of the complete redistribution of the albite component in alkali feldspar.

Retrograde metamorphism

Petrographic evidence indicates that the response of prograde assemblages to retrograde metamorphism associated with F_2 and F_3 was dependent on the prograde mineralogy and the particular structural domain of the outcrop. Some rocks show well-developed S_2 foliations of secondary mica and/or chlorite, but most show only local mineralogical adjustment in the form of zoning of rims or replacement of grain margins (e.g. garnet by chlorite/biotite). Temperatures calculated by the garnet/biotite geothermometer, using the compositional data in Table 2, for S_2 biotite and garnet rims (mostly contacting grains) are lower than those obtained for M1, but no systematic variation is apparent (Table 9). The wide variation in calculated temperatures is taken to indicate partial re-equilibration.

Summary and discussion

The P-T fields defined by experimentally determined univariant curves and invariant points, together with calculations made using several geobarometers, indicate equilibration pressures of ~4 kb for zone C rocks. Rocks of lower grade are interpreted as having equilibrated at slightly lower pressure, 3–4 kb. Equilibration temperatures of the prograde sequence are constrained by critical dehydration reactions in pelites and cation-exchange reactions (garnet-biotite), and range from ~450–550°C in zone A to 550–600°C in zone B and 600–680°C in zone C (Fig. 9). In places, temperatures were sufficient to form synmetamorphic melts. The disposition of the isograds and the estimated P-T fields conflict with Holdaway's (1971) Al_2SiO_5 phase boundaries. However, the discrepancy could be removed if the andalusite-sillimanite boundary were placed some 50°C higher, as suggested by Greenwood (1976). Retrograde metamorphism has resulted in secondary mineral assemblages in some rocks, but mainly consists of local re-equilibration, as shown by zoning of mineral rims. The estimated prograde P-T conditions imply a high geothermal gradient (45–50°C km^{-1}) at the time of metamorphism.

The grade of regional metamorphism in the southeast part of the Selwyn Range appears to be at least as high as any previously reported from the Mount Isa Inlier. Comparable upper-amphibolite facies (sillimanite-grade) pelites and calc-silicate rocks have been described from near Mary Kathleen (Derrick, 1980) and also from parts of the Duchess region (Bultitude & others, in press), and Carter & others (1961, p. 165) reported 'apparently high-grade metamorphics', some containing sillimanite, at several localities at the western margin of the inlier. Derrick (1980) estimated pressures of 3.5–4.8 kb and temperatures of 600–650°C for the Mary Kathleen rocks.

It has commonly been supposed that the various metamorphic episodes in the Mount Isa Inlier are related to the intrusion of granitoids (e.g. Plumb & others, 1980), since, on a regional scale, the axes of granite intrusions commonly coincide with areas of highest metamorphic grade. However, in the Selwyn Range area, the metamorphic isograds are independent of the granite plutons, which appear to both pre-date and post-date the main metamorphic episode, M1. The Selwyn Range region is similar to many other low-medium pressure metamorphic terrains in terms of the close association of extensive granitoid bodies, but further structural, petrologic, and geochronological studies are required before a comprehensive picture of the metamorphism, deformation and plutonism of the region can be obtained.

Acknowledgements

We gratefully acknowledge helpful discussions with our colleagues and former colleagues at BMR and GSQ, particularly L. A. Wyborn and R. J. Bultitude. N. G. Ware kindly provided access to the TPD electron microprobe at the Australian National University. We also thank R. N. England, D. J. Ellis, V. Wall and an anonymous reviewer for constructive criticism of the manuscript.

References

ANDERSON, P. A. M., NEWTON, R. C., & KLEPPA, O. J., 1977—The enthalpy change of the andalusite-sillimanite reaction and the Al_2SiO_5 diagram. *Amercian Journal of Science*, 277, 585-93.

BLAKE, D. H., 1980—The early geological history of the Proterozoic Mount Isa Inlier, northwestern Queensland: an alternative interpretation. *BMR Journal of Australian Geology & Geophysics*, 5, 243-56.

BLAKE, D. H., JAQUES, A. L., & DONCHAK, P. J. T., 1979—Precambrian geology of the Selwyn region, northwestern Queensland—preliminary data. *Bureau of Mineral Resources, Australia, Record* 1979/86 (unpublished).

BULTITUDE, R. J., BLAKE, D. H., DONCHAK, P. J. T., & MOCK, C. M., in press—Duchess region, Queensland. *Bureau of Mineral Resources, Australia, 1:100 000 Geological Map Commentary.*

CARTER, E. K., BROOKS, J. H., & WALKER, K. R., 1961—The Precambrian mineral belt of northwestern Queensland. *Bureau of Mineral Resources Australia, Bulletin* 51.

CHATTERJEE, N. D., & JOHANNES, W., 1974—Thermal stability and standard thermodynamic properties of synthetic $2M_1$ -muscovite, $K\ Al_2\ [AlSi_3O_{10}(OH)_2]$. *Contributions to Mineralogy and Petrology*, 48, 89-114.

DAY, H. W., & KUMIN, H. J., 1980—Thermodynamic analysis of the aluminium silicate triple point. *American Journal of Science*, 280, 265-87.

DERRICK, G. M., 1979—Geochemical data, Marraba 1:100 000 Sheet area, northwest Queensland. *Bureau of Mineral Resources, Australia, Record* 1979/85 (unpublished).

DERRICK, G. M., 1980—Marraba, Queensland. *Bureau of Mineral Resources, Australia, 1:100 000 Geological Map Commentary.*

DONCHAK, P. J. T., BLAKE, D. H., & JAQUES, A. L., 1979—Precambrian geology of the Mount Angelay 1:100 000 Sheet area (7055), northwestern Queensland—preliminary data. *Bureau of Mineral Resources, Australia, Record* 1979/93 (unpublished).

EDWARDS, A. B., & BAKER, G., 1954—Scapolitization in the Cloncurry district of northwestern Queensland. *Journal of the Geological Society of Australia*, 1, 1-33.

ELLIS, D. J., 1980—Osumilite-sapphirine-quartz granulites from Enderby Land, Antarctica: P-T conditions of metamorphism, implications for garnet-cordierite equilibria and the evolution of the deep crust. *Contributions to Mineralogy and Petrology*, 74, 201-10.

ELLIS, D. J., & GREEN, D. H., 1979—An experimental study of the effect of Ca upon garnet-clinopyroxene Fe-Mg exchange equilibria. *Contributions to Mineralogy and Petrology*, 71, 13-22.

ENGLAND, R. N., 1971—Progressive metamorphism of amphibolites from the Cloncurry and Petermann Ranges area. *Bureau of Mineral Resources, Australia, Record* 1971/109 (unpublished).

FERRY, J. M., & SPEAR, F. S., 1978—Experimental calibration of Fe and Mg partitioning between biotite and garnet. *Contributions to Mineralogy and Petrology*, 66, 113-17.

GHENT, E. D., 1976—Plagioclase-garnet-Al_2SiO_5-quartz: a potential geobarometer-geothermometer. *American Mineralogist*, 61, 710-14.

GHENT, E. D., & STOUT, M. Z., 1981—Geobarometry and geothermometry of plagioclase-biotite-garnet-muscovite assemblages. *Contributions to Mineralogy and Petrology*, 76, 92-7.

GLIKSON, A. Y., & DERRICK, G. M., 1978—Geology and geochemistry of middle Proterozoic basic volcanic belts, Mount Isa/Cloncurry, northwest Queensland. *Bureau of Mineral Resources, Australia, Record* 1978/48 (unpublished).

GLIKSON, A. Y., DERRICK, G. M., WILSON, I. H., & HILL, R. M., 1976—Tectonic evolution and crustal setting of the middle Proterozoic Leichhardt River fault trough, Mount Isa region, northwestern Queensland. *BMR Journal of Australian Geology & Geophysics*, 1, 115-29.

GRAPES, R. H., & GRAHAM, C. M., 1978—The actinolite-hornblende series in metabasites and the so-called miscibility gap: A review. *Lithos*, 11, 85-97.

GREENWOOD, H. J., 1976—Metamorphism at moderate temperatures and pressures. *In* BAILEY, D. K., & MACDONALD, R. (editors), The evolution of the crystalline rocks. *Academic Press, London*, 187-259.

HELGESON, H. C., DELANY, J. M., NESBITT, H. W., & BIRD, D. K., 1978—Summary and critique of the thermodynamic properties of the rock-forming minerals. *American Journal of Science*, 278-A, 1-229.

HOLDAWAY, M. J., 1971—Stability of andalusite and the aluminium silicate phase diagram. *American Journal of Science*, 271, 97-131.

HOSCHEK, G., 1969—The stability of staurolite and chloritoid and their significance in metamorphism of pelitic rocks. *Contributions to Mineralogy and Petrology*, 11, 208-32.

HSU, L. C., 1968—Selected phase relationships in the system Al-Mn-Si-O-H. *Journal of Petrology*, 9, 40-83.

JOPLIN, G. A., & WALKER, K. R., 1961—The Precambrian granites of northwestern Queensland. *Proceedings of the Royal Society of Queensland*, 72, 21-57.

LE ROUX, A. P., & REID, D. L., 1978—Geochemistry of Karroo dolerite sills in the Calvinia District, Western Cape Province, South Africa. *Contributions to Mineralogy and Petrology*, 66, 351-60.

LEAKE, B. E., 1978—Nomenclature of amphiboles. *American Mineralogist*, 63, 1023-52.

MERRILL, R. B., ROBERTSON, J. K., & WYLLIE, P. J., 1970—Melting reactions in the systems $NaAlSi_3O_8$-$KAlSi_3O_8$-SiO_2-H_2O to 20 kilobars compared with results for other feldspar-quartz-H_2O and rock-H_2O systems. *Journal of Geology*, 78, 558-69.

NEWTON, R. C., & WOOD, B. J., 1979—Thermodynamics of water in cordierite and some petrologic consequences of cordierite as a hydrous phase. *Contributions to Mineralogy and Petrology*, 68, 391-405.

PAGE, R. W., 1978—Response of U-Pb zircon and Rb-Sr total-rock and mineral systems to low grade regional metamorphism in Proterozoic igneous rocks, Mount Isa, Australia. *Journal of the Geological Society of Australia*, 25, 141-64.

PAGE, R. W., in preparation—Early to middle Proterozoic evolution in the Mount Isa Inlier, Australia, as revealed by U-Pb zircon systems in superposed felsic volcanic sequences.

PERKINS, D., III, & NEWTON, R. C., 1981—Charnockite geobarometers based on coexisting garnet-pyroxene-plagioclase-quartz. *Nature*, 292, 144-46.

PLUMB, K. A., DERRICK, G. M., & WILSON, I. H., 1980—Precambrian geology of the McArthur River-Mount Isa region of northern Australia. *In* HENDERSON, R. A., & STEPHENSON, P. J. (editors), The geology and geophysics of northeastern Australia. *Geological Society of Australia, Queensland Division*, 71-88.

POWELL, M., & POWELL, R., 1977—Plagioclase-alkali feldspar geothermometry revisited. *Mineralogical Magazine*, 41, 253-56.

RAMSAY, C. R., & DAVIDSON, L. R., 1970—The origin of scapolite in the regionally metamorphosed rocks of Mary Kathleen, Queensland, Australia. *Contributions to Mineralogy and Petrology*, 25, 41-51.

REED, S. J. B., & WARE, N. G., 1975—Quantitative electron microprobe analysis of silicates using energy-dispersive X-ray spectrometry. *Journal of Petrology*, 16, 499-519.

RICHARDSON, S. W., 1968—Staurolite stability in a part of the system Fe-Al-Si-O-H. *Journal of Petrology*, 9, 467-88.

ROSSITER, A. G., & FERGUSON, J., 1980—A Proterozoic tectonic model for northern Australia and its economic implications. *In* FERGUSON, J., & GOLEBY, A. B. (editors), Uranium in the Pine Creek Geosyncline. *International Atomic Energy Agency, Vienna*, 209-32.

SLAUGHTER, J., KERRICK, D. M., & WALL, V. J., 1975—Experimental and thermodynamic study of equilibria in the system CaO-MgO-SiO_2-H_2O-CO_2. *American Journal of Science*, 275, 143-62.

SPEAR, F. S., 1980—NaSi $\rightleftharpoons$ CaAl exchange equilibrium between plagioclase and amphibole. *Contributions to Mineralogy and Petrology*, 72, 33-41.

STANTON, R. L., & VAUGHAN, J. P., 1979—Facies of ore formation: a preliminary account of the Pegmont deposit as an example of potential relations between small iron formations and stratiform sulphide ores. *Proceedings of the Australasian Institute of Mining and Metallurgy*, 270, 25-38.

STORMER, J. C., Jnr., & WHITNEY, J. A., 1977—Two-feldspar geothermometry in granulite facies metamorphic rocks. Sapphirine granulites from Brazil. *Contributions to Mineralogy and Petrology*, 65, 123-33.

TAYLOR, B. E., & LIOU, T. K., 1978—The low temperature stablity of andradite in C-O-H fluids. *American Mineralogist*, 63, 378-93.

THOMPSON, A. B., 1976—Mineral reactions in pelitic rocks: I. Prediction of P-T-X(Fe-Mg) phase relations. *American Journal of Science*, 276, 401-24.

THOMPSON, J. B. JNR, 1957—The graphical analysis of mineral assemblages in pelitic schists. *American Mineralogist*, 42, 842-58.

TUTTLE, O. F., & BOWEN, N. L., 1958—Origin of granite in the light of experimental studies in the system $NaAlSi_3O_8$-$KAlSi_3O_8$-SiO_2-H_2O. *Geological Society of America, Memoir* 74.

WALL, V. J., & ESSENE, E. J., 1972—Subsolidus equilibria in CaO-Al_2O_3-SiO_2-H_2O. *Geological Society of America, Abstracts*, 4, 700.

WALKER, K. R., JOPLIN, G. A., LOVERING, J. F., & GREEN, R., 1960—Metamorphic and metasomatic convergence of basic igneous rocks and lime-magnesia sediments of the Precambrian of northwestern Queensland. *Journal of the Geological Society of Australia*, 6, 149-78.

WARE, N. G., 1981—Computer programs and calibration with the PIBS technique for quantitative electron probe analysis using a lithium-drifted silicon detector. *Computers & Geoscience*, 7, 167-84.

WEILL, D. F., 1966—Stability relations in the Al_2O_3-SiO_2 system calculated from solubilities in the Al_2O_3-SiO_2-Na_2AlF_6 system. *Geochimica et Cosmochimica Acta*, 30, 223-37.

WINKLER, H. G. F., 1979—Petrogenesis of metamorphic rocks. (5th edition) *Springer-Verlag, New York.*

WYBORN, L. A., 1981—Aspects of the geochemistry and economic potential of the felsic igneous rocks of the Mt Isa region (abstract). *BMR Journal of Australian Geology & Geophysics*, 6, 276.

YARDLEY, B. W. D., LEAKE, B. F., & FARROW, C. M., 1980—The metamorphism of Fe-rich pelites from Connemara, Ireland. *Journal of Petrology*, 21, 365-99.

Appendix: Notation

A. Phases

ab	albite	gr	grossularite
act	actinolite	hbl	hornblende
ad	andradite	hd	hedenburgite
alm	almandine	hm	hematite
amph	amphibole	ilm	ilmenite
an	anorthite	kfs	K-feldspar
and	andalusite	mag	magnetite
ap	apatite	mu	muscovite
bi	biotite	pl	plagioclase
cc	calcite	qz	quartz
chl	chlorite	scap	scapolite
cpx	clinopyroxene	si	sillimanite
di	diopside	sph	sphene
dol	dolomite	st	staurolite
epi	epidote	tour	tourmaline
fs	feldspar	tr	tremolite
ga	garnet	zo	zoisite

B. Components

Ab	$NaAlSi_3O_8$	Gr	$Ca_3Al_2Si_3O_{12}$
Alm	$Fe_3Al_2Si_3O_{12}$	Hd	$(CaFe)_2Si_2O_6$
An	$CaAl_2Si_2O_8$	Tr	$Ca_2Mg_5Si_8O_{22}(OH)_2$

C. Other

a_A^b	activity of component A in phase b
X_A	mole fraction of component A
K	equilibrium coefficient
$K_{D_{A-B}}^{Fe-Mg}$	distribution coefficient of Fe-Mg exchange between A and B
ln	natural logarithm
$\triangle G_r$	free energy for reaction
$\triangle H_r$	enthalpy of reaction
$\triangle H_f$	enthalpy of formation
$\triangle S_r$	entropy of reaction
$\triangle V_r$	volume change of reaction
P_{total}	lithostatic pressure
P_{fluid}	fluid pressure
R	gas constant

BMR Journal of Australian Geology & Geophysics, 7,197–213

MULTIELEMENT COMPOSITION OF THE CONODONT *ICRIODUS EXPANSUS* BRANSON & MEHL FROM THE UPPER DEVONIAN OF THE CANNING BASIN, WESTERN AUSTRALIA

Robert S. Nicoll

The apparatus structure of the conodont *Icriodus expansus* Branson & Mehl is here recognised as consisting of seven element types—I, Ca, Cb, Cc, Cd, Ce and Cf. The apparatus contains one pair of I elements and over 140 associated cone elements. The orientation of the I element is reversed. The study is based on a large collection of fused clusters found in a sample from the Upper Devonian (Frasnian) Napier Formation in the Oscar Range of the Canning Basin, Western Australia.

Introduction

Collection of conodont-bearing limestone samples from the early Late Devonian Napier Formation at the margin of a small leucite lamproite plug (Nicoll, 1981) in the Oscar Range, Canning Basin, of Western Australia (Fig. 1) in 1978 produced one sample (WCB 804/5) that contained about 100 fragments of fused conodont clusters belonging to the genera *Icriodus* and *Polygnathus*. Recollection from the sample site in 1980 has resulted in a collection of over 1000 clusters or cluster fragments and several thousand discrete elements from 25 kg of limestone. All the conodont elements have a conodont colour alteration index of five (CAI 5).

Specimens contained in the clusters and in the associated discrete element fauna are assigned to three multielement taxa: *Icriodus expansus* Branson & Mehl, 1938; *Polygnathus xylus xylus* Stauffer, 1940; and *Ozarkodina brevis* (Bischoff & Ziegler, 1957). *I. expansus* is the most abundant with more than 850 clusters recovered. *P. xylus xylus* is represented by over 200 clusters and *O. brevis* by only 10 clusters. In no case is there any indication of mixing of the three species in any of the clusters. The abundance of clusters accurately mirrors the abundance of discrete elements. Description of *P. xylus xylus* and *O. brevis* will follow in a later paper.

The indicated age range of the three species recovered from the cluster bed is Middle to Late Devonian (Givetian to Frasnian). *P. xylus xylus* is supposed to range as high as the Lower *asymmetricus* Zone (Klapper & Ziegler, 1979) or Upper *asymmetricus* Zone (Seddon, 1970). A sample collected from traverse section (WCB 318), part of a study of the Oscar Range-Napier Range Devonian conodonts, contains *Ancyrodella lobata* (sample WCB 318/11) and is located stratigraphically below the cluster bed. This would indicate an age no older than the Middle *asymmetricus* Zone and would thus suggest that the age

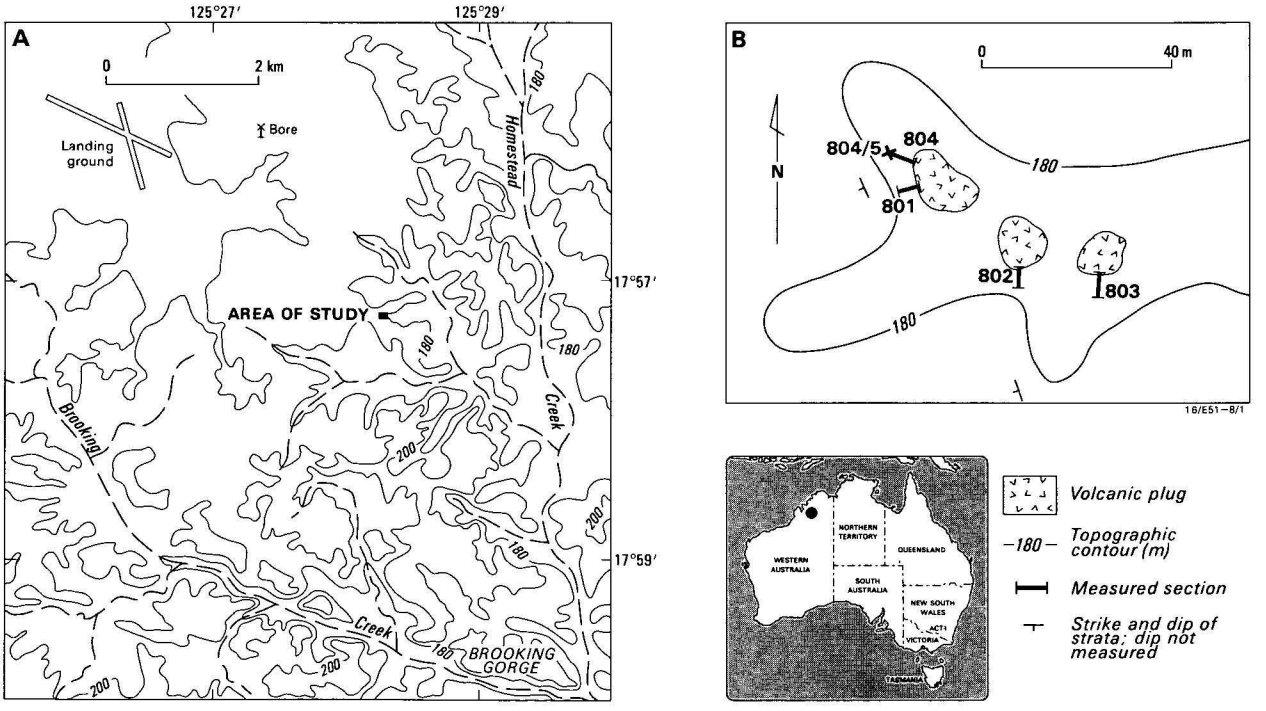

Figure 1. Locality maps.
A—Study area near the eastern end of the Oscar Range, Leopold Downs 1:100 000 topographic map, grid reference 3962-618132.
B—Location of *Icriodus*-bearing material (sample 804/5).

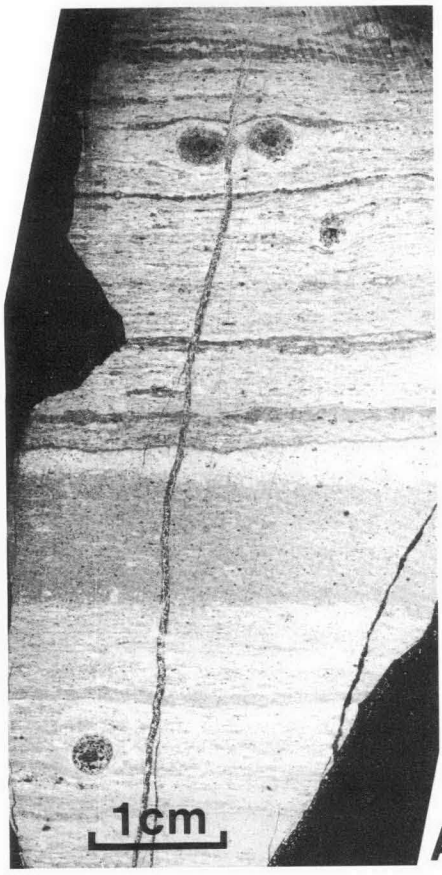

Aa

Ab

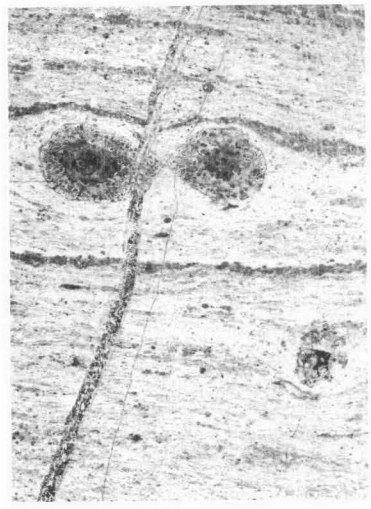

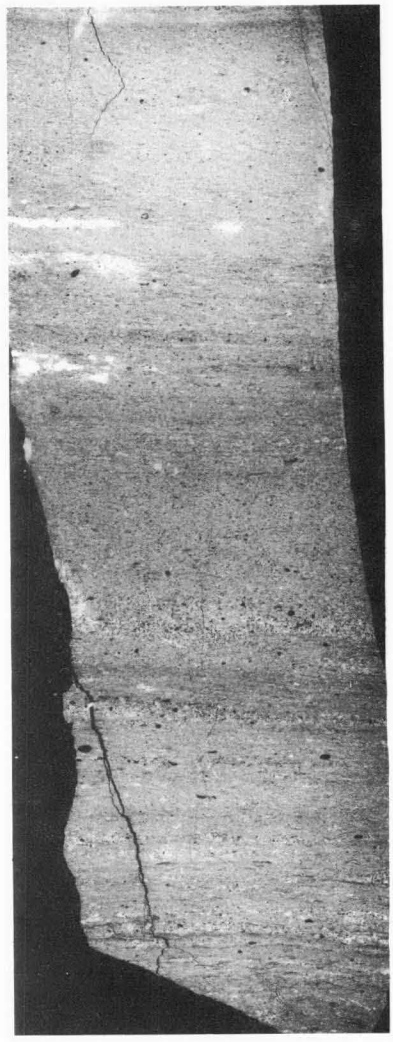

B

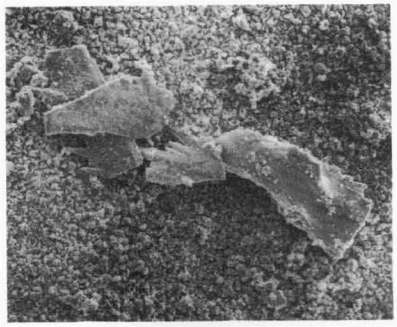

C

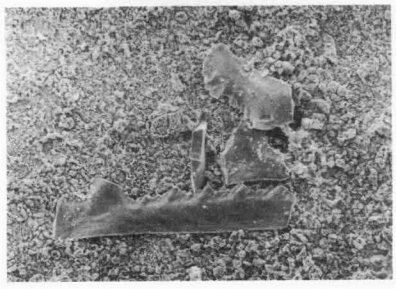

D

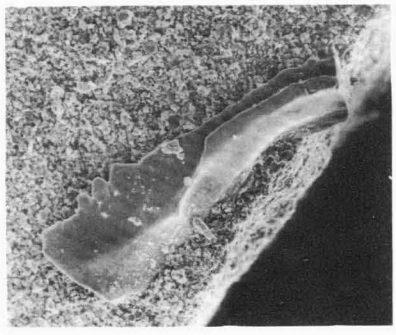

E

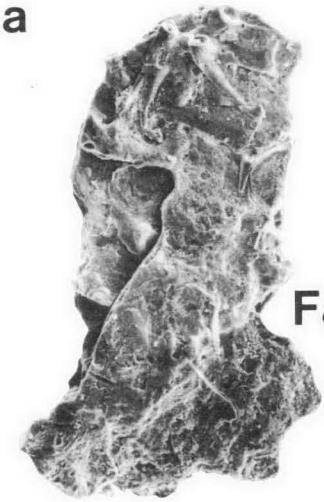

Fa

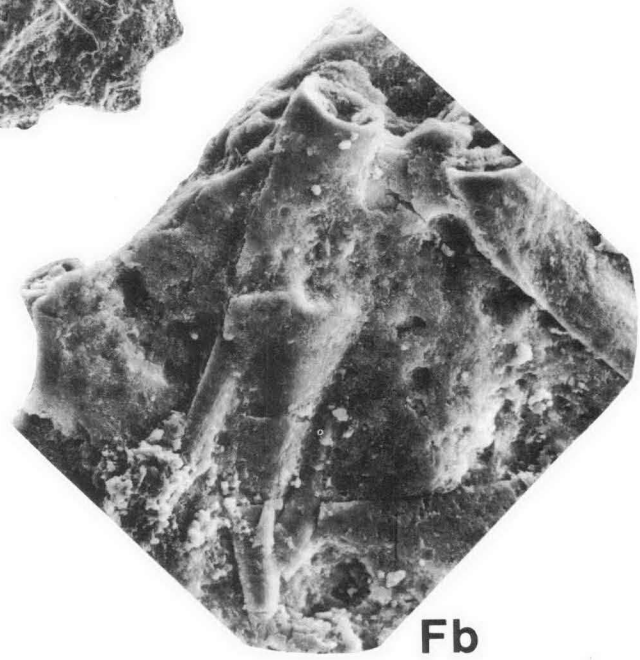

Fb

range of both *O. brevis* and *P. xylus xylus* could be as high as the Upper *asymmetricus* Zone, as was indicated by Seddon (1970). The age of the cluster bed fauna is thus Late Devonian (Frasnian) and more specifically, Middle *asymmetricus* Zone.

The limestone bed containing the conodont clusters is a micrite about 10 cm thick. The composition and texture of the bed (Fig. 2 A,B) are not uniform, but show a distinct layering, in part, owing to the distribution of small fossils. The fossils are mostly ostracods, some small gastropods, a few small brachiopods, and what may be a calcareous sponge. One acid-etched surface contained a small echinoid spine. Burrows, up to 5 mm in diameter, found mostly in the upper half of the bed, are generally in the plane of the bedding and filled with sparry calcite.

To determine the distribution and relationship of conodont elements in the bed, a series of slabs, each about 10 mm thick, was cut parallel to the bedding and then partly etched with acid. Conodonts, as discrete elements or clusters, were found on the slab surfaces throughout the bed and do not appear to be related to any lithology or level within the bed.

Eighteen discrete elements or clusters were observed on the 0.3 m^2 of etched slab surface. None of the elements were observed either within the burrows or along the margin of the burrow structures. The distribution of conodonts appears to be random within the bed and not related to any variation of microfacies of the bed. Elements appear as single discrete elements (Fig. 2E), fused clusters (Fig. 2C), and as related elements in close proximity (Fig. 2D). No other skeletal phosphatic material is associated with the elements.

Processing of samples to obtain the clusters was done using acetic acid on lumps of rock 5-10 cm across. Acid was changed daily and the residue washed by decanting. This last step was taken because the cone elements of the *Icriodus* apparatus are so small that they would have been lost through standard sieves. Some specimens may have been lost, owing to surface tension during decanting of excess water, but virtually all conodont elements in the rock were recovered.

A number of the figured specimens were lost or damaged when two SEM stubs were dropped during photography. In addition, some of the most delicate clusters, most notably the fused juvenile I elements shown in Figure 9, disintegrated while being removed from the stubs. The specimens from this study are lodged in the Commonwealth Palaeontological Collection (CPC) at the Bureau of Mineral Resources in Canberra.

Multielement *Icriodus*

The first documented interpretation of the multielement structure of *Icriodus* was by Lange (1968) on material that he considered to be of probable coprolitic origin. Lange assigned his material to *I. alternatus* and recognised an assemblage consisting of a single pair of I elements in association with an indeterminate number, 30 to 56, of acodinan cone elements. Lange's line drawings (1968, pl. 6) show some differentiation of the cone elements, but do not have sufficient detail to allow comparison with the cone element types recognised in the present study.

Klapper & Philip (1971, 1972) described the apparatus structure of *Icriodus* as well as *Pelekysgnathus* and *Pedavis*. At that time they thought that *Icriodus* consisted of only two element types, the I and the acodinan S_2 elements. Later, Klapper & Ziegler (1975) recognised that *Icriodus* might also contain an M_2 element.

Other workers, most notably Bultynck (1972) and van den Boogaard & Kuhry (1979) have argued that the *Icriodus* apparatus lacked cone elements. These authors cited the low levels of occurrence together of I and cone type elements in samples as the principal reason for rejecting an *Icriodus* plus cone apparatus structure.

In 1977, I recognised an *Icriodus* apparatus structure consisting of I, M_2 and S_2 elements (Nicoll, 1977). At the time, I speculated that, on the basis of a size-graded series of four I elements, the *Icriodus* apparatus might contain as many as four pairs of I elements. The present study has not substantiated that speculation, but it should be noted that the former material represented a different *Icriodus* species.

Several recent studies have tended to support the multielement composition of genera in the family Icriodontidae. Uyeno & Klapper (1980) have defined an apparatus structure of I, S_2, and M_2 elements in *Steptotaxis* and recognised three types of S_2 elements in *S.* n.sp. A and *S.* n.sp. B. Uyeno (*in* Norris & Uyeno, 1981) has recognised three acodinan cone element types (S_{2a}, S_{2b}, S_{2c}) in association with *Icriodus subterminus*. Johnson & Klapper (1981) have established statistically the presence of both S_2 and M_2 elements associated with I elements in *Icriodus nevadenis* and *T. trojani*.

Notation applied to elements

As the number of element types recognised as part of the *Icriodus* apparatus has changed over the years, there has been established a patchwork notational scheme modified from that originally proposed by Klapper & Philip (1971). This has meant that the notational scheme has grown without an overall plan

Figure 2. Thin sections of cluster bed (A-B), three examples of conodont elements from acid-etched surfaces of limestone slabs, (C-E) and phosphatic chips (F).
A—Thin section (Aa) of cluster bed and enlargement of burrows (Ab) showing microfacies variation; circular features near top and bottom are cross sections of burrows and are about 3 mm in diameter; CPC 22459. B—Thin section from another specimen, showing the degree of lateral variation of microfacies; CPC 22460. C—*Polygnathus xylus xylus;* Pa element and broken S elements; (56x) CPC 22461. D.—*Polygnathus xylus xylus;* broken Sa and Sc elements; (40x) CPC 22462. E. *Polygnathus xylus xylus;* single Pa element; (65x) CPC 22463.
A number of thin phosphatic chips were recovered in the residue and many of these contained conodonts, both *Icriodus expansus* and *Polygnathus xylus xylus*. As in the other clusters, there is no mixing of taxa on the chips. F—Cone elements of *I. expansus* in phosphatic chip. CPC 22464. Fa—view of chip (65x) and Fb—enlargement of cones (330x).

and that there is no unity between schemes that have been applied to different genera of the Icriodontidae. In an attempt to resolve some of the these problems I suggest a new notational scheme that can be applied to all the Icriondontidae.

The notational scheme devised by Klapper & Philip (1971) for their type 4 apparatuses (I, S & M) is too tied to form-element nomenclature to be used in the present situation, where six distinct cone element types are recognised in the *Icriodus* apparatus.

Barrick (1977) has applied the Sweet & Schonlaub (1975) notational system to his simple-cone element apparatuses. I feel it is improbable that there is either a close positional or functional analogue between the simple cone elements M and Sb-Sd, as used by Barrick, and the platform-ramiform elements to which Sweet & Schonlaub applied the original notation scheme. If this contention is accepted, then the forcing of cone elements into a platform-ramiform notational scheme is not relevant when a functional and positional interpretation is applied to the analysis of the elements.

I also find the letter-code system applied by Barnes & others (1979) to simple cones difficult to apply to the style of morphologic variation found in *Icriodus* elements, especially as the *Icriodus* apparatus does not fit any of their categories of apparatus type.

For the above reasons I will here apply yet another notational scheme, specifically to the genus *Icriodus*, but which is also probably relevant to related taxa (e.g. *Pelekysgnathus, Pedavis, Steptotaxis*). The notation of the *Icriodus* apparatus is I, Ca, Cb, Cc, Cd, Ce, and Cf. The notation I is applied to the platform element and is used as originally defined by Klapper & Philip (1971). All cone elements are described by an upper case C and the lower case letters a-f. The notations Ca to Cf are applied to distinct element morphologies and do not imply a symmetry transition series with morphologic or functional intergradation between element types. As a general statement the cone element types Ca-Cd are comparable to the Klapper & Philip S_2 acodinan element. The cone elements Ce and Cf are analogous to the M_2 element of other authors.

Orientation of I element

Branson & Mehl (1934, 1938) in their original description of the genus *Icriodus* oriented the specimens with the tips of the basal cavity posterior and the three-rowed process anterior. This orientation has been followed by most subsequent workers (Klapper & Ziegler, *in* Ziegler, 1975). The direction of curvature of the tips of the basal cavity has been cited as confirming the validity of this orientation (Lindstrom, 1964).

From this study, it is apparent that this orientation of the I element of the genus *Icriodus*, and thus all members of the family Icriodontidae, should be questioned. I propose that the correct orientation of the I element of the genera *Icriodus*, *Pelekysgnathus*, *Pedavis*, and *Steptotaxis*, is with the dual-tipped basal cavity anterior and the platform-like denticle supporting structure posterior. This proposal is based on the interpretation of a number of morphologic features shown by the *I. expansus* material from this study, including: (1) the origin of the dual-tipped basal cavity; (2) the shape of the basal cavity; (3) the growth pattern of the upper surface.

The apparent pattern of growth of the Pa element of many genera, such as *Polygnathus, Gnathodus*, and *Siphonodella*, is for the anterior blade to be well

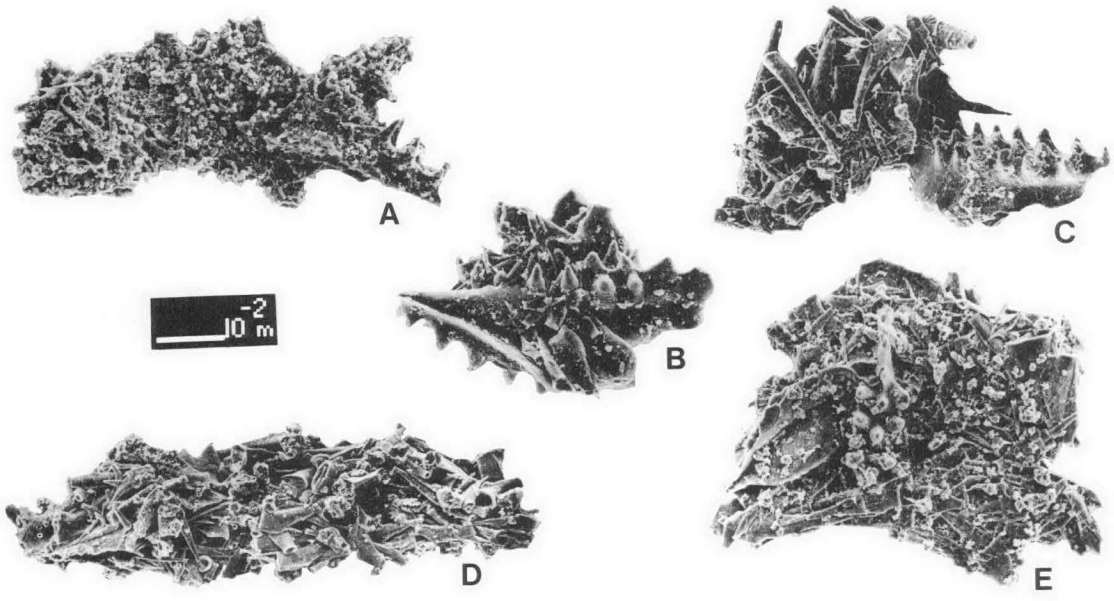

Figure 3. *Icriodus expansus* **clusters (all specimens 115 x).**
A—Cluster with one pair of I elements and an indeterminate number of cone elements; I elements configuration anterior-anterior, bases outward; CPC 22465. B—Cluster with one pair of I elements and more than 30 cone elements; I element configuration anterior-anterior, bases outward; CPC 22466. C—Cluster with single I element and more than 60 cone elements; CPC 22467. D—Cluster with single I element and 130 cone elements counted from exposed view; one Ca element is located almost touching anterior end of I element; CPC 22468. E—Cluster with one pair of I elements and 105 cone elements counted on exposed view; I element configuration anterior-anterior, bases outward; CPC 22469.

formed at a very early growth stage. This does not necessarily mean that additional denticles will not be added to the anterior margin of the blade as the specimen matures, but that, by comparison with the platform, the blade attains a mature morphology at an early stage. Subsequent major growth modification of most platform elements takes place as a modification of the platform, principally by its posterior and lateral expansion. By orienting the *Icriodus* I element with the three-row platform posterior, a similar growth pattern is observed.

The outline shape of the basal cavity of the I element, when conventionally oriented, is not the shape displayed when most Pa elements with enlarged basal cavities are oriented with the blade anterior. The morphology of the basal cavity of genera such as *Gnathodus*, *Clydagnathus*, and *Polygnathus* is for the cavity to open laterally, very abruptly, at or near the posterior end of the blade and to then gradually taper posteriorly. If *Icriodus* is oriented with the rounded, dual-tipped lip of the basal cavity anterior, then the outline of the basal cavity is similar to that of other genera. The outline of the cavity reflects the morphology of the surface to which the conodont element is attached, and one would not expect the attachment structure of *Icriodus* to be the reverse of that of other conodont organisms.

The mode of origin of the dual-tipped basal cavity suggested below, that is the fusion of a cone element to the margin of the I element, is only possible if the margin is the anterior margin. If the I element of *Icriodus* is analogous to the Pa element of genera such as *Polygnathus* or *Ozarkodina*, then the position of the I element is at the posterior end of the element sequence, assuming a linear rather than radial pattern (Nicoll, 1977). There would thus have been no cone elements located behind the I element to fuse with it, if the previously accepted element orientation is used.

I conclude, therefore, that, for the family Icriodonitidae, the dual-tipped basal cavity is located at the anterior rather than the posterior margin of the I element. An analogy between platform type Pa elements and the I element can be made; the I element has a short anterior blade, usually no more than two or three denticles, located in front of a platform composed of three rows of denticles

In members of the *Icriodus latericrescens* group the lateral process is anteriorally directed, but the spurs and lateral processes of *Icriodus* and *Pedavis* species are posteriorly directed.

Table 1. Configuration of I-element clusters of *I. expansus* and associated cone elements

	Associated cone elements		
Two-I elements configuration	*>10*	*<10*	*Totals*
ant-ant bases opposed	15	23	38
ant-pos bases opposed	1	4	5
ant-ant bases same	6	10	16
ant-pos bases same	5	—	5
other orientations	6	13	19
One-I element & cone element association	92	172	264

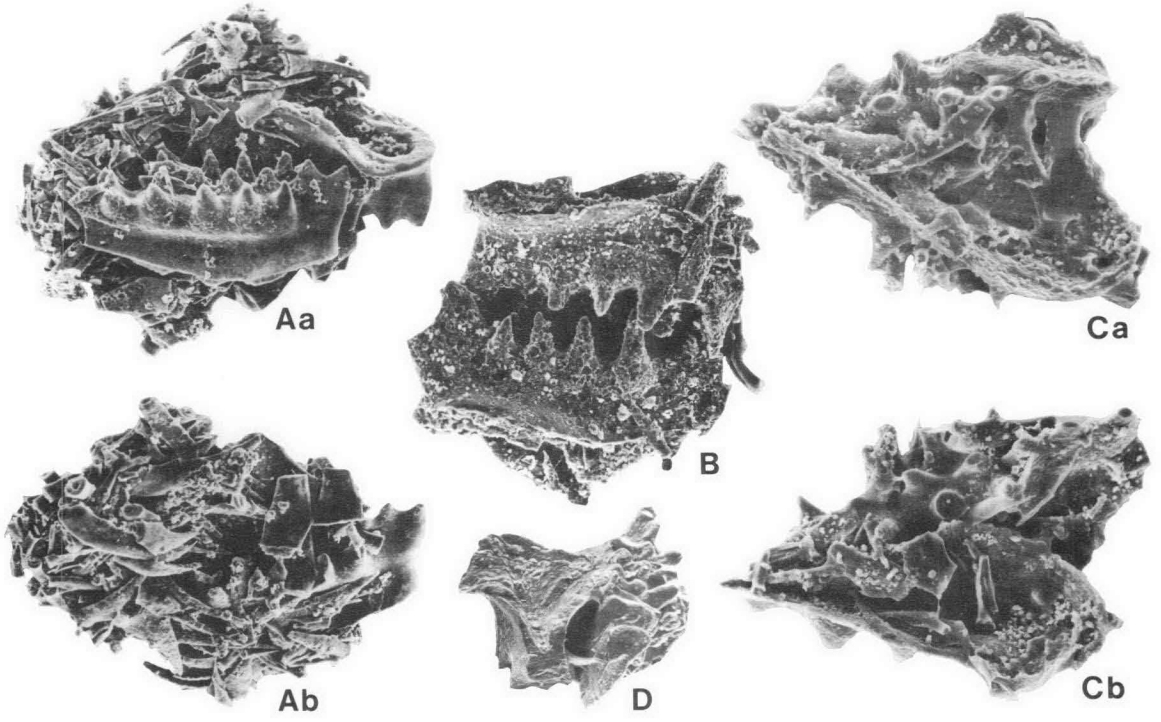

Figure 4. *Icriodus expansus* **clusters (all specimens 110x).**
A—Two sides of cluster containing single pair of I elements and at least 140 cone elements. Care was taken in counting the reverse side cone elements not to count any denticle that might have been observable from other side, and thus the denticle count is probably conservative; I elements anterior-anterior, bases outward; CPC 22470. B—Cluster with single pair of I elements and at least 25 cone elements. I element configuration anterior-anterior, upper surfaces touching; CPC 22471. C—Two sides of cluster containing single pair of I elements and at least 40 cone elements; I element configuration anterior-anterior, bases outward; CPC 22472. D—Cluster with single pair of I elements and only a few cone elements; I element configuration anterior-anterior, bases outward; CPC 22473.

Clusters

In this study over 850 clusters have been recovered that contain elements of *Icriodus expansus*. Over 350 of the clusters contain cone elements and at least one I element. The rest consist of only cone elements. These figures may be misleading, because the clusters are relatively easily fragmented and many may have been broken into smaller clusters during physical preparation of the samples (washing, heavy liquid separation).

Of 347 clusters containing at least one I element, roughly 25 per cent contained two I elements and a number of cone elements. In no cluster is there any indication of more than two I elements. Owing to the three-dimensional nature of the clusters and mineral overgrowth in some examples, accurate counts of the total cone elements and numbers of individual cone types are not possible. At least 141 cone elements have been counted in one of the larger and cleaner clusters (Fig. 4A).

The orientation and relationship of elements within the clusters have been examined. There is a general tendency for the clusters to be elongated and for the I elements to be located at or toward one end of the clusters (Figs. 3A,D). Cone element types Ca, Cb, Cc, and Cd, may be randomly distributed, but are frequently associated with the I elements. There is no observable size gradation of the Ce and Cf cone elements from one end of a cluster to another.

The relative configuration of the I elements has been examined (Table 1). Almost half the 83 clusters with

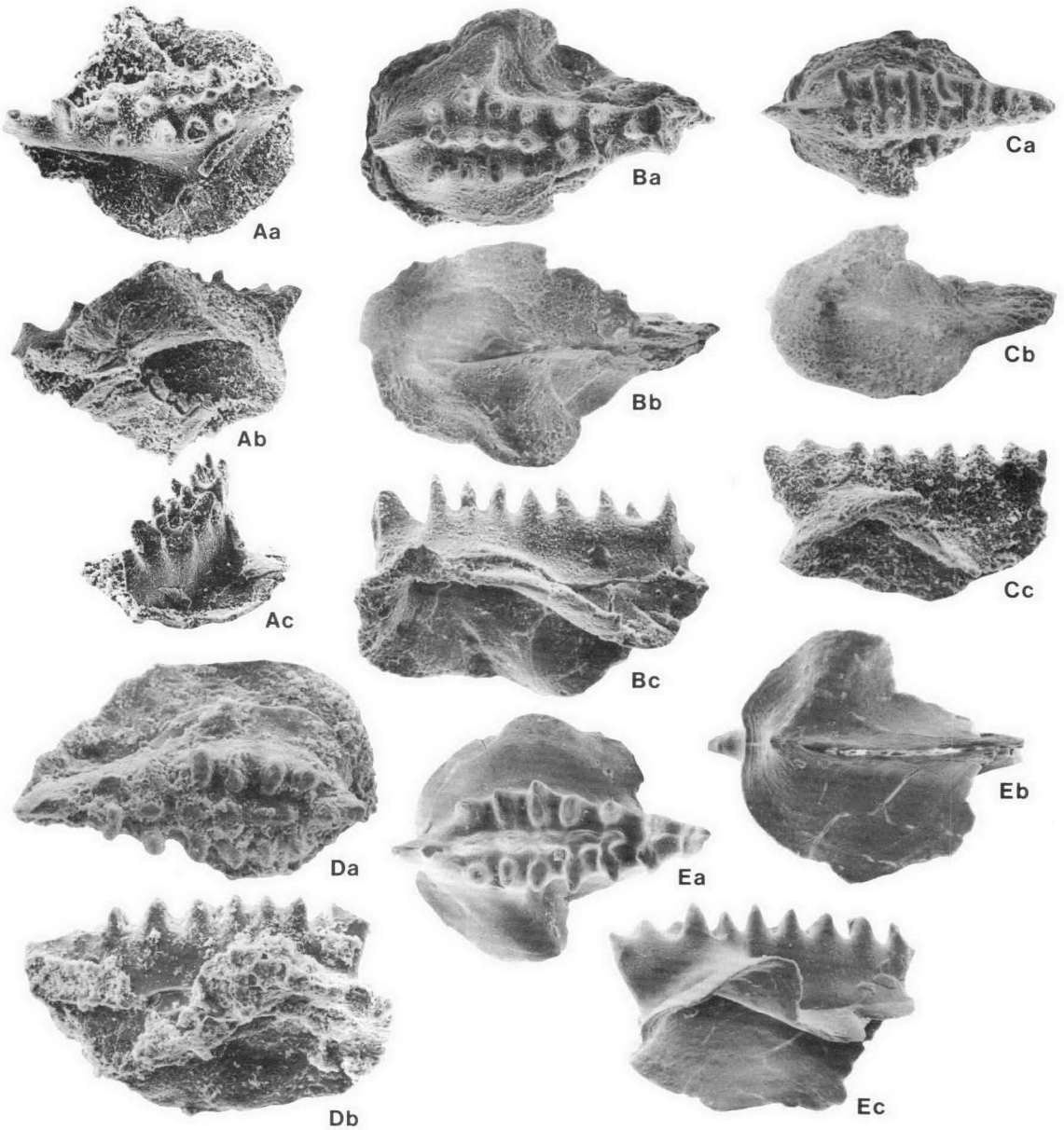

Figure 5. I element basal plate morphology (all specimens 90x).
A—I element: Upper (Aa), basal (Ab), and posterior (Ac) views; CPC 22474. B—I element: Upper (Ba), basal (Bb), and lateral (Ac) views; CPC 22475. C—I element: Upper (Ca), basal (Cb), and lateral (Cc) views; CPC 22476. D—I element: Upper (Da) and lateral (Db) views; CPC 22477. E—I element; Upper (Ea), basal (Eb), and lateral (Ec) views; CPC 22478.

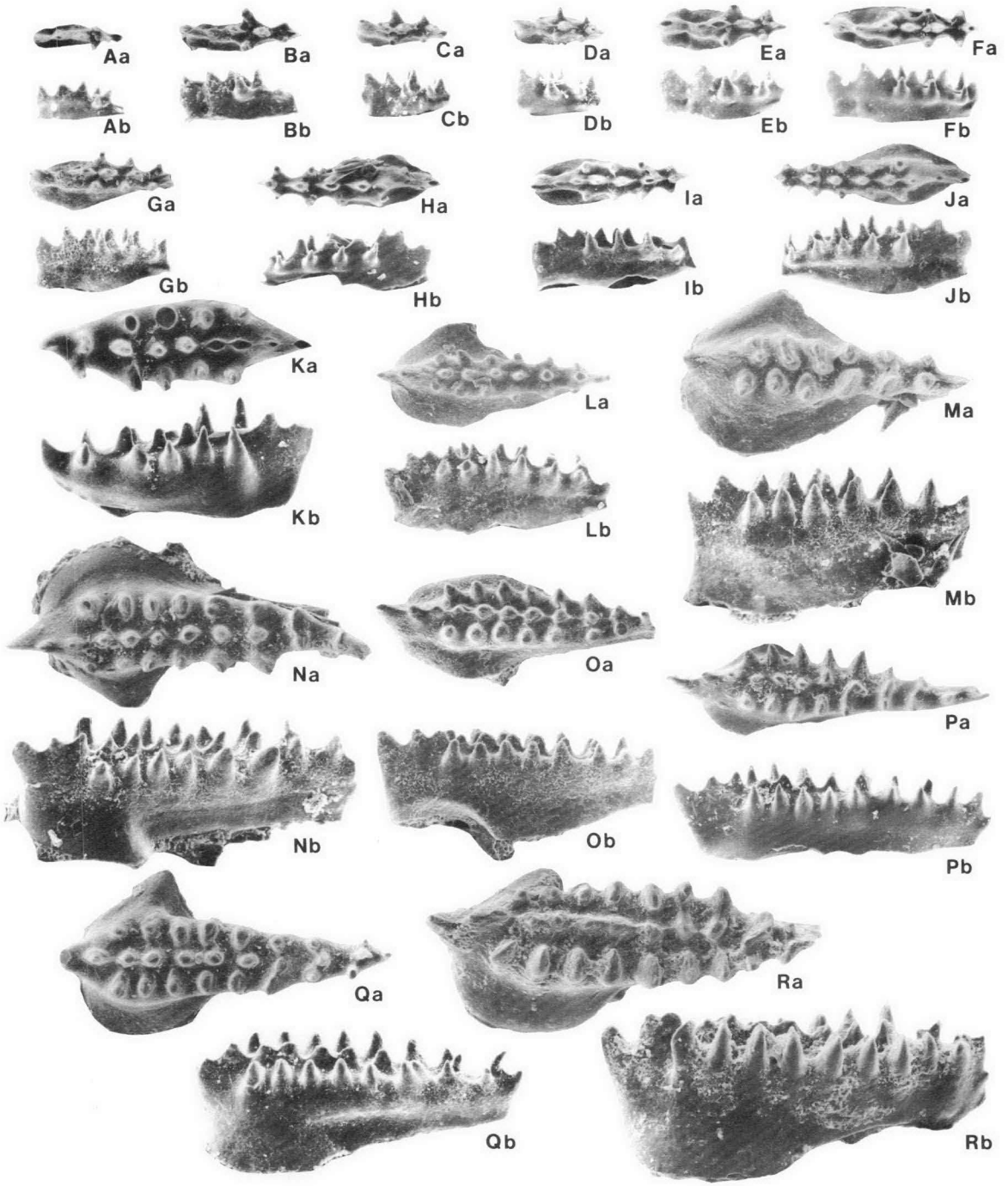

Figure 6. Growth series of I elements of *Icriodus expansus* from the first triad (one pair lateral denticles) stage to the ninth triad (nine pair lateral denticles) stage (all specimens 80x).

A—First triad and developing second triad stage, three blade denticles; CPC 22479. B—First triad and developing second triad stage, three blade denticles; CPC 22480. C—Second triad stage, two blade denticles; CPC 22481. D—Second triad stage, two blade denticles; CPC 22482. E—Second triad stage, three blade denticles; CPC 22483. F—Third triad stage, three blade denticles; CPC 22484. G—Third triad stage, three blade denticles; CPC 22485. H—Fourth triad stage, three blade denticles; CPC 22486. I—Fourth triad stage, three blade denticles; CPC 22487. J—Fifth triad stage, three blade denticles; CPC 22488. K—Fifth triad stage, three blade denticles; CPC 22489. L—Sixth triad stage, three blade denticles; CPC 22490. M—Sixth triad stage, two blade denticles; CPC 22491. N—Seventh triad stage, three blade denticles; CPC 22492. O—Seventh triad stage, three blade denticles; CPC 22493. P—Eighth triad stage, two blade denticles; CPC 22494. Q—Eighth triad stage, two blade denticles; CPC 22495. R—Ninth triad stage, three blade denticles; CPC 22496.

two I elements have those elements oriented with the long axes roughly parallel, the basal cavities facing outward, and the anterior ends pointing in the same direction. The elements are either in a side by side configuration (Fig. 4A, C, D) or with denticles intermeshed (Fig. 4B). Other configurations occur with less frequency.

In all examples where two I elements are observed together in a cluster, both elements are at the same stage of development. The elements are of about the same size and have the same number of lateral denticles. There is no indication of loss and replacement of one of the I elements in any of these clusters.

From the data, it seems clear that the configuration of the I elements in the living conodont animal must have been with the denticulate surfaces close together on either side of a groove. This differs from the orientation suggested by Schmidt (1950), in which the Pa elements are side by side with the upper surfaces not opposed.

Systematic palaeontology

GENUS *ICRIODUS* BRANSON & MEHL, 1938

Type species. *Icriodus expansus* Branson & Mehl, 1938

Icriodus expansus Branson & Mehl, 1938
(Figures 3–12)

1938 *Icriodus expansus* Branson & Mehl, p. 160, Pl. 26, Fig. 19.

1975 *Icriodus expansus* Branson & Mehl; Klapper & Ziegler in Ziegler ed. p. 109, Pl. Icriodus 1, Figs. 1, 2 (with synonymy).

Diagnosis. Multielement taxa with seven element types —I, Ca, Cb, Cc, Cd, Ce, and Cf. I element is incriodontan, C elements are cone type.

Description of elements

I Element. (Figs. 5–8); material studied—more than 1000 discrete elements.

The crown of the I element has from three to twelve central row denticles and one to nine pairs of lateral row denticles. In juvenile specimens all denticles are discrete with the central row denticles laterally compressed and the lateral row denticles rounded. Mature specimens with five or more pairs of lateral row denticles may show fusion of the central row denticles with one or the other of the lateral row denticles of the denticle triad. However, most specimens show little or no denticle fusion.

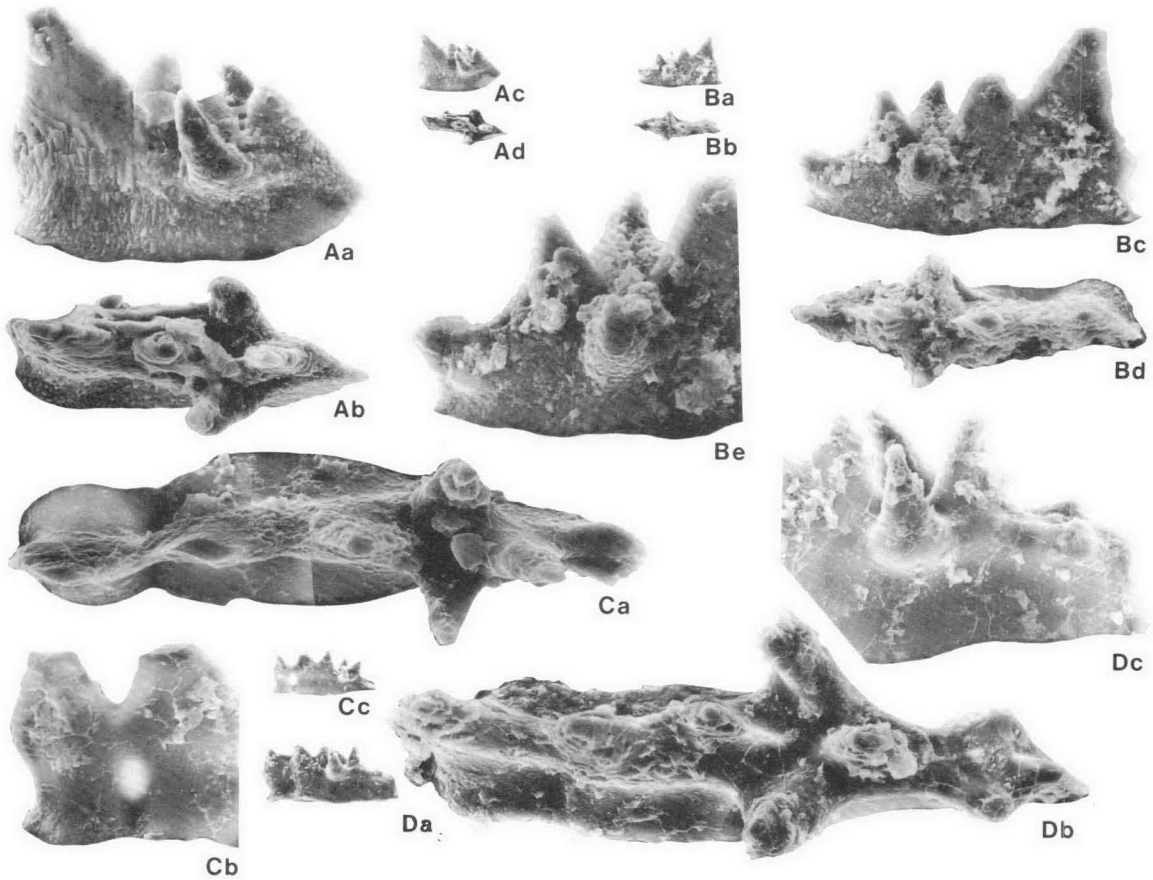

Figure 7. Juvenile I elements—first triad stage (small views 80x, enlargements 420x except as noted).
A—I element with two blade denticles; earliest growth stage recovered with first triad of denticles and no indication of second denticle triad; CPC 22497; lateral views Aa, Ac; upper views Ab, Ad. B—I element with two blade denticles; early growth stage with first denticle triad and buds of second denticle triad at initial growth stage; CPC 22498; lateral views Ba, Bc, Be (650x); upper views Bb, Bd. C.—I element with three blade denticles and first triad of denticles developed; growth of second denticle triad showing at posterior tip; same specimen as Fig. 6A; CPC 22479; Ca—enlarged upper view; Cb—enlarged view of anterior blade denticles with thin spot between denticles; Cc—lateral view. D—I element with three blade denticles; first triad of denticles well developed and second triad at an early growth stage; same specimen as Fig. 6B; CPC 22480; Da—lateral view; Db—enlarged upper view; Dc—enlarged lateral view of posterior showing early growth stage of denticles.

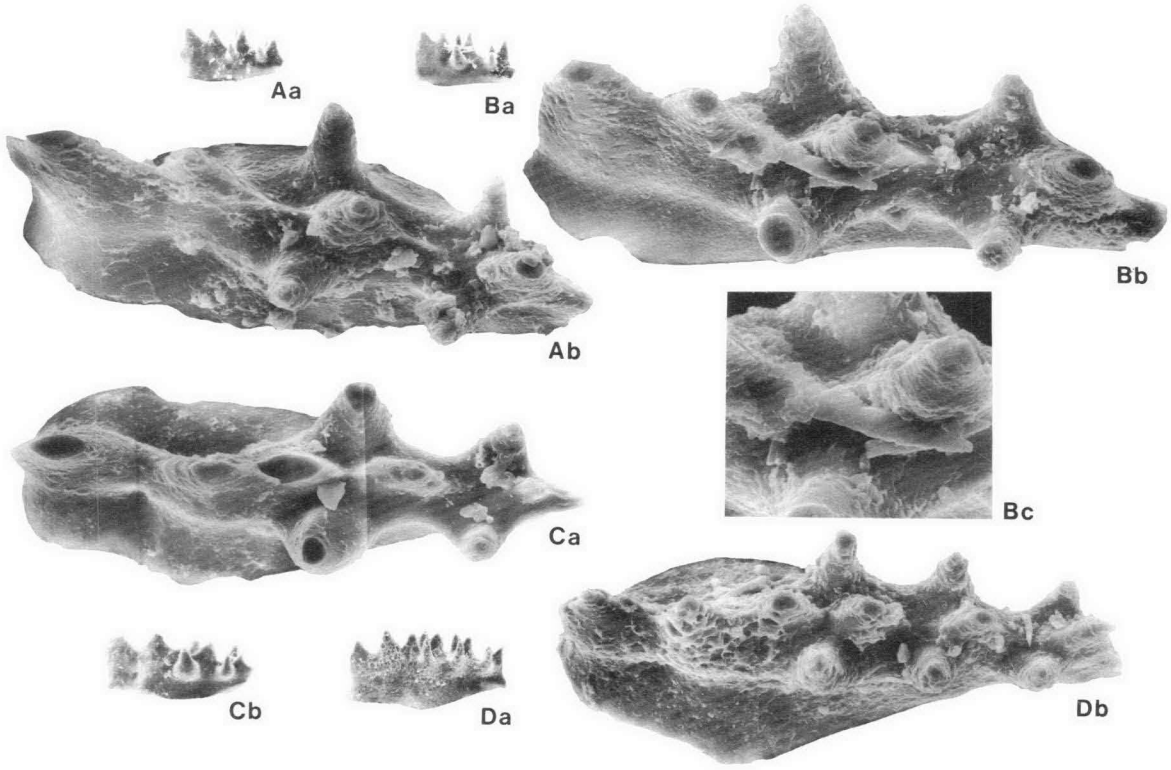

Figure 8. Juvenile I elements—second and third triad growth stage (small views 80x, enlargements 420x except as noted).
A—I element with two blade denticles, second triad growth stage; same specimen as Fig. 6C; CPC 22481; Aa—lateral view; Ab—enlarged upper view. B—I element with two blade denticles, second triad growth stage; same specimen as Fig. 6D; CPC 22482; Ba—lateral view; Bb—enlarged upper view; Bc—enlargement of two very small denticles fused to upper surface (700x). C—I element with three blade denticles, second triad growth stage; same specimen as Fig. 6E; CPC 22483; Ca—enlarged upper view; note that flange at base of crown has not filled out to smooth margin between anterior two denticles; Cb—lateral view. D—I element with three blade denticles, third triad growth stage; same specimen as Fig. 6G; CPC 22485; Da—lateral view; Db—enlarged upper view; note that flange at base of crown has almost filled out to smooth margin.

A short anterior blade is formed by the first two or three anterior-denticles before the first triad of central and lateral row denticles. The basal cavity is deeply excavated with two basal cavity tips. The outline of the cavity is slightly asymmetrical in juvenile specimens, but mature specimens may have a pronounced, slightly posteriorly directed, inner lateral spur. The outer margin is smoothly rounded.

Many specimens (Fig. 5) have a well-preserved basal plate, that extends outward beyond the crown for a width equal to about one third the height of the crown. Around the anterior margin the flange of the basal plate is directed outward, but as the basal cavity narrows posteriorly the flange is directed downward so that the cavity width of the basal plate is no more than that of the crown.

A growth series of the I element is shown in Figure 6. The smallest juvenile form (Fig. 7A) consists of only a single pair of lateral denticles and three central row denticles, two of which form the blade. Growth takes place in a posterior direction with the addition of successive denticle triads composed of one central row denticle and a pair of lateral row denticles. It appears that denticle growth of each triad may be initiated from a central point. Denticles of each triad appear to grow to moderate size before the next denticle triad appears.

No speciments have been observed at a stage prior to the first denticle triad. However, the pre-triad growth stage must have consisted of only two or three laterally compressed denticles.

An interesting morphologic pattern in early growth stages may explain the origin of the dual tip of the basal cavity of *Icriodus*, as well as the related genera of *Pelekysgnathus* and *Pedavis*. Some I elements (Figs. 7, 9) show the anterior blade denticle partly separated from the adjacent blade denticle. In one or two examples there appears to be a very thin spot or cavity at mid-denticle height between the two denticles (Fig. 7C). This is also reflected in a corresponding "coke bottle"-like constriction or waist in the margin of the crown. It appears that the blade of *Icriodus* may have originated with the fusion of two cone denticles.

Cone elements

In this study six cone element types are recognised in the apparatus structure of *Icriodus expansus*. All cone elements have in common the development of striations on the upper part of the element and a shoulder effect that interrupts the smooth taper of the anterior and posterior edges of these laterally compressed elements.

Four of the cone types (Ca, Cb, Cc, and Cd) appear to be represented by only a single pair of elements in the apparatus and are analogous to the S_2 elements of other authors. The rest of the cone elements, in excess of 130 elements, are divided between Ce and Cf type cones and are analogous to the M_2 element. Owing to the partial preservation and three dimensional

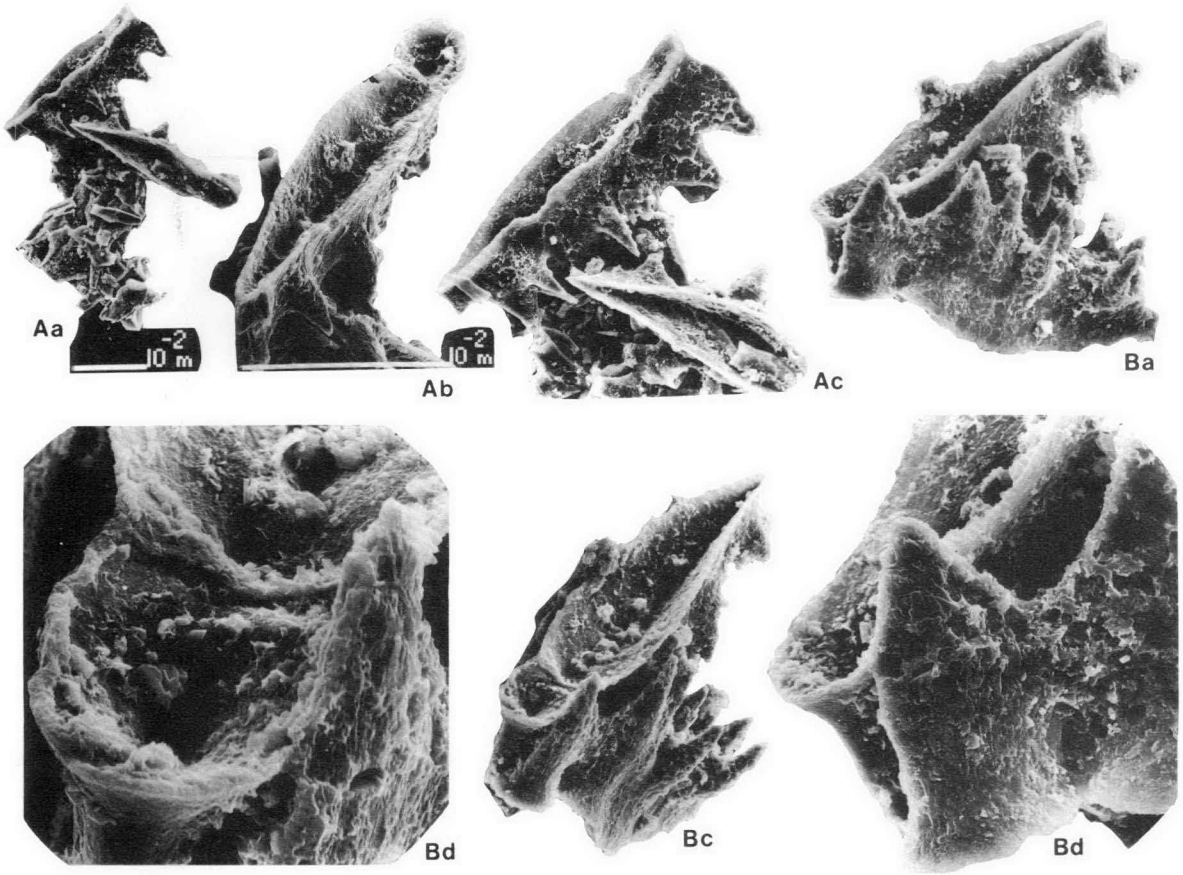

Figure 9. Juvenile I element clusters.
A—Cluster of single pair I elements, at second triad growth stage, and 55 cone elements; I elements are slightly skewed, but with posterior ends together; CPC 22499; Aa—view of cluster (100x); Ab—basal view of one I element showing dual basal cavity (290x); Ac—lateral view of same I element showing what appears to be lack of complete fusion of anterior blade denticles (290x). B—Cluster of single pair I elements, at second triad growth stage, and a few cone elements; I element configuration anterior-anterior, bases outward; the blade consists of three denticles, the anterior one showing a separate basal cavity and not at this stage surrounded by the same width of the lower flange of the crown found on the posterior part of blade; note the depression separating the two denticles at mid denticle height; CPC 22500; Ba—lateral view of element pair (300x); Bb—enlarged view of dual tip basal cavity (900x); Bc—oblique view showing base of one element and anterior view of second I element (300x); Bd—enlarged lateral view of anterior blade denticles (850x).

nature of the clusters, it is impossible to make an accurate count of the number of elements in larger, and thus presumably more complete, clusters. Two of the larger clusters contained 120 and 141 cone elements, mostly of types Ce and Cf.

Ca Element (Fig. 10N–R); material studied: 90 discrete elements.

Erect, bilaterally asymmetrical, laterally compressed cone element with bowed outer lateral margin and a slightly posteriorly directed outer lateral spur. In lateral view the element expands slightly, in the plane of the anterior-posterior axis, above the base and then narrows abruptly to form the shoulder on the anterior and posterior margins. Above the shoulder the element tapers gradually to the tip. The anterior and posterior margins have sharp keels. The cross-sectional shape of the base is similar to that of a large I element with a prominent spur that is directed slightly posteriorly. Fine striations are present on the lateral surfaces of the element above the shoulder. Some specimens (Fig. 10N) have a prominent costa associated with the lateral spur.

Cb element. (Fig. 10J–M); material studied—16 discrete elements.

Erect, bilaterally asymmetrical element with a triangular basal outline. The anterior side is broad and the element tapers posteriorly. There is a shoulder on the posterior margin and there may be a slight anterior shoulder. The striation pattern is similar to that of the Ca element.

Cc element. (Fig. 10E–I); material studied—53 discrete elements.

Bilaterally asymmetrical, laterally recurved element with straight outer lateral margin and an expanded inner basal flange. The anterior margin of the base is broadly rounded and expands slightly to mid-length before tapering toward the posterior margin. The thickness of the element is reduced along the anterior and posterior margins just above the base of the element, so that the margins are both sharp, as in the Ca element. There are prominent shoulders on both anterior and posterior margins.

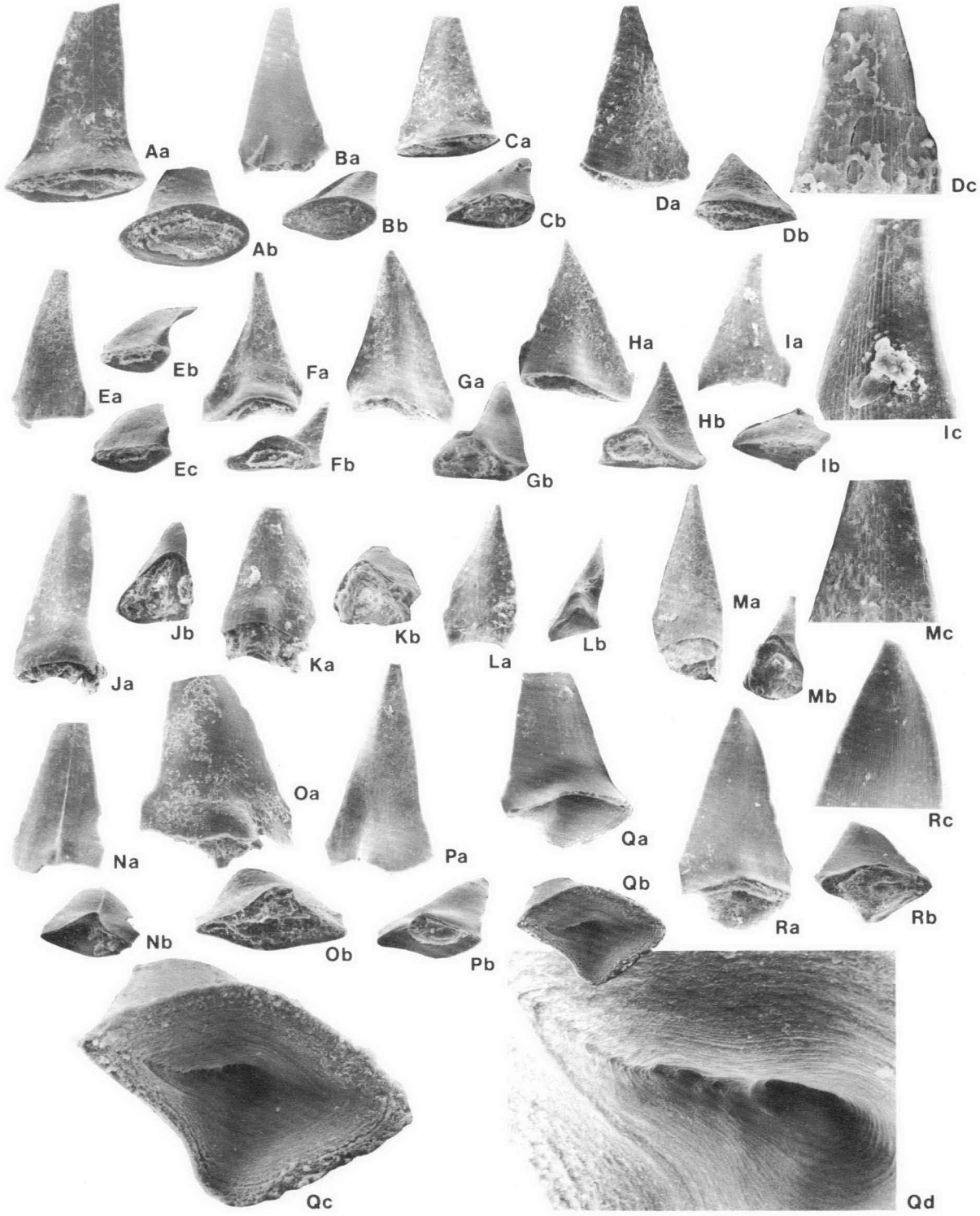

Figure 10. Cone elements Ca, Cb, Cc and Cd (All specimens 110x, except as noted).
A-D—Cone element Cd. A—CPC 22501, inner lateral (Aa) and basal (Ab) views; B—CPC 22502, outer lateral (Ba) and basal (Bb) views; C—CPC 22503, inner lateral (Ca) and basal (Cb) views; D—CPC 22504, outer lateral (Da), basal (Db) views, and enlargement (Dc) showing striation (385x). E-I—Cone element Cc. E—CPC 22505, outer lateral (Ea), oblique (Eb) and basal (Ec) views; F—CPC 22506, inner lateral (Fa) and basal (Fb) views. G—CPC 22507, inner lateral (Ga) and basal (Gb) views. H—CPC 22508, inner lateral (Ha) and basal (Hb) views. I—CPC 22509, outer lateral (Ia), basal (Ib) views, and enlargement (Ic) showing striations (385x). J-M—Cone element Cb. J—CPC 22510, lateral (Ja) and basal (Jb) views; K—CPC 22511, lateral (Ka) and basal (Kb) views; L—CPC 22512, lateral (La) and basal (Lb) views; M—CPC 22513, lateral (Ma), basal (Mb) views, and enlargement (Mc) showing striations (270x). N-R—Cone element Ca. N—CPC 22514, outer lateral (Na) and basal (Nb) views; O—CPC 22515, outer lateral (Oa) and basal (Ob) views; P—CPC 22516, outer lateral (Pa) and basal (Pb) views; Q—CPC 22517, inner lateral (Qa), basal (Qb), and enlarged basal interior views Qc (250x), Qd (800x) showing attachment grooves on inner basal surface of crown. R—CPC 22518, inner lateral (Ra), basal (Rb) views, and enlargement (Rc) showing striations (200x).

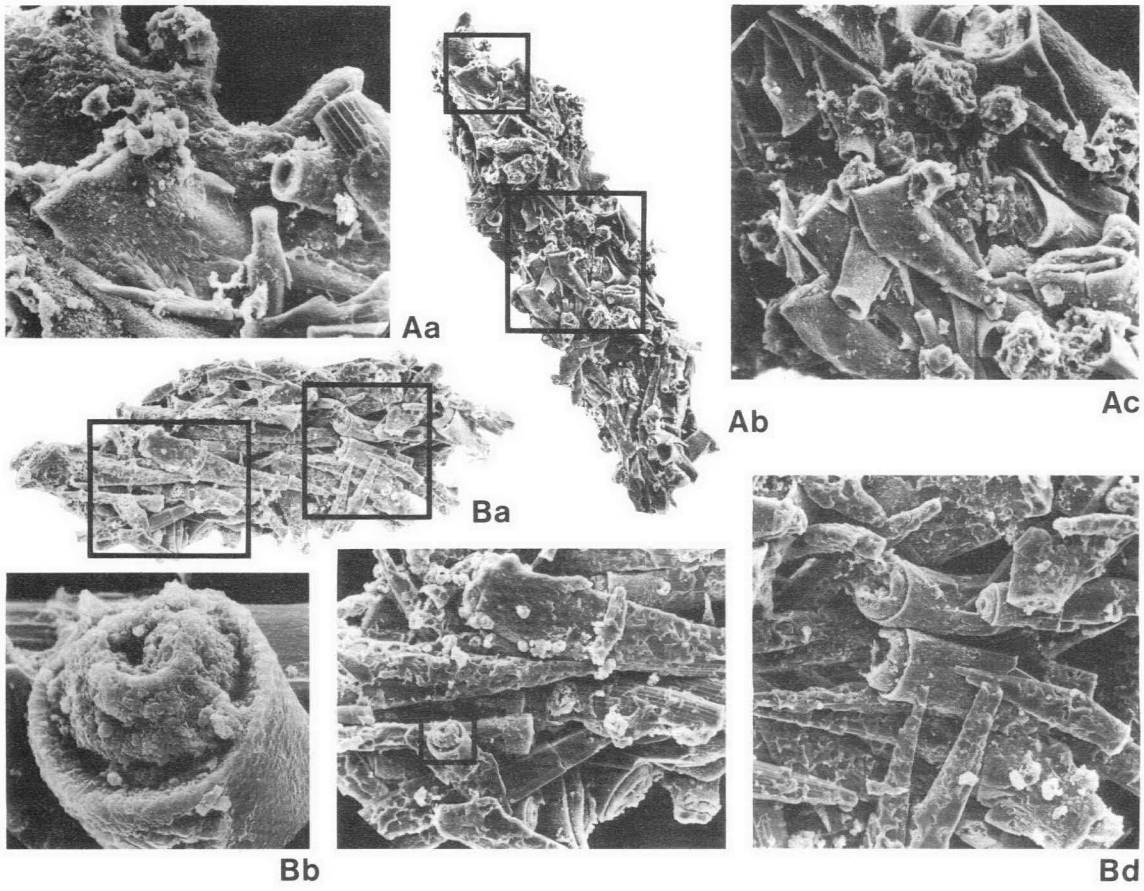

Figure 11. Cone elements Ce and Cf.
A—Cluster with single I element and 130 cone elements, many showing the slightly ovate basal cross-section typical of the Ce element; same specimen as Fig. 3D; CPC 22468; Aa—enlargement showing very small Ce element with well-developed shoulder spurs (550x); Ab—view of cluster, I element toward top of plate (115x); Ac—enlargement showing several Ce elements as well as a Ca element near top right corner (325x). B—Cone cluster (Ba) with more than 80 elements, mostly Cf elements and some Ce elements (120x) CPC 22519. Bb—enlargement of area outlined in view Bc, showing basal plate of Cf element (1800x); Bc—enlargement showing striation on elements and basal plates (285x); Bd enlargement showing basal plates of Cf elements (350x).

Cd element. (Fig. 10A–D); material studied—20 discrete elements.

Erect, bilaterally symmetrical to slightly asymmetrical element with oval base. Element tapers from base to tip with only very minor shoulders on anterior and posterior margins. The striation pattern is similar to that of the Ca element.

Ce element. (Fig. 11); material studied—more than 1000 specimens in clusters.

Cf element. (Fig. 11); material studied—more than 1000 specimens in clusters.

Erect to slightly recurved elements with fewer but coarser, more prominent, striations than those found on the Ca-Cd elements. The shoulders are also generally more prominent than those of the Ca-Cd elements, and are developed relatively higher above the base of the element. These are less robust elements than those described above, and taper to a finer point.

The elements are morphologically similar in all respects except for the cross-section outline of the base. The Ce element has an oval base and the Cf element has a circular base. There does not appear to be any significant intergradation of these two element types.

Apparatus element numbers

The number of discrete elements in the apparatus structure of *Icriodus expansus*, here estimated to be more than 140, seems excessive when compared with an element abundance of 15 in genera such as *Ozarkodina* or *Polygnathus*. However, a direct comparison of apparatus element numbers between *Icriodus* and other genera is misleading, and it may be more accurate to compare total apparatus denticle numbers. The multielement *Oulodus angulatus*, described by Nicoll (1979), can be taken as a simple example. That almost complete multielement apparatus with its simple morphology of large discrete denticles, which make a count easy, had a total of 189 denticles when allowance is made for missing fragments of elements by doubling the denticle count of the comparable complete element. The total number of denticles of some individual hindeodelliform Sc element is in excess of 50. Thus, by comparison, the 140+ denticles of the *I. expansus* apparatus is well within what might be expected for denticle numbers of a Devonian platform type conodont species.

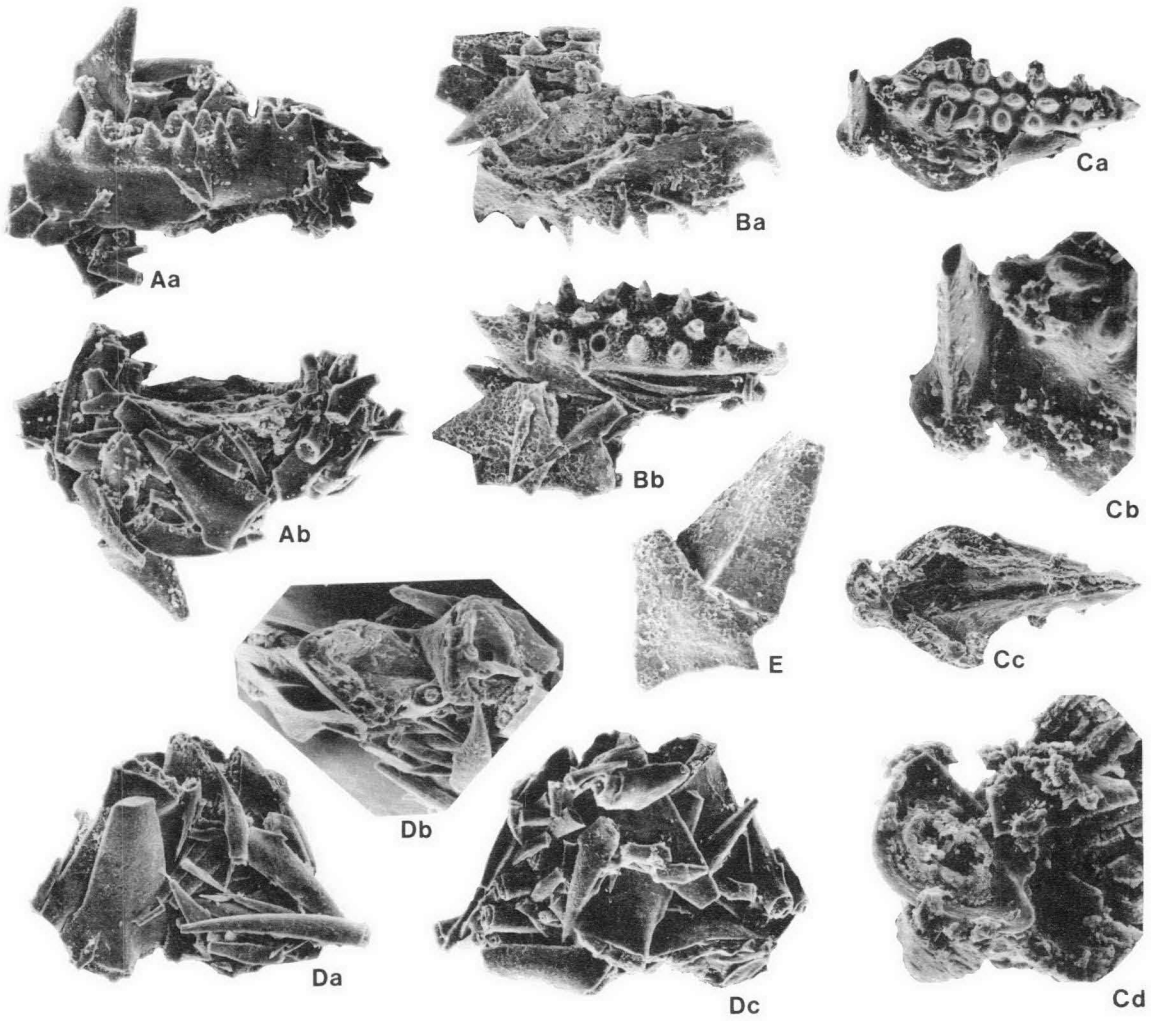

Figure 12. Cone element types in clusters.
A—Two views of cluster containing a single I element and at least 55 cone elements; two of the cones are Cc type elements and one may be a type Cd element; most of the elements are cone types Ce and Cf; CPC 22520 (100x). B—Two views of cluster containing a single I element and at least 30 cone elements; cone element types Cc, Ce, and Cf are recognised; CPC 22521 (105x). C—four views of cluster containing a single I element and at least five cone elements; cone element attached to anterior of I element is type Ca and large element on side is a Cd element; CPC 22522; Ca—upper view (75x); Cb—upper view, enlargement of anterior margin (180x); Cc—basal view (75x); Cd—basal view, enlargement of Ca element showing basal plate (260x). D—Three views of cone cluster containing at least 60 elements; cluster contains two Ca elements and two Cb elements as well as Ce and Cf elements; CPC 22523; Da and Dc—lateral views; Db—view showing distinctive outline of Ca and Cb elements (85x). E—Cluster of two cone elements, one Ca and one Cc element. CPC 22524 (120x).

Phyletic composition and origin of the Family Icriodontidae

Several authors (Klapper & Philip, 1972; Klapper & Murphy, 1975; Cooper, 1977) have recently discussed the composition of the Family Icriodontidae, with general agreement. Genera usually included in the family are *Icriodus*, *Pelekysgnathus*, *Pedavis*, *Steptotaxis*, *Sannemannia*, and *Icriodella*. However, in light of our present knowledge of the apparatus structure of these taxa, it is probable that *Icriodella* should be excluded from the Icriodontidae.

The oldest recognised species of the Icriodontidae, excluding *Icriodella* species, is *Pelekysgnathus dubius* Jeppsson (1972) from the Yass Basin sequence of eastern Australia, and is dated as early Ludlovian. The Australian material, originally described as *Corysso-gnathus dentatus* by Link & Druce (1972), has been considered to be conspecific with *Pelekysgnathus dubius* Jeppsson (1972) by both Jeppsson (1974) and Klapper & Murphy (1975). Klapper & Murphy, on morphologic grounds, did not believe that *P. dubius* should be assigned to *Pelekysgnathus*. However, examination of additional samples from the Euralie Limestone Member of the Laidlaw Formation of the Yass Basin has produced cone elements associated with *P. dubius* (= *C. dentatus*) that are nearly identical with the cone elements of *P. index* Klapper & Murphy from the Pridoli of the Roberts Mountains of Nevada and of *P. australis* Nicoll & Druce from the Famennian of the Canning Basin of Western Australia. For this reason, I suggest that Jeppsson was correct in this original assignment of the species to *Pelekysgnathus*. The importance of this discussion is that the oldest recognised elements of a species assigned to the Icriodontidae, *P. dubius*, are simple in character, and the cone elements lack secondary denticulation.

The next oldest taxon assigned to the Icriodontidae is *Pedavis latialata* (Walliser), which differs significantly from the *Pelekysgnathus* group by the development of triad denticulation on processes of the I element and the presence of denticulation on the S_1 (sagittodontan) cone element. In this morphology, both the I and S_1 elements of *Pedavis* are more similar to *Icriodella* than to *Pelekysgnathus*. The other recognised cone element of *Pedavis*, the M_2, is more similar to the cone element of *Pelekysgnathus* than to the denticulate elements of *Icriodella*.

The relationship of *Pelekysgnathus*, *Pedavis*, *Steptotaxis*, and *Icriodus* is not well defined, and there are some significant gaps in the geologic record as well as a lack of species that show morphologic intergradation between species or genera. Cone element types of the above genera are generally similar, but it is probable that only in the present case has the full nature of the range and number of element types in the apparatus structure been recognised. *Pelekysgnathus* generally lacks the development of denticle triads in the I element. *Icriodus*, *Pelekysgnathus*, and *Steptotaxis* all have cone elements of acodinan (Ca, S_2) morphology, and these are generally similar to the sagittodontan (S_1) element of *Pedavis*, except for the minor denticle development of the latter. The other cone elements, M_{2a} and M_{2b}, recognised for *Pel. australis* by Nicoll & Druce (1979) and also found with *Pel. index* (Klapper, pers. comm.), are generally similar to the M_2 element of *Pedavis pesavis pesavis* (Bischoff & Sannemann) and the Ce and Cf elements here recognised for *I. expansus*. I think that using the present study of *I. expansus* as a model will mean that other workers may more closely examine the cone elements associated with Icriodontidae I elements and differentiate more elements in the apparatuses of *Pelekysgnathus*, *Pedavis*, and *Steptotaxis*.

The possible relationship of *Icriodella*, if any, to the Icriodontidae is not known. Most elements in the *Icriodella* apparatus, except for the saggittodontiform element, are denticulate. If *Icriodella* is ancestral to the Icriodontidae, this would mean that, between its last occurrence in the Llandovery and the first occurrence of *Pelekysgnathus* in the early Ludlow, all the elements lost their secondary denticulation and there were other gross morphologic changes. Because the icriodontid type of process denticulation has been repeated in several taxa, from *Icriodella* in the Ordovician to *Eotaphrus* in the Carboniferous, the presence of a triad style denticulation may be the result of an adaptation to a feeding mode rather than an indication of a close phyletic relationship.

It is possible that ancestral forms to *Pelekysgnathus* and *Pedavis* should be looked for in cone elements of the late Ordovician or the Silurian.

Interpretation of the structure of *Icriodus expansus*

The linear sequence of elements in the conodont organism, suggested by myself (Nicoll, 1977) and many others, would seem to be confirmed by the linear pattern of elements in some of the better-preserved *Icriodus* clusters recovered in this study. The general sequence of ramiform anterior elements to platform or platform-like posterior elements, well developed in *Polygnathus* and *Ozarkodina* clusters, appears to be analogous to the cone to platform sequence in *Icriodus*.

The general pattern of element and denticle distribution in the condont organism is that of numerous anterior denticles and a few posterior denticles with the posterior elements frequently having broad, flat surfaces, which may contain trough structures or complex patterns of ribs or nodes. There thus appears to be some fundamental functional differentiation between the anterior and posterior elements of this sequence. I have suggested earlier (Nicoll, 1977, p. 277) that the conodont elements were structures located along a food groove, the function being to filter, pass, and direct food particles into the gut opening and that the Pa elements had a special function, which may have been the final manoeuvring of the food particles into the gut opening.

In the *Icriodus* apparatus, there is less differentiation of the cone element types than usually found for the ramiform elements of other genera. However, the triad denticle pattern of the posterior part of the I element is clearly analogous to the platform of other genera. The central denticle row is equivalent to the carina of the *Polygnathus* Pa element and the lateral rows to the nodose or upturned inner and outer platform margins of the Pa element.

In this study it is apparent that the configuration of the I elements is of opposition rather than the side by side configuration suggested in some conodont reconstructions. This configuration is also suggested by the *Polygnathus xylus xylus* Pa elements recovered in this study, many of which are fused with upper surfaces together.

Conclusions

- The apparatus structure of *Icriodus expansus* consisted of seven element types: one pair of I elements, probably one pair each of the cone element types Ca, Cb, Cc, and Cd, and numerous cone elements of types Ce and Cf.
- The apparatus contained in excess of 150 discrete elements.
- The orientation of the I elements is laterally opposed with upper surfaces together or in close proximity when the conodont organism was alive.
- Despite its apparent morphologic differences, the apparatus structure *Icriodus* was probably functionally very similar to the apparatus structures of other genera, such as *Polygnathus* or *Ozarkodina*.
- The lack of recognition of the apparatus structure components of *Icriodus* in discrete element collections is probably a function of sorting. Part of this sorting probably occurred at the time of deposition, when the small and thus lighter cones were separated from the I element by current action. In support of this, one should remember that there have been very few examples of early growth stages of the I element described or illustrated in the literature. The second part of the sorting has probably occurred in the laboratory, where the small Ce and Cf cone elements would be washed through most sieves.

Acknowledgements

I wish to thank Arthur Wilson for assistance in photography and plate preparation. I especially wish to thank Gilbert Klapper and Tom Uyeno who critically read the manuscript. Their suggestions did much to improve it.

References

BARNES, C. R., KENNEDY, D. J., MCCRACKEN, A. D., NOWLAN, G. S. & TARRANT, G. A., 1979—The structure and evolution of Ordovician conodont apparatuses. *Lethaia*, 12, 125-51.

BARRICK, J. E., 1977—Multielement simple-cone conodonts from the Clarita Formation (Silurian), Arbuckle Mountains, Oklahoma. *Geologica et Palaeontologica*, 11, 47-68.

BISCHOFF, G. & ZIEGLER, W., 1957—Die Conodontenchronologie des Mitteldevons und des tiefsten Oberdevons. *Abhandlungen des Hessischen Landesametes fur Bodenforchung*, 22, 1-136.

BRANSON, E. B., & MEHL, M. G., 1934—Conodonts from the Grassy Creek Shale of Missouri. *University of Missouri Studies*, 8, 171-259.

BULTYNCK, P., 1972—Middle Devonian *Icriodus* assemblages (Conodonta). *Geologica et Palaeontologica*, 6, 71-86.

COOPER, B. J., 1977—Toward a familial classification of Silurian conodonts. *Journal of Palaeontology*, 51, 1057-71.

JEPPSSON, L., 1972—Some Silurian conodont apparatuses and possible conodont dimorphism. *Geologica et Palaeontologica*, 6, 51-69.

JEPPSSON, L., 1974—Aspects of Late Silurian conodonts. *Fossils and Strata*, 6, 1-54.

JOHNSON, D. B. & KLAPPER, G., 1981—New Early Devonian conodont species of central Nevada. *Journal of Paleontology*, 55, 1237-50.

KLAPPER, G., 1969—Lower Devonian conodont sequence, Royal Creek, Yukon Territory, and Devon Island, Canada. *Journal of Paleontology*, 43, 1-27.

KLAPPER, G. & MURPHY, M. A., 1975—Silurian-Lower Devonian conodont sequence in the Roberts Mountains Formation of Central Nevada. *University of California Publications in Geological Sciences*, 111.

KLAPPER, G., & PHILIP, G. M., 1971—Devonian conodont apparatuses and their vicarious skeletal elements. *Lethaia*, 4, 429-52.

KLAPPER, G., & PHILIP, G. M., 1972—Familial classification of reconstructed Devonian conodont apparatuses. *Geologica et Palaeontologica*, SB1, 97-114.

KLAPPER, G. & ZIEGLER, W. 1975—*Icriodus*. *In* ZIEGLER, W. (editor), Catalogue of conodonts. *E. Schweizerbart'sche Verlagsbuchhandlung*, 2, 67-8.

KLAPPER, G. & ZIEGLER, W. 1979—Devonian conodont biostratigraphy. *In* HOUSE, M. R., SCRUTTON, C. T., & BASSET, M. G. (editors). The Devonian System, *Special Papers in Palaeontology*, 23, 199-224.

LANGE, F. G., 1968—Conodonten-Gruppenfunde aus Kalken des tieferen Oberdevon. *Geologica et Palaeontologica*, 2, 37-57.

LINDSTROM, M., 1964—Conodonts. *Elsevier, Amsterdam.*

LINK, A. G. & DRUCE, E. C., 1972—Ludlovian and Gedinnian conodont stratigraphy of the Yass Basin, New South Wales. *Bureau of Mineral Resources, Australia, Bulletin* 134.

NICOLL, R. S., 1977—Conodont apparatuses in an Upper Devonian palaeoniscoid fish from the Canning Basin, Western Australia. *BMR Journal of Australian Geology & Geophysics*, 2, 217-28.

NICOLL, R. S., 1981—Conodont colour alteration adjacent to a volcanic plug, Canning Basin, Western Australia. *BMR Journal of Australian Geology & Geophysics*, 6, 265-7.

NICOLL, R. S. & DRUCE, E. C., 1979—Conodonts from the Fairfield Group, Canning Basin, Western Australia. *Bureau of Mineral Resources, Australia, Bulletin* 190.

NORRIS, A. W. & UYENO, T. T., 1981—Stratigraphy and paleontology of the lowermost Upper Devonian Slave Point Formation on Lake Claire and the lower Upper Devonian Waterways Formation on Birch River, northeastern Alberta. *Geological Survey of Canada, Bulletin* 334.

SEDDON, G., 1970—Frasnian conodonts from the Sadler Ridge—Bugle Gap area, Canning Basin, Western Australia. *Journal of the Geological Society of Australia*, 16, 723-53.

SCHMIDT, H., 1950—Nachtrage zur Deutung der Conodonten. *Decheniana*, 104, 11-19.

SWEET, W. C. & SCHONLAUB, H. P., 1975—Conodonts of the genus *Oulodus* Branson and Mehl, 1933. *Geologica et Paleontologica*, 9, 41-59.

UYENO, T. T. & KLAPPER, G., 1980—Summary of conodont biostratigraphy of the Blue Fiord and Bird Fiord Formations (Lower-Middle Devonian at the type and adjacent areas, southwestern Ellesmere Island, Canadian Arctic Archipelago. *In* Current Research, Part C, *Geological Survey of Canada, Paper* 80-1C, 81-93.

VAN DEN BOOGAARD, M. & KUHRY, B., 1979—Statistical reconstruction of the *Palmatolepis* apparatus (Late Devonian conodontophorids) at the generic, subgeneric, and specific level. *Scripta Geologica*, 49, 1-57.

BMR Journal of Australian Geology & Geophysics, 7, 213–218

EXTENT OF ARCHAEAN AND LATE PROTEROZOIC ROCKS UNDER THE ICE CAP OF PRINCESS ELIZABETH LAND, ANTARCTICA, INFERRED FROM GEOPHYSICS

P. Wellman & J. W. Williams

A helicopter survey has mapped gravity and magnetic anomalies and ice thickness over a 100 km by 100 km ice cap area, inland from coastal outcrops of Archaean and Late Proterozoic rocks of the Princess Elizabeth Land coast. The gravity and magnetic anomalies indicate that there is no major change in crustal structure across the boundary between Archaean and Late Proterozoic rocks. The Archaean rocks of the Vestfold Hills do not extend further inland, but they may extend under Prydz Bay or as a narrow coastal strip under ice inland from the West Ice Shelf, 150 km to the northeast of the Vestfold Hills. Late Proterozoic rocks probably underlie most of the ice cap along the coast.

Introduction

Along the coast of Princess Elizabeth Land, Antarctica, high-grade metamorphic rocks form two groups with different metamorphic histories (Ravich & Krylov, 1964; Tingey, 1982) (Fig. 1). The first group consists of Archaean rocks which crop out for 70 km at the northeastern end of the coast and are best exposed in the Vestfold Hills. These give Rb-Sr whole rock (WR) ages of 2570 m.y., K-Ar (WR) ages of 1185-1500 m.y., and are intruded by unmetamorphosed basaltic dykes about 1400 m.y. old. The rocks are mainly orthogneiss, but with a paragneiss component (Oliver & others, 1982). The other group consists of rocks metamorphosed in the Late Proterozoic and without unmetamorphosed dykes. They crop out in scattered exposures for over 200 km along the southwestern end of the coast (Fig. 1), and extend 600 km southwest of the coast to the Mawson Escarpment, and 1000 km west to Edward VIII Gulf. In Princess Elizabeth Land they were metamorphosed to mainly granulite grade between 900 and 1100 m.y. ago, and give K-Ar WR ages of 420 to 520 m.y. The rocks are mainly paragneiss with no relics of metamorphosed dykes. Orthogneiss occurs at the southwestern extremity of the Princess Elizabeth Land coast, and orthogneiss with relic dykes occurs southwest of and immediately adjacent to the Archaean rocks (J. W. Sheraton, BMR, pers. comm.).

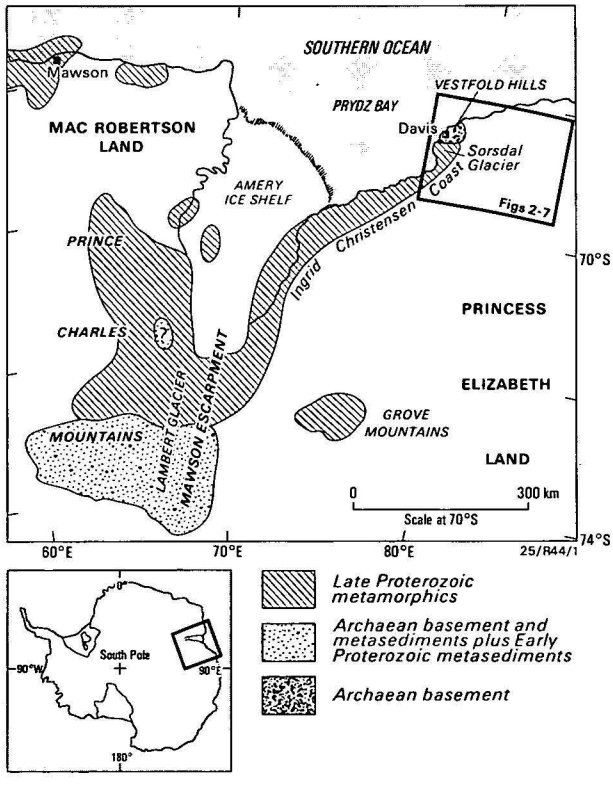

Figure 1. Locality sketch, and generalised geology from Tingey (1982).

Away from the coast little is known about Princess Elizabeth Land. Previous work on the ice cap consisted of early reconnaissance by aircraft and later surface and aircraft altitude traverses. A Soviet expedition carried out a reconnaissance airborne survey of unreported flight pattern in the period 1971 to 1974 and measured ice altitude, radar ice thickness and the total magnetic field (Demenitskaya, 1977; Federov & others, 1982; Kadmina, 1980).

This paper reports a geophysical survey inland of the northeastern half of the Princess Elizabeth Land coast (Fig. 1). The object of the survey was to define any geophysical anomalies over the contact between Archaean and Proterozoic rocks, and to investigate the position of the contact inland. Similar investigations have been carried out in the Prince Charles Mountains (Wellman & Tingey, 1976) and in Enderby and Kemp Lands (Wellman & Tingey, 1982, and unpublished data).

Survey details

The survey was carried out between 8 January and 22 February 1981, using Hughes 500C helicopters for transport (Williams, 1981). Station positions away from the coast were determined by a combination of dead-reckoning and either a single sun shot or two sun shots one hour apart; these positions are estimated to be accurate to 2–6 km. Station positions within sight of or on coastal rocks have an estimated accuracy of better than 1 km. Station height was measured in the field using two Mechanism microbarometers. Field readings were corrected for diurnal pressure changes, using three-hourly readings at Davis Base, and field and base temperatures. Altitude precision is probably similar to earlier surveys of this type (standard deviation about 10 m; Wellman & Tingey, 1982); however, on this survey there were no control stations on the ice cap, so the higher altitudes may have a

Table 1. Observations

Station number	*Lat. (°S)*	*Long. (°E)*	*Meter altitude (m)*	*Observed gravity (μms⁻²)*	*Rock altitude (m)*	*Free air anomaly (μms⁻²)*	*Bouguer anomaly (μms⁻²)*	*Bouguer correction 100 x 100 km area (μms⁻²)*	*Terrain corrected free air (μms⁻²)*	*Total magnetic field (nT)*
6905.0020	68.56	77.96	8.0	9825897.0	8.0	621.1	612.2	20	590	
8007.0000	68.58	77.97	28.7	9825854.3	28.7	628.2	596.1	20	580	55238
8007.0001	68.72	78.28	96.9	9824737.4	−807.3	−364.0	197.7	−90	300	55407
8007.0002	68.83	78.78	786.3	9823557.6	−16.5	516.7	232.7	−220	450	56305
8007.0003	68.92	79.08	1086.5	9822573.4	13.4	404.3	−15.0	−300	280	56339
8007.0004	69.12	79.37	1245.5	9821993.0	−64.3	193.8	−227.8	−400	170	56298
8007.0005	69.29	79.85	1464.7	9821052.8	—	−105.9	—	−500	—	56458
8007.0006	69.48	80.17	1608.2	9820804.0	5.8	09.3	−592.3	−560	−30	56663
8007.0007	68.57	78.65	273.4	9825032.9	95.6	568.0	394.2	−90	480	55305
8007.0008	68.72	78.79	604.2	9823944.9	−114.1	309.0	166.0	−210	380	56197
8007.0009	68.88	79.38	1022.6	9822789.5	−33.7	447.4	87.1	−330	420	55556
8007.0010	68.82	79.67	1034.2	9822718.9	28.7	449.1	38.2	−350	390	56591
8007.0011	68.98	80.12	1284.1	9822247.0	75.8	651.4	111.4	−450	560	56327
8007.0012	69.15	80.57	1502.1	9821699.5	193.9	674.2	−35.4	−530	480	56058
8007.0013	68.98	81.00	1513.7	9821456.6	18.1	569.5	−14.2	−540	530	56541
8007.0014	68.85	80.57	1382.7	9821629.1	−96.1	416.5	−33.2	−460	430	56657
8007.0015	68.70	80.08	1216.9	9822012.0	8.6	379.2	−85.7	−360	270	56504
8007.0016	68.58	79.82	1038.5	9822697.4	66.8	587.5	146.8	−280	430	55199
8007.0017	69.12	79.25	1231.3	9822024.1	−19.3	181.1	−268.5	−380	110	56328
8007.0018	69.30	79.62	1413.2	9821242.3	−386.7	−147.2	−393.1	−480	90	56483
8007.0019	69.58	78.98	1398.5	9821745.5	−12.7	144.4	−373.0	−480	110	56093
8007.0020	69.45	78.60	1285.8	9822236.6	60.6	364.7	−164.6	−410	240	55583
8007.0021	69.35	78.27	1001.8	9823134.7	114.6	445.8	−16.5	−330	310	55461
8007.0022	69.20	77.76	582.2	9824333.8	75.2	439.7	164.6	−190	350	55496
8007.0023	68.82	78.05	58.4	9825685.8	58.4	404.7	339.4	−80	410	55835
8007.0024	68.25	79.20	524.0	9823904.8	42.4	504.4	275.6	−90	370	55557
8007.0025	68.37	79.53	839.9	9822953.6	37.2	360.2	16.2	−180	200	55677
8007.0026	68.48	79.85	1086.0	9822476.5	80.5	574.7	105.9	−260	370	55949
8007.0027	68.47	80.03	1146.1	9822165.1	−113.0	454.9	106.9	−280	390	56108
8007.0028	68.60	80.33	1311.8	9821651.5	−65.6	372.6	−73.0	−360	290	56117
8007.0029	68.45	80.62	1249.6	9821694.0	66.6	315.5	−204.6	−350	150	56051
8007.0030	69.05	78.15	613.2	9824187.5	80.9	479.2	188.2	−180	370	55570
8007.0031	69.15	78.55	943.5	9823034.7	−28.3	285.5	−49.0	−310	260	56206
8007.0032	69.25	78.93	1270.5	9821998.5	19.9	198.5	−294.9	−380	90	55593
8007.0033	69.42	79.42	1439.9	9821439.8	−38.9	61.2	−452.4	−480	30	56341
8007.0034	69.52	79.77	1573.5	9820770.0	(618.7)	−255.6	(−1306.8)			56576
8007.0035	68.17	79.48	360.3	9824156.3	−3.1	207.1	73.6	−100	170	55719
8007.0036	68.30	79.95	848.8	9822848.0	−13.1	325.5	15.4	−220	240	55901
8007.0037	68.42	80.22	1124.0	9822069.6	−388.6	322.1	186.5	−290	480	56175
8007.0038	68.57	80.47	1279.3	9821710.5	−22.0	349.9	−115.8	−390	270	56363
8007.0039	68.68	80.98	1433.2	9821159.9	−79.4	206.8	−274.3	−470	200	57012
8007.0040	68.83	81.53	1566.3	9820739.5	−182.9	105.7	−348.9	−560	210	57205
8007.0041	68.40	78.93	533.4	9824183.0	34.9	625.2	398.4	−90	490	55564
8007.0042	68.53	79.32	796.8	9823297.0	53.2	471.9	132.2	−200	330	55718
8007.0043	68.63	79.70	1023.6	9822625.6	−49.6	439.1	90.2	−280	370	56296
8007.0269	68.63	77.83	39.3	9825792.2	39.3	568.1	524.2	10	510	55151
8007.0263	68.65	78.00	72.2	9825659.8	72.2	525.0	444.3	−20	460	55089
8007.0262	68.65	78.22	82.1	9825549.8	82.1	445.5	353.8	−50	400	55864
8007.0257	68.50	78.27	127.8	9825557.1	127.8	686.0	543.1	−10	550	56781
8007.0268	68.23	78.73	22.4	9825407.3	22.4	378.0	352.9	0	350	56374
8007.0259	68.37	78.42	29.6	9825661.6	29.6	567.6	534.6	10	520	57445
8007.0261	68.51	78.50	158.0	9825402.2	158.0	618.1	441.5	−30	470	56331
8007.0272	68.36	78.55	40.9	9825596.3	40.9	543.4	497.6	0	500	58140
8007.0258	68.47	78.41	137.3	9825460.3	137.3	637.0	483.5	0	480	58367
8007.0264	68.50	78.10	73.7	9825768.4	73.7	730.3	647.0	0	650	55537
8007.0115	68.56	77.93	52.1	9825808.1	52.1	666.5	608.2	0	610	55902
8007.0267	68.31	78.64	15.9	9825550.8	15.9	451.7	434.0	0	430	58706

systematic error. Ice thickness was measured using a Mark V 100 MHz ice-radar set constructed by the Antarctic Division of the Australian Department of Science and Technology. Ice-thickness measurements have a precision of about ±10 m for the first return echo. However, if the upper surface of the rock is irregular the mean ice thickness underneath the station will have a greater uncertainty, so the accuracy of the mean thickness is probably about 100 m. Acceleration due to gravity was measured with a precision of better than ± 1 μm s^{-2}, using a LaCoste & Romberg gravity meter. The calculated gravity anomalies were made compatible with anomalies of the Gravity Map of Antarctica (Grushinsky & Sazhina, 1975) by adopting a Potsdam value of 9 825 897 μm s^{-2} for Davis B station (BMR No. 6905.0020), and calculating

anomalies using the 1930 International Gravity Formula. The calculated Bouguer anomalies are corrected for the differences in rock altitude and ice thickness between stations. No terrain corrections have been made.

Total intensity magnetic measurements were made using a Geometrics 816 proton precession magnetometer. Field readings were reduced by subtracting the diurnal magnetic variation recorded at Davis Base (less than 140 km away); this diurnal correction has a magnitude of less than 170 nT, and is thought to be accurate to better than 40 nT.

Survey results

The survey results are summarised in Table 1. The ice surface altitude shown in Figure 2 is similar to published contours (Natmap 1971) based on the few previous measurements. However, the trough in the ice cap over the Sorsdal Glacier is deeper and longer than previously sketched.

Rock altitude (Fig. 3) is between +200 and −400 m, except under the lower Sorsdal Glacier, where there is a trough with a base at least 800 m below sea level. The average rock altitude is near sea level. The present rock surface is depressed below its de-glacial level by the isostatic loading effect of the ice cap, the amount of depression being approximately one-third of the present ice thickness because the density of ice is about one-third of upper mantle density. Allowing for this depression, the de-glacial rock surface inland from the present coast would all be above sea level, with a highest altitude of at least 700 m.

Federov & others (1982) have reported rock altitudes to the immediate west and southwest of the survey area, based on ice radar measurements. These are consistent with the new results in the area of overlap. The Princess Elizabeth Land coast is, therefore, an extensive region with rock altitude averaging near sea

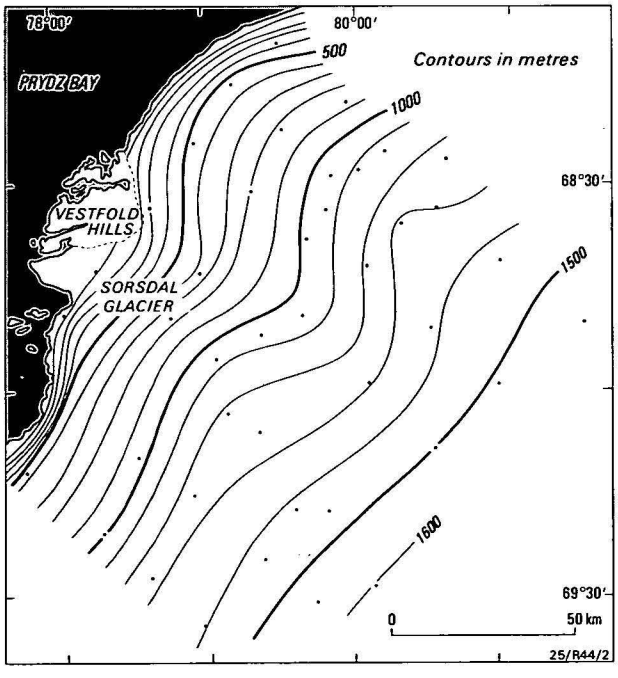

Figure 2. Ice surface altitude (contour interval 100 m).

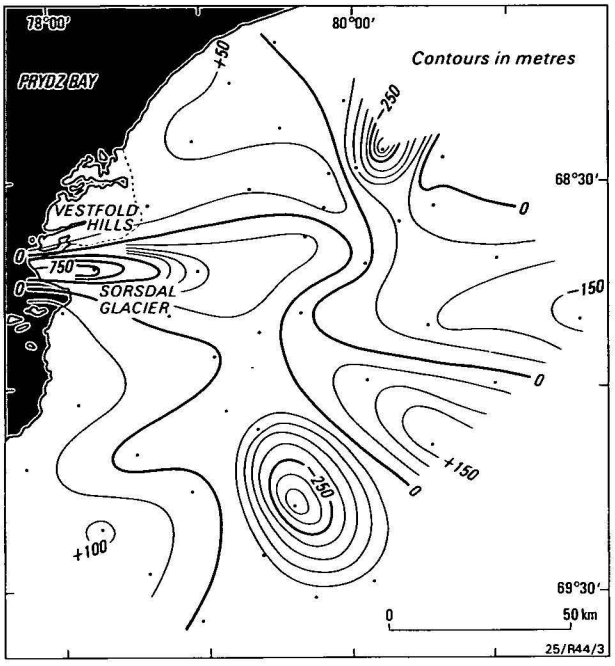

Figure 3. Rock altitude (contour interval 50 m).

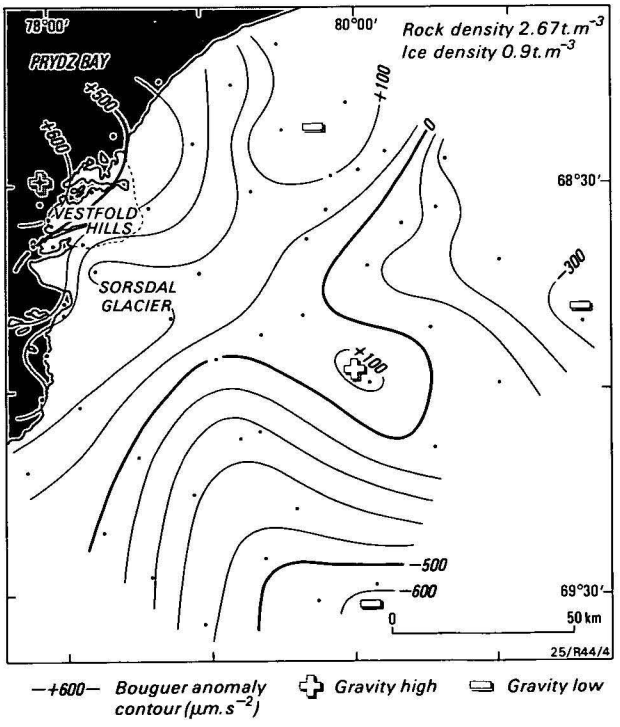

Figure 4. Bouguer gravity anomalies (contour interval 100 μm s^{-2}).

level. It is bounded in the west by the trough of the Lambert Glacier and Amery Ice Shelf (Fig. 1), and in the southwest at 70°20′S by the higher land of the Grove Mountains. It extends east possibly as far as 90°E (Znachko-Yarorskii, 1980), and is bounded on the north by the coast.

The Bouguer anomalies have been calculated by using a density of 2.67 t m^{-3} for rock and 0.9 t m^{-3} for ice. No terrain corrections were applied. The Bouguer anomaly map (Fig. 4) mainly reflects the variation in rock density in the upper crust superimposed on a

regional trend, evident as a gradual southeast decrease in anomaly from an average of about +400 μm s^{-2} at the coastline to −600 μm s^{-2} inland. The regional anomaly is due to a regional increase inland in the depth of the base of the crust below sea level; this in turn is due to increased mass above sea level inland. The regional anomaly is given approximately by the mean Bouguer correction for 100 × 100 km areas (Fig. 5). Anomalies calculated by removing this effect (Fig. 6) are here referred to as Faye isostatic gravity anomalies. They do not show a significant correlation with ice altitude.

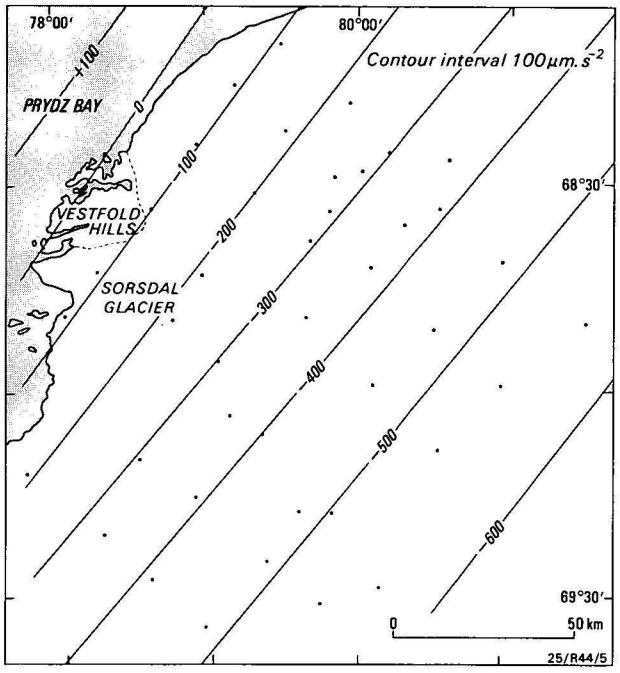

Figure 5. Mean Bouguer correction for 100 km x 100 km areas (contour interval 100 μms^{-2}).

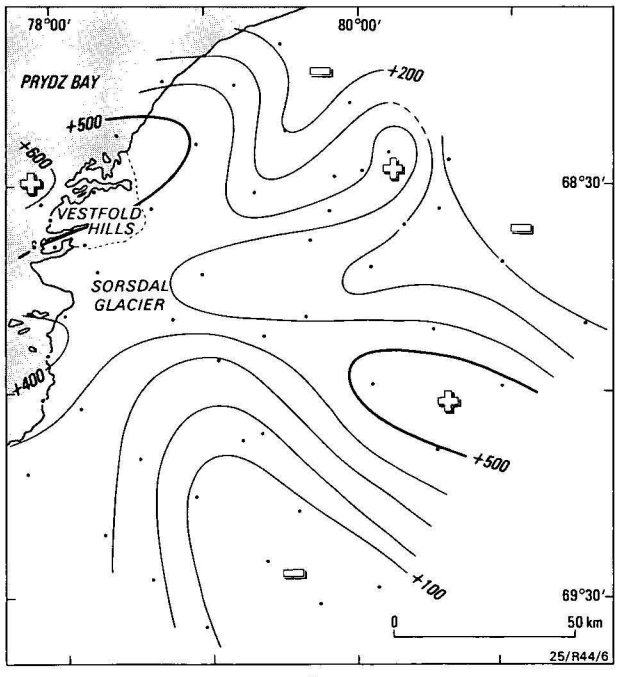

Figure 6. Regional free air (Faye) gravity anomalies (contour interval 100 μm s^{-2}).

The Faye anomalies of Figure 6 are higher than +400 μm s^{-2} over the exposed Archaean rocks of the Vestfold Hills, and are generally less than +400 μm s^{-2} over the exposed Late Proterozoic rocks along the coastline, both in the mapped area and further southwest (Grushinsky & Sazhina, 1975).

Residual total force magnetic anomalies (Fig. 7) have been calculated by taking the regional magnetic field determined by the Geographical Survey Institute of Japan (1978), correcting it for secular variation, and subtracting it from the total force magnitudes listed in Table 1. Over most of the survey area the residual anomalies vary smoothly from −600 to +600 nT. The area of Archaean outcrop has high, irregular values, which are almost certainly due to the relatively high magnetic susceptibilities of the numerous thick basaltic dykes (Glebovskii, 1964).

The position of the high and low trends of the residual magnetic anomalies (Fig. 7) are similar to the position of the Faye regional gravity anomalies (Fig. 6), the signs of the anomalies being opposite except over the Archaean outcrop. The coastal outcrops of Late Proterozoic rock southwest of Davis Base are on the flank of a southeast-trending gravity low (Fig. 6) and magnetic high (Fig. 7). Anomalies of similar character continue to the east, so it is inferred that the Late Proterozoic rocks extend over the southern two thirds of the mapped area. The area of Archaean outcrop in the Vestfold Hills has both a gravity and magnetic high; areas with anomalies with this sign combination are not found elsewhere in the mapped area. The area immediately east of the Archaean outcrops has a nearly flat magnetic field and northeast-trending gravity anomalies similar in direction to the east-northeast geological structure in the Archaean Vestfold Hills area (Oliver & others, 1982). The rocks of this area east of the Vestfold Hills are inferred to be a rock type not now exposed.

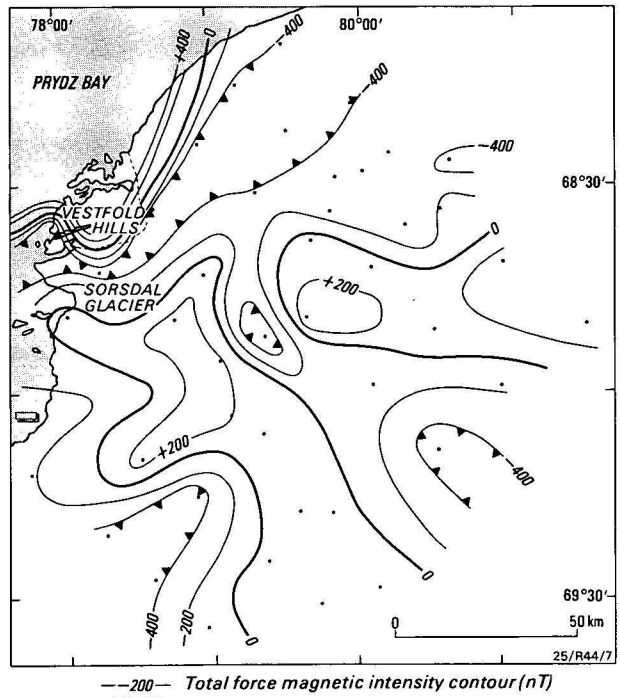

Figure 7. Residual total force magnetic intensity (contour interval 200 nT).

The gravity and magnetic results of this survey show that the boundary between the Archaean and Late Proterozoic rocks is not coincident with a large gravity anomaly or gradient, and the magnetic anomaly change is not great, although it looks large in Figure 7. The boundary is, therefore, not an abrupt and major change in crustal density or apparent susceptibility, and the deep crustal structure is probably similar on the two sides of the boundary. In particular, there is no major dipole gravity anomaly caused by an abrupt change in mean crustal density, as found along the boundaries between many dissimilar crustal blocks in Canada and Australia (Gibb & Thomas, 1976; Wellman, 1978). The geophysical evidence, therefore, supports the field interpretation of Sheraton (personal communication) that between the Archaean rocks of the Vestfold Hills and the area to the southwest there is a gradational increase in intensity of late Proterozoic metamorphism and the amount of paragneiss relative to orthogneiss.

Regional comparisons

The pattern of regional magnetic residuals reported by Demenitskaya (1977) (Fig. 8) is consistent with the pattern of Figure 7. In particular, the magnetic high over the Vestfold Hills does not extend inland, but may be part of an extensive high over the continental shelf. An area under ice, 150 km to the northeast, just inland from the West Ice Shelf, is along the strike from the Archaean outcrop, and has a well-defined magnetic high (Fig. 8) and a poorly defined free air anomaly high, averaging +400 μm s^{-2} (Grushinsky & Sazhina, 1975). This area may also be Archaean.

The irregular magnetic anomalies covering the southern two-thirds of Figure 7 are part of a regional high extending 350 km in an east-northeasterly direction (Fig. 8). The area of this anomaly is thought to be

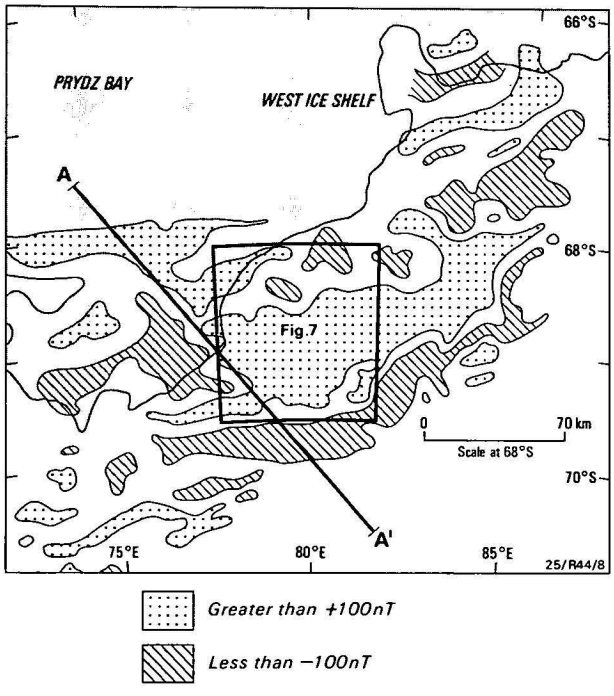

Figure 8. Residual total force magnetic intensity, from Demenitskaya (1977).
The small square shows the area of Figure 7.

the conservative minimum extent of Late Proterozoic rocks exposed along the southwest end of Princess Elizabeth Land coast. In Figure 8 the dominant magnetic trend for the whole Princess Elizabeth Land coastal area is east-northeast. This direction is consistent with trends of rock type variation and foliation in the Archaean rocks (Oliver & others, 1982) and schistosity and banding trends in the Late Proterozoic rocks (Federov & others, 1982).

A major northwest-trending magnetic anomaly discontinuity crosses the coastline at 77.5°E (line A-A', Fig. 8). This feature has the same direction as the gravity and magnetic anomalies in the southern two-thirds of Figures 6 and 7, and the same direction as linear sediment-filled depressions between the Grove Mountains and Prydz Bay reported by Federov & others (1982). The real nature of these northwest-trending structures is not known, but they are the major disturbances on the east-northeast trend of folds and large regional structures.

Acknowledgements

The authors are grateful to the Antarctic Division (Australian Department of Science and Technology) for logistic support, and to the Glaciology Section, Antarctic Division for the loan of ice-radar equipment.

References

DEMENITSKAYA, R. M., 1977—Earth's crust structure in Antarctica and some problems of its geodynamics. Presented at the Third Symposium on Antarctic Geology and Geophysics, Madison, USA, 1977 (unpublished).

FEDEROV, L. V., GRIKUROV, R. E., KURININ, R. G., & MASOLOV, V. M., 1982—Crustal structure of the Lambert Glacier area from geophysical data. *In* CRADDOCK, C. (editor), Antarctic geoscience. *University of Wisconsin Press, Madison*, 931-6.

GEOGRAPHICAL SURVEY INSTITUTE OF JAPAN, 1978—Magnetic maps 1975 of the Antarctic. *Geographical Survey Institute of Japan.*

GIBB, R. A., & THOMAS, M. D., 1976—Gravity signature of fossil plate boundaries in the Canadian Shield. *Nature*, 262, 199-200.

GLEBOVSKII, YU, S., 1964—The magnetic anomalies of the Vestfold Hills. Soviet Antarctic Expedition information bulletin, 2, 21-4. *Elsevier, Amsterdam.*

GRUSHINSKY, N. P., & SAZHINA, N. B., 1975—Gravity map of the Antarctic. Scale 1:5 000 000. *Ministry of Geology of the USSR, Moscow.*

KADMINA, I. N., 1980—Structure of the magnetic layer of the crust in Lambert Glacier Regional. Geophysical research in Antarctica. *Research Institute of Arctic Geology, Leningrad*, 44-51.

NATMAP, 1971—Australian Antarctic Territory SR43-44. 1:1 000 000 scale. *Division of National Mapping, Canberra.*

OLIVER, R. L., JAMES, P. R., COLLERSON, K. D., & RYAN, B., 1982—Precambrian geologic relationships in the Vestfold Hills, Antarctica. *In* CRADDOCK, C. (editor), Antarctic geoscience. *University of Wisconsin Press, Madison*, 435-44.

RAVICH, M. G., & KRYLOV, A. YA., 1964—Absolute ages of rocks from East Antarctica. *In* ADIE, R. J. (editor), Antarctic geology. *Proceedings of the First International Symposium on Antarctic Geology, Cape Town, 16-21 September 1963*, 579-89.

SHERATON, J. N., OFFE, L. A., TINGEY, R. J., & ELLIS, D. J., 1980—Enderby Land, Antarctica—an unusual Precambrian high grade metamorphic terrain. *Journal of the Geological Society of Australia*, 27, 1-18.

TINGEY, R. J., 1982—The geology and geological evolution of the Prince Charles Mountains, Antarctica. *In* CRADDOCK, C. (editor), Antarctic geoscience. *University of Wisconsin Press, Madison*, 455-64.

WELLMAN, P., 1978—Gravity evidence for abrupt changes in mean crustal density at the junction of Australian crustal blocks. *BMR Journal of Australian Geology & Geophysics*, 3, 153-62.

WELLMAN, P., & TINGEY, R. J., 1976—Gravity evidence for a major crustal fracture in eastern Antarctica. *BMR Journal of Australian Geology & Geophysics*, 1, 105-8.

WELLMAN, P., & TINGEY, R. J., 1982—A gravity survey of Enderby and Kemp Lands, Antarctica. *In* CRADDOCK, C. (editor), Antarctic geoscience. *University of Wisconsin Press, Madison*, 937-40.

WILLIAMS, J. W., 1981—Geophysical and surveying work along the Ingrid Christensen Coast near Davis Base, Antarctica, 1980/1981 Summer. *Bureau of Mineral Resources, Australia, Record* 1981/59 (unpublished).

ZNACHKO-YARORSKII, 1980—Bedrock relief of Antarctica, 1:20 000 000. *In* GRIKUROV, G. R. (editor), Tectonic map of Antarctica, 1:10 000 000. *Ministry of Geology of the USSR, Moscow.*

BMR Journal of Australian Geology & Geophysics, 7, 219–223

THE APPIN (NEW SOUTH WALES) EARTHQUAKE OF 15 NOVEMBER 1981

David Denham, Gunter Bock* & Ron S. Smith.

The earthquake that occurred near Appin, New South Wales, on 15 November 1981 and its aftershock of 19 November were both associated with thrust faulting in the middle crust (10–20 km), caused by east-west compressive forces. The magnitudes of the main earthquake were estimated to be 3.9 M_S, 4.3 m_b, 4.6 M_L and 4.1 M_W, and a seismic moment of about 1.4 x 10^{15} N-m was estimated. Although no damage was reported, the main earthquake was felt over about 60 000 km^2 of New South Wales, with a maximum felt intensity of 5 on the Modified Mercalli Scale experienced near the epicentral region and along the coastal plain from Wollongong to Nowra. The radius of the MMIV isoseismal was about 200 km.

Introduction

The Appin earthquake of 15 November 1981, which was felt over a wide area of southeast New South Wales, occurred in a region where earthquakes have been felt for about 200 years (Drake, 1974). The most important of these have been the Robertson earthquake of 1961 (Cleary & Doyle, 1962; Cleary, 1963; Doyle & others, 1968; Denham, 1980) and the Picton earthquake of 1973 (Fitch, 1976; Denham, 1976; Mills & Fitch, 1977). Both these earthquakes had Richter magnitudes of about 5.5 (Drake, 1974), occurred at depths of close to 20 km, and caused minor damage in the epicentral areas.

Figure 1 shows the distribution of earthquakes known to have occurred in the region, and for which five or more stations have been used in the hypocentral locations. The data set plotted in this figure covers the period from 1959, when the ANU network was commissioned (Cleary & Doyle, 1962), through 1981. Earlier earthquakes have not been plotted, because of uncertainties in their locations.

Although there is a suggestion of northwest-southeast trends in the southern Sydney Basin (see the Robertson earthquake in Cleary & Doyle, 1962), there are no obvious correlations between the earthquake distribution patterns and the main geological features.

Focal parameters

Location of hypocentre

The main Appin earthquake was recorded at most seismograph stations in eastern Australia, as far west as Roopena (RPA) in South Australia, and even as far north as the Warramunga array in the Northern Territory. It was followed on 19 November by a single aftershock, which was recorded by only 12 stations, the farthest being Young (YOU), 230 km away.

The main earthquake and aftershock were located using the program HYPOELLIPSE (Lahr, 1980) and a crustal model (Table 1) based on Finlayson & McCracken's figure 5 (1981). Corrections for Sydney Basin sediments were applied to the Riverview and

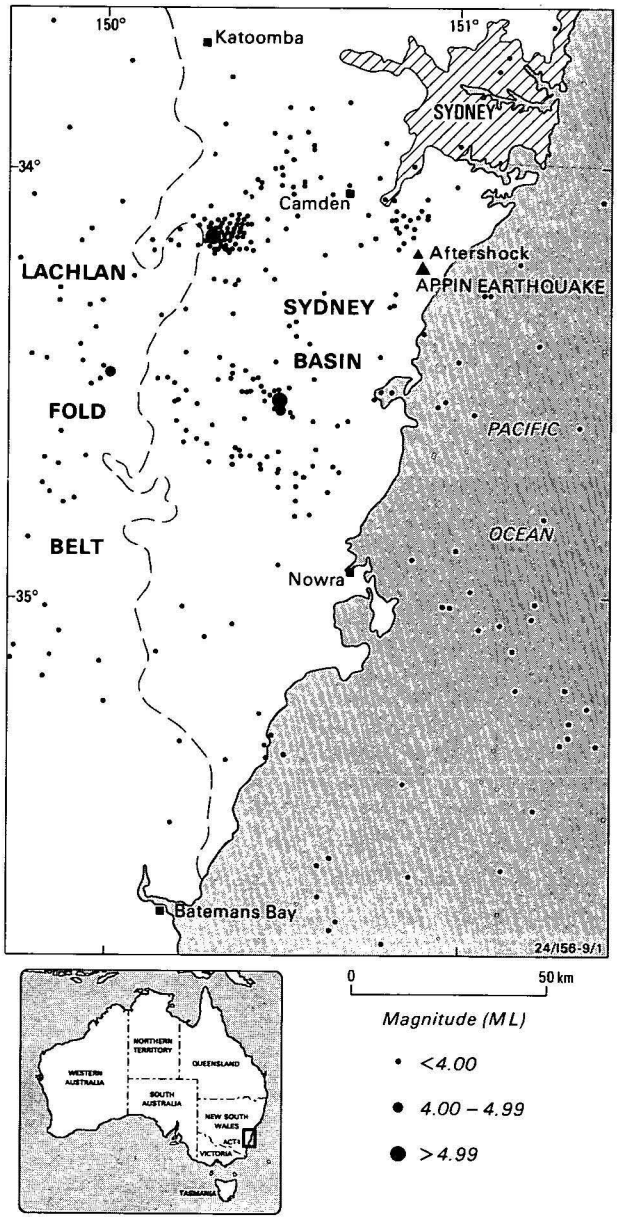

Figure 1. Distribution of earthquakes in the Sydney Basin region located by 5 or more stations from 1959–1981, and the locations of the main Appin earthquake of 15 November 1981 and the aftershock on 19 November 1981.

* Research School of Earth Sciences, Australian National University, PO Box 4, ACT 2600.

Table 1. Crustal model used to determine hypocentres.

Layer	*P-wave velocity (km/s)*	*Depth (km)*	*Thickness (km)*
1	5.8	0	5
2	5.85	5	2
3	6.1	7	4
4	6.11	11	4
5	6.5	15	10
6	6.8	25	9.5
7	7.0	34.5	4.5
8	7.83	39.0	2.5
9	8.15	41.5	18.5
10	8.20	60.0	10.00

Table 2. Hypocentral parameters of the Appin earthquake and aftershock.

Date	*Origin time*	*Lat. (°S)*	*Long. (°E)*	*Depth (km)*	*Number of stations used*
15 Nov. 1981	16h 58m 10.4s	34.249	150.897	14.4	12
19 Nov. 1981	12h 18m 52.8s	34.227	150.886	11.6	11

Avon arrivals. The hypocentral parameters of the main earthquake and the aftershocks are shown in Table 2. Only stations closer than 240 km to the epicentre were used in the solutions.

The standard errors in depth are 1.8 and 3.6 km respectively for the main shock and the aftershock, and the epicentral standard errors are similarly about 2 km and 4 km. These numbers relate to the precision of the solutions; the uncertainty of the hypocentre is probably somewhat larger.

We tried to locate the aftershock relative to the main shock with the master-event technique. Although this method was originally applied to teleseismic events (e.g. Fukao, 1972), it can also be employed for local earthquakes, if the aftershock is close enough to the master event, i.e. if the distance between main shock and aftershock is far less than the hypocentral distance to the nearest station. We assumed a P-wave velocity of 6.5 km/s at the focus, and used 10 stations that recorded the aftershock as well as the main shock. The origin-time of the aftershock, as obtained with the master-event location, was 12h 18m 52.6s ± 0.14s, the focal depth, 12.4 km, and the distance to the main shock, 4.0 ± 2.1 km. Relative to the main shock, the aftershock was located at an azimuth of 300° and a dip angle of 120° (measured from downwards vertical).

Magnitude and moment

Surface wave (M_S), Richter (M_L) and P-wave (m_b) magnitudes were measured wherever possible (Table 3). For body waves the standard relation $m_b = \log \frac{A}{T} + Q$ was used, where A is the ground amplitude in μm, T, the period in seconds, and Q, the depth-distance factor given by Richter (1958, pp. 688-9). Surface-wave magnitudes were determined using Marshall & Basham's (1973) formula, $M'_S = \log A + B'(\Delta) + P(\Delta)$, where $B'(\Delta)$ is a distance-correction term, $P(\Delta)$, a path-correction term, and A is measured in nanometres. This relation was derived to extend the M_S scale to higher frequencies and distances less than 20 degrees. At 20 degrees and 20 second period it gives the same result as the 1967 IASPEI formula (McGregor & Ripper, 1976), $M_S = \log \frac{A}{T} + 1.66 \log\Delta + 3.3$. The Richter magnitude was determined by using Richter's standard distance factors extended by Eiby & Muir (1961) to cater for greater distances.

Table 3. Magnitude of the Appin earthquake.

Station	*Distance (degrees)*	m_b	M_S	M_L	M_W
ADE	10.1	4.4	<4.0		
ASP	18.2	3.9	3.7		4.1
BFD	7.5	4.5		4.4	
BRS	7.0		4.1		
CNB	1.7			4.3	
COO	3.7			5.0	
CTA	14.7	4.1	3.8		
ISQ	16.8	4.1			
RIV	0.5			4.3	
STK	8.1	4.4			
TAU	9.1		<4.0		
TOO	5.5	4.4		4.8	
WRA	20.4	4.2			
Mean Values		4.3 ± 0.2	3.9 ± 0.2	4.6 ± 0.3	4.1

The surface waves recorded on the long-period seismographs at Alice Springs were large enough for the seismic moment to be estimated by the AR parameter method, introduced by Brune & others (1963) and developed by Williams (1979). A value of M_o of 1.37 × 10^{15} N-m* was obtained, which yielded an M_W value of 4.1, based on Kanamori's (1978) relation,

$$M_W = \frac{\log M_o - 60}{1.5}.$$

The seismic energy, E, released by the earthquake can be calculated from the different magnitude values (using Richter's relations) and from the seismic moment, using Kanamori's (1978) estimate. Log E values are given below:

$$\log E = 2.9 + 1.9\, M_L - 0.024\, M_L^2 = 11.13$$
$$= 4.8 + 1.5\, M_S = 10.65$$
$$= 2.4\, m_b - 1.2 = 9.12$$
$$= M_o/2 \times 10^4 = 10.81$$

We therefore estimate the seismic energy release as about 5 x 10^{10} Joules, although there is obviously considerable uncertainty in this figure, because of the scatter in the values of log E given above.

Focal mechanism

First motion directions from 23 stations that recorded the main shock are displayed in a stereographic equal-area Schmidt projection of the lower half of the focal sphere in Figure 2. Data from the South Australian network have not been plotted, because of the poor signal-to-noise ratio at these stations. For the same reason, only three of the Tasmanian stations were used.

The westerly dipping nodal plane is well constrained, but the easterly dipping plane is poorly determined. However, lack of control for this plane does not affect the faulting model for the earthquake, which appears to be almost pure reverse dip-slip motion caused by east-west horizontal compressive stress. It is not possible to ascertain which of the two planes is the fault

* 1 N-m = 10^7 dyn-cm

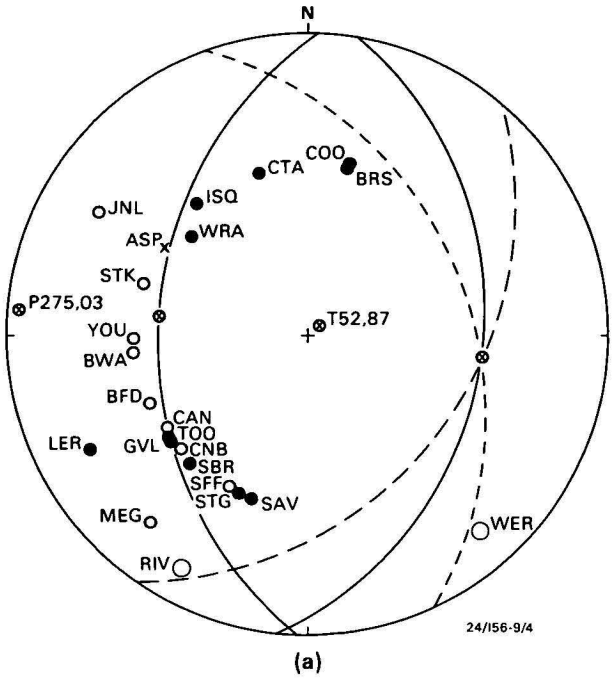

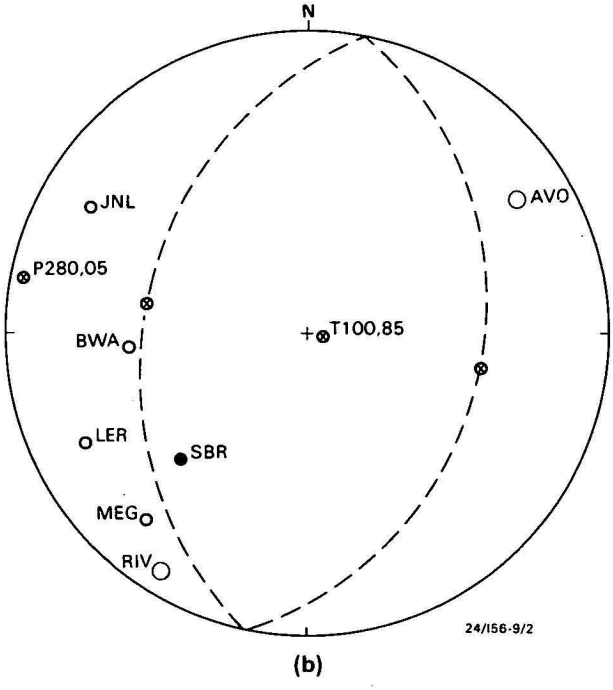

Figure 2. Fault-plane solutions for the main Appin earthquake (a) and the aftershock (b).
Solid circles, open circles, and crosses represent compressive, dilative, and emergent first motions, respectively, plotted on equal-area projections of the lower focal sphere. Larger circles represent data transposed from the upper focal sphere. The circumscribed crosses show the nodal poles and the pressure and tension axes. The numbers represent the trend and plunge of the poles, respectively, the letters are the standard 3-letter codes for Australian seismograph stations, as adopted by the International Seismological Centre, UK.

plane. However, by comparing the two depths obtained from the master-event technique, the easterly dipping nodal plane is favoured as the one that ruptured. The dip of the pressure axis, which is very close to zero, can vary only by about two degrees, and the azimuth by about 15 degrees, for the mechanism to be consistent with the observations. The tension axis is similarly constrained, and must dip between 72 degrees and vertical.
Stations Lerida, NSW (LER) and Sheffield, Tasmania (SFF) appear to be inconsistent with the solution. However, a slight change in crustal model would bring Lerida back close to the nodal plane, and as the signal-to-noise ratio is poor at Sheffield these discrepancies are not considered to be serious.

Table 4 lists the adopted focal parameters. They are consistent with those from the 1961 Robertson and 1973 Picton earthquakes (Denham, 1980), which also give solutions indicative of thrust faulting caused by horizontal compressive stress.

The aftershock that took place on 19 November 1981 had an M_L magnitude of about 3.3, and was recorded well enough by seven stations to obtain clear first

Table 4. Adopted parameters for focal mechanism of the Appin earthquake.

	Trend	*Plunge*
Poles of nodal planes	092	42
	277	48
Axis of compression	275	03
Axis of tension	052	80
Null axis	184	02

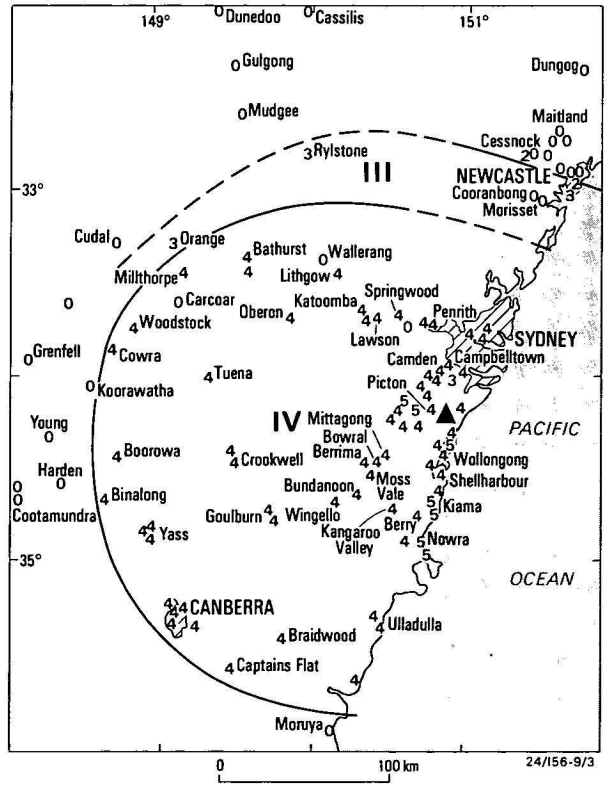

Figure 3. Isoseismal map of the main Appin earthquake.

motions (Fig. 2b). While the data are insufficient to determine a well-constrained focal mechanism, they also are consistent with a thrust-faulting mechanism. The direction of first motion at Lerida for the aftershock is opposite to that for the main shock. However, this is a consequence of the difference in take-off angle from the two earthquakes to that station, and does not imply a different faulting mechanism.

Felt-reports

About 300 felt-report questionnaires were distributed, up to 300 km from the epicentre. About half were returned. The isoseismal map (Fig. 3) was compiled from these data, using Eiby's (1966) version of the Modified Mercalli Scale.

Because the earthquake took place at night (4 a.m. local time) the range of responses is limited. The level of shaking assigned, Modified Mercalli 4, which is defined below (Table 5), was felt over a very wide area, and MM 5 was experienced along the coast from Nowra to Wollongong and near the epicentre.

The mean radius of the MM IV isoseismal is about 200 km, and there is a suggestion that the ground motion was stronger to the south of the epicentre than to the north. A similar effect was noticed after the 1973 Picton earthquake (Denham, 1976).

Table 5. MM 4 Intensity: typical effects.

Generally noticed indoors, but not outside.
Very light sleepers may be wakened.
Vibration may be likened to the passing of heavy traffic, or to the jolt of a heavy object falling or striking the building.
Walls and frame of buildings are heard to creak.
Doors and windows rattle.
Glassware and crockery rattles.
Liquids in open vessels may be slightly disturbed.
Standing motorcars may rock, and the shock can be felt by their occupants.
No confirmed damage was reported.

Discussion

The Appin earthquake of 15 November 1981 was caused by east-west compressive stress beneath the Sydney Basin. The focal processes were similar to those of other recent earthquakes in the region (Denham & others, 1981). This implies that the region is still being uplifted (Wellman, 1979), although the cause of the tectonic stress is not known. Only one aftershock was recorded, so it is not possible to ascertain which plane is the fault plane or to estimate the displacement on the fault associated with the earthquake. However, the aftershock was shallower and to the northwest of the main earthquake, so it appears that the easterly dipping nodal plane was associated with the faulting. This is supported by the results of the master-event analysis.

The ground motion resulting from the main earthquake did not cause any damage, but it was felt over a larger area than some higher-magnitude earthquakes that have occurred in southeast Australia. For example, the Bowning earthquake of July 1977 (Smith & McEwin, 1980) had a Richter magnitude of 5.0, and a similar depth (13 km), and yet was felt only up to 120 km away. The 1973 Picton earthquake (Denham, 1976), which took place close to the Appin earthquake, was also felt over a very large area (radius of MM IV isoseismal of 300 km for an M_L~5.5 earthquake). This effect may, therefore, be attributable to the earthquake occurring beneath the Sydney Basin.

Acknowledgements

We thank H. A. Doyle and J. Rynn for reviewing the manuscript, the Universities of Adelaide, Queensland, and Tasmania for providing seismograms, and Janet Weekes and Clemetine Krayshek for assistance with the analysis of the seismograms.

References

BRUNE, J., ESPINOSA, A., & OLIVER, J., 1963—Relative excitation of surface waves by earthquakes and underground explosions in California and Nevada. *Journal of Geophysical Research*, 68, 3501-13.

CLEARY, J. R., 1963—Near earthquake studies in southeastern Australia. *Ph.D. thesis, Australian National University, Canberra* (unpublished).

CLEARY, J. R., & DOYLE, H. A., 1962—Application of a seismograph network and electronic computer in near earthquake studies. *Bulletin of the Seismological Society of America*, 52, 673-82.

DENHAM, D., 1976—Effects of the 1973 Picton and other earthquakes in Eastern Australia. *In* DENHAM, D. (editor), Seismicity and earthquake risk in eastern Australia. *Bureau of Mineral Resources, Australia, Bulletin* 164, 15-31.

DENHAM, D., 1980—The 1961 Robertson Earthquake—more evidence for compressive stress in southeast Australia. *BMR Journal of Australian Geology & Geophysics*, 5, 153-6.

DENHAM, D., WEEKES, J., & KRAYSHEK, C., 1981—Earthquake evidence for compressive stress in the southeast Australian crust. *Journal of the Geological Society of Australia*, 28 (3), 323-32.

DOYLE, H. A., CLEARY, J. R., & GRAY, N. M., 1968—The seismicity of the Sydney Basin. *Journal of the Geological Society of Australia*, 15, 175-81.

DRAKE, L., 1974—The seismicity of New South Wales. *Journal & Proceedings of the Royal Society of New South Wales*, 107, 35-40.

EIBY, G. A., 1966—The Modified Mercalli Scale of earthquake intensity and its use in New Zealand. *New Zealand Journal of Geology & Geophysics*, 9, 122-9.

EIBY, G. A., & MUIR, M. G., 1961—Tables to facilitate the study of the near earthquakes. *New Zealand Department of Scientific and Industrial Research, Seismological Observatory Bulletin*, S-109.

FINLAYSON, D. M., & MCCRACKEN, H. M., 1981—Crustal structure under the Sydney Basin and Lachlan Fold Belt, determined from explosion seismic studies. *Journal of the Geological Society of Australia*, 28, 177-190.

FITCH, T. J., 1976—The Picton earthquake of March 9, 1973: a seismic view of the source. *In* DENHAM, D. (editor), Seismicity and earthquake risk in eastern Australia. *Bureau of Mineral Resources, Australia, Bulletin* 164, 11-14.

FUKAO, Y., 1972—Source process of a large deep-focus earthquake and its tectonic implications—the western Brazil earthquake of 1963. *Physics of the Earth and Planetary Interiors*, 5, 61-76.

KANAMORI, H., 1978—Quantification of earthquakes. *Nature*, 271, 411-14.

LAHR, J. C., 1980—Hypoellipse/Multics: a computer program for determining local earthquake hypocentral parameters, magnitude, and first motion pattern. *United States Geological Survey, Open-file Report* 80-59.

McGregor, P. M., & Ripper, I. D., 1976—Notes on earthquake magnitude scales. *Bureau of Mineral Resources, Australia, Record* 1976/56 (unpublished).

Marshall, P. D., & Basham, P. W., 1973—Rayleigh wave magnitude scale M_S. *Pure and Applied Geophysics*, 103, 406-14.

Mills, J. M., & Fitch, T. J., 1977—Thrust faulting and crust—upper mantle structure in east Australia. *Geophysical Journal of the Royal Astronomical Society*, 48, 351-84.

Richter, C. F., 1958—Elementary seismology. *Freeman & Co., San Francisco.*

Smith, R. S., & McEwin, A. J., 1980—Earthquake accelerograms and attenuation of seismic waves at Oolong, New South Wales. *BMR Journal of Australian Geology & Geophysics*, 5(1), 63-7.

Wellman, P., 1979—On the Cainozoic uplift of the southeastern Australian highland. *Journal of the Geological Society of Australia*, 26(1), 1-9.

Williams, B. R., 1979—M_o calculations from a generalised AR parameter method for WWSSN instruments. *Bulletin of the Seismological Society of America*, 69 (2), 329-51.

BMR Journal of Australian Geology & Geophysics, 7, 225-226

IMPREGNATION OF UNCONSOLIDATED SEDIMENT SAMPLES, USING A LARGE VACUUM CHAMBER

M. H. Tratt & R. V. Burne

A large cylindrical vacuum chamber has been constructed (1180 mm long, 405 mm diameter) and used for impregnating unconsolidated, undisturbed sediment samples. To ensure complete sample impregnation and to avoid stress fracturing of the resin, a very slow-curing impregnating mixture of Daystar 'Escon CR6-1' polyester resin with 0.5% by volume cumene hydroperoxide hardener is used in this chamber. This gives a curing time for large samples of about 1–3 months. With such long curing times, all but the finest-grained samples have been successfully impregnated.

Introduction

We have designed, constructed and used a large vacuum chamber for impregnating undisturbed and unconsolidated core samples (Fig. 1). The apparatus operates on the same principles as described by Jongerius & Heintzberger (reviewed by Bouma, 1969, pp. 107–8), although it is larger and less complicated.

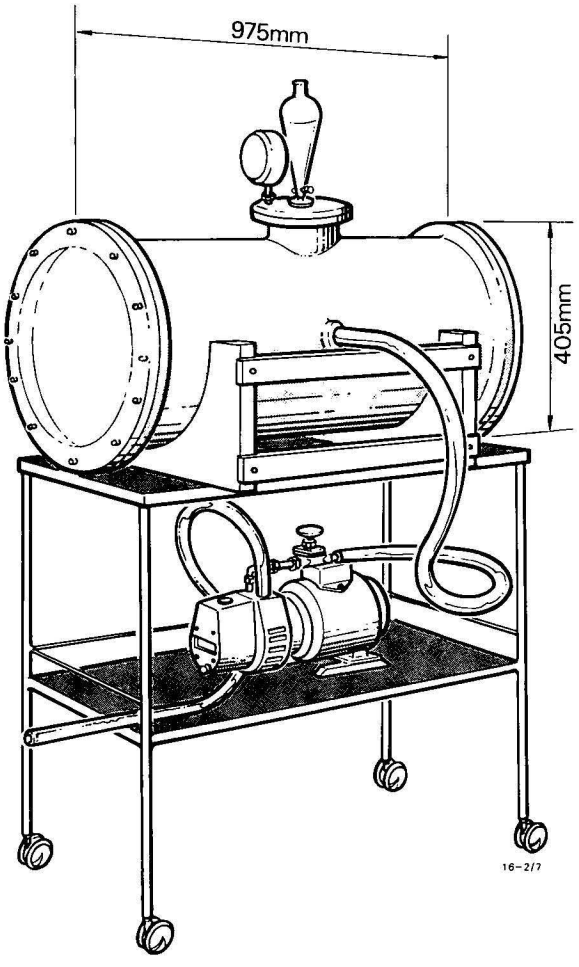

Figure 1. Vacuum impregnation chamber.
The apparatus consists of a cylinder of 10 g stainless steel, 1180 mm long and 405 mm in diameter, with 12-mm thick flanges welded to the ends. The cylinder is closed by 25-mm clear polycarbonate plates sealed with O rings and fixed by 12 bolts. The top of the cylinder is fitted with a 12 mm stainless steel plate, drilled and tapped to take a vacuum gauge and a pear-funnel with a stopcock for introducing the resin. A vacuum line connection is made with the side of the cylinder, and the chamber is connected directly by a vacuum hose to a vacuum pump. The pump used is a "DYNAVAC" 100 series 100L/min direct-drive, two-stage vacuum pump.

We use an impregnating medium with a very long curing time, and have achieved good results in impregnating all but the finest-grained materials. The excellent results of this method lead us to conclude that, for most materials, pressurised impregnation, as described by Ginsburg & others, (1966), is unnecessary, provided that the curing time of the resin is relatively long. It is worth noting that, even with higher pressure, the impregnation of fine-grained, calcareous, clay-sized sediments and terrigenous clays is not successful (Ginsburg & others, 1966). This note describes the impregnating chamber, and outlines the impregnating procedure.

Impregnating materials

The polyester resin used is Daystar 'Escon CR6–1' casting resin. Experiments were carried out to find the type and quantity of catalyst that would give the longest practicable curing time, to enable complete impregnation of the sample and to avoid stress cracks in the cured plastic. Bouma (1969) reviewed the gelling properties of various impregnating mixtures, but did not experiment with the effects of gelling times greater than about 3 days. We found that a suitable mixture for slow-curing impregnation used 0.5% by volume of the catalyst cumene (isopropylbenzene) hydroperoxide. The curing time for 1.5 litres of this mixture in a sandy sample of 270 mm x 210 mm x 120 mm is about 30–35 days, although it has gelled within 20 days.

The chemicals used are potentially harmful. Special care should be taken when handling the cumene hydroperoxide and skin contact should be avoided. All mixing and preparation should be done in a fume cabinet, and the exhaust from the impregnation chamber should also be led to a fume cabinet.

Operation

Sample preparation

The sample to be impregnated must be completely dry. Freeze-drying of large core slabs has been found unsatisfactory, as moisture is not always completely expelled. Samples are, therefore, dried in an oven at 95°C, for 5–6 days.

The specimen is placed in a mould that gives about 20 mm clearance around the sides: polythene freezer boxes are ideal. Moulds can also be made from aluminium sheet; the sides should be angled for easy removal of the sample. Plywood moulds may also be used, and these are cut with the sample during slab-

bing. Split cores are generally impregnated in the cut core barrel liner, and slabs of box-cores may be held together with tape bandages, or impregnated in cut core tins; put the whole into a mould.

Impregnation

Remove one polycarbonate end plate from the chamber and position the specimen in its mould in the chamber so that the resin falls from the funnel into the mould, but not directly on to the specimen. Check that the O ring is in good order, lightly smear it with vacuum grease and refit the polycarbonate end plate.

Close the stopcock on the pear-funnel, open the vacuum pump isolating valve, and start the vacuum pump. The chamber takes about 5 minutes to evacuate. When the vacuum gauge is steady, close the pump isolating valve and switch off the pump. Leave the system for about 10 minutes to check that the vacuum is holding. If it is, the resin may be introduced.

Thoroughly mix the resin and hardener and pour the mixture into the pear-funnel on top of the chamber. Open the stopcock to let the resin drip *slowly* into the specimen mould. If the resin is introduced too quickly, it boils and spatters the chamber.

When the resin has covered the specimen by about 15 mm, break the vacuum carefully by slowly opening the stopcock on the now-empty pear-funnel. Transfer the specimen and mould to a fume cabinet and leave them to gell for about 2–3 weeks. Top up the resin as necessary. When the resin has gelled and hardened, it can be removed from the mould. Complete curing of the resin takes 1–3 months, depending on the volume of resin used.

Results

With the long curing times, most materials are completely impregnated and even very fine-grained sediments are partly impregnated. Some examples of slabbed and polished box-core samples are shown in Figure 2.

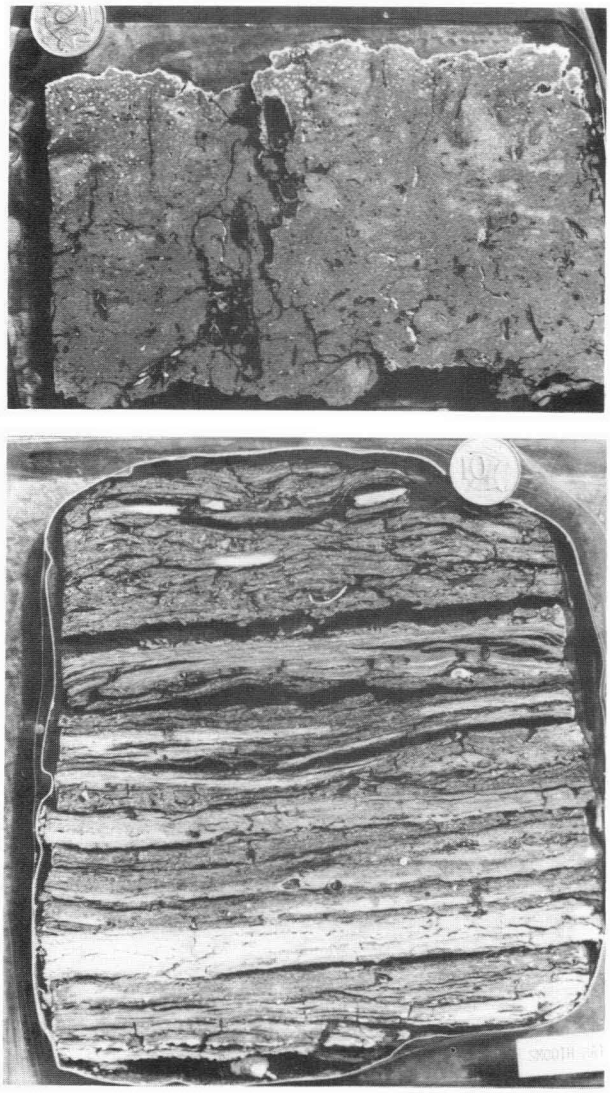

Figure 2. Examples of impregnated box core samples, slabbed and polished:
(a) mixed carbonate/terrigenous silty clay with gastropods and mangrove roots; (b) flat laminated algal stromatolitic sediments.

References

BOUMA, A. H., 1969—Methods for the study of sedimentary structures. *Wiley-Interscience, New York.*

GINSBURG, R. N., BERNARD, H. A., MOODY, R. A. & DAIGLE, E. E., 1966—The Shell method of impregnating cores of unconsolidated sediments. *Journal of Sedimentary Petrology*, 36, 1118-25.

BMR Journal of Australian Geology & Geophysics, 7, 227–229

NEW MICROFORM PUBLICATIONS

Lithostratigraphy of the Ninmaroo Formation (Upper Cambrian—Lower Ordovician), Georgina Basin, Queensland and Northern Territory.

B. M. Radke

BMR Report 181; Microform MF153

ISBN 0 642 07060

1981, 2 fiche, $8.50

The Ninmaroo Formation (Upper Cambrian—Lower Ordovician) has a widespread distribution in the south-eastern Georgina Basin of Queensland and the Northern Territory, extending from northwest of the Toko Syncline to the east and south over the Smoky Anticline to the Burke River Structural Belt. It overlies Middle and Upper Cambrian units with disconformity and unconformity, except in the Toko Syncline and southern Burke River Structural Belt, where the sequence is conformable. To the west of the Toko Syncline it interfingers laterally with the Tomahawk Beds. The upper boundary is an erosional surface everywhere except in the central Toko Syncline, where it is apparently conformably overlain by the Kelly Creek Formation. The formation is up 950 m thick, and comprises bituminous limestone, limestone, sandy limestone, dolostone, calcareous sandstone, siltstone, and minor shale. Lithofacies distribution in the Ninmaroo Formation indicates a sequence that is progradational to the east and southeast. The sequence consists of a basal ooid carbonate lithofacies overlain by peloid carbonate lithofacies, a terrigenous lithofacies in the Toko Syncline, flat-pebble conglomerate lithofacies, mixed carbonate lithofacies in the Toko Syncline, skeletal carbonate and peloid carbonate lithofacies in the Burke River Structural Belt. A crystalline dolostone lithofacies occurs mainly along fault zones. Most of these lithofacies accumulated by cyclic sedimentation, which produced sheet deposits 0.1–4.5 m thick. Three cycles are recognised; cryptalgal carbonate, peloid carbonate, and skeletal-ooid carbonate.

Tectonic setting of the easternmost Arunta Block.

R. G. Warren

BMR Report 221; Microform MF154

ISBN 0 642 06981 6

1981, 1 fiche, $0.75

Crystalline basement in the Field River Block, between the Tarlton and Toomba Faults (adjacent to and west of the Queensland-Northern Territory border), consists of metamorphic rocks and granites typical of the northern Arunta zone. The metamorphic rocks are placed in Divisions II and III of the Arunta Block. The granites are dominantly leucogranites, but older, more melanocratic granites are also present. The Field River Block is part of a large tectonic unit exposed in the Tennant Creek Block, Arunta Block, and along the western margin of the Mount Isa Orogen, all of which began to form before 1800 m.y. ago. The eastern and southern margins of the major tectonic unit remained mobile. The rocks of the Field River Block have suffered only very limited cratonic-type dislocation since the Middle Proterozoic.

Catalogue of palaeontological type specimens located in the Department of Geology and Geophysics, University of Sydney—supplement to Report 149.

G. Z. Foldvary

BMR Report 224; Microform MF155

ISBN 0 642 06503 9

1981, 1 fiche, $0.75

Lord Howe Rise area, offshore Australia: preliminary results of a co-operative Federal Republic of Germany/Australia geophysical survey.

J. B. Willcox, P. A. Symonds, D. Bennett, & K. Hinz

BMR Report 228; Microform MF157

ISBN 0 642 06825 9

1981, 1 fiche, $0.75

During October 1978 the Bundesanstalt für Geowissenschaften und Rohstoffe (BGR) and the Bureau of Mineral Resources, under the auspices of the Federal Republic of Germany/Australia Science & Technology Agreement, conducted a co-operative survey of the central Lord Howe Rise area aboard the R/V *Sonne*. The main objectives were to examine the structure, geological evolution, and petroleum potential of the Lord Howe Rise. About 4000 line kilometres of multichannel seismic, gravity, and magnetic profiles were recorded. The survey lines were also extended across the Norfolk/West Norfolk Ridge, New Caledonia Basin, Middleton Basin, Lord Howe Basin, and Dampier Ridge. The results of a preliminary seismic stratigraphic analysis based on the high-quality on-line monitor records, ties to DSDP Sites 207 and 208, and shallow refraction studies are discussed in this Report. The *Sonne* survey has confirmed that numerous horsts and grabens underlie the western part of the Lord Howe Rise, but that there is no single sediment-filled depression resulting from rifting or pull-apart tectonics like that on the southern 'Atlantic-type' margin of Australia (Bremer, Great Australian Bight, and Otway Basins). The grabens probably trend north-northwest; they are each 30–40 km wide and of considerable but unknown length; and they are filled with 2000 m or more of pre-break-up (rift-fill) sediments. The horst and graben province extends westwards across the Middleton and Lord Howe Basins, where the basement appears to be more crystalline, and onto the Dampier Ridge, which is considered to be at least partly of continental origin. Within the sedimentary sequence

on the northern Lord Howe Rise, pinnacle reefs appear to be built on and just above a ?Late Cretaceous 'break-up unconformity'. The New Caledonia Basin appears to be older than the Tasman Basin, and the eastern flank of Lord Howe Rise was probably the margin of the Australia-Antarctica supercontinent before Late Cretaceous time. The overburden of post-break-up sediments on the Lord Howe Rise is probably too thin to have led to the maturation of any hydrocarbon source material within the marine transgressive rocks deposited just after break-up. However, sediments within the grabens, possibly mainly Cretaceous fluvial-deltaic deposits, may have some petroleum potential in the long term.

Geological Branch annual summary of activities, 1980.

BMR Report 230; Microform MF159

ISBN 0 642 07063 6

1981, 5 fiche, $3.75

Geophysical Branch summary of activities, 1980.

BMR Report 231; Microform MF160

ISBN 0 620 06941 7

1981, 3 fiche, $2.25

Ehrenberg Range airborne magnetic and gamma-ray spectrometer survey, NT 1976—operational report.

A. J. Mutton

BMR Report 232; Microform MF161

ISBN 0 642 06886 0

1981, 1 fiche, $0.75

In September 1976, the Bureau of Mineral Resources conducted a semi-detailed airborne magnetic and radiometric survey of the Ehrenberg Range in the northeast of the MOUNT RENNIE 1:250 000 Sheet area, west of Alice Springs, Northern Territory. This report describes the acquisition, processing, and presentation of the data, and shows at reduced scale the total magnetic intensity contours and profiles, and total count radiometric profiles which are available through the Australian Government Printer Copy Service.

Definitions of newly named and revised Precambrian stratigraphic and intrusive rock units in the Duchess and Urandangi 1:250 000 Sheet areas, Mount Isa Inlier, northwestern Queensland.

D. H. Blake, R. J. Bultitude, & P. J. T. Donchak

BMR Report 233; Microform MF164

ISBN 0 642 07057 1

1981, 1 fiche, $0.75

The new nomenclature results from a detailed reconnaissance survey of the Precambrian parts of the Duchess and Urandangi Sheet areas carried out between 1975 and 1980 by geologists from the Bureau of Mineral Resources and the Geological Survey of Queensland. Forty stratigraphic and intrusive rock units are defined. All definitions have been approved by the Queensland Stratigraphic Nomenclature Sub-Committee.

Investigations of the geology and hydrology of the Great Artesian Basin, 1878–1980.

M. A. Habermehl

BMR Report 234; Microform MF169

ISBN 0 644 01898 4

1982, 1 fiche, $0.75

A review is given of the significant literature dealing with the groundwater development and investigations of the geology and hydrology of the Great Artesian Basin. This compilation was prepared as part of the hydrogeological study of the Great Artesian Basin, carried out by BMR from 1971 to 1980.

Springs in the Great Artesian Basin, Australia—their origin and nature.

M. A. Habermehl

BMR Report 235; Microform MF179

ISBN 0 644 01897 6

1982, 1 fiche, $0.75

Springs and areas of seepage are abundant in the marginal areas of the Great Artesian Basin. About 600 spring locations, concentrated in eleven groups, are described. Artesian springs are generally associated with (1) faults along which the water flows upwards, (2) the abutment of aquifers in the sedimentary Jurassic and Cretaceous sequence against impervious bedrock, or (3) pressure water breaking through thin confining beds near the discharge margins of the basin. Many artesian springs have built up conical mounds by mechanical deposition of particles derived from the pressure aquifers and the confining beds, and by chemical precipitation of solids dissolved in the artesian groundwater. Artesian springs and their deposits in the Lake Eyre region show a range from topographically high springs to younger, topographically lower springs as a result of the lowering of the land-surface and spring outlet levels in Quaternary times. Discharges from springs in the Great Artesian Basin generally are small and most springs produce much less than 10 l/s; few have larger discharges, which range up to 85 l/s. The accumulated discharge of about 600 springs is estimated at about 1500 l/s. Discharges have declined since water-well development started in the basin. Aquifers in the eastern recharge margin produced overflow springs where the topographic surface incised into the aquifers. Many springs in the eastern marginal area are not related to aquifers of the Great Artesian Basin, but issue from capping basalt sheets. Springs in the central area of the basin issue from overlying Tertiary deposits.

Geophysical characteristics of some near-surface magnetic sources in the Cobar area, NSW.

P. R. Gidley

BMR Report 236; Microform MF167

ISBN 0 642 07059 8

1981, 1 fiche, $0.75

The characteristics of near-surface magnetic sources in the Cobar area were investigated by BMR during 1978 and 1979. Three areas known to have prominent aeromagnetic anomalies and noisy ground magnetic anomalies were studied. The studies included drilling and laboratory analyses which showed the near-surface magnetic materials to be a combination of the minerals maghemite and hematite. The distribution of these mineral concentrations was found to vary rapidly, both laterally and vertically. Drilling and logging evidence indicated that the magnetic mineral concentrations occurred in thin layers, generally only a few metres thick. Magnetic anomalies produced by this material are the result of two effects: firstly, that due to the near-surface magnetic materials which have high susceptibilities (up to 250 000 x 10^{-6} SI), and secondly, that due to their high remanence, which is reflected in observed Koenigsberger ratios up to 92. Oriented measurements on material collected from surface magnetic sources suggest that the remanent component is parallel to the earth's present magnetic field.

The results of the studies provide guidelines for the development of methods to detect bedrock sources in the presence of near-surface sources. These methods involve the application of spectral analysis and filtering to high-resolution data which permits the depths of magnetic sources to be determined, thereby resolving the responses of bedrock and near-surface sources.

Size and distribution statistics, Wenlock brachiopods from Canberra, Australia.

D. L. Strusz

BMR Report 237; Microform MF183

ISBN 0 644 01823 2

1982, 1 fiche, $0.75

The Wenlockian Walker Volcanics brachiopod fauna is listed systematically, and statistical data are presented on: 1. Community structure—distribution of specimens by locality and species, and occurrence of dominant species; 2. Size and shape—including a diagrammatic key to parameters measured, using photographs of specimens, for each species.

Geophysical Branch summary of activities, 1981.

BMR Report 238; Microform MF178

ISBN 0 644 01739 2

1982, 3 fiche, $2.25

Geological Branch annual summary of activities, 1981.

BMR Report 239; Microform MF182

ISBN 0 644 01829 1

1982, 4 fiche, $3.00

GREAT BARRIER REEF MARINE PARK AUTHORITY

AUGMENTATIVE RESEARCH SUPPORT 1983

The Great Barrier Reef Marine Park Authority invites applications for augmentative support of the research projects of recent graduate and post-graduate students.

It is intended that the supplementary support be given to projects that can be augmented to contribute to the Authority's work of planning the Great Barrier Reef Marine Park and in particular for the responsible use of the Great Barrier Reef region by man. The Authority will therefore consider applications from a variety of disciplines.

At the conclusion of the research successful applicants will be expected to submit a report to the Authority. The report should include a section specifically explaining the relevance and application of the results to management for conservation and use of the Great Barrier Reef.

Applicants should already be supported by their organisation for basic expenses and have access to general equipment, library, laboratory and computing facilities necessary for the research. Applications should include

(1) A description of the research project.
(2) A brief discussion of the relevance of the proposed research to planning and management of the Great Barrier Reef Marine Park.
(3) A detailed budget for the amount sought (generally of the order of $800 or less).
(4) A statement by the applicant's supervisor/head of department supporting the application.
(5) A statement by the head of institution, or his delegated officer, confirming the basic support of the institution for the applicant.
(6) A statement of the existing financial support (grants, etc.) held by, or available to, the applicant.

Applications should be sent to :

The Executive Officer,
Great Barrier Reef Marine Park Authority,
P.O. Box 1379,
TOWNSVILLE, QLD. 4810.
CLOSING DATE FOR APPLICATIONS :
31st DECEMBER, 1982.

CONTENTS

G. Playford
A latest Devonian palynoflora from the Buttons beds, Bonaparte Gulf Basin, Western Australia 149

G. F. Taylor & K. M. Scott
Evaluation of gossans in relation to lead-zinc mineralisation in the Mount Isa Inlier, Queensland 159

A. L. Jaques, D. H. Blake, & P. J. T. Donchak
Regional metamorphism in the Selwyn Range area, northwest Queensland 181

R. S. Nicoll
Multielement composition of the conodont *Icriodus expansus* Branson & Mehl from the Upper Devonian of the Canning Basin, Western Australia 197

P. Wellman & J. W. Williams
Extent of Archaean and Late Proterozoic rocks under the ice cap of Princess Elizabeth Land, Antarctica, inferred from geophysics 213

D. Denham, G. Bock, & R. S. Smith
The Appin (New South Wales) earthquake of 15 November 1981 219

NOTE

M. H. Tratt & R. V. Burne
Impregnation of unconsolidated sediment samples, using a large vacuum chamber 225

ABSTRACTS

New microform publications 227

R81/103 (3) Cat. No. 82 0640 0